

**R**  
**ADIOLGY**  
**AND**  
**ONCOLOGY**

**vol.55 no.3**

**september 2021**





## Publisher

Association of Radiology and Oncology

## Aims and Scope

*Radiology and Oncology is a multidisciplinary journal devoted to the publishing original and high quality scientific papers and review articles, pertinent to diagnostic and interventional radiology, computerized tomography, magnetic resonance, ultrasound, nuclear medicine, radiotherapy, clinical and experimental oncology, radiobiology, medical physics and radiation protection. Therefore, the scope of the journal is to cover beside radiology the diagnostic and therapeutic aspects in oncology, which distinguishes it from other journals in the field.*

## Editor-in-Chief

**Gregor Serša**, Institute of Oncology Ljubljana, Department of Experimental Oncology, Ljubljana, Slovenia (Subject Area: Experimental Oncology)

## Executive Editor

**Viljem Kovač**, Institute of Oncology Ljubljana, Department of Radiation Oncology, Ljubljana, Slovenia (Subject Areas: Clinical Oncology, Radiotherapy)

## Editorial Board

### Subject Areas:

#### Radiology and Nuclear Medicine

**Sotirios Bisdas**, University College London, Department of Neuroradiology, London, UK

**Boris Brkljačić**, University Hospital "Dubrava", Department of Diagnostic and Interventional Radiology, Zagreb, Croatia

**Maria Gódný**, National Institute of Oncology, Budapest, Hungary

**Gordana Ivanac**, University Hospital Dubrava, Department of Diagnostic and Interventional Radiology, Zagreb, Croatia

**Luka Ležaić**, University Medical Centre Ljubljana, Department for Nuclear Medicine, Ljubljana, Slovenia

**Katarina Šurlan Popovič**, University Medical Center Ljubljana, Clinical Institute of Radiology, Ljubljana, Slovenia

**Jernej Vidmar**, University Medical Center Ljubljana, Clinical Institute of Radiology, Ljubljana, Slovenia

## Deputy Editors

**Andrej Čör**, University of Primorska, Faculty of Health Science, Izola, Slovenia (Subject Areas: Clinical Oncology, Experimental Oncology)

**Božidar Casar**, Institute of Oncology Ljubljana, Department for Dosimetry and Quality of Radiological Procedures, Ljubljana (Subject Area: Medical Physics)

**Maja Čemažar**, Institute of Oncology Ljubljana, Department of Experimental Oncology, Ljubljana, Slovenia (Subject Area: Experimental Oncology)

### Subject Areas:

#### Clinical Oncology and Radiotherapy

**Serena Bonin**, University of Trieste, Department of Medical Sciences, Cattinara Hospital, Surgical Pathology Bg, Molecular Biology Lab, Trieste, Italy

**Luca Campana**, Veneto Institute of Oncology (IOV-IRCCS), Padova, Italy

**Christian Dittrich**, Kaiser Franz Josef - Spital, Vienna, Austria

**Blaž Grošelj**, Institute of Oncology Ljubljana, Department of Radiation Oncology, Ljubljana

**Luka Milas**, UT M. D. Anderson Cancer Center, Houston, USA

**Miha Oražem**, Institute of Oncology Ljubljana, Department of Radiation Oncology, Ljubljana

**Gaber Plavc**, Institute of Oncology Ljubljana, Department of Radiation Oncology, Ljubljana

**Csaba Polgar**, National Institute of Oncology, Budapest, Hungary

**Dirk Rades**, University of Lubeck, Department of Radiation Oncology, Lubeck, Germany

**Luis Souhami**, McGill University, Montreal, Canada

**Borut Štabuc**, University Medical Center Ljubljana, Division of Internal Medicine, Department of Gastroenterology, Ljubljana, Slovenia

**Andrea Veronesi**, Centro di Riferimento Oncologico- Aviano, Division of Medical Oncology, Aviano, Italy

**Branko Zakotnik**, Institute of Oncology Ljubljana, Department of Medical Oncology, Ljubljana, Slovenia

**Miklós Kásler**, National Institute of Oncology, Budapest, Hungary

**Maja Osmak**, Ruder Bošković Institute, Department of Molecular Biology, Zagreb, Croatia

**Igor Kocijančič**, University Medical Center Ljubljana, Institute of Radiology, Ljubljana, Slovenia (Subject Areas: Radiology, Nuclear Medicine)

**Karmen Stanič**, Institute of Oncology Ljubljana, Department of Radiation Oncology, Ljubljana, Slovenia (Subject Areas: Radiotherapy; Clinical Oncology)

**Primož Strojjan**, Institute of Oncology Ljubljana, Department of Radiation Oncology, Ljubljana, Slovenia (Subject Areas: Radiotherapy, Clinical Oncology)

### Subject Area: Experimental Oncology

**Metka Filipič**, National Institute of Biology, Department of Genetic Toxicology and Cancer Biology, Ljubljana, Slovenia

**Janko Kos**, University of Ljubljana, Faculty of Pharmacy, Ljubljana, Slovenia

**Tamara Lah Turnšek**, National Institute of Biology, Ljubljana, Slovenia

**Damijan Miklavčič**, University of Ljubljana, Faculty of Electrical Engineering, Ljubljana, Slovenia

**Ida Ira Skvortsova**, EXTRO-lab, Dept. of Therapeutic Radiology and Oncology, Medical University of Innsbruck, Tyrolean Cancer Research Institute, Innsbruck, Austria

**Gillian M. Tozer**, University of Sheffield, Academic Unit of Surgical Oncology, Royal Hallamshire Hospital, Sheffield, UK

### Subject Area: Medical Physics

**Robert Jeraj**, University of Wisconsin, Carbone Cancer Center, Madison, Wisconsin, USA

**Mirjana Josipović**, Rigshospitalet, Department of Oncology, Section of Radiotherapy, Copenhagen, Denmark

**Håkan Nyström**, Skandionkliniken, Uppsala, Sweden

**Ervin B. Podgoršak**, McGill University, Medical Physics Unit, Montreal, Canada

**Matthew Podgorsak**, Roswell Park Cancer Institute, Departments of Biophysics and Radiation Medicine, Buffalo, NY, USA

## Advisory Committee

**Tullio Giraldi**, University of Trieste, Faculty of Medicine and Psychology, Department of Life Sciences, Trieste, Italy

**Vassil Hadjidekov**, Medical University, Department of Diagnostic Imaging, Sofia, Bulgaria

**Marko Hočevar**, Institute of Oncology Ljubljana, Department of Surgical Oncology, Ljubljana, Slovenia

Editorial office

**Radiology and Oncology**

Zaloška cesta 2

P. O. Box 2217

SI-1000 Ljubljana

Slovenia

Phone: +386 1 5879 369

Phone/Fax: +386 1 5879 434

E-mail: gsera@onko-i.si

Copyright © Radiology and Oncology. All rights reserved.

Reader for English

**Vida Kološa**

Secretary

**Mira Klemenčič**

**Zvezdana Vukmirović**

Design

**Monika Fink-Serša, Samo Rován, Ivana Ljubanović**

Layout

**Matjaž Lužar**

Printed by

**Tiskarna Ozimek, Slovenia**

Published quarterly in 400 copies

*Beneficiary name: DRUŠTVO RADIOLOGIJE IN ONKOLOGIJE*

*Zaloška cesta 2*

*1000 Ljubljana*

*Slovenia*

*Beneficiary bank account number: SI56 02010-0090006751*

*IBAN: SI56 0201 0009 0006 751*

*Our bank name: Nova Ljubljanska banka, d.d.,*

*Ljubljana, Trg republike 2,*

*1520 Ljubljana; Slovenia*

SWIFT: LJBASIX

*Subscription fee for institutions EUR 100, individuals EUR 50*

*The publication of this journal is subsidized by the Slovenian Research Agency.*

Indexed and abstracted by:

- Baidu Scholar
- Case
- Chemical Abstracts Service (CAS) - CAplus
- Chemical Abstracts Service (CAS) - SciFinder
- CNKI Scholar (China National Knowledge Infrastructure)
- CNPIEC - cnpLINKer
- Dimensions
- DOAJ (Directory of Open Access Journals)
- EBSCO (relevant databases)
- EBSCO Discovery Service
- Embase
- Genamics JournalSeek
- Google Scholar
- Japan Science and Technology Agency (JST)
- J-Gate
- Journal Citation Reports/Science Edition
- JournalGuide
- JournalTOCs
- KESLI-NDSL (Korean National Discovery for Science Leaders)
- Medline
- Meta
- Microsoft Academic
- Naviga (Softweco)
- Primo Central (ExLibris)
- ProQuest (relevant databases)
- Publons
- PubMed
- PubMed Central
- PubsHub
- QOAM (Quality Open Access Market)
- ReadCube
- Reaxys
- SCImago (SJR)
- SCOPUS
- Sherpa/RoMEO
- Summon (Serials Solutions/ProQuest)
- TDNet
- Ulrich's Periodicals Directory/ulrichsweb
- WanFang Data
- Web of Science - Current Contents/Clinical Medicine
- Web of Science - Science Citation Index Expanded
- WorldCat (OCLC)

*This journal is printed on acid-free paper*

On the web: ISSN 1581-3207

<https://content.sciendo.com/raon>

<http://www.radioloncol.com>

# contents

## *review*

- 247 **Microwave ablation compared with radiofrequency ablation for the treatment of liver cancer: a systematic review and meta-analysis**  
Antonios E. Spiliotis, Gereon Gäbelein, Sebastian Holländer, Philipp-Robert Scherber, Matthias Glanemann, Bijendra Patel

## *nuclear medicine*

- 259 **Can dynamic imaging, using <sup>18</sup>F-FDG PET/CT and CT perfusion differentiate between benign and malignant pulmonary nodules?**  
Aleksander Marin, John T. Murchison, Kristopher M. Skwarski, Adriana A.S. Tavares, Alison Fletcher, William A. Wallace, Vladka Salapura, Edwin J.R. van Beek, Saeed Mirsadraee

## *radiology*

- 268 **MRI of Morel-Lavallée lesion - a case series**  
Tajda Srot Volavc, Mitja Rupreht
- 274 **Are radiation-induced cavernomas clinically relevant findings? Results from long-term follow-up with brain magnetic resonance imaging of childhood cancer survivors**  
Lucas Becker, Judith Gebauer, Jan Küchler, Christian Staackmann, Hannes Schacht, Melchior Lauten, Ulf Jensen-Kondering, Peter Schramm, Thorsten Langer, Alexander Neumann
- 284 **Sialendoscopy and CT navigation assistance in the surgery of sialolithiasis**  
Aleksandar Anicin, Jure Urbancic

## *experimental oncology*

- 292 **Morphological features of breast cancer circulating tumor cells in blood after physical and biological type of isolation**  
Tanja Jesenko, Ziva Modic, Cvetka Grasic Kuhar, Maja Cemazar, Urska Matkovic, Simona Miceska, Jerneja Varl, Anamarija Kuhar, Veronika Kloboves-Prevodnik
- 305 **Simvastatin is effective in killing the radioresistant breast carcinoma cells**  
Bertram Aschenbrenner, Giulia Negro, Dragana Savic, Maxim Sorokin, Anton Buzdin, Ute Ganswindt, Maja Cemazar, Gregor Sersa, Sergej Skvortsov, Ira Skvortsova

## *clinical oncology*

- 317 **Five-year follow-up and clinical outcome in euthyroid patients with thyroid nodules**  
Katica Bajuk Studen, Simona Gaberscek, Edvard Pirnat, Katja Zaletel

- 323 **The importance of flaps in reconstruction of locoregionally advanced lateral skull-base cancer defects: a tertiary otorhinolaryngology referral centre experience**  
Domen Vozel, Peter Pukl, Aleš Grošelj, Aleksandar Aničin, Primož Strojjan, Saba Battelino
- 333 **State of the art in breast intraoperative electron radiation therapy after intraoperative ultrasound introduction**  
Cristiana Vidali, Mara Severgnini, Gabriele Bellio, Fabiola Giudici, Vittorino Milan, Zaira Pellin, Sara Savatovic, Serena Scomersi, Gerd Fastner, Antonella Ciabattoni, Marina Bortul
- 341 **Preoperative serum CA-125 level as a predictor for the extent of cytoreduction in patients with epithelial ovarian cancer**  
Sebastjan Merlo, Nikoloa Besic, Eva Drmota, Nina Kovacevic
- 347 **Predictive impact of the inflammation-based indices in uveal melanoma liver metastases treated with transarterial hepatic chemoperfusion**  
Johannes M. Ludwig, Johannes Haubold, Sebastian Baue, Heike Richly, Jens T. Siveke, Julia Wimmer, Lale Umutlu, Benedikt M. Schaarschmidt, Jens M. Theysohn
- 354 **Adverse events during immunotherapy in Slovenian patients with metastatic melanoma reveal a positive correlation with better treatment outcome**  
Tanja Mesti, Vid Ceplak Mencin, Biljana Mileva Boshkoska, Janja Ocvirk
- 362 **Breast cancer during pregnancy: retrospective institutional case series**  
Erika Matos, Tanja Ovcaricek

### *medical physics*

- 369 **A protocol for accurate radiochromic film dosimetry using Radiochromic.com**  
Ignasi Méndez, Juan Jose, Rovira-Escutia, Bozidar Casar

### *slovenian abstracts*

review

# Microwave ablation compared with radiofrequency ablation for the treatment of liver cancer: a systematic review and meta-analysis

Antonios E. Spiliotis<sup>1</sup>, Gereon Gäbelein<sup>1</sup>, Sebastian Holländer<sup>1</sup>, Philipp-Robert Scherber<sup>1</sup>, Matthias Glanemann<sup>1</sup>, Bijendra Patel<sup>2</sup>

<sup>1</sup> Department of General, Visceral, Vascular and Pediatric Surgery, University Clinic of Saarland, Homburg, Saarland, Germany

<sup>2</sup> Barts Cancer Institute, Queen Mary University of London, London, UK

Radiol Oncol 2021; 55(3): 247-258.

Received 5 April 2021

Accepted 10 May 2021

Correspondence to: Antonios E. Spiliotis, Department of General, Visceral, Vascular and Pediatric Surgery, University of Saarland, Kirrberger Straße, 66421, Homburg, Saarland, Germany. E-mail: antonios.spiliotis@uks.eu

Disclosure: No potential conflicts of interest were disclosed.

This is an open access article under the CC BY-NC-ND license (<http://creativecommons.org/licenses/by-nc-nd/4.0/>).

**Background.** Guidelines have reported that although microwave ablation (MWA) has potential advantages over radiofrequency ablation (RFA), superiority in efficacy and safety remain unclear. Aim of the study is to compare MWA with RFA in the treatment of liver cancer.

**Methods.** Meta-analysis was conducted according to the PRISMA guidelines for studies published from 2010 onwards. A random-effects model was used for the meta-analyses. Complete ablation (CA), local tumor progression (LTP), intrahepatic distant recurrence (IDR), and complications were analyzed.

**Results.** Four randomized trials and 11 observational studies with a total of 2,169 patients met the inclusion criteria. Although overall analysis showed no significant difference in LTP between MWA and RFA, subgroup analysis including randomized trials for patients with hepatocellular cancer (HCC) demonstrated statistically decreased rates of LTP in favor of MWA (OR, 0.40; 95% CI, 0.18–0.92;  $p = 0.03$ ). No significant differences were found between the two procedures in CA, IDR, complications, and tumor diameter less or larger than 3 cm.

**Conclusions.** MWA showed promising results and demonstrated better oncological outcomes in terms of LTP compared to RFA in patients with HCC. MWA can be utilized as the ablation method of choice in patients with HCC.

Key words: liver; carcinoma hepatocellular; liver neoplasms; radiofrequency ablation; microwaves

## Introduction

Over the past 30 years, several ablative methods have been developed for the treatment of hepatic cancer as an alternative to surgical resection and liver transplantation in patients with unresectable cancer or in selected patients with resectable disease. Recent guidelines recommend radiofrequency ablation (RFA) and microwave ablation (MWA) as the ablative methods with the highest efficacy in the treatment of liver cancer.<sup>1,2</sup>

Tumor location near to the main biliary tree, abdominal organs, or diaphragm is a relative contraindication for RFA because of the risk of severe complications.<sup>2</sup> RFA is prone to heat-sink effect, which reduces further the efficacy of the treatment.<sup>1,2</sup> On the other hand, MWA, which is a more recent thermal ablation technique, is associated with higher intratumoral temperatures, resulting in faster, larger, and more homogenous ablation compared to RFA.<sup>2</sup> Furthermore, MWA is less prone to heat-sink effect and can be utilized in tumors adjacent to vessels.

According to the European Association for the Study of the Liver (EASL) recommendations, MWA showed promising results for local tumor control in patients with hepatocellular cancer (HCC).<sup>1</sup> The guidelines by the American Association for the Study of Liver Diseases (AASLD) reported that MWA has potential advantages over RFA; however, further studies are required to provide safety and efficacy data.<sup>2</sup> The Cochrane meta-analysis conducted in 2013 failed to provide evidence regarding the role of ablative methods in the treatment of HCC since only one randomized clinical trial (RCT) with high risk of bias was available.<sup>3</sup> The last conducted meta-analysis in 2019 reported beneficial outcomes in favor of MWA.<sup>4</sup> However, low quality randomized and observational studies, which were affected by confounding bias were included in this meta-analysis, which could influence the reliability of the outcomes.

Despite the promising results of MWA in the treatment of liver cancer, efficacy and safety of MWA compared to RFA is unclear. Aim of this meta-analysis is to compare RFA and MWA in the treatment of HCC and liver metastases. Our hypothesis is that the beneficial characteristics of MWA are translated into better oncological outcomes compared to RFA.

## Methods

### Inclusion and exclusion criteria

A protocol was developed to pre-specify criteria for including and excluding studies in the review. Eligibility criteria were based on the PICO elements (population, interventions, comparators, and outcomes) plus a specification of the type of studies that have addressed these questions. RCTs and observational studies (prospective or retrospective cohort and case-control studies) were eligible for inclusion. Studies conducted before 2010 were excluded from the meta-analysis.

Studies meeting the following criteria were included: (1) population: adults with primary liver cancer or hepatic metastases; (2) interventions: RFA and MWA as monotherapy or combined with surgical resection; (3) MWA and RFA conducted percutaneously, laparoscopically, or through laparotomy; (4) comparators: effectiveness and safety of MWA compared to RFA; (5) outcomes: results provided data relative to complete ablation (CA), local tumor progression (LTP), intrahepatic distant (IDR), complications; (6) full text available in English or German; (7) studies with low or moderate risk of bias.

Exclusion criteria were the following: (1) studies with benign liver tumors; (2) pediatric population; (3) animal or in vitro studies; (4) RFA or MWA combined with other interventions such as transarterial chemoembolization (TACE); (5) gender and geographical criteria were not utilized; (6) stage of liver cancer, size, and location of tumors did not constitute exclusion criteria; (7) duplicate data.

### Study outcomes

Primary outcomes were the CA rates and the LTP. CA was defined as the no enhancement of the tumor in the hepatic arterial or portal venous phase in dynamic enhanced imaging (CT, MRI), which was conducted after ablation. As incomplete ablation was defined the enhancement of the tumor in dynamic enhanced imaging.<sup>5</sup> As LTP was defined the reappearance of the tumor within or adjacent to the ablation zone during the follow-up period. Studies that reported recurrence rates without to define if that is local or distant were excluded from this analysis. In studies where 1-year, 3-year, and 5-year LTP rates were reported, only the overall 5-year LTP rate was included in the analysis. In the majority of cases, patients were presented with multinodular disease. For that reason, CA and LTP were recorded for every treated lesion. Studies, where LTP and CA were recorded per patient and not per lesion, were excluded from the analysis.

IDR and complications were included in the secondary outcomes. IDR was defined as distant recurrence within the liver. In studies where 1-year, 3-year, and 5-year IDR rates were reported, the overall 5-year rate was included in the meta-analysis. Minor complications, which required no intervention or were not associated with prolonged hospital stay, were not included in the analysis. Major complications were defined as post-interventional events that lead to substantial morbidity or disability, require intervention, and result in prolonged hospital stay.

A subgroup analysis was conducted, comparing CA and LTP for tumors  $\leq 3$  cm and tumors  $> 3$  cm in diameter. RFA and MWA were compared separately in patients diagnosed with HCC and colorectal liver metastases (CRLM).

### Search strategy and data collection

The systematic review was conducted according to the Preferred Reporting Items for Systematic Reviews and Meta-Analyses (PRISMA) guidelines.<sup>6</sup> A systematic search of MEDLINE (PubMed

and Ovid) and the Cochrane Central Register of Controlled Trials was conducted for relevant systematic reviews, RCTs, and observational studies. Access to Embase was not available for the review team. The search was accomplished in July 2020.

The search strategy included the following keywords: (((("Carcinoma, Hepatocellular"[Mesh]) OR (hepatic tumor)) AND ("Radiofrequency Ablation"[Mesh]) AND ("Microwaves"[Mesh])). The search strategy was not limited by geographical criteria. English and German language articles were reviewed for inclusion. Studies conducted between 2010 and 2020 were screened. Reference lists of retrieved studies and relevant reviews were hand-searched.

Eligibility for inclusion was evaluated in the title and abstract of each publication. If the title and abstract were relevant to the review question, full-text screening was conducted. Reviewers were not blinded to the name of authors and institutions. Screening of articles was conducted by two reviewers. Discrepancies were resolved by consensus. If consensus was not reached, discrepancies were resolved by adjudication from a third reviewer. Data were extracted independently by two reviewers and checked from a third reviewer. When further information was required during data extraction, the reviewers tried to contact the corresponding author with email.

### Risk of bias assessment

Non-randomized studies were included since available RCTs were limited. The quality of RCTs and observational studies was assessed using the Cochrane Risk of Bias version 2 (RoB 2) tool and The Risk of Bias In Non-randomized Studies of Interventions (ROBINS-I) tool, respectively.<sup>7</sup> Risk of bias was assessed independently by two reviewers. In case of disagreement, a third author adjudicated the final judgement. High risk RCTs were excluded from the analysis.

Non-randomized studies vary with respect to their intrinsic ability to estimate the causal effect of an intervention. Therefore, to reach reliable conclusions and to eliminate the risk of bias in our results, only studies with low and moderate risk of bias were included in the meta-analysis. Studies with "Serious", "Critical" risk of bias, or "No information" were excluded from the meta-analysis.

Review authors have defined confounding domains in the review protocol. Confounding domain is a preintervention prognostic factor of the outcome that also predicts whether an individual receives RFA or MWA. Non-randomized studies

were assessed as 'Low Risk of Bias' in this domain when patients in both groups were matched using propensity score based on the confounding factors. Surveys that compared confounding factors at baseline without propensity score matching and reported no statistical differences were included as studies with 'Moderate Risk of Bias'. Finally, studies with statistically different baseline characteristics or not reported or not compared baseline characteristics were assessed as 'Serious Risk' or 'Critical Risk' and were excluded from the analysis.

### Statistical analysis

For all outcomes of interest, meta-analyses for the Odds Ratio (OR) have been performed. The amount of heterogeneity (measured by  $I^2$ ) among studies varied strongly between outcomes, ranging from very low to substantially. However, in order to be consistent with respect to the modelling strategy, random effects estimates for the OR have been chosen for all outcomes. Sensitivity analyses for this modelling found high agreement between estimates derived from random and fixed effect models. Within the random effects model, the DerSimonian-Laird estimator<sup>8</sup> has been used for the calculation of between-studies variance ( $\tau^2$ ) in combination with the Mantel-Haenszel method<sup>9</sup> for the calculation of between-study heterogeneity statistic  $Q$ .<sup>10</sup> Overall treatment effects (overall ORs) were derived from the random effects models and presented as point estimates and corresponding 95% confidence intervals (CI). In all analyses,  $p$ -value  $< 0.05$  was regarded as statistically significant.

The amount of heterogeneity among studies has been measured by the  $I$  value. In addition, tests of heterogeneity were performed on the  $Q$  statistic, which provides  $p$ -values. Funnel plots have been created to examine publication bias in meta-analysis outcomes with more than five included studies. Asymmetry in funnel plots has been analyzed using Egger's test of the intercept in meta-analysis outcomes with more than ten included studies.<sup>11</sup> For statistical analysis, the R software for statistical computing (R version 4.0.1, R Core Team, 2020) has been used in combination with the meta package and dmetar package.<sup>12</sup>

## Results

### Studies selection

A total of 716 publications were identified from database searching. After removing duplicates, 581

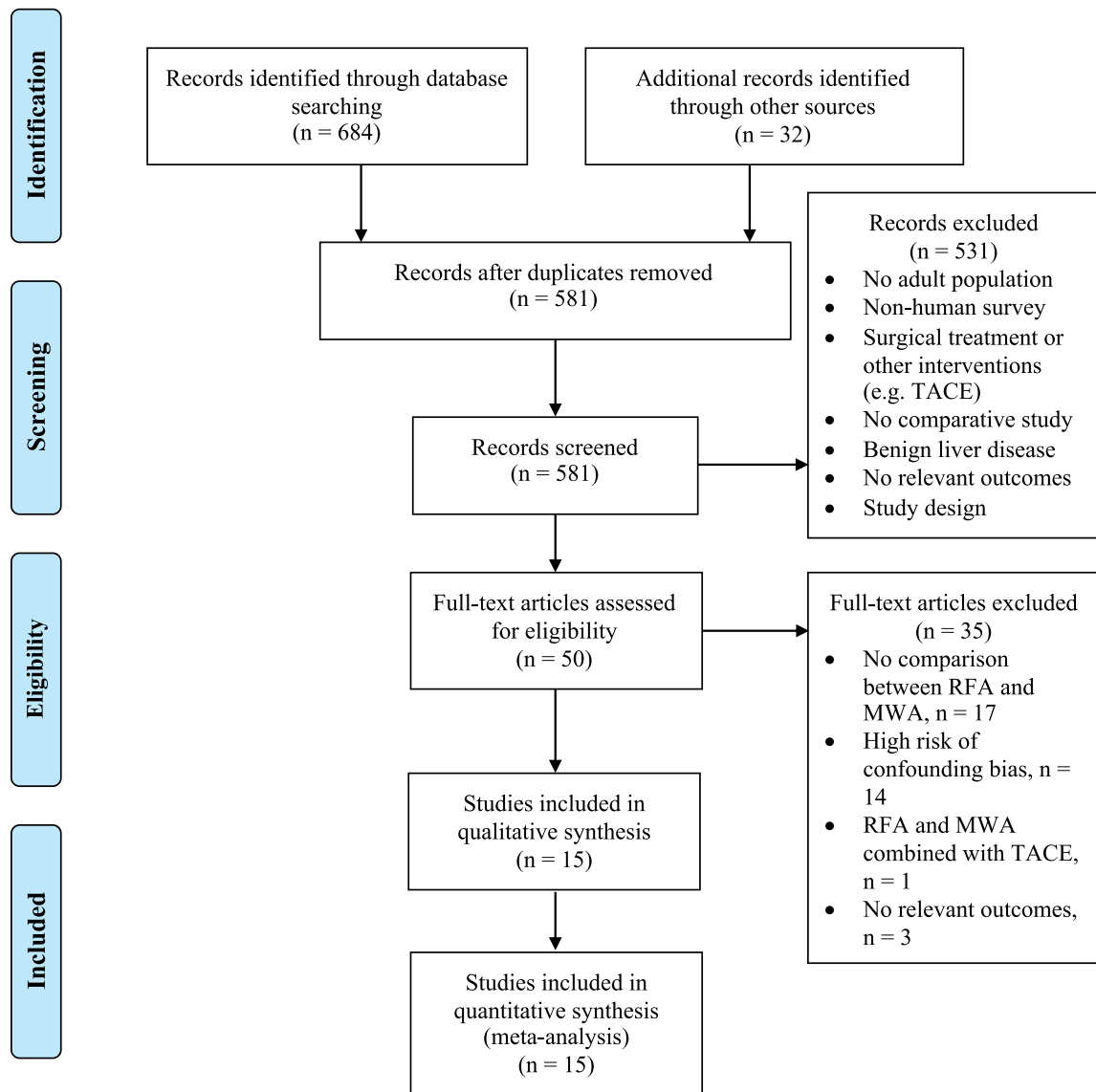


FIGURE 1. Prisma flow diagram.

MWA = microwave ablation, RFA = radiofrequency ablation, TACE = transarterial chemoembolization

unique articles were screened for inclusion. During the title-abstract screening phase, a total of 531 irrelevant studies were excluded. Fifty articles were selected for full-text review. Thirty-five articles were excluded because of no comparison between RFA and MWA (n = 17), increased risk of bias in confounding domain for observation studies (n = 14), combined treatment with TACE (n = 1), and no relevant outcomes (n = 3). The RCT by Yu *et al.* was assessed as a trial with high risk of bias and was excluded from the meta-analysis.<sup>13</sup> Finally, 15 studies (four RCTs, one prospective study, ten retrospective studies), were included in our review. PRISMA diagram is demonstrated in Figure 1.

### Characteristics of included studies

Fifteen studies with a total of 2,169 patients were included in the analysis.<sup>14-28</sup> The recruitment period ranged from 2001 to 2018. The sample size ranged from 40 to 460 patients. The average age across studies ranged from 52 to 68 years. The mean or median tumor size ranged from 1.7 cm to 3.75 cm. All studies reported no significant differences in tumor size between the two treatment groups. Study characteristics and baseline characteristics are demonstrated in Table 1.

Eight studies evaluated the role of thermal ablation in patients with HCC.<sup>14-16,18,22,24,26,28</sup> Child-Pugh

TABLE 1. Study and baseline characteristics of studies included in the meta-analysis

Study	Country	Study Design	Tumor	RFA, n	MWA, n	Age, RFA	Age, MWA	Child-Pugh A/B/C, RFA	Child-Pugh A/B/C, MWA	Tumor size (cm), RFA	Tumor size (cm), MWA	Tumor lesions, RFA	Tumor lesions, MWA
Kamal 2019 (13)	Egypt	RCT	HCC	28	28	55	55	22.6/2000	22.6/2000	3.28 ± 0.91	3.25 ± 0.92	34	34
Vietti Violi 2018 (14)	France/ Switzerland	RCT	HCC	73	71	65 (median)	68 (median)	53/20/0	57/14/0	1.8 ± 0.71	1.8 ± 0.65	104	98
Abdelaziz 2014 (15)	Egypt	RCT	HCC	45	66	56.8 ± 7.3	53.6 ± 5	24/21/0	25/41/0	2.95 ± 1.03	2.9 ± 0.97	52	76
Di Vece 2013 (16)	Italy	RCT	HCC/ Metastases	20	20	59 (median)	63 (median)	N/R	N/R	3.2 (median)	3.6 (median)	20	20
Qian 2012 (17)	China	Prospective	HCC	20	22	56 ± 11	52 ± 12	20/0/0	22/0/0	2 ± 0.5	2.1 ± 0.4	20	22
Sparchez 2019 (18)	Romania	Retrospective	Metastases	44	17	60.18 ± 9.96	62.12 ± 10.73	-	-	2.maj	feb.55	62	20
Takahashi 2018 (19)	USA	Retrospective	CRLM	54	51	N/R	N/R	-	-	2.4 (median)	2.1 (median)	155	121
Shady 2018 (20)	USA	Retrospective	CRLM	62	48	N/R	N/R	-	-	1.8 (median)	1.7 (median)	85	60
Xu 2017 (21)	China	Retrospective	HCC	159	301	54 ± 11	54.2 ± 11	140/19/0	278/23/0	1.7 ± 0.3	1.7 ± 0.3	159	301
van Tilborg 2016 (38)	Netherlands	Retrospective	CRLM	Total number of participants: 122		N/R	N/R	-	-	2.apr	2.maj	151	48
Potretzke 2016 (23)	USA	Retrospective	HCC	55	99	62	61	N/R	N/R	2.apr	2.feb	69	136
Zhang X. 2014 (24)	China	Retrospective	HCC/ Metastases	92	230	51.5 ± 14.3	55.7 ± 13.2	N/R	N/R	5.4 ± 1.9	5.7 ± 2.1	173	349
Zhang L. 2013 (25)	China	Retrospective	HCC	78	77	54 ± 10.5	54 ± 9.5	78/0/0	77/0/0	2.3 ± 0.4	2.2 ± 0.4	97	105
Liu 2013 (26)	China	Retrospective	Metastases	54	35	53.1 ± 12.7	53.4 ± 15.3	-	-	2.5 ± 1.0	2.3 ± 1.0	70	62
Ding 2013 (27)	China	Retrospective	HCC	85	113	58.64 ± 8.52	59.06 ± 11.68	49/36/0	75/30/0	2.38 ± 0.81	2.55 ± 0.89	98	131

Age and tumor size are recorded as mean, mean ± standard deviation (SD), or median.

CRLM = colorectal liver metastases, HCC = hepatocellular cancer, MWA = microwave ablation, RCT = randomized clinical trial, RFA = radiofrequency ablation, N/R = not reported

score, which was estimated in the majority of studies, was not statistically different between RFA and MWA groups. In the retrospective study conducted by Potretzke *et al.*, MELD score was estimated, which was similar in the RFA and MWA group.<sup>24</sup> Four studies included patients with hepatic metastases of different origins<sup>17,19,25,27</sup>, whereas three studies included only patients with CRLM.<sup>20,21,23</sup> In the RCT conducted by Di Vece *et al.*, the primary origin of liver metastases was not reported.<sup>17</sup>

## Quality assessment

The quality of included RCTs was acceptable (Supporting Information, Figure S1). Two out of four RCTs were judged to be at low risk of bias across all domains.<sup>15,17</sup> The RCT conducted by Abdelaziz *et al.* was judged to raise some concerns in bias due to deviations from intended interventions since important non-protocol interventions during follow-up were not recorded.<sup>16</sup>

Three studies reported the method of randomization and allocation sequence generation. Coin flip<sup>16</sup> and centralized computer-generated randomization<sup>15,17</sup> were utilized as methods for random sequence generation. In these RCTs, the allocation

sequence was adequately concealed. The study by Kamal *et al.* did not report the method of randomization and was judged to raise some concerns in the domain of bias arising from the randomization process.<sup>14</sup> Simple randomization was used in two studies<sup>4,16</sup>, whereas the other two RCTs utilized blocked-restricted randomization.<sup>15,17</sup>

Physicians, who conducted the ablations, were not blinded, since different equipment was utilized in each treatment modality. Patients were masked to the treatment in one trial.<sup>15</sup> In two RCTs, independent outcome assessors, who were masked to the treatment allocation, reviewed all images and recorded the outcomes.<sup>15,17</sup> In the studies conducted by Kamal *et al.* and Abdelaziz *et al.*, outcome assessors were not blinded.<sup>14,16</sup> However, the risk of bias due to blinding of outcome assessors was considered to be low, since assessment of CT or MRI imaging was objective and specific criteria were utilized for the evaluation of CA and LTP.

All retrospective studies were judged to be at moderate risk of overall and confounding bias (Supporting Information, Table S1). Studies that evaluated the role of ablation in hepatic metastases did not report the histological stage of the primary tumors.<sup>19-21,23,25, 27</sup> Two studies that included HCC

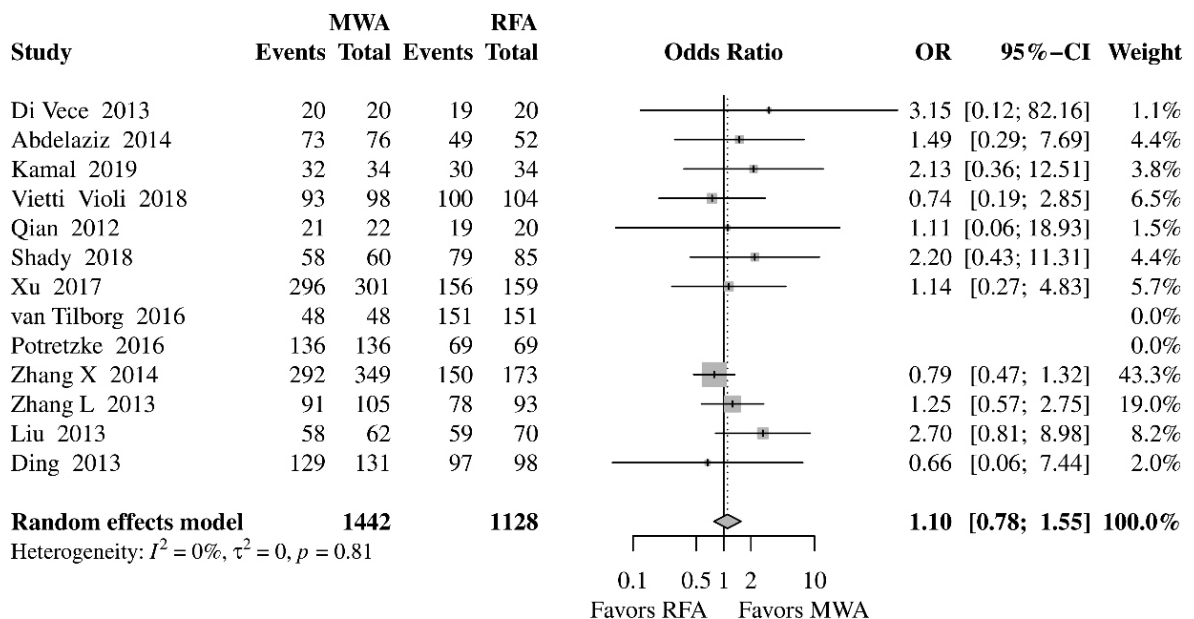


**FIGURE 2.** Forest plot of random-effects meta-analysis results for complete ablation rates in the MWA and RFA group.

CI = confidence interval, MWA = microwave ablation, OR = odds ratio, RFA = radiofrequency ablation

patients did not compare the BCLC stage at baseline.<sup>25,26</sup> Tumor size was comparable between the two groups in all studies.

Four studies were affected by selection bias.<sup>18,20,22,23</sup> In these studies, the number of excluded patients and the reason of exclusion were not reported. Bias due to deviations from intended interventions was seen only in the survey by van Tilborg *et al.*<sup>23</sup> Eleven patients underwent retreatments during follow-up, using the alternative ablation technique.

## Meta-analysis outcomes

### Complete ablation

Non-significant difference was found in CA rates between MWA and RFA (OR, 1.10; 95% CI, 0.78–1.55;  $p = 0.5898$ ) (Figure 2). No evidence of heterogeneity was found between the included studies ( $I^2$ , 0%;  $\tau^2$ , 0%,  $p = 0.81$ ). In order to evaluate the influence of retrospective studies in the results, a further analysis was performed, calculating OR separately for RCTs and retrospective studies (Supporting Information, Figure S2). Since only one prospective study was included in the meta-analysis<sup>18</sup>, further stratification by prospective studies was not performed. For the four RCTs, meta-analysis outcomes remained consistent with the main overall results (OR, 1.28; CI, 0.54–3.05;  $p = 0.5706$ ). Similarly, meta-analysis of the retrospec-

tive studies showed no significant difference between the two approaches (OR, 1.07; CI, 0.73–1.56;  $p = 0.7373$ ).

### Local tumor progression

LTP rates were comparable between MWA and RFA (OR, 0.79; 95% CI, 0.53–1.20;  $p = 0.2689$ ) (Figure 3). However, inter-study heterogeneity was significant ( $I^2$ , 56%;  $\tau^2$ , 0.2556;  $p = 0.01$ ). In the subgroup analysis, which included two RCTs, significantly reduced rates of LTP were found in the MWA group compared to RFA (OR, 0.40; 95% CI, 0.18–0.92;  $p = 0.03$ ). Furthermore, inter-study heterogeneity was not significant ( $I^2$ , 0%;  $\tau^2$ , 0;  $p = 0.47$ ). On the other hand, in the subgroup analysis of retrospective studies, the rates of LTP were similar in both groups (OR, 0.87; 95% CI, 0.55–1.39;  $p = 0.5731$ ), whereas heterogeneity remained significant ( $I^2$ , 63%;  $\tau^2$ , 0.2766;  $p < 0.01$ ) (Figure 4).

### Intrahepatic distant recurrence

Analysis of seven studies showed no statistically significant differences in IDR between MWA and RFA (OR, 0.73; 95% CI, 0.45–1.16;  $p = 0.1826$ ) (Figure 5). Inter-study heterogeneity was significant ( $I^2$ , 56%;  $\tau^2$ , 0.1977;  $p = 0.03$ ). Meta-analysis of RCTs showed no significant difference between the two procedures (OR, 0.66; 95% CI, 0.29–1.52;  $p = 0.3266$ ). No evidence of heterogeneity was found

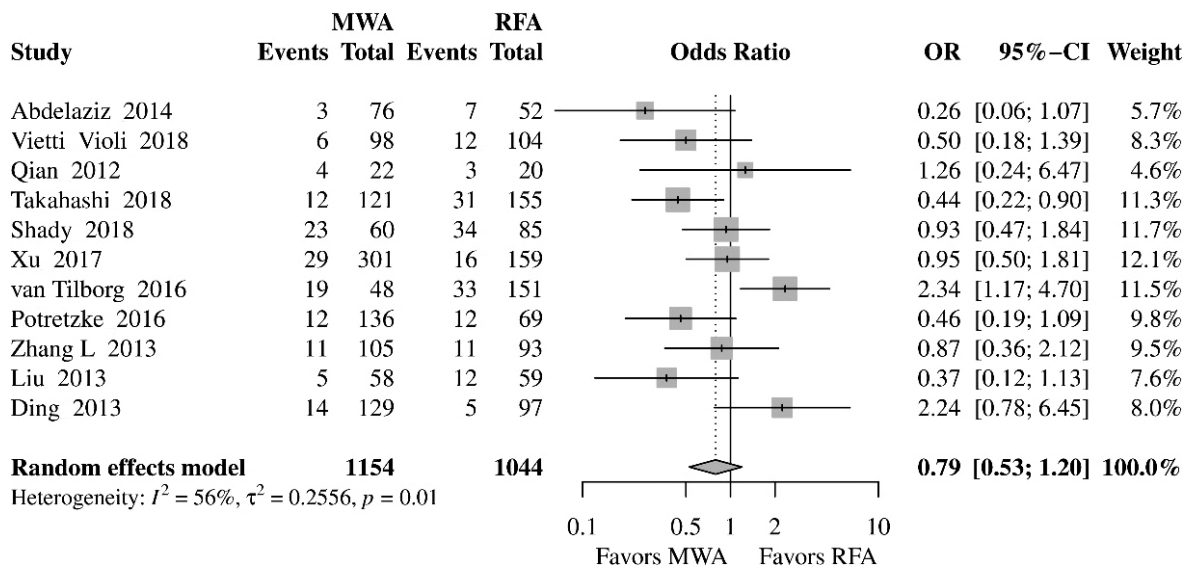


FIGURE 3. Forest plot of random-effects meta-analysis results for local tumor progression in the RFA and MWA group.

CI = confidence interval, MWA = microwave ablation, OR = odds ratio, RFA = radiofrequency ablation

between the two randomized trials ( $I^2$ , 0%;  $\tau^2$ , 0;  $p = 0.52$ ). Similarly, no difference between RFA and MWA was demonstrated when only retrospective studies were included in the meta-analysis (OR, 0.79; 95% CI, 0.43–1.46;  $p = 0.4529$ ). However, heterogeneity among retrospective studies was statistically significant ( $I^2$ , 75%;  $\tau^2$ , 0.2848;  $p < 0.01$ ).

### Complications

The most commonly reported major complications in both groups were subcapsular hepatic hematoma, perihepatic hematoma, arterial bleeding requiring embolization or surgical treatment, hepatic abscess, biliary fistula, bowel perforation, abdominal wall skin burn, and pleural effusion. The risk of major complications was not different between the two approaches (OR, 0.80; 95% CI, 0.46–1.37;  $p = 0.4129$ ) (Figure 6). In the subgroup meta-analysis, comparing RFA and MWA based on the type of study, results remained consistent without significant differences in the rate of complications in the RCTs<sup>14-17</sup> and retrospective studies.<sup>19,21,22,24,26-28</sup>

### Tumor size

Four studies assessed the rates of CA in patients with tumor  $< 3$  cm.<sup>6,18,24,28</sup> Heterogeneity among the surveys was not significant ( $I^2$ , 0%;  $\tau^2$ , 0;  $p = 0.54$ ). Results of meta-analysis showed no significant difference in CA between RFA and MWA (OR, 2.18; 95% CI, 0.34–13.88;  $p = 0.4095$ ). For the outcome of

LTP, three studies were included in the meta-analysis.<sup>18,24,28</sup> Results revealed no significant differences between the two modalities (OR, 0.99; 95% CI, 0.49–2.01,  $p = 0.9729$ ).

Regarding tumors with size larger than 3 cm, three studies reported CA rates<sup>16,24,28</sup> and two studies evaluated LTP.<sup>24,28</sup> Meta-analysis showed no significant difference in CA and LTP between RFA and MWA ( $p = 0.7682$ ;  $p = 0.8168$ , respectively).

### Hepatocellular cancer

Meta-analysis showed no significant difference in CA between RFA and MWA in patients with HCC (OR, 1.18; 95% CI, 0.70–1.99;  $p = 0.5437$ ). When only RCTs were included in the meta-analysis<sup>14-16</sup>, the results remained constant and significant differences were not found (OR, 1.20; 95% CI, 0.49–2.94;  $p = 0.6904$ ).

LTP was not significantly different between RFA and MWA (OR, 0.77; 95% CI, 0.49–1.22,  $p = 0.2723$ ). However, when only pooling RCTs<sup>15,16</sup>, rates of LTP were statistically decreased in the MWA group compared to RFA (OR, 0.40; 95% CI, 0.18–0.92,  $p = 0.03$ ). On the other hand, meta-analysis results of the retrospective studies<sup>22,24,26,28</sup> showed no difference between the two procedures (OR, 0.92; 95% CI, 0.52–1.60;  $p = 0.7614$ ).

Differences between RFA and MWA in the incidence of IDR were not found (OR, 0.75; 95% CI, 0.43–1.30;  $p = 0.3041$ ). However, heterogeneity among surveys was significant ( $I^2$ , 63%;  $\tau^2$ , 0.2594;

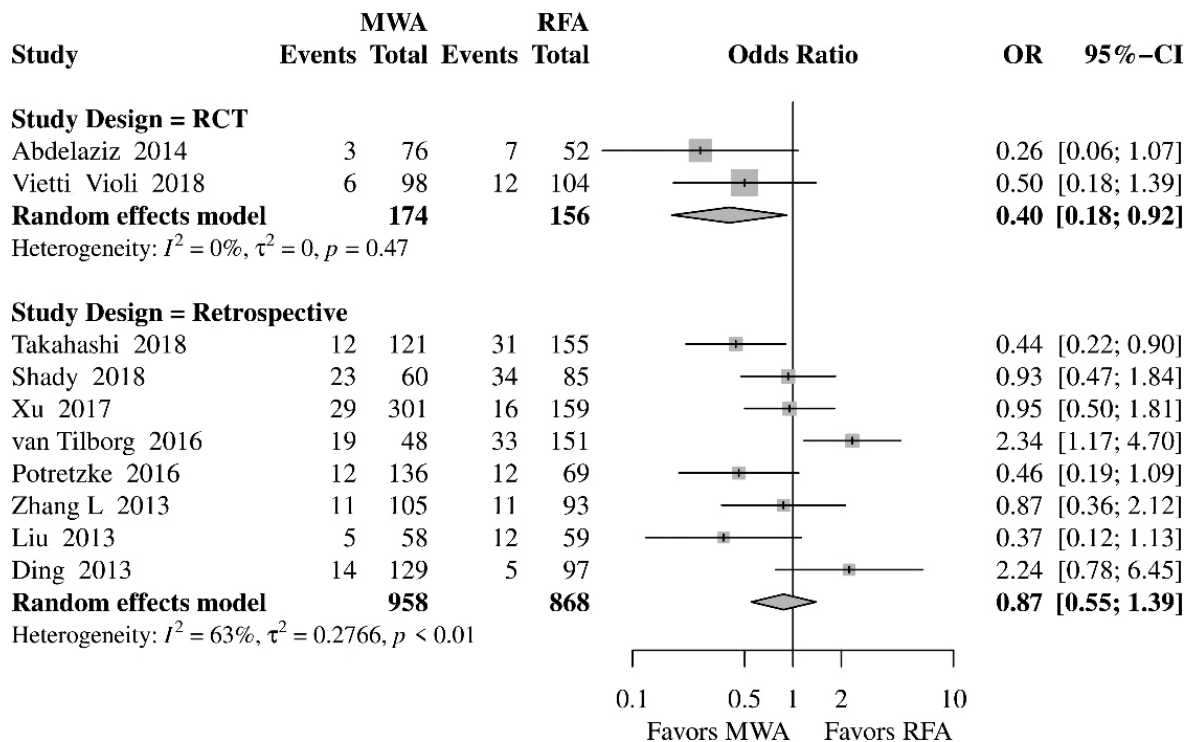


**FIGURE 4.** Forest plot of random-effects meta-analysis results for local tumor progression in the RFA and MWA group based on the study type.

CI = confidence interval, MWA = microwave ablation, OR = odds ratio, RFA = radiofrequency ablation

$p = 0.02$ ). Subgroup analysis of RCTs<sup>14,16</sup> and retrospective studies<sup>22,26,28</sup> showed no statistically different results between the two procedures ( $p = 0.3266$ ;  $p = 0.6975$ , respectively). Inter-study heterogeneity was not significant across RCTs; however, heterogeneity remained significant among retrospective studies.

### Colorectal liver metastases

CA and LTP were compared between RFA and MWA in patients with CRLM. Meta-analysis included three retrospective studies.<sup>20,21,23</sup> For both outcomes, no significant differences were found between the two procedures ( $p = 0.3441$ ;  $p = 0.9826$ , respectively).

### Publication bias

CA, LTP, IDR, complications, CA in HCC patients, LTP in HCC patients, and IDR in HCC patients were examined for publication bias (Supporting Information, Figure S3, S4). Results demonstrated a low risk of publication bias for the outcomes assessed. Egger's test was utilized in the outcomes with more than ten included studies. No obvious

asymmetry or  $p$ -value  $< 0.05$  were detected, which is associated with no evidence of publication bias.

## Discussion

RFA is currently one of the most widely used thermal ablation modalities. On the other hand, utilization of MWA has been increased the last years as a result of significant advancements in technology of new generation devices. These advancements are translated into higher temperatures and faster heating compared to RFA, large ablation volumes, and less heat sink effect.<sup>29</sup> However, MWA has not been adequately compared with RFA and selection of appropriate treatment is not based on high level of evidence.<sup>30</sup> On the basis of these considerations, we conducted the present meta-analysis to evaluate the role of MWA in the treatment of liver cancer.

Meta-analysis of CA rates, which included more than 2,500 tumor lesions, demonstrated no significant differences between MWA and RFA. In the subgroup analysis of RCTs with 438 tumors, similar rates of CA were found between the two methods. Analysis of all included studies revealed no significant difference in LTP between MWA and

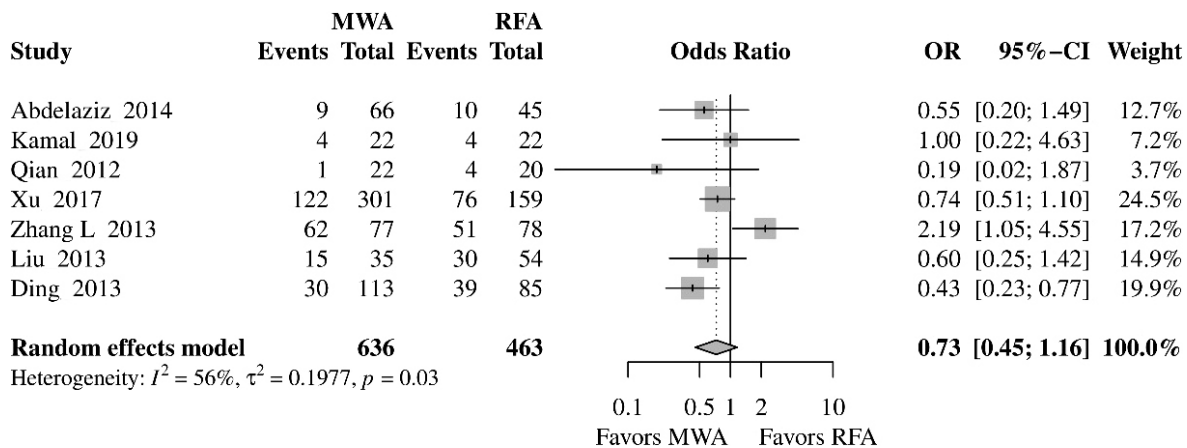


FIGURE 5. Forest plot of random-effects meta-analysis results for intrahepatic distant recurrence rates in the RFA and MWA group.

CI = confidence interval, MWA = microwave ablation, OR = odds ratio, RFA = radiofrequency ablation

RFA. Since increased heterogeneity was detected among the studies, subgroup analysis of RCTs was conducted to decrease heterogeneity and to evaluate the influence of observational studies on the outcomes. The RCTs by Abdelaziz *et al.* and Vietti Violi *et al.* included 255 patients with HCC and up to three lesions with less than 5 cm and 4 cm tumor size, respectively.<sup>15,16</sup> Furthermore, new generation MWA devices with 2,450 MHz generators were utilized. Meta-analysis of the two RCTs demonstrated statistically decreased rates of LTP in the MWA group. Specifically, LTP was reported in 5.2% and 12.2% of tumor lesions treated with MWA and RFA, respectively.

The finding of the RCTs is consistent with the physics and characteristics of radiofrequency and microwave energies. MWA is associated with higher temperatures, faster heating, larger ablation volumes, and less heat sink effect compared to RFA, which are translated into better oncological outcomes in terms of LTP in the present meta-analysis. On the other hand, meta-analysis of retrospective studies failed to demonstrate superiority of MWA over RFA, which is attributed to the significant inter-study heterogeneity.

Consequently, though CA was comparable between the two procedures, LTP was beneficial in favor of MWA. These conflicting results are not surprising given the limitations associated with measurement and evaluation of complete ablation response. Imaging modalities cannot detect with 100% accuracy whether neoplastic cells have been sufficiently ablated. For that reason, ablation response cannot be considered as the most reliable indicator of treatment effectiveness. On the other hand, follow-up imaging examinations and LTP

have been considered of great importance in detecting treatment failure. LTP is the most reliable indicator of treatment effectiveness and can be utilized as assessment tool of treatment efficacy.

IDR was comparable between the two ablative methods. Subgroup analysis of two RCTs demonstrated similar rates of IDR between MWA and RFA. The RCT by Kamal *et al.* reported IDR rates of 18.2% at 12-month follow-up<sup>14</sup>, while the survey by Abdelaziz *et al.* reported rates between 13.6% and 22.22% at 27-month follow-up.<sup>16</sup> The beneficial outcomes in LTP were not associated with a decreased incidence of intrahepatic recurrence in the MWA group. This result is attributed to a variety of factors, which are associated with cancer disease, underlying liver disease, and indications of treatment. Patients were oft assigned to treatment based on tumor proximity to blood vessels or biliary tract. These tumors are characterized by increased incidence of local metastases, which in the majority of cases cannot be prevented with an effective ablation therapy. Furthermore, an underlying hepatic disease in patients with HCC or an advanced primary tumor in patients with hepatic metastases are predisposing factors for tumor recurrence, which cannot be eliminated with an ablation procedure.

The risk of complications was not significantly different between the groups and both procedures presented a limited number of adverse events. This finding is important since larger ablation zones, which are achieved through MWA, could be perceived to cause more perioperative complications and damage to liver function compared to RFA. This assumption was refuted with the results of our meta-analysis.

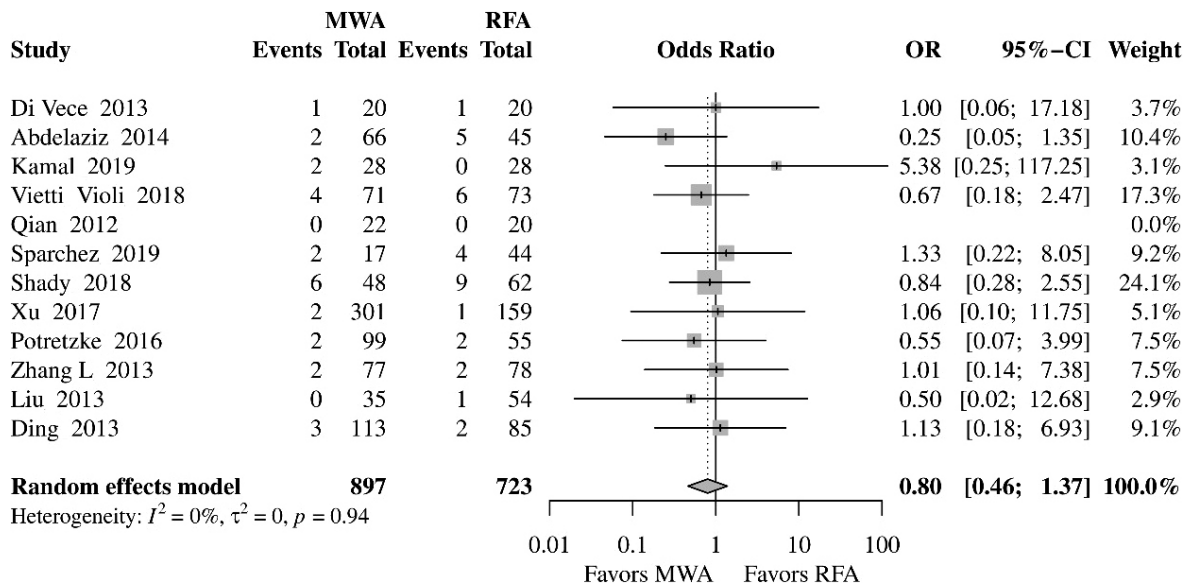


FIGURE 6. Forest plot of random-effects meta-analysis results for complication rates following RFA and MWA.

CI = confidence interval, MWA = microwave ablation, OR = odds ratio, RFA = radiofrequency ablation

CA and LTP were compared separately among patients with HCC and CRLM. As mentioned above, results derived from the two RCTs in HCC patients showed statistically decreased rates of LTP following MWA compared to RFA.<sup>15,16</sup> In the present meta-analysis, only three retrospective studies compared the two methods in patients with CRLM; consequently, reliable conclusions cannot be drawn, though results showed no significant difference.

In accordance with our results, previous studies reported similar rates of CA between RFA and MWA.<sup>4,31-34</sup> Glassberg *et al.* reported statistically decreased rates of LTP in the MWA group compared to RFA. Systematic reviews and meta-analyses conducted before 2015 reported comparable rates of LTP between RFA and MWA.<sup>31-34</sup> However, results were derived from studies that in many cases utilized first generation MWA devices. In our meta-analysis, studies published before 2010 were excluded to eliminate this factor. Since the majority of surveys in our analysis utilized new generation devices, which provide controlled and enhanced ablation, beneficial results of MWA over RFA can be attributed to this factor.

Subgroup analysis showed no difference between RFA and MWA for tumor size less or larger than 3 cm. Similar to our findings, Luo *et al.* concluded that CA and LTP were comparable between RFA and MWA in tumors with diameter larger than 3 cm.<sup>34</sup> In contrast to our results, Facciorusso *et al.* reported significantly decreased incidence of LTP

in the MWA group compared to RFA when meta-analysis was restricted to studies with high tumor burden.<sup>32</sup> However, the authors failed to define the size of lesions with high tumor burden. This subgroup analysis was performed without clear criteria and results should be evaluated with caution.

In contrast to our results, Glassberg *et al.* found that LTP in patients with tumor sizes > 2.5 cm was statistically reduced in MWA group compared to RFA.<sup>4</sup> However, authors did not report the studies that were included in this subgroup analysis. For that reason, level and quality of evidence cannot be assessed. At this point, we should mention that Glassberg *et al.* included observational studies with low quality, which were excluded from our meta-analysis, since were associated with high risk of confounding bias and insufficient comparison of baseline characteristics.<sup>35-40</sup> Furthermore, studies that compared RFA or MWA combined with TACE were included in the meta-analysis by Glassberg *et al.*, which could influence the results of the ablation methods.

Contrary to our findings, the meta-analysis conducted by Glassberg *et al.* reported that distant recurrence was significantly reduced by 15% with MWA compared to RFA when only RCTs were included in the subgroup meta-analysis.<sup>4</sup> These results were derived from the RCTs conducted by Abdelaziz *et al.* as well as by Yu *et al.*<sup>13,16</sup> The second RCT was assessed as high risk of bias in all domains during full-text screening in our study. Consequently, results from a high risk study can-

not be assessed as reliable and interpretation should be performed with caution.

The findings in the present meta-analysis should be interpreted in view of certain limitations. First, observational studies without randomization were included in the analysis, which is associated with potential confounding, selection, measurement, and reporting bias. In order to eliminate bias attributed to observational studies, only surveys with low or moderate overall risk of bias were included. Second, significant inter-study heterogeneity was observed for certain outcomes. In these cases, influence of retrospective studies on the results and sources of heterogeneity were examined with subgroup analysis of RCTs and retrospective studies separately. Third, different MWA and RFA devices were utilized across the surveys, which could influence the results of our analysis. Since various devices were used, a subgroup analysis based on the type of devices was not possible. Fourth, limited number of studies included patients with liver metastases or CRLM. Consequently, further RCTs are required to compare MWA with RFA in patients with hepatic metastases.

In addition, in the present study, the proved superiority of MWA over RFA in terms of LTP cannot be translated into better long-term oncological outcomes, since survival outcomes were not evaluated. Overall survival and disease-free survival were not included in our analysis, since limited data can be drawn from the available studies. The majority of surveys were retrospective in design and have included patients with no 100% matching in oncological characteristics. Furthermore, some patients underwent simultaneously surgical resection and ablation. Survival of these patients is multifactorial in etiology and causality. Regarding patients with liver metastases, neoadjuvant or adjuvant treatment and tumor stage were not 100% similar between the two groups. For that reason, survival after ablation is associated with several parameters, which could not be attributed only to the effectiveness of the ablative procedures. In fact, LTP and CA are generally considered the best indicators of treatment effectiveness for ablative methods rather than overall survival or disease-free survival.

The meta-analysis is strengthened by its broad inclusion of 15 studies with a total of 2,169 patients. In contrast to other meta-analyses, low quality studies were excluded. Consequently, results were derived from high or moderate quality studies. Taking into consideration the results of the present meta-analysis, we suggest that MWA should be the ablation method of choice in the treatment of HCC.

Finally, since the majority of studies included patients with HCC, further RCTs are required to evaluate the role of ablation treatments in patients with liver metastases.

## References

1. European Association for the Study of the Liver. Electronic address: easloffice@easloffice.eu; European Association for the Study of the Liver. EASL Clinical Practice Guidelines: management of hepatocellular carcinoma. *J Hepatol* 2018; **69**: 182-236. doi: 10.1016/j.jhep.2018.03.019
2. Marrero JA, Kulik LM, Sirlin CB, Zhu AX, Finn RS, Abecassis MM, et al. Diagnosis, staging, and management of hepatocellular carcinoma: 2018 Practice Guidance by the American Association for the Study of Liver Diseases. *Hepatology* 2018; **68**: 723-50. doi: 10.1002/hep.29913
3. Weis S, Franke A, Mössner J, Jakobsen JC, Schoppmeyer K. Radiofrequency (thermal) ablation versus no intervention or other interventions for hepatocellular carcinoma. *Cochrane Database Syst Rev* 2013; **12**: Cd003046. doi: 10.1002/14651858.CD003046.pub3
4. Glassberg MB, Ghosh S, Clymer JW, Wright GWJ, Ferko N, Amaral JF. Microwave ablation compared with hepatic resection for the treatment of hepatocellular carcinoma and liver metastases: a systematic review and meta-analysis. *World J Surg Oncol* 2019; **17**: 98. doi: 10.1186/s12957-019-1632-6
5. Zhou J, Sun HC, Wang Z, Cong WM, Wang JH, Zeng MS, et al. Guidelines for diagnosis and treatment of primary liver cancer in China (2017 Edition). *Liver Cancer* 2018; **7**: 235-60. doi: 10.1159/000488035
6. Moher D, Liberati A, Tetzlaff J, Altman DG, Group PRISMA. Preferred reporting items for systematic reviews and meta-analyses: the PRISMA statement. *PLoS Med* 2009; **6**: e1000097. doi: 10.1371/journal.pmed.1000097
7. Sterne JA, Hernan MA, Reeves BC, Savovic J, Berkman ND, Viswanathan M, et al. ROBINS-I: a tool for assessing risk of bias in non-randomised studies of interventions. *BMJ* 2016; **355**: i4919. doi: 10.1136/bmj.i4919
8. DerSimonian R, Laird N. Meta-analysis in clinical trials revisited. *Contemp Clin Trials* 2015; **45**: 139-45. doi: 10.1016/j.cct.2015.09.002
9. Robins J, Breslow N, Greenland S. Estimators of the Mantel-Haenszel variance consistent in both sparse data and large-strata limiting models. *Biometrics* 1986; **42**: 311-23. PMID: 3741973
10. Cochran WG. The combination of estimates from different experiments. *Biometrics* 1954; **10**: 101-29. doi: 10.2307/3001666
11. Egger M, Davey Smith G, Schneider M, Minder C. Bias in meta-analysis detected by a simple, graphical test. *BMJ* 1997; **315**: 629-34. doi: 10.1136/bmj.315.7109.629
12. Balduzzi S, Rucker G, Schwarzer G. How to perform a meta-analysis with R: a practical tutorial. *Evid Based Ment Health* 2019; **22**: 153-60. doi: 10.1136/ebmental-2019-300117
13. Yu J, Yu XL, Han ZY, Cheng ZG, Liu FY, Zhai HY, et al. Percutaneous cooled-probe microwave versus radiofrequency ablation in early-stage hepatocellular carcinoma: a phase III randomised controlled trial. *Gut* 2017; **66**: 1172-3. doi: 10.1136/gutjnl-2016-312629
14. Kamal A, Elmoety AAA, Rostom YAM, Shater MS, Lashen SA. Percutaneous radiofrequency versus microwave ablation for management of hepatocellular carcinoma: a randomized controlled trial. *J Gastrointest Oncol* 2019; **10**: 562-71. doi: 10.21037/jgo.2019.01.34
15. Vietti Violi N, Duran R, Guiu B, Cercueil JP, Aubé C, Digkila A, et al. Efficacy of microwave ablation versus radiofrequency ablation for the treatment of hepatocellular carcinoma in patients with chronic liver disease: a randomised controlled phase 2 trial. *Lancet Gastroenterol Hepatol* 2018; **3**: 317-25. doi: 10.1016/S2468-1253(18)30029-3
16. Abdelaziz A, Elbaz T, Shousha HI, Mahmoud S, Ibrahim M, Abdelmaksoud A, et al. Efficacy and survival analysis of percutaneous radiofrequency versus microwave ablation for hepatocellular carcinoma: an Egyptian multidisciplinary clinic experience. *Surg Endosc* 2014; **28**: 3429-34. doi: 10.1007/s00464-014-3617-4

17. Di Vece F, Tombesi P, Ermili F, Maraldi C, Sartori S. Coagulation areas produced by cool-tip radiofrequency ablation and microwave ablation using a device to decrease back-heating effects: a prospective pilot study. *Cardiovasc Intervent Radiol* 2014; **37**: 723-9. doi: 10.1007/s00270-013-0733-9
18. Qian GJ, Wang N, Shen Q, Sheng YH, Zhao JQ, Kuang M, et al. Efficacy of microwave versus radiofrequency ablation for treatment of small hepatocellular carcinoma: experimental and clinical studies. *Eur Radiol* 2012; **22**: 1983-90. doi: 10.1007/s00330-012-2442-1
19. Sparchez Z, Mocan T, Hajjar NA, Bartos A, Hagiuc C, Matei D, et al. Percutaneous ultrasound guided radiofrequency and microwave ablation in the treatment of hepatic metastases. A monocentric initial experience. *Med Ultrason* 2019; **21**: 217-24. doi: 10.11152/mu-1957
20. Takahashi H, Kahramangil B, Kose E, Berber E. A comparison of microwave thermosphere versus radiofrequency thermal ablation in the treatment of colorectal liver metastases. *HPB (Oxford)* 2018; **20**: 1157-62. doi: 10.1016/j.hpb.2018.05.012
21. Shady W, Petre EN, Do KG, Gonen M, Yarmohammadi H, Brown KT, et al. Percutaneous microwave versus radiofrequency ablation of colorectal liver metastases: ablation with clear margins (A0) provides the best local tumor control. *J Vasc Interv Radiol* 2018; **29**: 268-75.e1. doi: 10.1016/j.jvir.2017.08.021
22. Xu Y, Shen Q, Wang N, Wu PP, Huang B, Kuang M, et al. Microwave ablation is as effective as radiofrequency ablation for very-early-stage hepatocellular carcinoma. *Chin J Cancer* 2017; **36**: 14. doi: 10.1186/s40880-017-0183-x
23. van Tilborg AA, Scheffer HJ, de Jong MC, Vroomen LG, Nielsen K, van Kuijk C, et al. MWA versus RFA for perivascular and peribiliary CRLM: a retrospective patient- and lesion-based analysis of two historical cohorts. *Cardiovasc Intervent Radiol* 2016; **39**: 1438-46. doi: 10.1007/s00270-016-1413-3
24. Potretzke TA, Ziemlewicz TJ, Hinshaw JL, Lubner MG, Wells SA, Brace CL, et al. Microwave versus radiofrequency ablation treatment for hepatocellular carcinoma: A comparison of efficacy at a single center. *J Vasc Interv Radiol* 2016; **27**: 631-8. doi: 10.1016/j.jvir.2016.01.136
25. Zhang XG, Zhang ZL, Hu SY, Wang YL. Ultrasound-guided ablative therapy for hepatic malignancies: a comparison of the therapeutic effects of microwave and radiofrequency ablation. *Acta Chir Belg* 2014; **114**: 40-5. PMID: 24720137
26. Zhang L, Wang N, Shen Q, Cheng W, Qian GJ. Therapeutic efficacy of percutaneous radiofrequency ablation versus microwave ablation for hepatocellular carcinoma. *PLoS One* 2013; **8**: e76119. doi: 10.1371/journal.pone.0076119
27. Liu Y, Li S, Wan X, Li Y, Li B, Zhang Y, et al. Efficacy and safety of thermal ablation in patients with liver metastases. *Eur J Gastroenterol Hepatol* 2013; **25**: 442-6. doi: 10.1097/MEG.0b013e32835cb566
28. Ding J, Jing X, Liu J, Wang Y, Wang F, Wang Y, et al. Comparison of two different thermal techniques for the treatment of hepatocellular carcinoma. *Eur J Radiol* 2013; **82**: 1379-84. doi: 10.1016/j.ejrad.2013.04.025
29. Farina L, Weiss N, Nissenbaum Y, Cavagnaro M, Lopresto V, Pinto R, et al. Characterisation of tissue shrinkage during microwave thermal ablation. *Int J Hyperthermia* 2014; **30**: 419-28. doi: 10.3109/02656736.2014.957250
30. Vogel A, Cervantes A, Chau I, Daniele B, Llovet JM, Meyer T, et al. Hepatocellular carcinoma: ESMO Clinical Practice Guidelines for diagnosis, treatment and follow-up. *Ann Oncol* 2018; **29** (Suppl 4): iv238-iv55. doi: 10.1093/annonc/mdy510
31. Chinnaratha MA, Chuang MY, Fraser RJ, Woodman RJ, Wigg AJ. Percutaneous thermal ablation for primary hepatocellular carcinoma: a systematic review and meta-analysis. *J Gastroenterol Hepatol* 2016; **31**: 294-301. doi: 10.1111/jgh.13028
32. Facciorusso A, Di Maso M, Muscatiello N. Microwave ablation versus radiofrequency ablation for the treatment of hepatocellular carcinoma: a systematic review and meta-analysis. *Int J Hyperthermia* 2016; **32**: 339-44. doi: 10.3109/02656736.2015.1127434
33. Huo YR, Eslick GD. Microwave ablation compared to radiofrequency ablation for hepatic lesions: a meta-analysis. *J Vasc Interv Radiol* 2015; **26**: 1139-46 e2. doi: 10.1016/j.jvir.2015.04.004
34. Luo W, Zhang Y, He G, Yu M, Zheng M, Liu L, et al. Effects of radiofrequency ablation versus other ablating techniques on hepatocellular carcinomas: a systematic review and meta-analysis. *World J Surg Oncol* 2017; **15**: 126. doi: 10.1186/s12957-017-1196-2
35. Hompes R, Fieuws S, Aerts R, Thijs M, Penninckx F, Topal B. Results of single-probe microwave ablation of metastatic liver cancer. *Eur J Surg Oncol* 2010; **36**: 725-30. doi: 10.1016/j.ejso.2010.05.013
36. Kuang M, Xie XY, Huang C, Wang Y, Lin MX, Xu ZF, et al. Long-term outcome of percutaneous ablation in very early-stage hepatocellular carcinoma. *J Gastrointest Surg* 2011; **15**: 2165-71. doi: 10.1007/s11605-011-1716-2
37. Lee KF, Wong J, Hui JW, Cheung YS, Chong CC, Fong AK, et al. Long-term outcomes of microwave versus radiofrequency ablation for hepatocellular carcinoma by surgical approach: a retrospective comparative study. *Asian J Surg* 2017; **40**: 301-8. doi: 10.1016/j.asjsur.2016.01.001
38. Simo KA, Sereika SE, Newton KN, Gerber DA. Laparoscopic-assisted microwave ablation for hepatocellular carcinoma: safety and efficacy in comparison with radiofrequency ablation. *J Surg Oncol* 2011; **104**: 822-9. doi: 10.1002/jso.21933
39. Vogl TJ, Farshid P, Naguib NN, Zangos S, Bodelle B, Paul J, et al. Ablation therapy of hepatocellular carcinoma: a comparative study between radiofrequency and microwave ablation. *Abdom Imaging* 2015; **40**: 1829-37. doi: 10.1007/s00261-015-0355-6
40. Yang B, Li Y. A comparative study of laparoscopic microwave ablation with laparoscopic radiofrequency ablation for colorectal liver metastasis. *J BUON* 2017; **22**: 667-72. PMID: 28730772

research article

# Can dynamic imaging, using <sup>18</sup>F-FDG PET/CT and CT perfusion differentiate between benign and malignant pulmonary nodules?

Aleksander Marin<sup>1,2</sup>, John T. Murchison<sup>3</sup>, Kristopher M. Skwarski<sup>4</sup>, Adriana A.S. Tavares<sup>1</sup>, Alison Fletcher<sup>1</sup>, William A. Wallace<sup>5</sup>, Vladka Salapura<sup>2</sup>, Edwin J.R. van Beek<sup>1</sup>, Saeed Mirsadraee<sup>1,6</sup>

<sup>1</sup> Edinburgh Imaging facility Queens Medical Research Institute, University of Edinburgh, Edinburgh, United Kingdom

<sup>2</sup> Faculty of Medicine, University of Ljubljana, Ljubljana, Slovenia

<sup>3</sup> Department of Radiology, Royal Infirmary of Edinburgh, Edinburgh, United Kingdom

<sup>4</sup> Department of Respiratory Medicine, Royal Infirmary of Edinburgh, Edinburgh, United Kingdom

<sup>5</sup> Department of Pathology, Royal Infirmary of Edinburgh, Edinburgh, United Kingdom

<sup>6</sup> National Heart and Lung Institute, Imperial College London, London, United Kingdom

Radiol Oncol 2021; 55(3): 259-267.

Received 26 March 2021

Accepted 24 April 2021

Correspondence to: Aleksander Marin, M.D., Radiology Department, University Hospital Llandough, Penlan Road, Penarth CF64 2XX, United Kingdom. E-mail: aleksander.marin@wales.nhs.uk

Disclosure: No potential conflicts of interest were disclosed.

This is an open access article under the CC BY-NC-ND license (<http://creativecommons.org/licenses/by-nc-nd/4.0/>).

**Background.** The aim of the study was to derive and compare metabolic parameters relating to benign and malignant pulmonary nodules using dynamic 2-deoxy-2-[fluorine-18]fluoro-D-glucose (<sup>18</sup>F-FDG) PET/CT, and nodule perfusion parameters derived through perfusion computed tomography (CT).

**Patients and methods.** Twenty patients with 21 pulmonary nodules incidentally detected on CT underwent a dynamic <sup>18</sup>F-FDG PET/CT and a perfusion CT. The maximum standardized uptake value (SUV<sub>max</sub>) was measured on conventional <sup>18</sup>F-FDG PET/CT images. The influx constant (K<sub>i</sub>) was calculated from the dynamic <sup>18</sup>F-FDG PET/CT data using Patlak model. Arterial flow (AF) using the maximum slope model and blood volume (BV) using the Patlak plot method for each nodule were calculated from the perfusion CT data. All nodules were characterized as malignant or benign based on histopathology or 2 year follow up CT. All parameters were statistically compared between the two groups using the nonparametric Mann-Whitney test.

**Results.** Twelve malignant and 9 benign lung nodules were analysed (median size 20.1 mm, 9–29 mm) in 21 patients (male/female = 11/9; mean age ± SD: 65.3 ± 7.4; age range: 50–76 years). The average SUV<sub>max</sub> values ± SD of the benign and malignant nodules were 2.2 ± 1.7 vs. 7.0 ± 4.5, respectively (p = 0.0148). Average K<sub>i</sub> values in benign and malignant nodules were 0.0057 ± 0.0071 and 0.0230 ± 0.0155 min<sup>-1</sup>, respectively (p = 0.0311). Average BV for the benign and malignant nodules were 11.6857 ± 6.7347 and 28.3400 ± 15.9672 ml/100 ml, respectively (p = 0.0250). Average AF for the benign and malignant nodules were 74.4571 ± 89.0321 and 89.200 ± 49.8883 ml/100g/min, respectively (p = 0.1613).

**Conclusions.** Dynamic <sup>18</sup>F-FDG PET/CT and perfusion CT derived blood volume had similar capability to differentiate benign from malignant lung nodules.

Key words: pulmonary nodule, perfusion, CT, dynamic, PET/CT

## Introduction

Pulmonary nodules are detected with increasing frequency due to widespread use of computed to-

mography (CT).<sup>1,2</sup> The prevalence of incidental pulmonary nodules on standard CT studies is around 13%, while lung cancer screening will detect lung nodules in up to 53% of subjects, leading to a lung

cancer prevalence of around 1.4% (0.5–2.7%).<sup>3</sup> The optimal diagnostic approach for the management of indeterminate pulmonary nodules has been the subject of much discussion.<sup>4</sup>

The widely accepted guidelines published by the British Thoracic Society (BTS) and the Fleischner Society recommend the minimum nodule diameter thresholds and CT follow-up time intervals for surveillance of solitary nodules smaller than 8 mm.<sup>3,5</sup> For nodules of  $\geq 8$  mm (300 mm<sup>3</sup>), the BTS guidelines recommend risk assessment using the Brock model. The above guidelines recommend either 3-month CT follow-up, work-up with positron emission tomography (PET) with 2-deoxy-2-[fluorine-18]fluoro-D-glucose (<sup>18</sup>F-FDG), tissue sampling, or resection for nodules of  $\geq 8$  mm. CT characterisation using only morphological features is imprecise<sup>6,7</sup>, leading to an increased interest in computer-based radiomics assessment.<sup>8–15</sup> Serial CT imaging to monitor nodule size can be problematic as nodule growth varies with different cancers and causes patient anxiety.<sup>16–18</sup> <sup>18</sup>F-FDG PET has high sensitivity but lower specificity of 82% for detecting malignant pulmonary nodules, particularly in those smaller than 10 mm.<sup>19</sup> Imaging guided sampling of small nodules is also difficult, is associated with complications, and its diagnostic yield decreases further as nodule size decreases.<sup>3,20,21</sup>

Neovascularisation is a complex process known to be central to carcinogenesis.<sup>22</sup> Advances in the imaging technology in the last two decades have enabled the study of perfusion characteristics within pulmonary nodules.<sup>23–27</sup> As benign and malignant lesions have different vascularity, different perfusion parameters and dynamic <sup>18</sup>F-FDG uptake properties can be expected.<sup>27–32</sup>

The purpose of this pilot study was to evaluate the feasibility and accuracy of CT perfusion and dynamic <sup>18</sup>F-FDG PET imaging in differentiating proven benign and malignant pulmonary nodules.

## Patients and methods

This single-centre prospective study was approved by the local Research Ethics Committee (13/SS/0153) and written informed consent was obtained from all participants.

Between December 2014 and December 2015, 20 consecutive patients who were referred to our respiratory outpatient clinic for an indeterminate incidental pulmonary nodule were recruited. The inclusion criteria were: a) incidentally detected soft tissue (solid) pulmonary nodules measuring  $\geq 8$

mm and  $< 30$  mm on CT, b) either surgical excision, imaging guided biopsy or imaging follow up of the nodule planned. The exclusion criteria were: a) abnormal renal function, b) previous adverse reaction to iodinated contrast agent, c) known history of malignancy, d) pregnancy or breast feeding, e) patients who refused or were unable to provide informed consent.

The patients underwent a dynamic <sup>18</sup>F-FDG PET/CT and dynamic perfusion CT imaging within a 3 week time frame (mean, 6.4 days: range 1–18 days). Due to technical reasons, the dynamic PET data could not be used in 4 patients for the analysis, one of these patients had two synchronous nodules. CT perfusion analysis was performed in 17 of the nodules. One patient declined the CT perfusion scan and 3 patients had significant breathing artefact on the scans, rendering analysis non-feasible. All nodules were classified into either benign or malignant on the basis of a histopathological diagnosis (n = 16), or stability during 2 years follow up CT imaging (n = 5).

## Dynamic PET/CT image acquisition

All patients were fasted for at least six hours before the imaging. Following a low dose CT scan for attenuation correction and localisation (120 kV, 50 mAs, 5/3 mm), patients were administered 400 MBq of <sup>18</sup>F-FDG intravenously, and a dynamic 60 minute image acquisition was performed using a Siemens Biograph PET/CT scanner (Siemens Healthcare, Erlangen, Germany). Respiratory-gated PET data were reconstructed using a 15-frame protocol (7 frames $\times$ 180 s, 7 $\times$ 300 s, 1 $\times$ 240 s), a matrix size of 256 $\times$ 256 $\times$ 53 with a voxel size of 2.65 $\times$ 2.65 $\times$ 3.00 mm<sup>3</sup>, and subsets expectation maximization (OSEM) method. A conventional PET/CT scan was performed on completion of the dynamic phase of the scan at 1 hour after injection of the tracer.

## Perfusion volume CT acquisition

Dynamic perfusion CT scans were performed as previously described<sup>25,28,33,34</sup> on a 320-detector row CT scanner (Aquilion ONE; Toshiba Medical Systems, Tokyo, Japan) with 16 cm field of view coverage. Imaging was performed at 0, 2, 4, 6, 8, 10, 12, 14, 16, 18, 20, 24, 30, 40, 50, 60, 90, 120 seconds, 3 minutes, 4 minutes, and 10 minutes following the intravenous injection of 70 ml of iodinated contrast (Iomeron 400 mg/ml, Bracco, Milan, Italy) followed by a 30 ml bolus of saline both at 9 ml/s through a 16 G cannula sited in the ante cubital fos-

sa. Acquisition parameters were 100 kV, 100 mA, 0.5 seconds rotation time, 320 x 0.5 mm collimation, 512 x 512 matrix.

## Image analysis

### Dynamic PET/CT

Reconstructed images were imported into PMOD 3.409 software (PMOD Technologies, Zurich, Switzerland) and the input function was determined by placing a spherical volume of interest (VOI) with diameter of 1 cm in the ascending aorta. VOIs were drawn around the pulmonary nodules semi-automatically with a threshold of 50% of the maximum voxel value within the nodule, and then the VOIs were copied to the dynamic imaging sequence to obtain the time activity curves (TACs) (Figure 1). The influx constant  $K_i$  ( $\text{min}^{-1}$  or  $(\text{ml plasma}) \cdot (\text{ml tissue})^{-1} \cdot \text{min}^{-1}$ ) was determined by Patlak analysis.<sup>35</sup> The Patlak plot model is a graphical analysis technique based on a 2-tissue compartment model with irreversibly trapped tracer. A mathematical transformation of the tissue compartment and plasma TACs produces a straight line plot which provides information about the blood volume (BV) of the tissue compartment and the exchange rate ( $K_i$ ) (Figure 2).

### Conventional PET/CT scan

The maximum standardised uptake value ( $\text{SUV}_{\text{max}}$ ) was measured for each nodule on conventional FDG PET/CT images. For the semi-quantitative analysis, the mean standardised uptake values ( $\text{SUV}_{\text{mean}}$ ) were measured of the ascending aorta at the level of the arch, and within the right lobe of the liver. SUV ratios (SUR) were calculated between the nodule  $\text{SUV}_{\text{max}}$  and the  $\text{SUV}_{\text{mean}}$  of the mediastinal blood pool ( $\text{SUR}_{\text{BLOOD}}$ ) and liver ( $\text{SUR}_{\text{LIVER}}$ ). Criteria for malignancy were specified as  $\text{SUV}_{\text{max}} \geq 2.5$ ;  $\text{SUR}_{\text{BLOOD}} \geq 1.56$ ;  $\text{SUR}_{\text{LIVER}} \geq 1.12$ . Qualitative assessment PET features were specified as following: 0 = no visible uptake; 1 = uptake less than mediastinal blood pool; 2 = uptake comparable to mediastinal blood pool; 3 = uptake greater than mediastinal blood pool; 4 = distant metastases. Qualitative specified criteria for malignancy was PET grade  $\geq 3$ .<sup>36,37</sup> VOIs were placed over the nodules, the ascending aorta at the level of the arch, and within the right lobe of the liver for determination of the  $\text{SUV}_{\text{mean}}$  and  $\text{SUV}_{\text{max}}$  values using OsiriX software (OsiriX, version 8.0.1 64 bit; OsiriX Imaging Software, Geneva, Switzerland).

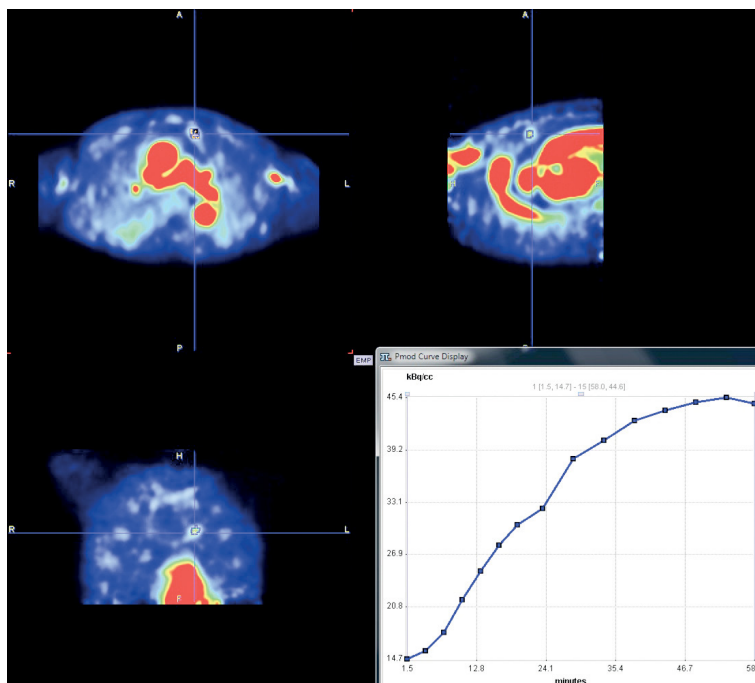


**FIGURE 1.** Dynamic PET images of a small pulmonary nodule in the left upper lobe and corresponding time activity curve (TAC) of the nodule displayed by PMOD 3.409 software.

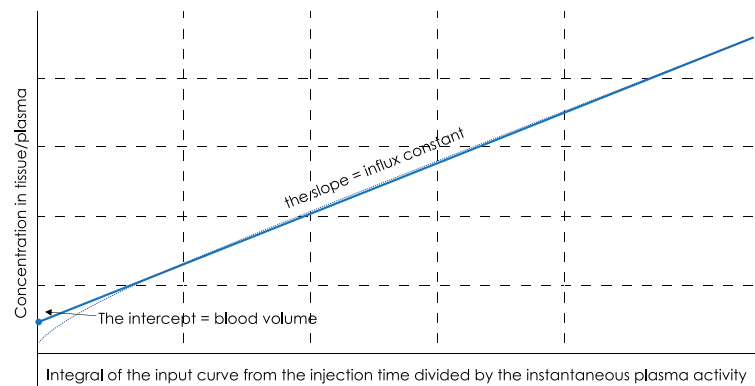


**FIGURE 2.** Patlak plot derived from the tissue time activity curve (TAC) and the input function (plasma TAC). The Patlak plot becomes linear after the tracer concentrations in reversible compartments and in plasma are in steady state.

### Perfusion CT

Perfusion analysis was performed using Body Perfusion Application on a Vitrea Workstation (Vitrea fx 6.0; Vital Images, Minnetonka, MN, USA). Regions of interest (ROIs) were placed over the pulmonary nodules and contralateral lung parenchyma (diameter range, 7–29 mm) on all perfusion CT images. Arterial input was determined by placing 1 cm ROI over the main pulmonary

**TABLE 1.** The demographic data, average nodule size, standardized uptake value ( $SUV_{max}$ ), metabolic parameter relating to the pulmonary nodules through dynamic  $^{18}F$ -FDG PET/CT, and perfusion parameters through perfusion CT for the benign and malignant nodules

	Benign Nodules	Malignant Nodules	p value
Total Number of nodules	9	12	
Number of male patients (%)	5/9 (55 %)	6/12 (50 %)	
Average patient age (years $\pm$ SD)	63 $\pm$ 7.5	68 $\pm$ 6.7	
Average nodule size, range (mm)	18, 9–29	22, 12–30	
Average $SUV_{max}$ $^{18}F$ -FDG PET/CT $\pm$ SD	2.2 $\pm$ 1.7	7.0 $\pm$ 4.5	0.0148
Number of nodules analysed for dynamic $^{18}F$ -FDG PET/CT	7	9	
Average $K_i$ $\pm$ SD ( $min^{-1}$ )	0.0057 $\pm$ 0.0071	0.0230 $\pm$ 0.0155	0.0311
Number of nodules analysed for perfusion CT parameters	7	10	
Average BV $\pm$ SD (Patlak, ml/100ml)	11.6857 $\pm$ 6.7347	28.3400 $\pm$ 15.9672	0.0250
Average AF $\pm$ SD (ml/100g/min)	74.4571 $\pm$ 89.0321	89.2000 $\pm$ 49.8883	0.1613

AF = Arterial flow; BV = blood volume;  $K_i$  = influx constant; SD = standard deviation; SUV = standardized uptake value

artery. Time-density graphs were then reviewed and adjustments to start point and end point of the maximum slope were made if needed to define the optimal slope range. Arterial flow perfusion maps overlaying CT images were visually analysed and ROIs were placed over the nodules to obtain the equivalent blood volume parameter calculated by Patlak plot model (BV, expressed in ml per 100 ml) and Arterial Flow (AF, expressed in ml per 100g per minute) using single-input maximum slope model for calculation.

### Statistical analysis

All results were expressed as mean  $\pm$  standard deviation (SD) unless indicated.  $K_i$  and perfusion indices BV and AF of benign and malignant nodules were statistically compared using the nonparametric Mann-Whitney U test. The accuracy of the different techniques and parameters was tested with area under the curve (AUC) in receiver operating characteristic (ROC) analysis with 95% confidence interval (CI). Comparison between the ROCs was performed using DeLong's test. Youdin index analysis was used to derive the optimised cut-point values. Mann-Whitney U test and ROC curve analyses were performed on GraphPad Prism version 8.2.1 for Windows (GraphPad Software, San Diego, CA, USA). Youdin index analysis and nonparametric DeLong's test were performed on MedCalc Statistical Software version 19.8 (MedCalc Software Ltd, Ostend, Belgium; <https://www.medcalc.org/>;

2021). A p value  $<$  0.05 was considered statistically significant.

## Results

The demographic data, average nodule size,  $SUV_{max}$ , metabolic parameter relating to the pulmonary nodules through dynamic  $^{18}F$ -FDG PET/CT, and perfusion parameters through perfusion CT for the benign and malignant nodules are summarised in Table 1 and Figure 3. We analysed 21 soft tissue nodules in 20 patients (male/female = 11/9; mean age  $\pm$  SD: 65.3  $\pm$  7.4; age range: 50–76 years) with mean nodule diameter  $\pm$  SD of 20.1  $\pm$  7.5 mm (9–29 mm); mean nodule volume  $\pm$  SD: 2849  $\pm$  2338.7 mm<sup>3</sup> (247–9348 mm<sup>3</sup>). 52% of the nodules were located in the upper lung lobes (right upper lobe 7/21, left upper lobe 4/21), 48% were in middle and lower lung lobes (right middle lobe 2/21, right lower lobe 6/21 and left lower lobe 2/21). Final diagnosis was determined after surgical resection in 10 patients, core CT guided biopsy or bronchoscopy in 6 patients, and over 2 years stability on follow up CT imaging in 5 patients.

As shown in Table 1 and Figure 3,  $SUV_{max}$  derived from the conventional  $^{18}F$ -FDG PET/CT and  $K_i$  derived from dynamic  $^{18}F$ -FDG PET/CT were significantly higher in malignant nodules than in benign nodules. Also, the Patlak model derived BV on perfusion CT was significantly higher in malignant nodules. The difference in AF between

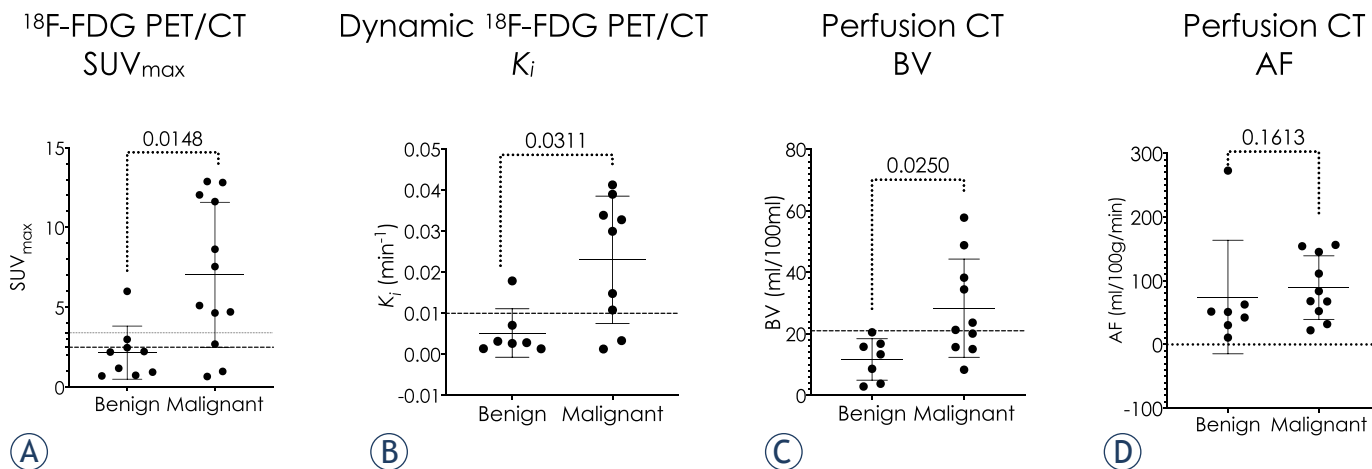


**FIGURE 3.** (A) standardized uptake value ( $SUV_{max}$ ), (B) Dynamic  $^{18}F$ -FDG PET/CT influx constant ( $K_i$ ), (C) Perfusion CT parameters blood volume (BV) and (D) Average arterial flow (AF) of the benign and malignant nodules.

the benign nodules and malignant nodules was not statistically significant.

The benign outlier on  $^{18}F$ -FDG PET/CT ( $SUV_{max} = 6.3$ ) and dynamic  $^{18}F$ -FDG PET/CT ( $K_i = 0.0179 \text{ min}^{-1}$ ) was an 18 mm nodule of inflammation and fibrosis (Figure 3A and B). The perfusion CT indices BV and AF in this nodule were relatively low, 3.8 ml/100ml and 51.5 ml/100g/min, respectively (Figure 3C and D). The two malignant outliers on conventional  $^{18}F$ -FDG PET/CT and dynamic  $^{18}F$ -FDG PET/CT were 12 mm and 16 mm mucinous adenocarcinomas *in situ* (12 mm nodule with  $SUV_{max} = 0.7$  and  $K_i = 0.0015 \text{ min}^{-1}$  (BV and AF analysis non-feasible due to respiratory motion artefact); 16 mm nodule with  $SUV_{max} = 1.0$ ,  $K_i = 0.0033$

$\text{min}^{-1}$ , BV = 48.8 ml/100ml and AF = 154.1 ml/100g/min) (Figure 3A and B). The mean CT densities of these two nodules on unenhanced CT images were 16.3HU and 15.9HU, while the mean density  $\pm$  SD of all benign and malignant nodules analysed was  $24.55 \pm 12.01$  HU. The benign outlier in AF on perfusion CT was a 10 mm perivascular epithelioid cell tumour (PEComa), AF = 272.7 ml/100g/min (Figure 3D). The BV in this nodule was 20.5 ml/100ml, the  $^{18}F$ -FDG PET/CT indices were low,  $SUV_{max} = 0.7$  and the  $K_i = 0.001 \text{ min}^{-1}$ .

Table 2 and Figure 4A show diagnostic accuracy of conventional PET/CT derived parameters with pre-specified and derived cut-point values though ROC analysis.<sup>36,37</sup>  $SUR_{BLOOD}$  parameter had overall

**TABLE 2.** Comparison of the diagnostic accuracy of different techniques and parameters with pre-specified and derived cut-point values for malignancy

Parameter	Cut-point value/grade		Sensitivity (95% CI)	Specificity (95% CI)	Accuracy	
$SUV_{max}$	Pre-specified	$\geq 2.5^*$	75.0% (46.8 to 91.1%)	66.7% (35.4 to 87.9%)	71.4%	
	Derived	$\geq 3.4$	75.0% (46.8 to 91.1%)	88.9% (56.5 to 99.43%)	81.0%	
$SUR_{BLOOD}$	Pre-specified	$\geq 1.56$	83.3% (55.2 to 97.0%)	88.9% (56.5 to 99.4%)	85.7%	
	Derived					
$SUR_{LIVER}$	Pre-specified	$\geq 1.12$	83.3% (55.2 to 97.0%)	66.7% (35.4 to 87.9%)	76.2%	
	Derived	$\geq 1.65$	75% (46.8 to 91.1%)	88.9% (56.5 to 99.4%)	81.0%	
SUV grade	Pre-specified & Derived		$\geq 3$	66.7% (39.0 to 86.2%)	77.8% (45.3 to 96.0%)	71.4%
$K_i$	Derived	$\geq 0.01 \text{ min}^{-1}$	77.8% (45.2 to 96.0%)	85.7% (48.7 to 99.3%)	81.3%	
BV	Derived	$\geq 21 \text{ ml/100ml}$	70% (39.7 to 89.2%)	100% (64.6 to 100%)	82.4%	
AF	Derived	$\geq 65 \text{ ml/100g/min}$	70% (39.7 to 89.2%)	85.7% (48.7 to 99.3%)	76.5%	

\* = adding cut-points standardized uptake value ( $SUV_{max}$ )  $\geq 1.75$  and  $\geq 3.6$  for nodules < 12 mm and > 16 mm, respectively,<sup>37</sup> resulted in sensitivity, specificity and accuracy of 72.7%, 70.0% and 71.4%, respectively;

AF = Arterial flow; BV = blood volume; CI = confidence interval;  $K_i$  = influx constant; SUR = SUV ratios; SUV = standardized uptake value

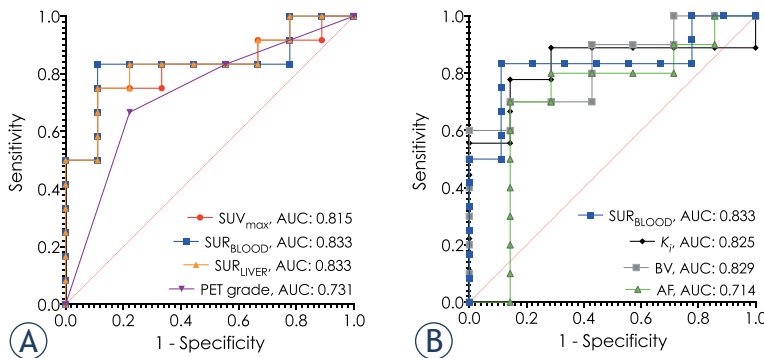


**FIGURE 4.** Comparison of AUCs on ROC curves (A)  $SUV_{max}$ ,  $SUR_{BLOOD}$ ,  $SUR_{LIVER}$ , PET grade and (B)  $SUR_{LIVER}$ ,  $K_i$ , BV and AF.

95% CI, p values for  $SUV_{max}$  /  $SUR_{BLOOD}$  /  $SUR_{LIVER}$  / PET grade /  $K_i$  / BV / AF: 0.6264 to 1.000, 0.0157/ 0.6486 to 1.000, 0.0105/ 0.6550 to 1.000, 0.0105/ 0.507 to 0.956, 0.0756/ 0.602 to 1.000, 0.0300/ 0.6322 to 1.000, 0.0248/ 0.4342 to 0.9944, 0.1432.

highest accuracy, however, pairwise comparison of AUCs showed no significant difference ( $p = 0.5308$  vs.  $SUV_{max}$ ;  $p = 1.0000$  vs.  $SUR_{LIVER}$ ;  $p = 0.1083$  vs. PET grade). ROC analysis and diagnostic accuracy for the diagnosis of malignancy by dynamic  $^{18}F$ -FDG PET/CT parameter  $K_i$  and perfusion CT indices BV and AF compared to  $SUR_{BLOOD}$  are further detailed in Table 2 and Figure 4B. Pairwise comparison of AUCs of  $SUR_{BLOOD}$ ,  $K_i$ , BV and AF showed no significant difference in their diagnostic performances ( $p > 0.1$  for all comparisons).

## Discussion

Our results demonstrate that the metabolic parameter  $K_i$  of dynamic  $^{18}F$ -FDG PET/CT and the BV parameter of perfusion CT are significantly lower in benign nodules.

Our study showed that the diagnostic accuracy of the conventional  $^{18}F$ -FDG PET/CT was best when semi-quantitative assessment and measuring the uptake ratio of the lung nodule to the mediastinal blood pool with cut-point criteria for malignancy  $SUR_{BLOOD} \geq 1.56$  was used. This has been confirmed in a larger multicenter trial by Evangelista *et al.*<sup>36</sup> Different to the SPUTNIK trial which has shown  $SUV_{max}$  to be the most accurate and reproducible technique with a caveat of introducing additional cut-point values altered according to the nodule size, we did not see significant improvement in diagnostic accuracy when replicating the multiple cut-points in our group of nodules (see \* in Table 2).<sup>37</sup>

The accuracies of the new metabolic parameter  $K_i$  and perfusion parameter BV were not signifi-

cantly different to the conventional  $^{18}F$ -FDG PET/CT. The derived  $K_i$  cut-point for malignancy was  $\geq 0.01 \text{ min}^{-1}$  resulting in sensitivity/specificity/accuracy of 77.8%/85.7%/81.3%, respectively. This is in good agreement with  $K_i$  cut-point  $\geq 0.014 \text{ min}^{-1}$  reported in the study by Huang *et al.* ( $n = 35$ ).<sup>26</sup> The derived BV cut-point value of  $\geq 21 \text{ ml/100ml}$  for malignancy showed comparable diagnostic accuracy to conventional and dynamic  $^{18}F$ -FDG PET/CT parameters. The high specificity of BV demonstrated in our nodules would need to be confirmed in larger studies.

The benign outlier on dynamic  $^{18}F$ -FDG PET/CT with a high  $K_i$  parameter histopathologically represented inflammation (Figure 3B). Higher metabolic activity is not only a feature of malignant cells, it can be observed in inflammatory nodules due to increased glucose metabolism in granulocytes and macrophages in a range of diseases, including fungal and necrobiotic rheumatoid nodules, sarcoidosis, tuberculosis, and other granulomas.<sup>38,39</sup> Dual time PET/CT did not prove to be useful for differentiating benign and malignant pulmonary nodules with an  $SUV_{max}$  less than 2.5 in regions with high prevalence of granulomatous disease.<sup>40,41</sup> Huang *et al.* showed that dynamic  $^{18}F$ -FDG PET/CT is valuable in differentiating benign from malignant pulmonary nodules with the potential to differentiate malignant from granulomatous disease.<sup>26</sup> Our study showed limited diagnostic accuracy of the dynamic  $^{18}F$ -FDG PET/CT in assessing inflammatory nodules.

The malignant outliers on dynamic  $^{18}F$ -FDG PET/CT with low  $K_i$  parameters were histopathologically mucinous adenocarcinoma *in situ*. Other malignant nodules in which low metabolic activity can be measured on  $^{18}F$ -FDG PET/CT are minimally invasive adenocarcinoma, carcinoid, and lung lymphoma.<sup>38,42</sup> Another important finding was that both malignant nodules with low metabolic activity were of lower CT density analysed on the initial perfusion CT images but also appreciable on low-dose CT scan of PET/CT examination. Further studies on low density lung nodules are needed for evaluation of using lower cut-point values for malignancy in conventional and dynamic PET/CT. Malignant lung nodules with low CT density and measuring less than 1 cm are known to have low metabolic activity on conventional  $^{18}F$ -FDG PET/CT.<sup>43,44</sup> Berger *et al.* have reported up to 41% of lung lesions to be false-negative on conventional  $^{18}F$ -FDG PET/CT in analysis of 25 mucinous, hypocellular lung lesions (3/9 false negative lesions were  $\leq 2 \text{ cm}$ , range, 1–5 cm).<sup>45</sup> Our study showed a

limited diagnostic accuracy of the dynamic  $^{18}\text{F}$ -FDG PET/CT in assessing low density malignant pulmonary nodules with  $K_i$  cut-point set at  $0.01 \text{ min}^{-1}$ .

Dynamic enhancement CT studies help identify false positive results in both inflammatory and infective conditions, and sometimes in benign vascular tumours.<sup>46,47</sup> The perfusion CT parameters for the inflammatory nodule in our study were low and indicative of a benign lesion despite high metabolic activity on  $^{18}\text{F}$ -FDG PET/CT. We have shown that the parameters of perfusion CT of both malignant nodules with low metabolic activity were higher than the BV and AF in benign nodules. Therefore, our findings indicate parameters of perfusion CT may aid in the identification of benign nodules with high glucose metabolic activity and in the identification of malignant nodules with low glucose metabolic activity. Ohno *et al.* have shown that perfusion CT is more specific and accurate than conventional  $^{18}\text{F}$ -FDG PET/CT.<sup>24,29</sup> Our study on a small sample of cases suggests that perfusion CT also performs better than dynamic  $^{18}\text{F}$ -FDG PET/CT.

The AF parameter of the perfusion CT obtained by the maximum slope method was not significantly different between benign and malignant nodules. Benign nodules had a lower AF parameter value than malignant nodules overall with one significant benign outlier with markedly high AF. Histopathologically, this represented an extremely rare 'light cell' or 'sugar type' PEComa. There are only about 50 cases of this neoplasm described in the literature.<sup>48,49</sup> PEComas are more commonly found as angiomyolipomas in the kidneys, or as lesions in the retroperitoneal space, gastrointestinal tract, or uterus. Only 7 cases of malignant pulmonary PEComa have been reported.<sup>50</sup> A case report of a benign pulmonary PEComa showing early wash-in enhancement with an early washout pattern of a malignant lesion on perfusion CT has been reported by Kim *et al.*<sup>51</sup> Despite a markedly high AF, the PEComa had a BV just under the cut-point value for malignancy and a low metabolic parameter  $K_i$  of dynamic  $^{18}\text{F}$ -FDG PET/CT. The BV parameter in combination with low  $K_i$  parameter proved to be more reliable for defining this extremely rare histological type of a pulmonary nodule.

Our study has limitations. This pilot study was performed in a small sample of patients and appropriately powered studies will be required for further validation. The mean nodule size was 18 mm for benign and 22 mm for malignant nodules, which would not normally be referred for imaging follow-up. The BTS and Fleischner Society recommended lower thresholds for nodule follow up (5

mm and 6 mm, respectively). More novel reconstruction methods in PET/CT such as specific point spread function (PSF) are enabling better spatial resolution and enable its use in 6 mm pulmonary nodules.<sup>52</sup>

Perfusion CT is quite demanding on patients with a prolonged breath-hold, which limits the availability of reliable data in some patients. All 3 nodules in which analysis was non-feasible due to the significant breathing artefact were near the diaphragm (2 in the right lower lobe and 1 in the right middle lobe). Segmentation of the pulmonary nodules on image analysis is restricted when the images were affected by respiratory motion artefact, especially in small nodules which were also abutting the chest wall or mediastinal structures. Some authors recommend quiet breathing during the perfusion CT scans but this is only acceptable in larger lung masses.<sup>53</sup> There is a need for further optimisation of nodule segmentation and advanced image registration techniques that allow accurate assessment of pulmonary nodules without need for long breath-hold.<sup>23,54</sup> The effective radiation dose for dynamic  $^{18}\text{F}$ -FDG PET/CT was around 8 mSv and for perfusion CT around 20 mSv. The radiation dose for perfusion CT can be improved by reducing the field of view from 16 cm to the nodule only and reducing tube voltage in smaller size patients.<sup>55</sup>

Potential increase in the demand for these not widely available novel dynamic imaging studies would consequently put additional strain on the imaging departments with increased demand for scanner time, funding and training of the staff. Limited capacity for a wider use of the dynamic imaging in lung nodules could be overcome by developing systems of identification of nodules with highest diagnostic benefit from dynamic imaging. A multicentre prospective cohort observational study initiated in 2016 is set to assess the performance and the cost-effectiveness of the dynamic CT and PET/CT in the characterisation of solitary pulmonary nodules.<sup>56</sup>

The small sample size limits the assessments of accuracy in our study. However, on this small sample we showed increase diagnostic improvement in the accuracy of diagnosis in both dynamic studies when compared to the conventional  $^{18}\text{F}$ -FDG PET/CT. Specificity in  $K_i$  and BV on our small sample size were higher at the estimated threshold values of  $0.01 \text{ min}^{-1}$  and 21 ml/100ml, respectively. This would need to be confirmed in larger studies.

Early identification of a lung nodule as benign or malignant by analysing its metabolic and per-

fusion parameters could reduce the need for CT to monitor lung nodule size, thereby reducing the number of CT scans required. It could also reduce the need for CT guided biopsy or other invasive procedures. Patients with malignant lung nodules could thus be identified more quickly and referred for radical treatment. With our study, we have demonstrated the potential of perfusion CT. The BV parameter assessed by perfusion CT was not only significantly lower in benign nodules, it also aided in correctly characterising the metabolically active inflammation, hypervascular benign PEComa and low density malignancy.

In conclusion, this study demonstrated the feasibility of dynamic <sup>18</sup>F-FDG PET/CT and CT perfusion studies in differentiating benign and malignant pulmonary nodules. The dynamic <sup>18</sup>F-FDG PET/CT and perfusion CT derived blood volume can assist to differentiate benign and malignant lung nodules and in indeterminate cases, a combined approach can be helpful.

## Acknowledgments

The authors would like to thank the late Martin Connell for his curiosity and analytical contribution; Dr. Dilip Patel, Dr. William Walker and the radiographers of the Queen's Medical Research Institute in Edinburgh for their support in this study.

## References

- Furtado CD, Aguirre DA, Sirlin CB, Dang D, Stamato SK, Lee P, et al. Whole-body CT screening: spectrum of findings and recommendations in 1192 patients. *Radiology* 2005; **237**: 385-94. doi: 10.1148/radiol.2372041741
- Brenner DJ, Hall EJ. Computed tomography – an increasing source of radiation exposure. *N Engl J Med* 2007; **357**: 2277-84. doi: 10.1056/nejra072149
- Callister MEJ, Baldwin DR, Akram AR, Barnard S, Cane P, Draffan J, et al. British thoracic society guidelines for the investigation and management of pulmonary nodules. *Thorax* 2015; **70**: ii1-54. doi: 10.1136/thoraxjnl-2015-207168
- Shinohara S, Hanagiri T, Takenaka M, Chikaishi Y, Oka S, Shimokawa H, et al. Evaluation of undiagnosed solitary lung nodules according to the probability of malignancy in the American College of Chest Physicians (ACCP) evidence-based clinical practice guidelines. *Radiol Oncol* 2014; **48**: 50-5. doi: 10.2478/raon-2013-0064
- MacMahon H, Naidich DP, Goo JM, Lee KS, Leung ANC, Mayo JR, et al. Guidelines for management of incidental pulmonary nodules detected on CT images: from the Fleischner Society 2017. *Radiology* 2017; **284**: 228-43. doi: 10.1148/radiol.2017161659
- Li F, Sone S, Abe H, MacMahon H, Armato SG, Doi K. Lung cancers missed at low-dose helical CT screening in a general population: comparison of clinical, histopathologic, and imaging findings. *Radiology* 2002; **225**: 673-83. doi: 10.1148/radiol.2253011375
- Joo HO, Je RY, Sung HK, Hyung SS, Soo KC. Clinical significance of small pulmonary nodules with little or no <sup>18</sup>F-FDG uptake on PET/CT images of patients with nonthoracic malignancies. *J Nucl Med* 2007; **48**: 15-21.
- Chen S, Harmon S, Perk T, Li X, Chen M, Li Y, et al. Diagnostic classification of solitary pulmonary nodules using dual time <sup>18</sup>F-FDG PET/CT image texture features in granuloma-endemic regions. *Sci Rep* 2017; **7**: 9370. doi: 10.1038/s41598-017-08764-7
- Wilson R, Devaraj A. Radiomics of pulmonary nodules and lung cancer. *Transl Lung Cancer Res* 2017; **6**: 86-91. doi: 10.21037/tlcr.2017.01.04
- Hawkins S, Wang H, Liu Y, Garcia A, Stringfield O, Krewer H, et al. Predicting malignant nodules from screening CT scans. *J Thorac Oncol* 2016; **11**: 2120-8. doi: 10.1016/j.jtho.2016.07.002
- Xu Y, Lu L, Lin-Ning E, Lian W, Yang H, Schwartz LH, et al. Application of radiomics in predicting the malignancy of pulmonary nodules in different sizes. *Am J Roentgenol* 2019; **213**: 1213-20. doi: 10.2214/AJR.19.21490
- Ather S, Kadir T, Gleeson F. Artificial intelligence and radiomics in pulmonary nodule management: current status and future applications. *Clin Radiol* 2020; **75**: 13-9. doi: 10.1016/j.crad.2019.04.017
- Khawaja A, Bartholmai BJ, Rajagopalan S, Karwoski RA, Varghese C, Maldonado F, et al. Do we need to see to believe? – radiomics for lung nodule classification and lung cancer risk stratification. *J Thorac Dis* 2020; **12**: 3303-16. doi: 10.21037/jtd.2020.03.105
- Feng B, Chen X, Chen Y, Liu K, Li K, Liu X, et al. Radiomics nomogram for preoperative differentiation of lung tuberculoma from adenocarcinoma in solitary pulmonary solid nodule. *Eur J Radiol* 2020; **128**: 109022. doi: 10.1016/j.ejrad.2020.109022
- Palumbo B, Bianconi F, Palumbo I, Fravolini ML, Ministrini M, Nuvoli S, et al. Value of shape and texture features from <sup>18</sup>F-FDG PET/CT to discriminate between benign and malignant solitary pulmonary nodules: an experimental evaluation. *Diagnostics* 2020; **10**: 696. doi: 10.3390/diagnostics10090696
- Henschke CI, Yankelevitz DF, Yip R, Reeves AP, Faroqi A, Xu D, et al. Lung cancers diagnosed at annual CT screening: volume doubling times. *Radiology* 2012; **263**: 578-83. doi: 10.1148/radiol.12102489
- Korosic MT, Bowman MH, Morris MJ, Skabelund AJ, Hersh AM. Effect of a pulmonary nodule fact sheet on patient anxiety and knowledge: a quality improvement initiative. *BMJ Open Qual* 2018; **7**: e000437. doi: 10.1136/bmjopen-2018-000437
- Slatore CG, Wiener RS, Golden SE, Au DH, Ganzini L. Longitudinal assessment of distress among veterans with incidental pulmonary nodules. *Ann Am Thorac Soc* 2016; **13**: 1983-91. doi: 10.1513/AnnalsATS.201607-555OC
- Cronin P, Dwamena BA, Kelly AM, Carlos RC. Solitary pulmonary nodules: Meta-analytic comparison of cross-sectional imaging modalities for diagnosis of malignancy. *Radiology* 2008; **246**: 772-82. doi: 10.1148/radiol.2463062148
- Wu CC, Maher MM, Shepard JAO. Complications of CT-guided percutaneous needle biopsy of the chest: prevention and management. *Am J Roentgenol* 2011; **196**: W678-82. doi: 10.2214/AJR.10.4659
- Huang MD, Weng HH, Hsu SL, Hsu LS, Lin WM, Chen CW, et al. Accuracy and complications of CT-guided pulmonary core biopsy in small nodules: a single-center experience. *Cancer Imaging* 2019; **19**: 51. doi: 10.1186/s40644-019-0240-6
- Folkman J. How is blood vessel growth regulated in normal and neoplastic tissue? – G. H. A. clowes memorial award lecture. *Cancer Res* 1986; **46**: 467-73. PMID: 2416426
- Cavalcanti PG, Shirani S, Scharcanski J, Fong C, Meng J, Castelli J, et al. Lung nodule segmentation in chest computed tomography using a novel background estimation method. *Quant Imaging Med Surg* 2016; **6**: 16-24. doi: 10.3978/j.issn.2223-4292.2016.02.06
- Ohno Y, Nishio M, Koyama H, Seki S, Tsubakimoto M, Fujisawa Y, et al. Solitary pulmonary nodules: comparison of dynamic first-pass contrast-enhanced perfusion area-detector CT, dynamic first-pass contrast-enhanced MR imaging, and FDG PET/CT. *Radiology* 2015; **274**: 563-75. doi: 10.1148/radiol.14132289
- Ohno Y, Nishio M, Koyama H, Miura S, Yoshikawa T, Matsumoto S, et al. Dynamic contrast-enhanced CT and MRI for pulmonary nodule assessment. *Am J Roentgenol* 2014; **202**: 515-29. doi: 10.2214/AJR.13.11888

26. Huang YE, Lu HI, Liu FY, Huang YJ, Lin MC, Chen CF, et al. Solitary pulmonary nodules differentiated by dynamic F-18 FDG PET in a region with high prevalence of granulomatous disease. *J Radiat Res* 2012; **53**: 306-12. doi: 10.1269/jrr.11089
27. Yuan X, Zhang J, Quan C, Cao J, Ao G, Tian Y, et al. Differentiation of malignant and benign pulmonary nodules with first-pass dual-input perfusion CT. *Eur Radiol* 2013; **23**: 2469-74. doi: 10.1007/s00330-013-2842-x
28. Ohno Y, Koyama H, Fujisawa Y, Yoshikawa T, Seki S, Sugihara N, et al. Dynamic contrast-enhanced perfusion area detector CT for non-small cell lung cancer patients: influence of mathematical models on early prediction capabilities for treatment response and recurrence after chemoradiotherapy. *Eur J Radiol* 2016; **85**: 176-86. doi: 10.1016/j.ejrad.2015.11.009
29. Ohno Y, Nishio M, Koyama H, Fujisawa Y, Yoshikawa T, Matsumoto S, et al. Comparison of quantitatively analyzed dynamic area-detector CT using various mathematic methods with FDG PET/CT in management of solitary pulmonary nodules. *Am J Roentgenol* 2013; **200**: W593-602. doi: 10.2214/AJR.12.9197
30. Karakatsanis NA, Lodge MA, Tahari AK, Zhou Y, Wahl RL, Rahmim A. Dynamic whole-body PET parametric imaging: I. Concept, acquisition protocol optimization and clinical application. *Phys Med Biol* 2013; **58**: 7391-418. doi: 10.1088/0031-9155/58/20/7391
31. Dimitrakopoulou-Strauss A, Pan L, Strauss LG. Quantitative approaches of dynamic FDG-PET and PET/CT studies (dPET/CT) for the evaluation of oncological patients. *Cancer Imaging* 2012; **12**: 283-9. doi: 10.1102/1470-7330.2012.0033
32. Yi CA, Kyung SL, Kim BT, Joon YC, Kwon OJ, Kim H, et al. Tissue characterization of solitary pulmonary nodule: comparative study between helical dynamic CT and integrated PET/CT. *J Nucl Med* 2006; **47**: 443-50. PMID: 16513614
33. Ohno Y, Koyama H, Matsumoto K, Onishi Y, Takenaka D, Fujisawa Y, et al. Differentiation of malignant and benign pulmonary nodules with quantitative first-pass 320-detector row perfusion CT versus FDG PET/CT. *Radiology* 2011; **258**: 599-609. doi: 10.1148/radiol.10100245
34. Mirsadraee S, Reid JH, Connell M, MacNee W, Hirani N, Murchison JT, et al. Dynamic (4D) CT perfusion offers simultaneous functional and anatomical insights into pulmonary embolism resolution. *Eur J Radiol* 2016; **85**: 1883-90. doi: 10.1016/j.ejrad.2016.08.018
35. Patlak CS, Blasberg RG, Fenstermacher JD. Graphical evaluation of blood-to-brain transfer constants from multiple-time uptake data. *J Cereb Blood Flow Metab* 1983; **3**: 1-7. doi: 10.1038/jcbfm.1983.1
36. Evangelista L, Cuocolo A, Pace L, Mansi L, Del Vecchio S, Miletto P, et al. Performance of FDG-PET/CT in solitary pulmonary nodule based on pre-test likelihood of malignancy: results from the ITALIAN retrospective multicenter trial. *Eur J Nucl Med Mol Imaging* 2018; **45**: 1898-907. doi: 10.1007/s00259-018-4016-1
37. Weir-McCall JR, Harris S, Miles KA, Qureshi NR, Rintoul RC, Dizdarevic S, et al. Impact of solitary pulmonary nodule size on qualitative and quantitative assessment using 18F-fluorodeoxyglucose PET/CT: the SPUTNIK trial. *Eur J Nucl Med Mol Imaging* 2020; **48**: 1560-9. doi: 10.1007/s00259-020-05089-y
38. Sim YT, Poon FW. Imaging of solitary pulmonary nodule-a clinical review. *Quant Imaging Med Surg* 2013; **3**: 316-26. doi: 10.3978/j.issn.2223-4292.2013.12.08
39. Ambrosini V, Nicolini S, Caroli P, Nanni C, Massaro A, Marzola MC, et al. PET/CT imaging in different types of lung cancer: an overview. *Eur J Radiol* 2012; **81**: 988-1001. doi: 10.1016/j.ejrad.2011.03.020
40. Chen CJ, Lee BF, Yao WJ, Cheng L, Wu PS, Ching LC, et al. Dual-phase 18F-FDG PET in the diagnosis of pulmonary nodules with an initial standard uptake value less than 2.5. *Am J Roentgenol* 2008; **191**: 475-9. doi: 10.2214/AJR.07.3457
41. Cloran FJ, Banks KP, Song WS, Kim Y, Bradley YC. Limitations of dual time point PET in the assessment of lung nodules with low FDG avidity. *Lung Cancer* 2010; **68**: 66-71. doi: 10.1016/j.lungcan.2009.05.013
42. Chiu CH, Yeh YC, Lin KH, Wu YC, Lee YC, Chou TY, et al. Histological subtypes of lung adenocarcinoma have differential 18F-fluorodeoxyglucose uptakes on the positron emission tomography/computed tomography scan. *J Thorac Oncol* 2011; **6**: 1697-703. doi: 10.1097/JTO.0b013e318226b677
43. Veronesi G, Bellomi M, Veronesi U, Paganelli G, Maisonneuve P, Scanagatta P, et al. Role of positron emission tomography scanning in the management of lung nodules detected at baseline computed tomography screening. *Ann Thorac Surg* 2007; **84**: 959-66. doi: 10.1016/j.athoracsurg.2007.04.058
44. Nomori H, Watanabe K, Ohtsuka T, Naruke T, Suemasu K, Uno K. Evaluation of F-18 fluorodeoxyglucose (FDG) PET scanning for pulmonary nodules less than 3 cm in diameter, with special reference to the CT images. *Lung Cancer* 2004; **45**: 19-27. doi: 10.1016/j.lungcan.2004.01.009
45. Berger KL, Nicholson SA, Dehdashti F, Siegel BA. FDG PET evaluation of mucinous neoplasms: Correlation of FDG uptake with histopathologic features. *Am J Roentgenol* 2000; **174**: 1005-8. doi: 10.2214/ajr.174.4.1741005
46. Yi CA, Lee KS, Kim EA, Han J, Kim H, Kwon OJ, et al. Solitary pulmonary nodules: Dynamic enhanced multi-detector row CT study and comparison with vascular endothelial growth factor and microvessel density. *Radiology* 2004; **233**: 191-9. doi: 10.1148/radiol.2331031535
47. Zhang M, Kono M. Solitary pulmonary nodules: Evaluation of blood flow patterns with dynamic CT. *Radiology* 1997; **205**: 471-8. doi: 10.1148/radiology.205.2.9356631
48. Hornick JL, Fletcher CDM. PEComa: What do we know so far? *Histopathology* 2006; **48**: 75-82. doi: 10.1111/j.1365-2559.2005.02316.x
49. Stallmann S, Fisseler-Eckhoff A. [Mesenchymal tumors of the lungs]. [German]. *Pneumologie* 2014; **12**: 34-43. doi: 10.1007/s10405-014-0808-6
50. Chakrabarti A, Bandyopadhyay M, Purkayastha B. Malignant perivascular epithelioid cell tumour (PEComa) of the lung-A rare entity. *Innov Surg Sci* 2020; **2**: 39-42. doi: 10.1515/iss-2016-0032
51. Kim WJ, Kim SR, Choe YH, Lee KY, Park SJ, Lee HB, et al. Clear cell "sugar" tumor of the lung: a well-enhanced mass with an early washout pattern on dynamic contrast-enhanced computed tomography. *J Korean Med Sci* 2008; **23**: 1121-4. doi: 10.3346/jkms.2008.23.6.1121
52. Suljic A, Tomse P, Jensterle L, Skrk D. The impact of reconstruction algorithms and time of flight information on PET/CT image quality. *Radiol Oncol* 2015; **49**: 227-33. doi: 10.1515/raon-2015-0014
53. Bhalla A, Das A, Naranje P, Irodi A, Raj V, Goyal A. Imaging protocols for CT chest: a recommendation. *Indian J Radiol Imaging* 2019; **29**: 236. doi: 10.4103/ijri.ijri\_34\_19
54. Dolde K, Naumann P, Dávid C, Kachelriess M, Lomax AJ, Weber DC, et al. Comparing the effectiveness and efficiency of various gating approaches for PBS proton therapy of pancreatic cancer using 4D-MRI datasets. *Phys Med Biol* 2019; **64**: 085011. doi: 10.1088/1361-6560/ab1175
55. McCollough CH, Primak AN, Braun N, Kofler J, Yu L, Christner J. Strategies for reducing radiation dose in CT. *Radiol Clin N Am* 2009; **47**: 27-40. doi: 10.1016/j.rcl.2008.10.006
56. Qureshi NR, Rintoul RC, Miles KA, George S, Harris S, Madden J, et al. Accuracy and cost-effectiveness of dynamic contrast-enhanced CT in the characterisation of solitary pulmonary nodules – The SPUTNIK study. *BMJ Open Respir Res* 2016; **3**: e000156. doi: 10.1136/bmjresp-2016-000156

## research article

# MRI of the Morel-Lavallée lesion - a case series

Tajda Srot Volavc<sup>1</sup>, Mitja Rupreht<sup>1,2</sup><sup>1</sup> Radiology Department, University Medical Center Maribor, Maribor, Slovenia<sup>2</sup> Medical Faculty, University of Maribor, Maribor, Slovenia

Radiol Oncol 2021; 55(3): 268-273.

Received 29 December 2020

Accepted 16 February 2021

Correspondence to: Assist. Prof. Mitja Rupreht, M.D., Ph.D., Radiology Department, UMC Maribor, Ljubljanska 5, 2000 Maribor, Slovenia. E-mail: mitja.rupreht@ukc-mb.si

Disclosure: No potential conflicts of interest were disclosed.

This is an open access article under the CC BY-NC-ND license (<http://creativecommons.org/licenses/by-nc-nd/4.0/>).

**Introduction.** The aim of the study was to review the appearances of Morel-Lavallée (ML) lesions on magnetic resonance imaging (MRI).

**Patients and methods.** 14 patients diagnosed with the ML lesion on MRI were analysed retrospectively (mean age = 35 years). Mechanism of injury, time frame from injury to MRI, location, shape, T1 and proton-density fat-suppression (PDFS) signal intensity (SI), presence of a (pseudo)capsule, septations or nodules within the collection, mass effect and fluid-fluid levels were analyzed. The Mellado and Bencardino classification was utilized to classify the lesions.

**Results.** In most cases, mechanism of injury was distortion. Mean time frame between the injury and MRI was 17 days. Lesions were located around the knee in 9 patients and in the peritrochanteric region in 5 patients. Collections were fusiform in 12 patients and oval in 2 patients. 9 collections were T1 hypointense and PDFS hyperintense. 4 collections had intermediate T1 and high PDFS SI. 1 collection had intermediate T1 and PDFS SI. (Pseudo)capsule was noted in 3 cases. Septations or nodules were found in 4 cases. According to the Mellado and Bencardino, collections were classified as seroma (type 1) in 9, subacute hematoma (type 2) in 1 and chronic organizing hematoma (type 3) in 4 cases.

**Conclusions.** Characteristic features of ML lesion include a fusiform fluid collection between the subcutaneous fat and the underlying fascia after shearing injury. Six types can be differentiated on MRI, with the seroma, the subacute hematoma and the chronic organizing hematoma being the commonest.

Key words: Morel-Lavallée; soft-tissue injury; hematoma; magnetic resonance imaging

## Introduction

Morel-Lavallée (ML) lesion has initially been presented by a French surgeon Victor Auguste Francois Morel-Lavallée in 1863, who described it as fluid collection which dissects the subcutaneous fat tissue.<sup>1</sup>

In most cases, it is a post-traumatic, closed, degloving soft-tissue injury caused by direct trauma or shearing forces, resulting in abrupt separation of skin and subcutaneous tissue from the underlying fascia.<sup>2-4</sup> Consequently, a dead space is formed, which can potentially fill with haemolymph, debris and fat, resulting in a formation of heterogeneous collection.<sup>2,3,5-6,7-9</sup>

Peritrochanteric region is particularly sensitive to this injury because of the increased mobility of the soft tissue in this area, the superficially located bone, strong underlying *fascia lata* attaching to the iliotibial band and a rich vascular plexus piercing the *fascia lata*.<sup>5,7,8</sup>

Clinically it usually presents as an enlarging painful swelling.<sup>2</sup> Clinical presentation and the imaging techniques are keys to a diagnosis. Ultrasound (US) is an excellent imaging modality for the evaluation of superficial soft tissues and collections. However, owing to both high contrast resolution and demonstration of deep tissues, magnetic resonance (MRI) is a gold standard for the identification and evaluation of the ML lesion.<sup>2-4,6-8,10,11</sup>

ML lesion can present with various shapes and signal intensities in standard MRI sequences due to the different stages and contents of the lesions. This can lead to underrecognition and misinterpretation of the ML lesions by the radiologists. In order to prevent complications such as infections or extensive tissue necrosis it is essential to diagnose and manage the lesion in a timely manner.<sup>2-4,7,10</sup>

In the literature, several forms of ML lesions have been described. In 2005, an extensive six-stage imaging-based classification on the shape of lesion, signal intensity (SI) on T1 and T2-weighted images, presence of the fibrous capsule, contrast enhancement and sinus tract formation capsule was proposed by Melado and Bencardino (Table 1).<sup>11</sup>

A type 1 ML lesion is a seroma, exhibiting fluid-like characteristics. It is seen as homogeneously hypointense on T1 and hyperintense on T2 MRI (Figure 1).<sup>5,12</sup> It can be acute or chronic and is mostly noncapsulated.<sup>5,11</sup>

A type 2 ML lesion is a subacute hematoma, which appears homogeneously hyperintense on both, T1 and T2 MRI.<sup>5,9,12</sup> The cause of high T1 SI is the presence of methaemoglobin. In the early subacute hematoma, the methaemoglobin is first observed in the periphery. With time it becomes more homogeneously distributed.<sup>5,11,13</sup> These lesions mostly have a hemosiderin-rich capsule on T1- and T2-WI. From time to time internal inhomogeneity can be seen, due to the fluid-fluid levels, internal septations and entrapped fat globules.<sup>5,13</sup>

Occasionally, patchy internal enhancement after intravenous contrast administration can be observed due to the presence of capillaries, which can lead to false interpretation of the lesion as a soft-tissue tumour. The subacute hematomas can be further divided in early and late subacute hematomas. The early ones are more homogeneous, while the late ones often present with a fibrous capsule and are seen as heterogeneous.<sup>5,14</sup>

A type 3 ML lesion is a chronic organizing hematoma, with hypo- or intermediate SI on T1 and as heterogeneous intermediate on T2 sequences. The heterogeneous signal is seen due to the content of the lesion: hemosiderin granulation tissue, necrotic debris, fibrin and blood clots (Figure 2).<sup>11</sup> Because of neovascularization and granulation tissue, patchy internal and peripheral enhancement can be seen on post-contrast MRI.<sup>5,12</sup> These types of lesions may be surrounded by a hemosiderin-rich fibrous capsule.<sup>5,14</sup>

Type 4-6 ML lesions are the chronic ones, often presenting atypically. A type 4 ML lesion is a closed fatty tissue laceration with a perifascial

dissection. It can be associated with or without a serous/haemorrhagic collection.<sup>5,11</sup> The collection is seen with low T1 SI and high T2 SI. It is not surrounded by a capsule and it enhances variably.<sup>5,14</sup>

A type 5 ML lesion is located perifascially and has a pseudonodular appearance. Occasionally, a peripheral enhancement and skin retraction are seen.<sup>5,11</sup>

A type 6 ML lesion is an infected lesion, it often presents with a thick capsule, internal septations, peripheral fluid leakage, inflammation of the adjacent fat tissue and fascia and sometimes even with an associated sinus tract.<sup>5,11</sup> The aim of our study was to retrospectively analyse the series of patients with ML lesions based on the Mellado-Bencardino classification and evaluate its presentations on MRI.

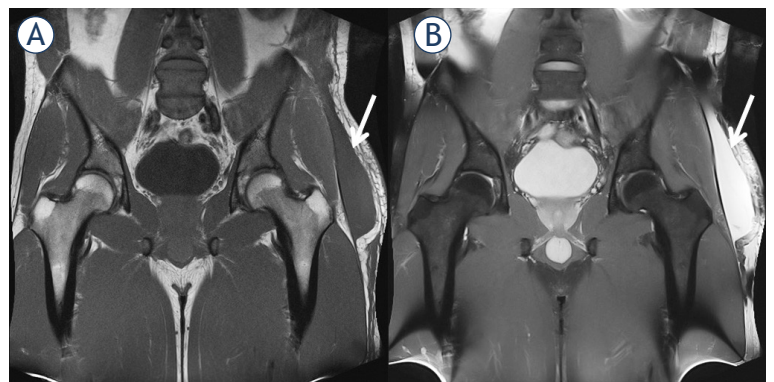


**FIGURE 1.** Morel-Lavallée lesion type 1. A 33-years-old professional skier 2 weeks after a fall. A large fusiform collection (arrows) between the subcutaneous fat and fascia lata demonstrating low signal intensity (SI) on T1 WI (A) and high SI on proton density fat-saturated image (PDFS) (B) in coronal plane indicating clear fluid i.e. seroma.

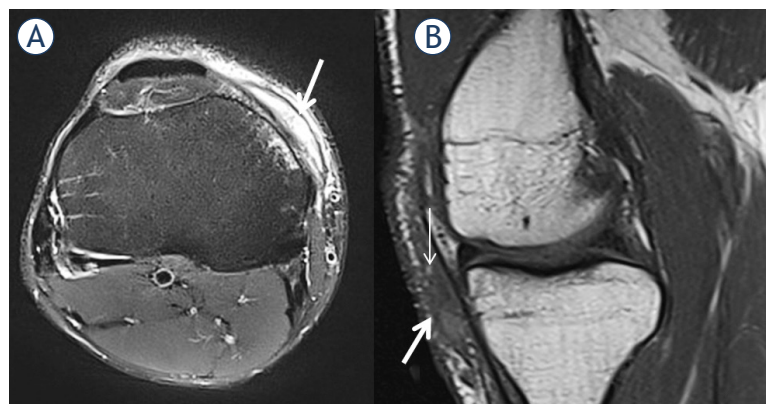


**FIGURE 2.** ML lesion type 3. A 34-year-old male after a distortion. On axial proton density fat-suppression (PDFS) MRI (A) a fusiform fluid collection with hypointense debris is demonstrated between the deep subcutaneous fat and layers of medial patellofemoral ligament (arrows). On T1 weighted sagittal image (B), in moderately hypointense collection several fat globules are visible (thin arrow).

TABLE 1. MRI classification of Morel-Lavallee lesions according to Mellado-Bencardino<sup>12</sup>

Lesion type	T1W	T2W	Morphology	Other
Type 1 - Seroma	Homogenously hypointense seroma	Hyperintense collection	Laminar	No evidence of outer capsule formation
Type 2 - Subacute hematoma	Homogenously hyperintense	Homogenously hyperintense	Oval	Presence of methaemoglobin Thin capsule formation
Type 3 - Chronic organizing hematoma	Hypointense	Heterogeneous hypointense/ isointense	Oval	Thick capsule formation Capsular and internal enhancement on postcontrast sequences
Type 4-Closed laceration	Hypointense	Hyperintense	Linear	No capsule formation
Type 5-Small, rounded pseudonodular appearance	Variable	Variable	Round	Variable capsule formation
Type 6-Superimposed infection	Variable	Variable	Variable sinus tract	Thick enhancing capsule

## Patients and methods

The study design was a single-center retrospective review, performed accordingly to the Declaration of Helsinki and approved by the local ethics committee. The search identified fourteen patients; ten male and four female. Their age ranged between 11–67 years with the mean age 34.8 years. The examinations were performed with various MRI scanners. MRI protocol consisted of T1 sequence in at least one plane and proton density fat-suppressed sequences (PDFS) in several planes. In addition, T2 sequence without fat suppression was utilized several times. Intravenous (I.V.) contrast was not administered in any case.

The mechanism of injury as well the time frame between injury and MRI were recorded, when provided. Additionally, the imaging reports and MRI images were reviewed. Also, the possible additional imaging modalities were identified. The following characteristics of the MR-images were evaluated by the radiology resident (first author) and musculoskeletal (MSK) radiologist with 14 years of experience (second author) in consensus: location, shape, signal intensity (SI), presence of a (pseudo) capsule, septations or nodules within the collection, mass effect and fluid-fluid levels.

## Results

### Mechanism of injury and time frame between the injury and MRI

In five patients out of fourteen (30.1%) the mechanism was distortion, in 3/14 patients (21.4%) fall, 2/14 (14.3%) were athletes without acute injury, 1/14 (7.1%) patient kneeled and one (7.1%) was injured in a motor vehicle accident. In 2/14 patients (14.3%), the mechanism of injury was unknown.

For 11/14 patients (78.6%) the time frame between the injury and MRI was 4 days to 4 months, with mean time of 17 days. For 3/14 patients (21.4%) the time frame was unknown.

### Additional ultrasound

Only one patient (7.1%) had an ultrasound before the MRI. One patient (7.1%) had a follow-up ultrasound.

### MRI characteristics

#### Location and shape

The collections were located around the knee in 9/14 patients (64.3%) and in the peritrochanteric region in 5/14 (35.7%) patients.

The majority (12/14, 85.7%) of collections was fusiform and only 2/14 (14.3%) had oval shape.

#### MRI signal intensity and lesion classification

Most collections (9/14, 64.3%) were T1 hypointense and PDFS hyperintense (Figure 1). 4/14 (28.5%) collections had intermediate T1 and high PDFS SI (Figure 2). 1/14 (7.1%) collection had intermediate T1 and PDFS SI. (Pseudo)capsule was noted in 3/14 cases (21.4%). Septations or nodules were found in 4/14 (28.5%) cases. No cases with mass effect or fluid-fluid levels were observed. Additionally, in 5/14 (35.7%) cases fat globules were found. Also, in 10/14 (71.4%) cases the oedema of subcutaneous fat was noted without lacerations.

The collections were classified according to the Mellado-Bencardino classification as seroma – type 1 in 9/14 (64.3%), subacute hematoma – type 2 in 1/14 (7.1%) and chronic organizing hematoma – type 3 in 4/14 (28.5%).

## Discussion

To our knowledge, the presented study is one of larger cohorts in the published literature, in particular with the focus on the MRI. ML lesions most commonly occur around the greater trochanter, although they can be found around the knee, trunk, peri-scapular etc.<sup>2-3,5-7,10,11,15</sup> Sometimes the collections may extend through thin sinus tract far from the original location (Figure 3). The location of the ML lesion around the knee was more frequent in our cohort than previously reported. Frequently, small fluid collections in the deep subcutaneous tissues around the knee joint are interpreted as simple seroma or hematoma whereas they could be also described as ML lesion. Alternatively, in the clinical practice, prepatellar fluid collections are commonly interpreted as a bursitis, which may represent the differential diagnosis. Prepatellar ML lesions often extend medially or laterally and proximally to the mid-thigh whereas a prepatellar bursitis does not extend beyond the mid-coronal plane and the boundaries of normal and slightly swollen bursa.<sup>16,17</sup> The exact definition of location might represent a challenge in the definition and classification of the ML lesions in the future. However, the distinction may not be clinically relevant as treatment is often the same. A chronic hemorrhagic prepatellar bursitis may mimic a type 3 ML lesion.<sup>14,18</sup> The shapes of the lesions were in line with the previous reports.<sup>5</sup> Septations and nodules, as well as fat globules, were less frequent in the presented group than in a published literature<sup>5</sup>, probably owing to a small patient group. The presence of intralesional fat globules (Figure 4) is not pathognomonic, although they may be found in some subacute hematomas.<sup>19</sup> However, their finding may contribute to the characterization of the

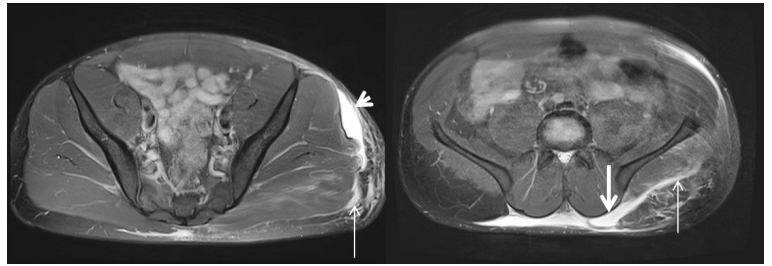


**FIGURE 3.** Extension of the Morel-Lavallée (ML) lesion. Same patient as in the Figure 1. On axial proton-density fat-suppression (PDFS) images, a thin communication (thin arrows) between *gluteus maximus* muscle and the deep gluteal fat connects the primary lesion (thick short arrow) and another collection posteriorly (thick arrow). Note also the mild oedema signal of the *gluteus maximus* muscle and gluteal fat indicating contusions.

collection as the ML lesion.<sup>20,21</sup> On the other hand, they are not among criteria of Mellado-Bencardino classification.

Most collections in the study group were classified as the Type 1 lesions. This could possibly be explained with the relative short time frame between the injury and the MRI. We could not find the time frame data in previous published reports. The results of less frequent type 2 and type 3 lesions are in line with other reports.<sup>5</sup>

We did not encounter type 3–6 lesions according to Mellado-Bencardino classification, possibly owing to their rarity, variable presentations on MRI, short time-frame between the injury and MRI, and a small patient group. Similar results were found in other small series.<sup>5</sup>

In the presented cohort, routine PDFS sequences were utilized as fluid-sensitive fat-suppressed sequences. The Mellado-Bencardino classification is based on T1/T2 MRI protocol, as it was most probably derived from MRI of soft tissue tumours as well as from other MSK protocols in mid-2000s, when it was introduced. The PDFS sequence was

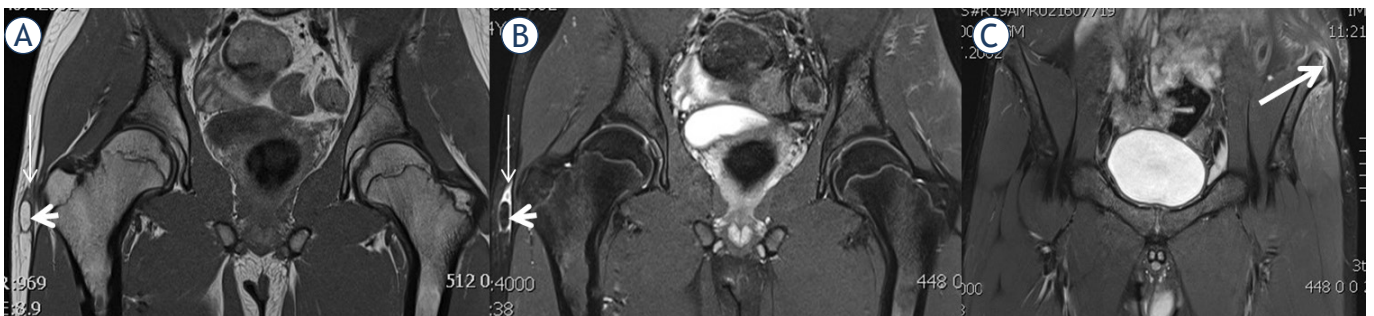


**FIGURE 4.** Fat globule and concomitant injury. In this 14-year-old boy with unknown time and mechanism of injury, a small fusiform fluid collection is visible at the right side between deep subcutaneous fat and *fascia lata* with low T1 (A) and high proton-density fat-suppression (PDFS) (B) SI (thin arrows) on coronal images. Note also a large fat globule in the lesion (short thick arrows). In addition, on the left side (C), an small avulsion of the *sartorius* tendon off the anterior superior iliac spine is visible (long thick arrow).

mostly not utilized routinely in the MSK MRI at the time, however owing to its robustness it has been a MSK workhorse since 2010, when the routine role of non-fat-suppressed T2 sequence was reduced. Therefore, to be strict, the classification in the presented series could be characterized as »Mellado-Bencardino related«. Furthermore, as in routine MSK MRI trauma settings, no contrast had been administered in the presented series. However, owing to other typical findings, follow-up examination with contrast was not indicated in any case. Modified MRI protocols, as well as not encountering types 3–6 lesions, might both imply the possible opportunity for an update and simplification of the Mellado-Bencardino classification to the three stages in the future. This should be verified in studies with larger patient cohorts and clinical correlation.

The specific location between the subcutaneous tissue and the fascia, the imaging signs and knowledge of the classification system may all be helpful in the differential diagnosis with other fluid-filled collections in the soft tissues.<sup>5</sup> In addition to bursitis, described above, other differential possibilities include soft tissue masses and other posttraumatic collections. Among soft tissue masses, sarcomas represent the most dangerous possibility which can mimic type 1 or 3 ML lesion. In short, sarcomas, as vascularized tumours, mostly demonstrate contrast enhancement, whereas collections do not. However, in most cases, particularly in trauma setting, I.V. contrast is not administered, as it was not in the presented cohort, as mentioned. Therefore, caution is warranted and low threshold to follow-up MRI with contrast or US Doppler examination (the role of US contrast in these settings is yet to be evaluated) should be set, particular in growing masses.

Other possible differential diagnoses include fat necrosis, where MRI signal depends on timing after trauma. It may appear spiculated or more laminar<sup>22</sup> and may sometimes mimic a type 4 ML lesion.<sup>11</sup> Another possibility is pseudolipoma, which can develop after blunt trauma as well as iatrogenic after surgery and hematoma.<sup>11</sup> On MRI, it usually presents as subcutaneous lipomatous mass without capsule or contrast enhancement.<sup>23</sup>

Owing to their superficial location, most of ML lesions can be detected with ultrasound (US). Interestingly, only one patient in the presented cohort had had US examination performed before the MRI. This could be explained with the lack of data of possible US examinations performed outside our institution. Mostly, similar as on MRI, the



**FIGURE 5.** Concomitant injuries. Same patient as in Figure 1 and 3. In proton-density fat-suppression (PDFS) coronal image, a mild hyperintensity of adductor muscles is visible (thick arrow) indicating mild distension without fibre disruption. In addition, note secondary cleft sign (thin arrow) at the lower right edge of the pubic symphysis indicating possible injury of the rectus/adductor aponeurosis. In such case, a dedicated MRI examination might be warranted.

US appearance depends on their age, often with heterogeneous echogenicity. The latter depends on the degradation stage of the blood products; acute and subacute (up to a month) lesions will appear heterogeneous with irregular margins and lobular shape. Over the time, the blood products will liquefy and become more hypochoic. Chronic lesions (more than 18 months) are more often homogenous with smooth margins.<sup>7,20,21,24</sup> MRI, however, enables more detailed analysis of deeper tissues and demonstration of possible concomitant muscle, nerve and bone injuries (Figures 4, 5). In our opinion, it is therefore preferred imaging modality at least before possible invasive therapeutic procedures or clinical suspicion of possible extension in different compartments, larger collections, superinfections or unclear differential diagnosis.<sup>5</sup> Nevertheless, US could be an excellent method for the follow-up of the lesion, particularly in conservatively managed cases, as well as in suspected complications after invasive treatment.

Computed tomography (CT) has minor role in the evaluation of the ML lesions. They may, however, incidentally show-up in the examinations, performed for the evaluation of possible bone injuries. On CT, they may demonstrate with fluid-fluid

levels and lower densities than simple hematomas owing to mixing of low-density lymphatic fluid.<sup>4</sup> Therefore, they may be easily overlooked, especially in the bone window.

Treatment of the ML lesion depends on the stadium. It varies from compression banding, aspiration or incision and evacuation, with or without injection of sclerosing agents.<sup>14,25</sup>

The lack of US data in the presented cohort represents a limitation of the presented study. Another limitation could be the lack of the data of further clinical and imaging management because most patients were outpatients who were lost to follow-up. However, both were not primary purposes of the study.

## Conclusions

Morel-Lavallée lesion results from the traumatic separation of the skin and subcutaneous fat from the underlying fascia where a fusiform fluid collection is demonstrated on imaging. On MRI, six types of ML lesion can be differentiated, with the seroma, the subacute hematoma and the chronic organizing hematoma being the most frequent presentations. Knowledge of the most common locations, imaging signs and classification system may be helpful in the differential diagnosis. The results of the presented study, as well as the modified MRI protocols in the last decade, might suggest the opportunity for the possible update and simplification of the Mellado-Bencardino classification.

## References

- Morel-Lavalle M. Decollements traumatiques de la peau et de couches. *Arch Gen Med* 1863; **1**: 20-38, 172-200, 300-332.
- Husein K, White B, Sampson M, Gupta S. Pictorial review of Morel-Lavallee lesions. *J Med Imaging Radiat Oncol* 2019; **63**: 212-15. doi: 10.1111/1754-9485.12854
- Myrick KM, Davis S. Morel-Lavallee injury - a case study. *Clin Case Rep* 2018; **6**: 1033-9. doi: 10.1002/ccr3.1518
- Diviti S, Gupta N, Hooda K, Sharma K, Lo L. Morel-Lavallee lesions review of pathophysiology, clinical findings, imaging findings and management. *J Clin Diagn Res* 2017; **11**: TE01-04. doi: 10.7860/jcdr/2017/25479.9689
- De Coninck T, Vanhoenacker F, Verstaete K. Imaging features of Morel-Lavallee lesions. *J Belg Soc Radiol* 2017; **101**: 15. doi: 10.5334/jbr-btr.1401
- Christian D, Leland HA, Osias W, Eberlin S, Howell L. Delayed presentation of a chronic Morel-Lavallee lesion. *J Radiol Case Rep* 2016; **10**: 30-9. doi: 10.3941/jrcr.v10i7.2698
- McLean K, Popovic S. Morel-Lavallee lesion: AIRP best cases in radiologic-pathologic correlation. *Radiographics* 2017; **37**: 190-96. doi: 10.1148/rg.2017160169
- Riemer K, Haukenes O, Kozak A. Morel-Lavallee lesion. *Tidsskr Nor Laegeforen* 2019; **139**. doi: 10.4045/tidsskr.18.0351
- Gilbert BC, Bui-Mansfield LT, Schyuler D. MRI of a Morel-Lavallee lesion. *Am J Roentgenol* 2004; **182**: 1347-8. doi: 10.2214/ajr.182.5.1821347
- Nair AV, Nazari PK, Sehkar R, Ramachandran PV, Moorthy S. Morel-Lavallee lesion: a closed degloving injury that requires real attention. *Indian J Radiol Imaging* 2014; **24**: 288-90. doi: 10.4103/0971-3026.137053
- Mellado JM, Bencardino JT. Morel-Lavallee lesion: review with emphasis on MR imaging. *Magn Reson Imaging Clin N Am* 2005; **13**: 775-82. doi: 10.1016/j.mric.2005.08.006
- Mellado JM, del Palomar LP, Diaz L, Ramos A, Sauri A. Long-standing Morel-Lavallee lesions of the trochanteric region and proximal thigh: MRI features in five patients. *Am J Roentgenol* 2004; **182**: 1289-94. doi: 10.2214/ajr.182.5.1821289
- Bush CH. The magnetic resonance imaging of musculoskeletal hemorrhage. *Skeletal Radiol* 2000; **29**: 1-9. doi: 10.1007/s002560050001
- Bonilla-Yoon I, Masih S, Patel DB, White EA, Levine BD, Chow K, et al. The Morel-Lavallee lesion: pathophysiology, clinical presentation, imaging features and treatment options. *Emerg Radiol* 2014; **21**: 35-43. doi: 10.1007/s10140-013-1151-7
- Parra JA, Fernandez MA, Encinas B, Rico M. Morel-Lavallee effusions in the thigh. *Skeletal Radiol* 1997; **26**: 239-41. doi: 10.1007/s002560050228
- Dye SF, Campagna-Pinto D, Dye CC, Shifflet S, Eiman T. Soft-tissue anatomy anterior to the human patella. *J Bone Joint Surg Am* 2003; **85**: 1012-17. doi: 10.2106/00004623-200306000-00005
- Yahyavi-Firouz-Abadi N, Demertzis JL. Prepatellar Morel-Lavallee effusion. *Skeletal Radiol* 2013; **42**: 151-2. doi: 10.1007/s00256-012-1398-1
- Borrero CG, Maxwell N, Kavanagh E. MRI findings of prepatellar Morel-Lavallee effusions. *Skeletal Radiol* 2008; **37**: 451-55. doi: 10.1007/s00256-008-0450-7
- Yu SJ. Magnetic resonance imaging of posttraumatic soft tissue disorders. *Emerg Radiol* 1996; **3**: 181-94. doi: 10.1007/BF01507739
- Mukherjee K, Perrin SM, Hughes PM. Morel-Lavallee lesion in an adolescent with ultrasound and MRI correlation. *Skelet Radiol* 2007; **36**: 43-5. doi: 10.1007/s00256-006-0122-4
- Neal C, Jacobson JA, Brandon C, Kalume-Brigido M, Morag Y, Girish G. Sonography of Morel-Lavallee lesions. *J Ultrasound Med* 2008; **27**: 1077-81. doi: 10.7863/jum.2008.27.1077
- Chan LP, Gee R, Keogh C, Munk PL. Imaging features of fat necrosis. *Am J Roentgenol* 2003; **181**: 955-9. doi: 10.2214/ajr.181.4.1810955.
- Theumann N, Abdelmoumene A, Wintermark M, Schynder P, Gailloud M-C, Resnick D. Posttraumatic pseudolipoma: MRI appearances. *Eur Radiol* 2005; **15**: 1876-80. doi: 10.1007/s00330-005-2757-2
- Choudhary AK, Methratta S. Morel-Lavallee lesion of the thigh: characteristic findings on US. *Pediatr Radiol* 2010; **40**: 49. doi: 10.1007/s00247-010-1587-9
- Dawre S, Shashank L, Gupta S, Sreekar H, Gupta AK. The Morel-Lavallee lesion: a review and proposed algorithmic approach. *Eur J Plast Surg* 2010; **35**: 489-94. doi: 10.1007/s00238-012-0725-z

## research article

# Are radiation-induced cavernomas clinically relevant findings? Results from long-term follow-up with brain magnetic resonance imaging of childhood cancer survivors

Lucas Becker<sup>1</sup>, Judith Gebauer<sup>2,7</sup>, Jan Kuchler<sup>3</sup>, Christian Staackmann<sup>4</sup>, Hannes Schacht<sup>1</sup>, Melchior Lauten<sup>5</sup>, Ulf Jensen-Kondering<sup>6</sup>, Peter Schramm<sup>1</sup>, Thorsten Langer<sup>5</sup>, Alexander Neumann<sup>1</sup>

<sup>1</sup> Department of Neuroradiology, University Medical Center Schleswig-Holstein, Luebeck, Germany

<sup>2</sup> Department of Internal Medicine I, University Medical Center Schleswig-Holstein, Luebeck, Germany

<sup>3</sup> Department of Neurosurgery, University Medical Center Schleswig-Holstein, Luebeck, Germany

<sup>4</sup> Department of Radiation Oncology, University Medical Center Schleswig-Holstein, Luebeck, Germany

<sup>5</sup> Department of Pediatric Oncology and Hematology, University Medical Center Schleswig-Holstein, Luebeck, Germany

<sup>6</sup> Department of Radiology and Neuroradiology, University Medical Center Schleswig-Holstein, Kiel, Germany

<sup>7</sup> Institute for Endocrinology and Diabetes, University of Luebeck, Germany

Radiol Oncol 2021; 55(3): 274-283.

Received 25 January 2021

Accepted 20 June 2021

Correspondance to: Alexander Neumann, MD, Department of Neuroradiology, University Medical Center Schleswig-Holstein, Ratzeburger Allee 160, 23538 Luebeck, Germany. E-mail: alexander.neumann@uksh.de

Lucas Becker and Judith Gebauer contributed equally and shared first authorship.

Disclosure: No potential conflicts of interest were disclosed.

This is an open access article under the CC BY-NC-ND license (<http://creativecommons.org/licenses/by-nc-nd/4.0/>).

**Introduction.** Radiation-induced cavernomas (RIC) after cranial radiotherapy have an unknown risk of hemorrhage. Zabramski magnetic resonance imaging (MRI) classification is touted as being able to indicate non-radiation-induced cavernomas hemorrhage risk. The aim of our study was to assess the hemorrhage risk of RIC during long-term follow-up of childhood cancer survivors based on brain MRI examinations.

**Patients and methods.** We analyzed retrospectively long-term follow-up data of 36 childhood cancer survivors after initial diagnosis with acute leukemia (n = 18) or brain tumor (n = 18), all treated with cranial radiotherapy. Detected RIC in long-term follow-up brain MRI (1.5 or 3 Tesla) were classified following the Zabramski MRI classification and were categorized into "high" (Zabramski type I, II or V) or "low" (type III or IV) risk of hemorrhage.

**Results.** 18 patients (50%) showed RIC with a significant relation to the original tumor entity (p = 0.023) and the cumulative radiation dose to the brain (p = 0.016): all 9 childhood cancer survivors diagnosed with medulloblastoma developed RIC. We classified RIC in only 3/36 childhood cancer survivors (8%) (1 patient with acute lymphoblastic leukemia [Zabramski type II] and 2 patients with medulloblastoma [type I and type II]) as high risk for hemorrhage, the remaining RIC were classified as Zabramski type IV with low risk for hemorrhage. None of the childhood cancer survivors with RIC showed symptomatic hemorrhages.

**Conclusions.** RIC are common late effects in childhood cancer survivors treated with cranial radiotherapy affecting half of these patients. However, only a few RIC (occurring in 8% of all reviewed childhood cancer survivors) were classified as high risk for hemorrhage and none of the childhood cancer survivors with RIC developed symptomatic hemorrhages. Thus, we conclude that RIC are low-risk findings in brain MRI and the course is mainly benign.

Key words: childhood cancer survivors; cranial radiotherapy; cavernomas; hemorrhage; brain magnetic resonance imaging

## Introduction

In recent decades, the percentage of children who can be cured from cancer has increased steadily, resulting in a growing number of childhood cancer survivors worldwide.<sup>1</sup> However, many of these childhood cancer survivors develop chronic health conditions emerging years to decades later as a consequence of cancer therapy.<sup>2</sup> Compared with chemo- or immunotherapy, late effects of radiation often occur in the former treated field, leading to subsequent neoplasms.<sup>3</sup> The cumulative radiation dose correlates with rates of subsequent tumors in the central nervous system (CNS) that include mostly meningiomas or gliomas.<sup>4</sup>

Furthermore, cranial radiotherapy is known to increase the risk of de novo formation of cerebral cavernomas (*syn.* cavernous angiomas, cavernous hemangiomas, cavernous malformation) as well, which also occur sporadically or following a familial etiology and represent benign venous malformations with low flow and low pressure.<sup>5,6</sup> However, while other radiation-induced neoplasms in most cases lead to rather clear-cut monitoring or therapy recommendations according to an interdisciplinary consensus, the handling approach for radiation-induced cavernomas (RIC) has yet to be defined, particularly in the context of the follow-up of childhood cancer survivors focused on here. Although the majority of cavernomas follow a complication-free course and do not require intervention, we are already aware of a tendency to symptomatic intracranial hemorrhage with potentially considerable clinical

impact and even subsequent need for surgery.<sup>7-10</sup> But so far systematic investigations concerning the hemorrhage risk of RIC, in particular, are not available.

Brain magnetic resonance imaging (MRI) is the modality of choice for the detection and follow-up imaging of cavernomas.<sup>11,12</sup> In 1994, Zabramski *et al.* defined a grading system for familial cavernomas depending on MRI findings (Table 1).<sup>13</sup> Nikoubashman *et al.* took up this classification in the recent past and investigated criteria to calculate prospective annual hemorrhage rates of cavernomas.<sup>14</sup> The study showed high bleeding risks for Zabramski type I (29.8%), type II (20.1%) and a proposed new type V (23.1%) and low bleeding risks for type III and IV (3.4% and 1.3% respectively). But in their study patients with a history of irradiation were explicitly excluded.<sup>14</sup>

Thus it remains unclear whether Nikoubashman's interpretation of the MRI appearance of cavernomas based on the Zabramski classification might be helpful for estimation of the hemorrhage risk of RIC. We would like to help clarify this and therefore set our sights on assessing for the first time the risk of hemorrhage of RIC in the long-term follow-up of childhood cancer survivors with brain MRI in this case series.

## Patients and methods

This study was approved by the Institutional Review Board of the University of Luebeck (14–180, 18–087).

**TABLE 1.** MRI classification of cerebral cavernomas according to Zabramski *et al.*: type I, type II and an additionally proposed new type V are associated with higher prospective hemorrhage rates, as published by Nikoubashman *et al.* in connection with non-radiation induced cavernomas<sup>13,14</sup>

Lesion type	MRI signal characteristics	Pathological characteristics
Type I	T1: hyperintense core T2: hyper- or hypointense core with surrounding hypointense rim	Subacute hemorrhage, surrounded by a rim of hemosiderin-stained macrophages and gliotic brain
Type II	T1: reticulated mixed-signal core T2: reticulated mixed-signal core with surrounding hypointense rim	Loculated areas of hemorrhage and thrombosis of varying ages, surrounded by gliotic, hemosiderin-stained brain; in large lesions, areas of calcification may be seen
Type III	T1: iso- or hypointense core T2: hypointense with a hypointense rim that magnifies the size of the lesion GE: hypointense with greater magnification than T2	Chronic resolved hemorrhage, with hemosiderin staining within and around the lesion
Type IV	T1: poorly seen or not visualized at all T2: poorly seen or not visualized at all GE: punctate hypointense lesions	Two lesions in the category were pathologically documented as telangiectasias
Type V	T1 and T2: visible parts in the center of the actual cavernoma; the cavernoma is not fully distinguishable from hemorrhage	

GE = gradient echo sequence

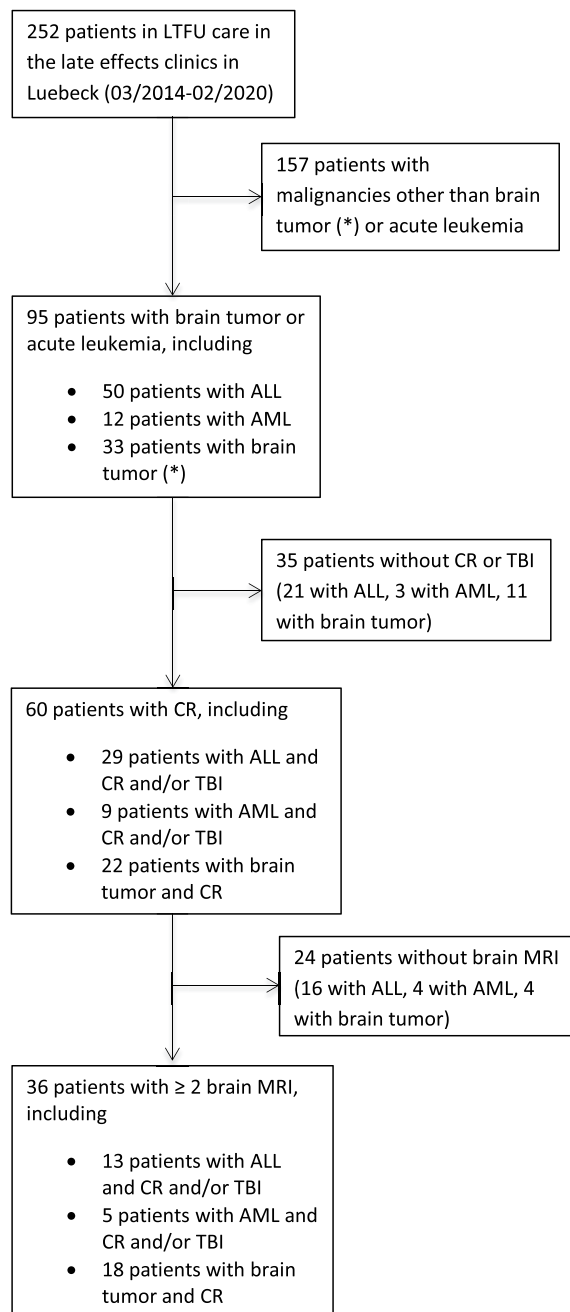


FIGURE 1. Flowchart of the patient selection process.

\* = craniopharyngeoma, ependymoma, germinoma, medulloblastoma; ALL = acute lymphoblastic leukemia; AML = acute myeloid leukemia; CR = cranial radiotherapy; LTFU = long-term follow-up; MRI = magnetic resonance imaging; TBI = total body irradiation

## Patients

We retrospectively analyzed 36 childhood cancer survivors out of 252 patients who were examined in the late effects clinic at the University Medical Center Schleswig Holstein in Luebeck over a pe-

riod of 6 years (03/2014–02/2020). We limited the analysis to patients with acute leukemia or brain tumors who had been treated with cranial radiotherapy (alone or as part of total body irradiation) and had received cranial imaging as part of their follow-up. Additionally, at least 2 brain MRI examinations (1 at the time of the initial tumor diagnosis and at least 1 in the follow-up) were required for inclusion in the study. The patients at the late effects clinic (i) were younger than 18 at cancer diagnosis, (ii) were at least 18 at first follow-up in the clinic and (iii) survived at least 5 years after the end of cancer therapy. Exclusion criteria for the study were (i) active malignancy and (ii) lack of consent. See the flowchart of the patient selection process in Figure 1.

## Magnetic resonance imaging of the brain including detection and classification of radiation-induced cavernomas

All patients received cranial imaging with at least one follow-up MRI of the brain on 1.5 or 3 Tesla scanners. The MRI sequence protocol for detection and classification of RIC included a T1, T2 and T2\*/susceptibility weighted imaging. Available brain MRI examinations were assessed and compared by two experienced neuroradiologists in consensual decisions. RIC were consensually detected and classified following the Zabramski classification and categorized into “high” ( $\geq 1$  type I and/or II and/or type V, in accordance with the proposal of Nikoubashman *et al.*<sup>14</sup>) or “low” (only type III and/or IV) risk of hemorrhage. Furthermore, other intracranial tumors as well as leukoencephalopathy and brain atrophy were analyzed. Leukoencephalopathy was graded into “mild” (focal lesions with hyper-intense signal in T2), “moderate” (confluent lesions) and “extensive” (diffuse lesions). Detected brain atrophy was divided semi-quantitatively into “mild”, “moderate” and “severe”.

## Statistical analysis

Clinical and imaging data were collected in a standardized pseudonymized data file. Most data were analyzed in a descriptive manner. For statistical analysis we used the software IBM® SPSS® (IBM Corp. Released 2016. IBM SPSS Statistics for Windows, Version 24.0. Armonk, NY: IBM Corp.). Categorical variables were analyzed in contingency tables using chi-squared test, or, if applicable, with the Fisher exact test. Mann-Whitney U test was used to compare continuous variables.

For the calculation of a possible association between the age at the initial tumor diagnosis (acute leukemia or brain tumor) and the occurrence of RIC the patients were dichotomized into the two groups “younger age” ( $\leq 8$  years) and “older age” ( $> 8$  years) based on the median age calculated in this collective.

Statistical significance was accepted at  $p < 0.05$ .

## Results

### Childhood cancer survivors

The study group of childhood cancer survivors consisted of 36 patients with the diagnosis of acute leukemia or brain tumor. At the time of the initial cancer diagnosis their age ranged from 1 to 25 years (median 8 years, interquartile range [IQR] 5–14 years). There were 19 female (median 7 years, IQR 3–14 years) and 17 male (median 10 years, IQR 6–15 years). We found no significant difference in the age profile between the two gender groups ( $p = 0.505$ ).

In particular, initial childhood cancer diagnoses were acute lymphoblastic leukemia (ALL) ( $n = 13$ ), acute myeloid leukemia (AML) ( $n = 5$ ), pilocytic astrocytoma ( $n = 2$ ), intracranial germinoma ( $n = 3$ ), medulloblastoma ( $n = 9$ ) and ependymoma ( $n = 3$ ) with need for cranial radiotherapy and polychemotherapy.

The median period of the last long-term follow-up examination in our late effects clinics after initial tumor diagnosis was 18 years (IQR 13–29).

### Cranial radiotherapy

Cranial radiotherapy was applied in conventional fractionation for patients with ALL, AML, pilocytic astrocytoma and germinoma. However, in patients with medulloblastoma, cranial radiotherapy was given in conventional fractionation or as hyperfractionated treatment. Moreover, one patient with craniopharyngeoma was treated with proton therapy. The exact cumulative radiation dose to the brain could not be evaluated in this case. In patients with acute leukemia, total body irradiation consisted of  $2 \times 2.0$  Gray (Gy) daily in three consecutive days. See Table 2 for scheme of cranial radiotherapy according to treatment protocols.

The median cumulative radiation dose in the 35 patients analyzed was 30.6 Gy (IQR 12–55 Gy). In all patients, no serious radiation-induced toxicities were reported. Individual's cumulative radiation doses to the brain are listed in Table 3.

TABLE 2. Cranial radiotherapy according to treatment protocols

Tumor entity	Dose/day	Number of fractions
ALL	1.5 Gy	8, 12, 16, 20 or 26
AML	1.5 Gy	8 or 10
Pilocytic Astrocytoma	1.8 Gy	28 or 30
Germinoma	1.6 Gy	15 or 25
Medulloblastoma	1.8 Gy	30 or 34
	$2 \times 1.0$ Gy (hyperfractionated)	30 or 34

ALL = acute lymphoblastic leukemia; AML = acute myeloid leukemia; Gy = Gray

### Follow-up brain magnetic resonance imaging and findings of radiation-induced cavernomas

Childhood cancer survivors received between 2 and 31 MRI examinations of the brain and we analyzed in total 383 MRI examinations. Radiation-induced meningiomas were found in four patients (11%), one of whom had 2 and another had 5 meningiomas. Furthermore, in one patient we found a possible vestibular schwannoma, which, however, could not be reliably distinguished from an aneurysmal bone cyst via imaging. Gliomas were not detected in long-term follow-up. Leukoencephalopathies were found in 28 patients (78%), while 12 of those 28 (43%) were mild, 10 were moderate (36%) and 6 extensive (21%). According to semi-quantitative analysis we found brain atrophy in 8 patients (22%): Five of them mild (62.5%) and three moderate (36.5%), but detected no cases of severe brain atrophy.

For further long-term comorbidities see Table 3.

In long-term follow-up 162 of 383 brain MRI examinations (42%) did not meet inclusion criteria because of lacking T2\*/susceptibility weighted imaging sequences or movement or other artifacts. Thus, we were able to analyze 221 brain MRI examinations (58%) concerning RIC.

18/36 patients (50%) showed RIC. We found a significant relation of existing RIC to the original tumor entity ( $p = 0.023$ ) and to the cumulative radiation dose to the brain ( $p = 0.016$ ).

The occurrence of RIC was equal in female ( $n = 9$ ) and male patients ( $n = 9$ ) ( $p = 0.500$ ). There was no significant association between the occurrence of RIC with the age at initial tumor diagnosis respectively start of cranial radiotherapy. Furthermore, we found no significant differences of RIC in the dichotomized patient groups “younger age” ( $\leq 8$  years, RIC  $n = 8$ ) and “older age” ( $> 8$  years, RIC  $n = 10$ ) ( $p = 0.370$ ).

TABLE 3. Patient characteristics, therapy data, findings of radiation-induced cavernomas and other comorbidities

No.	Gender (F=female; M=male)	Initial tumor diagnosis	Age at diagnosis (years)	Cumulative radiation dose to the brain (Gy)	Total number of brain MRI	Detection of RIC	Latency between CR and RIC (years)	Zabramski classification	RIC localization (1=supratentorial; 2=infratentorial; 3=both)	RIC dynamic	Other benign tumors in follow-up brain MRI	Leukoencephalopathy (mild; moderate; extensive)	Brain atrophy (mild; moderate; severe)	Other comorbidities in the long term	Period of follow-up (years)
1	F	ALL	17	24	9						Meningioma	moderate	-	COPD, hypercholesterolemia, hyperparathyroidism, migraine	44
2	F	ALL	1	12	2							mild	-	Lipedema, fibroepithelioma	26
3	F	ALL	3	12	2							-	-	Class I obesity	22
4	F	ALL	7	18	2							mild	-	CRF, class II obesity, hypercholesterolemia, hypopituitarism, thyroid nodules	37
5	F	ALL	3	24	4	+	40	II	3	+	Meningioma	extensive	mild	Hypercholesterolemia, class I obesity, thyroid nodules, scoliosis, myoma uteri	44
6	F	ALL	21	24	2	+	10	IV	1			mild	-	Reduced left ventricular ejection fraction, class III obesity, multiple vein thrombosis	13
7	M	ALL	5	12	2							-	-	Hypercholesterolemia	19
8	F	ALL	9	12	2							mild	-	Hypercholesterolemia	28
9	M	ALL	11	30	9							mild	-	Hypogonadism, hypercholesterolemia,	13
10	F	ALL	7	30.6	3	+	29	IV	1		Meningioma	moderate	-	Basalioma, hyperparathyroidism, class II obesity, thyroid nodules	33
11	F	ALL	5	39	6						Vestibular schwannoma, DD aneurysmal bone cyst	mild	-	Diabetes mellitus type 2, hypercholesterolemia, steatosis hepatitis, congestive heart failure, restrictive lung disease, thyroid nodules, deep vein thrombosis, basalioma, CRF, vestibular schwannoma	39
12	M	ALL	2	30	2							moderate	-	Thyroid Nodules, hypopituitarism, diabetes mellitus type 2, CRF, steatosis hepatitis, cataract	35
13	F	ALL	2	12	4							moderate	-	Intellectual disability	17
14	F	AML	14	12	2	+	21	IV	1			mild	-	Thyroid nodules, hypercholesterolemia, hypertension, spondyloarthritis	26
15	M	AML	15	12	2							-	-	Thyroid nodules, restrictive lung disease, diabetes mellitus type 1, hypogonadism, hypercholesterolemia	31
16	F	AML	16	12	3	+	28	IV	3			moderate	-	Thyroiditis	18
17	F	AML	2	15	2	+	21	IV	3			-	-	Cataract, hypercholesterolemia, depression	24
18	F	AML	8	12	3							-	-	CRF, class II obesity, chronic pain, visual impairment	14
19	M	PA	1	54	28	+	23	IV	3			moderate	moderate	Hypopituitarism, stroke, epilepsy, hearing loss, hypercholesterolemia, gallstones	29
20	M	PA	17	50.4	24							moderate	-	Hypercholesterolemia	11
21	M	Geminoma	17	40	16							mild	-	Hypopituitarism, chronic renal failure	5
22	M	Geminoma	14	24	20							mild	-	Hypopituitarism, class I obesity, depression, hypercholesterolemia	9

No.	Gender (F=female; M=male)	Initial tumor diagnosis	Age at diagnosis (years)	Cumulative radiation dose to the brain (Gy)	Total number of brain MRI	Detection of RIC	Latency between CR and RIC (years)	Zabramski classification	RIC localization (1=supratentorial; 2=infratentorial; 3=both)	RIC dynamic	Other benign tumors in follow-up brain MRI	Leukoencephalopathy (mild; moderate; extensive)	Brain atrophy (mild; moderate; severe)	Other comorbidities in the long term	Period of follow-up (years)
23	M	Germinoma	10	40	21	+	5	IV	1			moderate	-	Depression, hypercholesterolemia, hypopituitarism	12
24	M	CP	17	n.a.	15							mild	-	Hypopituitarism, class I obesity, hypercholesterolemia, autoimmune polyendocrine syndrome type 2 with diabetes mellitus type 1, vitiligo, thyroiditis	13
25	F	Medulloblastoma	7	55	3	+	27	IV	2		Meningioma	-	mild	Hypothyroidism, thyroid nodules, hearing loss, asthma	28
26	M	Medulloblastoma	8	54	25	+	5	IV	3	+		mild	-	Hypopituitarism, hearing loss	14
27	M	Medulloblastoma	8	54	21	+	2	I	3	+		moderate	moderate	Hypopituitarism, hearing loss	10
28	M	Medulloblastoma	13	54	24	+	5	IV	2	+		moderate	-	Hypopituitarism, epilepsy, hearing loss, class I obesity, tetraparesis	10
29	M	Medulloblastoma	11	68.6	24	+	2	IV	3	+		-	mild	Spinal hygroma, hypothyroidism, growth hormone deficiency	14
30	M	Medulloblastoma	6	68.6	18	+	7	IV	3	+		-	-	Hypopituitarism, hearing loss, intellectual disability	19
31	M	Medulloblastoma	9	60	3	+	29	II	2			mild	-	Basaloma, hearing loss, intellectual disability	30
32	F	Medulloblastoma	25	60	6	+	18	IV	3			extensive	moderate	Coxarthrosis with total endoprosthesis, gonarthrosis	18
33	M	Medulloblastoma	2	60	13	+	7	IV	3			moderate	mild	Visual impairment, growth hormone deficiency, hypothyroidism, intellectual disability, hearing loss, steatosis hepatis	17
34	F	Ependy-moma	12	68	31	+	13	IV	3			moderate	mild	Hypopituitarism, chronic renal failure	13
35	F	Ependy-moma	6	72	28							extensive	-	-	13
36	F	Ependy-moma	7	68	10							mild	-	Asthma bronchiale	13

ALL = acute lymphoblastic leukemia; AML = acute myeloid leukemia; CRF = cancer related fatigue; COPD = chronic obstructive pulmonary disease; CP = craniopharyngeoma; CR = cranial radiotherapy; DD = differential diagnosis; MRI = magnetic resonance imaging; n.a. = not available; PA = pilocytic astrocytoma; PCHT = polychemotherapy; RIC = radiation-induced cavernomas

The cumulative radiation dose differed significantly between childhood cancer survivors with RIC (median 54 Gy [IQR 24–60 Gy]) and childhood cancer survivors without RIC (median 24 Gy [IQR 12–40 Gy]) ( $p = 0.019$ ).

All 9 childhood cancer survivors with treated medulloblastoma developed RIC (100%). Occurrences of RIC dependent on the other tumor entities were: ALL 3/13 (23%), AML 3/5 (60%), pilocytic astrocytoma 1/2 (50%), germinoma 1/3 (33%) and ependymoma 1/3 (33%). One patient with craniopharyngeoma did not develop RIC. We classified RIC only in 1 patient (3%) with ALL (Zabramski type II) and in 2 patients (6%) with medulloblastoma (Zabramski type I and type II) as high risk for hemorrhage while

all other detected RIC were classified as Zabramski type IV with low risk for hemorrhage. We did not find any statistically significant difference between RIC with low and high risk for hemorrhage depending on the original tumor entity ( $p = 0.737$ ). We did not categorize RIC as Zabramski type III or V, in accordance with the proposal of Nikoubashman *et al.*<sup>14</sup> Thus, only 3/18 childhood cancer survivors with RIC (17%) and 3 (8%) of all reviewed childhood cancer survivors with at least 2 brain MRI examinations developed lesions with a high risk for hemorrhage. As a main result of the study none of the childhood cancer survivors with RIC showed symptomatic intracranial hemorrhages. The localization of RIC was only supratentorial in 15 of the 36 childhood cancer

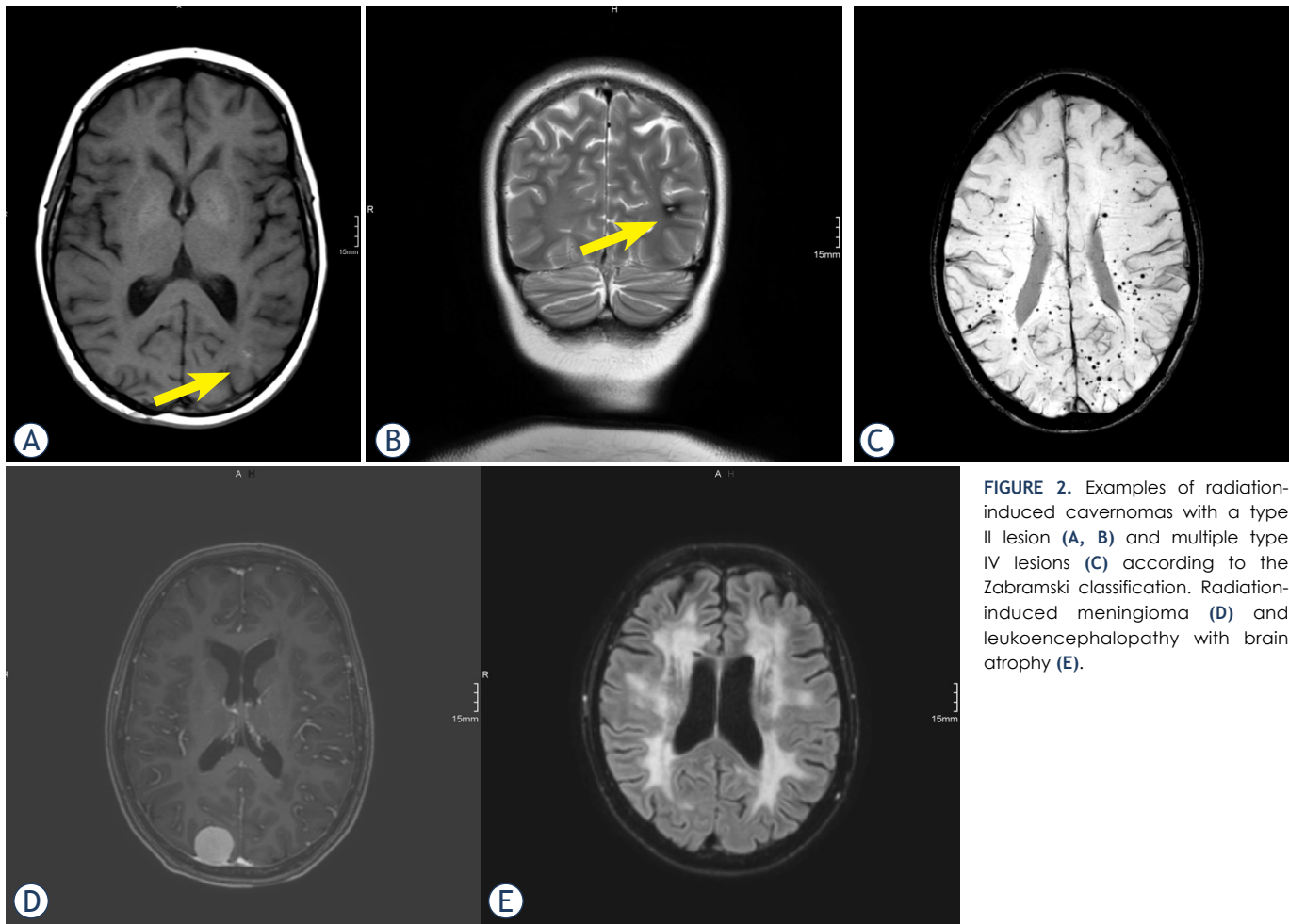


**FIGURE 2.** Examples of radiation-induced cavernomas with a type II lesion (A, B) and multiple type IV lesions (C) according to the Zabramski classification. Radiation-induced meningioma (D) and leukoencephalopathy with brain atrophy (E).

survivors (42%), in two childhood cancer survivors only infratentorial (5%) and in 19 childhood cancer survivors both supra- and infratentorial (53%). RIC occurred after cranial radiotherapy in a median time period of 15.5 years (IQR 5–27). Six of the 36 childhood cancer survivors (17%) showed dynamic findings of RIC, and there were changes in the number and/or size of individual RIC without any accompanying changes in the Zabramski classification. Three childhood cancer survivors (8%) developed only a single RIC documented in brain MRI. Table 3 shows the summarized results. Examples of brain magnetic resonance imaging from childhood cancer survivors during long long-term follow-up are shown in Figure 2.

## Discussion

The aim of this study was to describe for the first time the course of RIC during long-term follow-

up of childhood cancer survivors, those formerly treated with cranial radiotherapy in connection with the initial diagnosis of leukemia or brain tumor. We thus assessed the hemorrhage risk of RIC following Nikoubashman's interpretation of the MRI appearance of cavernomas based on the Zabramski classification and examined the question of how to deal with RIC that frequently appear in MRI follow-up examinations of childhood cancer survivors. In our experience to date this seems to be distinctly more difficult than providing recommendations regarding extraaxial or intraaxial neoplasms (especially meningiomas or gliomas), which have already been the subject of extensive discussion in relevant literature as long-term consequences.<sup>4</sup> Several guidelines, often based on a risk stratification system mainly taking into account the initial cancer diagnosis and the treatment received, recommend specific follow-up examinations to facilitate early diagnosis and treatment of these sequelae.<sup>15</sup>

Besides neoplasms, neurocognitive deficits in connection with pathological findings in brain MRI, such as leukoencephalopathy or brain atrophy, are reported in connection with childhood cancer survivors.<sup>16</sup> Also our results showed 4 radiation-induced meningiomas, but no gliomas. There were variable findings of leukoencephalopathy, brain atrophy and several other comorbidities, though this was not a focal point of our studies.

Our study focuses on RIC. An assumed correlation between cranial radiotherapy and cavernomas in children was primarily described in 1994.<sup>17</sup> In the following years this phenomenon was investigated extensively in several studies and summarized in review articles with a visible predominance in young patients treated for cancer.<sup>18-24</sup> Furthermore, researchers also looked into the question of whether RIC differ from other, sporadically or familiarly occurring cavernomas regarding their natural course. Baumgartner *et al.* showed findings after irradiation radiologically and pathologically similar to sporadically occurring cavernomas.<sup>25</sup> Cha *et al.*, on the other hand, found differences in histological findings in a comparison between 10 patients with “de novo” cavernomas and 7 patients with a total of 8 RIC and regarded the findings after radiation more as inactive organizing hematomas in blood-filled spaces after tissue destruction and thus different from proliferation of malformed vasculature in sporadic cavernomas.<sup>26</sup> According to a study with a specific histopathological focus based on 13 patients with RIC, there is, both histologically and with regard to immunohistochemistry, an overlap to non-radiation-induced cavernomas (5/13) as well as to organizing coagulum-like lesions (8/13), as described by Cha *et al.*, so that one must assume two different etiological mechanisms in the pathogenesis.<sup>27</sup>

Concerning RIC, our results include a significant relation to the initial tumor entity and the cumulative radiation dose to the brain, as reflected by the occurrence of RIC without exception in patients treated for medulloblastoma with high cumulative radiation doses. In 2007 Lew *et al.* looked at precisely such patients who had received radiation therapy for medulloblastomas in childhood and described cavernomas in this case as common with an increasing incidence over time.<sup>28</sup> They concluded that most of these lesions follow a benign course and do not require intervention.<sup>28</sup> Furthermore, results that show a correlation between RIC and the cumulative radiation dose can be found in a more recent study focusing on adult cancer patients.<sup>29</sup>

With regard to the correlation between RIC and cranial radiotherapy, data on the time lag of the oc-

currence after radiation are additionally available. Following examination of 5 patients with cavernomas after cranial or craniospinal irradiation, Jain *et al.* described a latency interval between treatment and time of detection of cavernomas with a mean of 19.5 years.<sup>5</sup> The latency that we found between cranial radiotherapy and detection of RIC with a median time period of 15.5 years matches these investigations (IQR 5–27). Moreover, Strenger *et al.* has published results that also focus on risk factors for the occurrence of RIC.<sup>30</sup> The investigations encompassed 171 patients and showed that particularly children < 10 years of age at the time of irradiation have a higher risk for RIC, whose occurrence was documented here as taking place in a period of 2.9–18.4 years after radiation.<sup>30</sup> Singla *et al.* examined the long-term course of irradiated patients and described for all of them an occurrence of cavernomas with a latency of 2–8 years – though only 5 patients with ALL were analyzed.<sup>31</sup>

Due to possible hemorrhage complications of RIC, the two latter studies very explicitly advocated imaging monitoring and Singla *et al.* described neurological symptoms and individual craniotomies because of RIC in 4 of 5 patients.<sup>30,31</sup> We did not document any symptomatic hemorrhages in connection with RIC in our patient group.

A number of studies have examined the hemorrhage risk of cavernomas in general. Flemming *et al.* calculated a prospective risk in this context in a group of 292 patients with cavernomas and consecutive hemorrhage.<sup>7</sup> It was determined that prior hemorrhage is one of the factors that may predict future hemorrhage.<sup>7</sup> One publication showed in a comparison of the features of RIC (32 patients) with other cavernomas (272 patients) no differences in symptomatic hemorrhages.<sup>32</sup> However, here RIC proved to be more likely to occur multilocular.<sup>32</sup> This matches our results, which predominantly showed multilocular and small lesions (Zabramski type IV). In particular, Nikoubashman *et al.* investigated those small, dot-like cavernomas in another study from 2013.<sup>33</sup> It shows a low bleeding rate of 0.7% per lesion-year according to a survey specifically of 18 children.<sup>33</sup> Nonetheless, it was propagated that even those small cavernomas are not purely benign lesions.<sup>33</sup>

It is certainly more difficult, however, to deal with lesions classified as Zabramski type I or II. As a reminder: type I is a (sub-)acute hemorrhage while type II as a “popcorn lesion” shows multiple hemorrhages. Here we again refer to data on the generally increased bleeding risk of cavernomas with already existing hemorrhage.<sup>7</sup> Among others,

Jeon *et al.* based their study of 326 adults with cavernomas, like us, on the Zabramski classification.<sup>34</sup> The study showed that not only prior symptomatic hemorrhage, but also MRI appearance could be related to prospective symptomatic hemorrhages of cavernomas.<sup>34</sup> The bleeding risk of cavernomas was also examined in a study by Al-Shahi Salman *et al.*, which additionally evaluated gender-specific differences.<sup>35</sup> This study found that the risk of recurrent hemorrhage is greater than the risk of a first bleeding event and greater for women than for men.<sup>35</sup>

As regards our results, we classified RIC as high risk for hemorrhage (Zabramski type I and II) in only 3 of 36 childhood cancer survivors (8%) and all other RIC were classified as low-risk lesions (Zabramski type IV [microhemorrhagic]). In this risk assessment we orient ourselves to the proposal made by Nikoubashman *et al.*<sup>14</sup> After analysis of 199 MRI examinations in total with 1558 distinct lesions this team depicted 5 different types of cavernomas via 1.5T MRI (T1, T2 and T2\*) while using a three-tier classification shown as graphic illustrations and corresponding MRI findings. It turned out that the cavernomas described as Zabramski type I, II and an additionally proposed new type V (with visible parts in the center of the actual cavernoma) had a significantly higher annual hemorrhage rate than type III and IV lesions.<sup>14</sup> Thus, the presence of acute or subacute blood degradation was statistically the strongest indicator for an increased hemorrhage risk with the conclusion that it is possible to predict hemorrhage rates based on the Zabramski classification.<sup>14</sup> As mentioned previously, these results were not related to RIC. Nevertheless, just in connection with RIC we consider the initial application of Nikoubashman's interpretation of the MRI appearance of cavernomas based on the Zabramski classification for an assessment of the hemorrhage risk to be a very meaningful approach.

It must be emphasized that in this retrospective case series half of the childhood cancer survivors examined in long-term follow-up showed RIC in follow-up brain MRI. Thus, our study supports the development of cavernomas after cranial radiotherapy as a common side effect in childhood cancer survivors, though most RIC are not likely to hemorrhage and are detected incidentally. Our results therefore suggest a mainly benign course of RIC. Consequently we conclude that the complication risk of RIC can definitely be described in good conscience as low in communication with childhood cancer survivors as long as one applies

assessments of existing classifications.<sup>13,14</sup> This ensures an advantageous aspect in dealing with patients who might feel anxious as a result of their prior cancer history. Studies with larger groups of patients and stronger study designs may possibly clarify whether dealing with RIC should be included and defined in the guidelines in connection with childhood cancer survivors.

Thus, we conclude that RIC are common late effects in childhood cancer survivors treated with cranial radiotherapy affecting half of the patients. However, only a few RIC (occurring in 8% of all reviewed childhood cancer survivors) were classified as high risk for hemorrhage and the majority of RIC follow a benign course. None of the childhood cancer survivors with RIC developed symptomatic hemorrhages. These results augment accurate risk assessment in individualized long-term follow-up also in order to reduce morbidity in childhood cancer survivors. In this context we are addressing an important point in the communication with childhood cancer survivors.

### Limitations

A retrospective approach with a relatively small sample size is a limitation of the present analysis. But, in particular, the accumulation of data concerning childhood cancer survivors also in the long-term follow-up, focused on here, is extremely rare, also in university hospitals. Nevertheless we strongly believe that this to our knowledge first study of this specific topic is valuable to assess the clinical relevance of radiation-induced cavernomas in brain MRI and add to be clear about their low risk for hemorrhage (with importance for patients and for physicians).

We are also restricted by the selection bias concerning inconsistent brain MRI data with lack of standardized imaging protocols in many MRI examinations conducted abroad and in some cases only a single follow-up examination with an extensive time lag until radiation. Furthermore, we did not focus on a detailed description of the irradiated fields, in particular, and the localization of RIC in our patient group, but we propose that this topic should be assessed after examination of larger collectives. The correlation between RIC and cranial radiotherapy that we assume in our results naturally remains unproven, also histologically, in the end (in this connection, the differential diagnoses cerebral microhemorrhages or teleangiectasias also have to be considered). The extent to which hemorrhages from cavernomas correlate with clinical

symptoms is a complex issue of its own that this study cannot resolve on the basis of a relatively small group without symptomatic hemorrhages.

## References

- Miller KD, Nogueira L, Mariotto AB, Rowland JH, Yabroff KR, Alfano CM, et al. Cancer treatment and survivorship statistics, 2019. *CA Cancer J Clin* 2019; **69**: 363-85. doi: 10.3322/caac.21565
- Oeffinger KC, Mertens AC, Sklar CA, Kawashima T, Hudson MM, Meadows AT, et al. Chronic health conditions in adult survivors of childhood cancer. *N Engl J Med* 2006; **355**: 1572-82. doi: 10.1056/NEJMsa060185
- Armstrong GT, Stovall M, Robison LL. Long-term effects of radiation exposure among adult survivors of childhood cancer: results from the childhood cancer survivor study. *Radiat Res* 2010; **174**: 840-50. doi: 10.1667/RR1903.1
- Bowers DC, Nathan PC, Constine L, Woodman C, Bhatia S, Keller K, et al. Subsequent neoplasms of the CNS among survivors of childhood cancer: a systematic review. *Lancet Oncol* 2013; **14**: e321-8. doi: 10.1016/S1470-2045(13)70107-4
- Jain R, Robertson PL, Gandhi D, Gujar SK, Muraszko KM, Gebarski S. Radiation-induced cavernomas of the brain. *AJNR Am J Neuroradiol* 2005; **26**: 1158-62.
- Hoz SS. Cavernoma and other malformations. In: Hoz SS, editor. *Vascular neurosurgery*. Berlin: Springer, Cham. 2017. p.p. 137-47. doi: 10.1007/978-3-319-49187-5\_4
- Flemming KD, Link MJ, Christianson TJ, Brown RD Jr. Prospective hemorrhage risk of intracerebral cavernous malformations. *Neurology* 2012; **78**: 632-6. doi: 10.1212/WNL.0b013e318248de9b
- Consales A, Piatelli G, Ravegnani M, Pavanello M, Striano P, Zoli ML, et al. Treatment and outcome of children with cerebral cavernomas: a survey on 32 patients. *Neural Sci* 2010; **31**: 117-23. doi: 10.1007/s10072-009-0157-0
- Giulioni M, Acciari N, Padovani R, Galassi E. Results of surgery in children with cerebral cavernous angiomas causing epilepsy. *Br J Neurosurg* 1995; **9**:135-41. doi: 10.1080/0268869950041467
- Acciari N, Galassi E, Giulioni M, Pozzati E, Grasso V, Palandri G, et al. Cavernous malformations of the central nervous system in the pediatric age group. *Pediatric Neurosurgery* 2009; **45**: 81-104. doi: 10.1159/000209283
- Hegde AN, Mohan S, Lim CC. CNS cavernous haemangioma: "popcorn" in the brain and spinal cord. *Clin Radiol* 2012; **67**: 380-8. doi: 10.1016/j.crad.2011.10.013
- Awad IA, Polster SP. Cavernous angiomas: deconstructing a neurosurgical disease. *J Neurosurg* 2019; **131**: 1-13. doi: 10.3171/2019.3.JNS181724
- Zabramski JM, Wascher TM, Spetzler RF, Johnson B, Golfinos J, Drayer BP, et al. The natural history of familial cavernous malformations: results of an ongoing study. *J Neurosurg* 1994; **80**: 422-32. doi: 10.3171/jns.1994.80.3.0422
- Nikoubashman O, Rocco FD, Davagnanam I, Mankad K, Zerah M, Wiesmann M. Prospective hemorrhage rates of cerebral cavernous malformations in children and adolescents based on MRI appearance. *AJNR Am J Neuroradiol* 2015; **36**: 2177-83. doi: 10.3174/ajnr.A4427
- Children's Oncology Group. Long-term follow-up guidelines for survivors of childhood, adolescent, and young adult cancer. Version 4.0, October 2013. [cited 2021-01-10]. Available at: [www.survivorshipguidelines.org/pdf/ltfuguidelines\\_40.pdf](http://www.survivorshipguidelines.org/pdf/ltfuguidelines_40.pdf)
- Cheung YT, Sabin ND, Reddick WE, Bhojwani D, Liu W, Brinkman TM, et al. Leukoencephalopathy and long-term neurobehavioural, neurocognitive, and brain imaging outcomes in survivors of childhood acute lymphoblastic leukaemia treated with chemotherapy: a longitudinal analysis. *Lancet Haematol* 2016; **3**: e456-e66. doi: 10.1016/S2352-3026(16)30110-7
- Ciricillo SF, Cogen PH, Edwards MS. Pediatric cryptic vascular malformations: presentation, diagnosis and treatment. *Pediatr Neurosurg* 1994; **20**: 137-47. doi: 10.1159/000120776
- Nimjee SM, Powers CJ, Bulsara KR. Review of the literature on de novo formation of cavernous malformations of the central nervous system after radiation therapy. *Neurosurgical Focus* 2006; **21**: 1-6. doi: 10.3171/foc.2006.21.1.5
- Di Giannatale A, Morana G, Rossi A, Cama A, Bertoluzzo L, Barra S, et al. Natural history of cavernous malformations in children with brain tumors treated with radiotherapy and chemotherapy. *J Neurooncol* 2014; **117**: 311-20. doi: 10.1007/s11060-014-1390-9
- Baumgartner JE, Ater JL, Ha CS, Kuttesch JF, Leeds NE, Fuller GN, et al. Pathologically proven cavernous angiomas of the brain following radiation therapy for pediatric brain tumors. *Pediatr Neurosurg* 2003; **39**: 201-7. doi: 10.1159/000072472
- Heckl S, Aschoff A, Kunze S. Radiation-induced cavernous hemangiomas of the brain. *Cancer* 2002; **94**: 3285-3291. doi: 10.1002/cncr.10596
- Lena G, Ternier J, Paz-Paredes A, Scavarda D. Central nervous system cavernomas in children. *Neurochirurgie* 2007; **53**: 223-37. doi: 10.1016/j.neuchi.2007.02.011
- Burn S, Gunny R, Phipps K, Gaze M, Hayward R. Incidence of cavernoma development in children after radiotherapy for brain tumors. *J Neurosurg* 2007; **106**: 379-83. doi: 10.3171/ped.2007.106.5.379
- Mottolose C, Hermier M, Stan H, Jouvét A, Saint-Pierre G, Froment JC, et al. Central nervous system cavernomas in the pediatric age group. *Neurosurg Rev* 2001; **24**: 55-71. doi: 10.1007/pl00014581
- Baumgartner JE, Ater JL, Ha CS, Kuttesch JF, Leeds NE, Fuller GN, et al. Pathologically proven cavernous angiomas of the brain following radiation therapy for pediatric brain tumors. *Pediatr Neurosurg* 2003; **39**: 201-7. doi: 10.1159/000072472
- Cha YJ, Nahm JH, Ko JE, Shin HJ, Chang J-H, Cho NH, et al. Pathological evaluation of radiation-induced vascular lesions of the brain: Distinct from de novo cavernous hemangioma. *Yonsei Med J* 2015; **56**: 1714-20. doi: 10.3349/ymj.2015.56.6.1714
- Kleinschmidt-DeMasters BK, Lillehei KO. Radiation-induced cerebral vascular "Malformations" at biopsy. *J Neuropathol Exp Neurol* 2016; **75**: 1081-92. doi: 10.1093/jnen/nlw085
- Lew SM, Morgan JN, Psaty E, Lefton DR, Allen JC, Abbott R. Cumulative incidence of radiation-induced cavernomas in long-term survivors of medulloblastoma. *J Neurosurg* 2006; **104**: 103-7. doi: 10.3171/ped.2006.104.2.103
- Cacho-Díaz B, Salmerón-Moreno K, Lorenzana-Mendoza N, Reyes A, Valdés-Ferrer SI, Gómez-Ahumada G, et al. Radiotherapy induced cavernomas in adult cancer patients. *Radiother Oncol* 2018; **127**: 287-291. doi: 10.1016/j.radonc.2018.02.026
- Strenger V, Sovinz P, Lackner H, Dornbusch HJ, Lingitz H, Eder HG, et al. Intracerebral cavernous hemangioma after cranial irradiation in childhood. Incidence and risk factors. *Strahlenther Onkol* 2008; **184**: 276-80. doi: 10.1007/s00066-008-1817-3
- Singla A, Brace O'Neill J, Smith E, Scott RM. Cavernous malformations of the brain after treatment for acute lymphocytic leukemia: presentation and long-term follow-up. *J Neurosurg Pediatr* 2013; **11**:127-32. doi: 10.3171/2012.11.PEDS12235
- Cutsforth-Gregory JK, Lanzino G, Link MJ, Brown Jr RD, Flemming KD. Characterization of radiation-induced cavernous malformations and comparison with a nonradiation cavernous malformation cohort. *J Neurosurg* 2015; **122**: 1214-22. doi: 10.3171/2015.1.JNS141452
- Nikoubashman O, Wiesmann M, Tournier-Lasserre E, Mankad K, Bourgeois M, Brunelle F, et al. Natural history of cerebral dot-like cavernomas. *Clin Radiol* 2013; **68**: e453-59. doi: 10.1016/j.crad.2013.02.010
- Jeon JS, Kim JE, Chung YS, Oh S, Ahn JH, Cho WS, et al. A risk factor analysis of prospective symptomatic haemorrhage in adult patients with cerebral cavernous malformation. *J Neurol Neurosurg Psych* 2014; **85**: 1366-70. doi: 10.1136/jnnp-2013-306844
- Al-Shahi Salman R, Hall JM, Horne MA, Moultrie F, Josephson CB, Bhattacharya JJ, et al. Untreated clinical course of cerebral cavernous malformations: a prospective, population-based cohort study. *Lancet Neurol* 2012; **11**: 217-24. doi: 10.1016/S1474-4422(12)70004-2

## research article

# Sialendoscopy and CT navigation assistance in the surgery of sialolithiasis

Aleksandar Anicin<sup>1,2</sup>, Jure Urbancic<sup>1,2</sup><sup>1</sup> Department of Otorhinolaryngology and Cervicofacial Surgery, University Medical Center Ljubljana, Ljubljana, Slovenia<sup>2</sup> Faculty of Medicine, University of Ljubljana, Ljubljana, Slovenia

Radiol Oncol 2021; 55(3): 284-291.

Received 8 February 2021

Accepted 25 February 2021

Corresponding author: Assist. Prof. Aleksandar Aničin, Ph.D., M.D., Department of Otorhinolaryngology and Cervicofacial Surgery, University Medical Center Ljubljana, Zaloška 2, SI-1000 Ljubljana, Slovenia. E-mail: aleksandar.anicin@kclj.si

Disclosure: No potential conflicts of interest were disclosed.

Authors' contributions: Both authors contributed equally to the article.

This is an open access article under the CC BY-NC-ND license (<http://creativecommons.org/licenses/by-nc-nd/4.0/>).

**Background.** A sialendoscopy-assisted combined approach is well established in the surgery of sialolithiasis. In cases of proximal salivary stones, transcutaneous sialendoscopy-assisted extractions with parotid and submandibular gland preservation is the primary intention of treatment. We recently added computer tomography (CT) navigation to improve the results of this challenging surgery equally in both localizations.

**Patients and methods.** All the patients who submitted to sialendoscopy and sialendoscopy-assisted procedures at the tertiary institution between January 2012 and October 2020 were included in the present study. From November 2019, CT navigation was added in cases with sialolithiasis and a presumably poor sialendoscopic visibility. We evaluated the parameters of the disease, diagnostic procedures, sialendoscopic findings and outcomes, with or without optical surgical navigation.

**Results.** We performed 178 successful salivary stone removals in 372 patients, of which 118 were combined sialendoscopy-assisted approaches, including 16 transcutaneous proximal, 10 submandibular and 6 parotid stone operations. Surgical navigation was used in six patients, four times for submandibular and twice for parotid sialolithiasis. These were all non-palpable, sialendoscopically invisible or partially visible stones, and we managed to preserve five of the six salivary glands.

**Conclusions.** The addition of CT navigation to sialendoscopy-assisted procedures for non-palpable, sialendoscopically invisible and fixed stones is a significant advantage in managing sialolithiasis. By consistently performing sialendoscopy and related preservation procedures, we significantly reduced the need for sialoadenectomies in patients with obstructive salivary gland disease.

Key words: sialendoscopy; sialolithiasis; surgical navigation; computer tomography

## Introduction

Sialendoscopy enables us to remove most salivary stones and, consequently, preserve salivary glands.<sup>1,2</sup> In cases with a tortuous course of the salivary ducts, far proximal stone position and corresponding narrow duct diameter, or with stones located behind the stricture, deeply embedded or positioned in an abscess formation, even the use of sialendoscopy can be insufficient in determining the exact position of the stone. Transcutaneous

sialendoscopy-assisted combined stone removals with intended gland preservation are particularly demanding, and their outcome may be unpredictable. The ongoing search for an additional guiding system is therefore justified.<sup>3</sup> Attempts to use ultrasound as guidance to help locate difficult salivary stones during surgery have been reported in previous years. However, its use is highly dependent on various factors, including the lack of direct stone visualization.<sup>4</sup> Surgical navigation using a computer tomography scan (CT) is regularly used in an-

terior skull base and paranasal sinus surgery with high precision.<sup>5</sup> Under clinical conditions, an accuracy of about 2 mm is expected.<sup>6</sup> It has been applied in various other therapeutic scenarios, including electrochemotherapy of deep-seated tumors in the head and neck region.<sup>7</sup> Following experiences reported by Capaccio *et al.*,<sup>8</sup> we therefore added CT-based navigation to the demanding combined approach to stone extractions to improve our results. To the best of our knowledge, we describe the first series in which navigation was used to locate the salivary stones and present it in the context of other endoscopic and combined salivary stone removals.

## Patients and methods

Data were prospectively collected in an institutional sialendoscopic database. On the proposal of the European Sialendoscopic Training Centre (ESTC), the database is a common source of data on imaging results before sialendoscopy, the exact indications for these procedures and their type, the procedure's findings, and follow-up.<sup>9,10</sup> All patients signed written consent for the respected procedure and data collection according to hospital policy.

### Ultrasound diagnostics

Ultrasound examination was carried out in all patients to evaluate major salivary glands and their ductal systems and to detect any ultrasonographically visible salivary stones and to exclude possible tumor growth.

### Mandibular occlusal radiography

We used mandibular occlusal radiography as a standard native X-ray method with a good sensitivity for radiopaque alterations of the floor of the mouth, including salivary calculi.<sup>11</sup>

### Computer tomography

The CT scan was primarily used to display more precisely the localization and number of salivary stones. Secondly, the use of CT enabled an estimation of the glands, their ducts and surrounding tissues. We performed contrast-enhanced CT in all cases of relapsing/persistent or complicated sialolithiasis, in order to show salivary stones, their embedded or even extraluminal position and possible abscess formation or other soft tissue formations related to sialolithiasis with a more chronic course.

### Magnetic resonance sialography

Standard and magnetic resonance imaging (MRI)-based sialography were used in sialendoscopically identified impassable distal strictures. We occasionally added standard MRI to estimate the status of glandular parenchyma.

### X-ray sialography

Conventional sialography is performed by retrograde injection of contrast agents into the salivary duct. The procedure involves instrumenting the duct for its cannulation and the possibility of injury or irritation. Although rarely used since other techniques have been readily available, in skilled hands, it produces characteristic imaging of the ductal anatomy, pathology (strictures and dilations) and adjacent parenchymal pathology.<sup>12</sup>

### Surgical navigation

After the workup described above, we performed sialendoscopic and sialendoscopy-assisted procedures. Our database was reviewed for less than sufficient endoscopic exposition in purely endoscopic and combined procedures from January 1st 2012 to October 31st 2020. We compiled the criteria for the use of the CT navigation listed in Table 1. CT navigation was added from November 2019 in all planned combined sialendoscopy-assisted surgery cases if three or more inclusion criteria were met.

A CT scan of the facial and salivary structures was done one day before surgery with 4 or 5 radiopaque surface fiducial markers (Figure 1). They were placed directly on the skin. Their position was additionally marked with a waterproof skin marker. The exact position was chosen according to the planned approach and incision placement. It has to be emphasized that the arrangement should preferably be on hard anatomical parts of the

**TABLE 1.** Inclusion criteria for the use of CT navigation (if three or more criteria were met)

Non-palpable stone
Difficult or impossible sialendoscopic visualization of the stone
Far proximal stone
Presumably fixed stone
Extraluminal stone (in an abscess or deeply embedded)
Salvage procedure with previously failed sialendoscopy or sialendoscopy-assisted procedure



FIGURE 1. Patient, prepared for surgery. With fiducial markers attached to the skin and navigational star on the patient's forehead (BrainLab, Munchen, Germany).

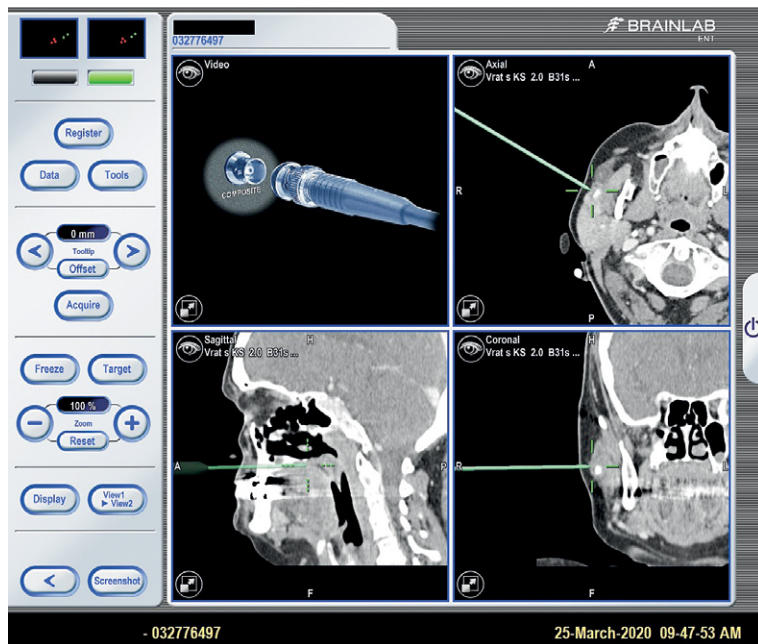


FIGURE 2. After identifying the skin's reference point with the stone being visible in the three-axis, the surgical trajectory is checked by the navigation.

face. Differences in jaw angle during CT imaging and when the patient is under general anesthesia were avoided by using a standard dental mouth gag in both situations. Acquired data in standard digital imaging and communication in medicine (DICOM) format were transferred to navigation Brainlab Kolibri (Brainlab, Munchen, Germany). Fiducial markers were automatically recognized

by the navigation software (Brainlab Cranial ENT V 2.1). No additional ad-hoc markers were chosen. The registration was done by touching the markers only. When the system perceived their order as ambiguous, the navigation itself chose the appropriate registration points sequence. When at least medium precision was achieved (self-assessment of the system), we checked the position of known anatomical landmarks and reconfirmed the accuracy to the surgeon's preference.

The first goal was to find the salivary stone's external approach path with the navigational tool lightly pressed on the skin. Since the CT presentation is divided into axial, coronal and sagittal planes, the surgeon must see the stone on all the planes. The trajectory may only then be approved. Both authors approved the trajectory before the continuation of the procedure. The contact point on the skin was marked as point zero, and the angle of the instrument was checked by both surgeons.

After incision and careful preparation, special care was taken not to change the position of the lower jaw. It can change the navigation accuracy when dealing with submandibular pathology; the same mouth gag in the same position was therefore used again.

The orientation axis is an imaginary line from point zero on the skin to the deep-seated stone (Figure 2). During the dissection, the surgeon is virtually travelling through tissue on the same three-dimensional pathway from a stone's skin reference point. When necessary, an additional sialendoscopic approach was made to control the position of the stone. It also represented backup guidance in the final approach to the stone (Figure 3). Stones were removed through transcutaneous (Figure 4) or transoral incisions. Routine facial nerve neuromonitoring (Medtronic, Jacksonville, USA) was used in all transcutaneous procedures. Data analysis and statistics were done using Microsoft Excel 2019 (Microsoft, Redmond, USA) and SPSS V20.0 (IBM, Armonk, USA).

The study was approved by the institutional Committee for Medical Ethics and the Slovene National Medical Ethics Committee approved data collection and review of outcomes (0120-80/2017/4). The study was performed according to the principles of the Helsinki Declaration.

## Results

Three hundred and seventy-two patients underwent a sialendoscopic approach for treating obstructed

tive salivary gland disease, of which 179 (48.12%) were female and 193 (51.88%) male, with an average age of 48 years (median 47.5 years) and an age span from 4 to 84 years. We performed 415 sialendoscopic and sialendoscopy-assisted procedures, roughly in two thirds because of submandibular pathology (273 operations or 66%). The essential data on the patients and sialendoscopic operations at the Department of Otorhinolaryngology and Cervicofacial Surgery January 2012 – November 2020 are shown in Table 2.

### Ultrasound diagnostics

In the present group, ultrasound examination proved accurate in evaluating the salivary glands' morphology and identifying stones, their size and localization, or possible dilatation of the ducts. In eight cases, ultrasound missed diagnosing rather long but narrow salivary stones (longer diameter of 8–10 mm and transverse diameter of 2–3 mm), which were all localized in the last distal 2 cm of Wharton's duct. We diagnosed these stones during sialendoscopy, four of them also by palpation in the office. Among 182 ultrasonographical examinations of submandibular glands, these eight cases resulted in a 4.4% false-negative rate.

### Mandibular occlusal radiography

Native mandibular occlusal radiography proved useful, showing a Wharton's duct salivary stone in 12 out of 17 examinations, five of them being non-palpable. In one patient, the examination revealed an osteoma of the mandible.

### Computer tomography

CT imaging was used in 143 patients (38.5%), mostly with sialolithiasis (122 patients or 85.31%). The proportion of all patients with sialolithiasis in whom a CT examination was performed was 62.24% (122/196). The percentage has been higher in the last four years (84.5%).

### MR sialography

MRI sialography was used in eight patients with sialendoscopically identified tight proximal strictures: four of them at a 30–45 mm depth of Wharton's duct and in the same number of patients with Stensen's duct strictures and a 50–60 mm endoscopic reach. A typical examination showed a sausage-like series of strictures and dilatations or

**TABLE 2.** Patients and sialendoscopic operations at the Department of Otorhinolaryngology and Cervicofacial Surgery, University Clinical Center Ljubljana, Slovenia, January 2012 – November 2020

All operations		415 (100%)
Operated salivary ductal system	Submandibular	273 (66%)
	Parotid	142 (34%)
Anesthesia	Local	302 (72.8%)
	General	113 (27.2%)
Patients	All	372
	Male	193 (51.8%)
	Female	179 (48.1%)
	Age (average, span – in years)	48 (4–84)
Radiology diagnostics	Ultrasound	372 (100%)
	Mandibular occlusal radiography	17 (4.6%)
	CT	143 (38.4%)
	MR sialography	8 (2.2%)
	X-ray sialography	2 (0.5%)
The type of interventional procedure	All	247
	Salivary stone extraction	178
	Stricture dilatation	69
	Stent insertion (after stricture dilatation or stone extraction)	145

long segments of the main and secondary duct strictures.

### X-ray sialography

Sialography was used in only two patients with tight distal strictures of Stensen's duct since



**FIGURE 3.** In case the stone is at least partially sialendoscopically visible, it can represent a backup guidance in a challenging final combined approach.

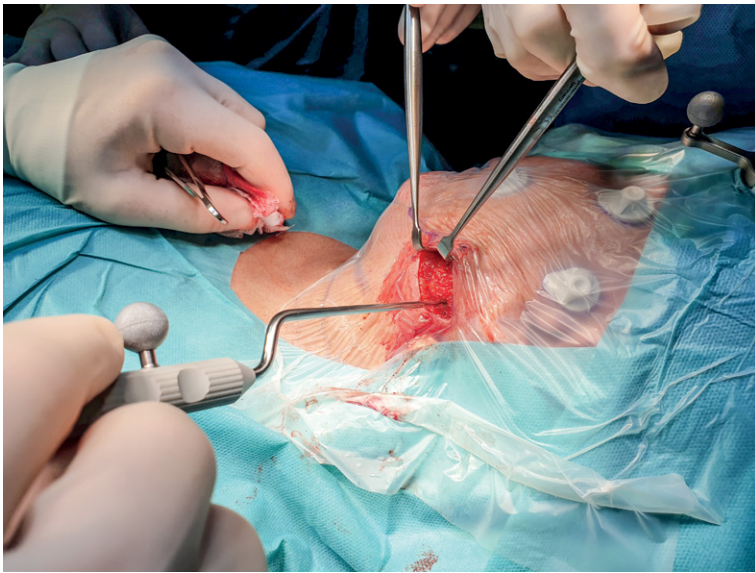


**FIGURE 4.** All stones were removed following the navigational trajectory with a transcutaneous or transoral approach.

**TABLE 3.** Sialendoscopy-assisted transcutaneous salivary stone extractions with or without the use of navigation at the Department of Otorhinolaryngology and Cervicofacial Surgery, University Medical Centre Ljubljana, Slovenia

Gland / Stone extraction outcome	Parotid gland	Submandibular gland	Total
Successful	4	6	10
Successful (with navigation)	2	3	5
Successful last attempt wire basket retrieval (transcutaneous approach failed)		1	1
Total	6	10	16

10.2.2012, when sialendoscopy was introduced in our department. The examination proved to be accurate, showing sausage-like series of strictures and dilatations. It also has apparent drawbacks, such as the need for cannulation and engagement of two teams (radiological and surgical). Damage to the duct can also be probable. We found one case with a ruptured stenotic segment 40 mm from the papilla.

### Types of anesthesia, procedures and use of additional tools

The majority of our sialendoscopies and sialendoscopy-assisted operations were performed under local anesthesia (302/415; 72.77%) and were well-tolerated. There were eight recorded cases of transient paresis of the buccal branch of the facial

nerve after parotid sialendoscopy, lasting from 3 to 6 hours; no other adverse reactions to local anesthesia were recorded. We performed 247 interventional procedures (59.5%), with 178 successful salivary stone extractions and 69 stricture dilations. A total of 145 temporary stents were inserted in these cases. In 168 cases (40.5%), no intervention procedure was carried out.

### Surgical approach and outcomes

The essential data on the patients and sialendoscopic operations at the Department of Otorhinolaryngology and Cervicofacial Surgery January 2012 – November 2020 are shown in Table 2.

Pure sialendoscopic stone removal was performed in 60 patients, and additional laser fragmentation was used in 8 (13.3%) of them. The combined sialendoscopy-assisted approach was the most common method of salivary stone extraction (118/178 procedures, 66.3%). The majority of the combined approach operations were performed through incisions of the oral mucosa (102 surgeries, 86.4%), mainly for the removal of submandibular stones (93 cases, 91.2%). A transcutaneous approach was employed in the remaining 16 procedures, in 10 of them using a transcervical approach (for submandibular stones) and six a transfacial approach (for parotid stones) (Table 3).

A salivary gland resection was performed in six out of 372 patients in whom sialendoscopy was part of their treatment.

A combination of sialendoscopy and navigation was used in six patients, four of them with submandibular and two with parotid stones (Table 4). Depending on their proximity along the duct, we used transcutaneous approaches in five patients (three transcervical and two transfacial approaches) and a transoral approach in one patient. We had two cases of complicated sialadenitis: a parotid abscess in one and an initial phlegmon of the mouth floor in the other case. Two cases with submandibular sialolithiasis were salvage procedures following previous unsuccessful non-guided sialendoscopy. In all six patients, the stones were non-palpable, and only two of them were partially visible on sialendoscopy. All but one stone were in a proximal position and fixed. With the use of CT guidance, we were able to preserve all but one salivary gland. The latter patient had an obstruction due to a severe far proximal stricture and a stone positioned behind it (i.e., more proximally than the stricture itself).

**TABLE 4.** Sialendoscopy and navigation-assisted combined approach procedures at the Department of Otorhinolaryngology and Cervicofacial Surgery November 2019 – November 2020

Patient	Age (years)	Sex	History	Site	Stone palpability	Stone location	Stone visibility	Fixation	Approach	Stone size (millimeters)	Final depth reached with sialendoscope (millimeters)	Follow-up
1	67	F	Acute abscess formation	Left parotid	No	Within the abscess cavity	Not visible	-	Transcutaneous sialendoscopy-assisted	5 (SPH)	72	Without complaints 14 months
2	46	M	Advanced sialolithiasis	Right submandibular	No	55 millimetres depth	Partially visible	Fixed	Transcutaneous sialendoscopy-assisted	10 (SPH)	60	Without complaints 12 months
3	60	F	Persisting swelling	Right parotid	No	45 millimetres depth	Partially visible	Fixed	Transcutaneous sialendoscopy-assisted	7 x 4 x 3	65	Without complaints 11 months
4	70	M	Advanced sialolithiasis	Left submandibular	No	64 millimetres depth	Non visible	Fixed	Transcutaneous sialendoscopy-assisted	10 (SPH)	75	Without complaints 11 months
5	21	M	Persistent swelling	Left submandibular	No	100 millimetres depth	Not visible	Fixed	Transcutaneous sialendoscopy-assisted	3 (intraglandular, found after gland resection)	90	After gland resection without complaints 7 months
6	34	M	Floor of the mouth phlegmona	Left submandibular	No	28** millimetres depth	Not visible	Fixed	Transoral sialendoscopy-assisted	6 x 4 x 3	62	Without complaints 14 months

SPH = spheric form; \*\* = depth at the time of extraction

## Discussion

Ultrasonography proved to be an accurate tool in our preoperative workup of submandibular sialolithiasis, with a 4.4% false-negative rate. All of the missed stones were in the distal Wharton's duct and had a narrow and elongated shape, with a transverse diameter 3 mm or less. Similar findings (5.1% false-negative cases) were published by German authors and explained by the mandible acoustic shadow.<sup>13</sup> In addition to the salivary stone position (proximity along the ductal tree), the ultrasonography's sensitivity for detecting the calculi mainly depends on their sheer size. Authors from Geneva report that stones with a diameter of less than 3 mm were missed in ultrasonical diagnosis in 10 out of 19 glands in their study and explain this by the absence of dorsal acoustic shadow of the calculi.<sup>14</sup> Our findings confirm the relationship between the sensitivity of the ultrasound examination and the size of the salivary stones. In our series, 8 lengthy but narrow salivary stones were missed (longer diameter 8–10 mm and transverse 2–3 mm). Ultrasonography also proved to be a sensitive tool in estimating the state of the related soft tissue, *i.e.*, for exclusion of nonobstructive pathology.

The proportion of patients with a CT examination has been more extensive in the last 4 years as a result of growing experience of the importance of input diagnostic information on possible multi-

plicity of stones.<sup>15</sup> High-resolution CT has a crucial role in post-treatment monitoring, especially in submandibular sialolithiasis, since it offers more information about possible residual stones than do clinical and ultrasound findings.<sup>16</sup> Due to its non-invasiveness and accuracy, sialo-MRI is the most appropriate method for assessing high-grade salivary duct strictures.<sup>17</sup> It is different from classic, CT-based or CBCT (cone beam computer tomography) sialography. There is no need for cannulation of the duct for endoluminal contrast injection. The procedure can therefore be used even during acute sialadenitis. Although we have used it relatively sparsely, in only eight patients, we believe that sialo-MRI has many advantages and should be used more often.

Most of the sialendoscopies and sialendoscopy-assisted operations were performed under local anesthesia (72.77%). With proper patient selection, procedures were well tolerated, and there were no adverse reactions to local anesthesia. Cases of transient, short-lasting paresis of the buccal branch of the 7<sup>th</sup> cranial nerve after parotid sialendoscopy were rare. Our experience is consistent with already reported good tolerance of sialendoscopies conducted under local anesthesia by Luers *et al*, provided that patients were in good general health and the operative procedure was not complicated or long-lasting.<sup>18</sup>

There were 178 successful salivary stone extractions in the present series, and the combined

sialendoscopy-assisted approach was the most common type of procedure. The reason was the lack of a laser or pneumatic lithotripter as a secondary minimally invasive stone fragmentation option. Slovenia was also a »sialendoscopic native« area, with a great proportion of previously untreated patients with large salivary stones.<sup>10</sup> On the other hand, there has been a general trend of a »combined approach come back« in the last few years. According to the recommendations of ESTC and some other authors, it still has an important place in calculi bigger than 7 mm.<sup>6,14,15</sup> Our own experience with deeply embedded, extraluminal and especially in abscess formation positioned stones corroborates their opinion.

The majority of salivary calculi were removed through oral mucosa incisions during combined approach surgery (102 surgeries). We had a significantly higher proportion of transcutaneous procedures than reported by authors from purely sialendoscopic quaternary centers.<sup>19</sup> The number of submandibular transcutaneous operations, in particular, was exceptionally high. Salivary stones are found significantly more often in the submandibular than in the parotid ductal system.<sup>20</sup> On the other hand, parotidectomy is often avoided in patients with sialolithiasis because of the risk of facial nerve injury.

For the same reason, the transfacial combined approach with gland preservation is well established for proximal stones of Stensen's duct.<sup>21</sup> On the other hand, submandibular gland resection was the most frequently performed type of end-stage treatment in patients with salivary stones.<sup>10</sup> The gland preservation procedure for far proximal submandibular sialolithiasis was reported and recommended more modestly.<sup>22</sup> The reason may be doubt in the long-term success of this type of procedure and a (repeated) possibility of marginal branch injury. Our attitude on the importance of salivary gland preservation, both parotid and submandibular, is based on findings of the indispensable role of saliva in maintaining the health of the oral and upper gastrointestinal system.<sup>23</sup> In addition, there is undoubtedly enough evidence of salivary gland function recovery after sialendoscopy.<sup>24</sup> For these reasons, we endeavored ten successful transcutaneous combined sialendoscopy-assisted procedures for far proximal submandibular stones; in three of them, CT navigation was also employed. With the consistent implementation of all kinds of sialendoscopic techniques, we significantly reduced the need for sialoadenectomies in patients with obstructive salivary gland disease. We were

forced to resect one of the salivary glands in only six of 372 patients (1.6%) in whom sialendoscopy was part of the treatment. Compared with the period before the introduction of sialendoscopy, the annual number of resections was reduced by 93.3% (15-fold), which represents an additional improvement of our previously published results.<sup>10</sup>

All six patients in our navigation subgroup had non-palpable salivary stones, even though their stones were relatively large (only one measured less than 5 mm). The reason for this seemingly paradoxical situation was the far proximal position of the stone in four cases, the phlegmon of the floor of the mouth in one and a parotid abscess formation in the remaining case. Good visibility on sialendoscopy is mandatory for all successfully performed solely endoscopic stone extractions and for a majority of combined approach procedures. Our inability to display calculi during sialendoscopy was also among the indications for the use of CT navigation in four cases: stone inside abscess formation<sup>1</sup>, far proximal position of the calculi (literally in the middle of the gland<sup>2</sup>), and terrible visibility inside the main duct.<sup>1</sup> There is only one procedure described so far combining salivary stone removal with both sialendoscopy and CT navigation assistance: the authors reported an excellent matching of the two guidance methods.<sup>8</sup> They therefore confirmed the probable validity of additional CT navigation guidance. Its introduction in sialolithiasis surgery represents a significant improvement and, in our opinion, has great added value, especially in challenging cases. We observed no facial nerve paresis or paralysis, sialocele or salivary fistula among the patients with the transcutaneous navigation-assisted approach. We therefore regard it as equally safe as a non-navigated combined approach.

It is essential to point out more or less obvious pitfalls of the CT navigation guidance method. Without the additional acquisition of (less than accessible) intraoperative CT, it does not allow any real-time correction, which makes CT navigation guidance an excellent method in patients with fixed salivary stones. The final step in locating the stone in virtually any type of approach is careful preparation of the last remnants of tissue over the stone. In difficult cases, the final position of the stone is easily missed; repeated axis check using the navigation may therefore be the only way to localize the stone or multiple stones. Since we had experience with a proximally shifted stone, the authors believe that the navigation in possibly non-fixed stones should be used with caution.

Even with navigation, the obstruction caused by a severe stricture containing the stone in an intraglandular position could not be resolved without gland resection. These challenging situations seem to be relatively infrequent.

## Conclusions

The combined use of sialendoscopy and CT navigation assistance is a step forward in minimally invasive surgery of sialolithiasis, especially in far proximal, intraparenchymal, non-palpable and sialendoscopically non-visible fixed stones, irrespective of the type of combined approach or salivary gland. CT navigation proved to be of help in demanding transcuteaneous submandibular stone extractions, with gland preservation. It is invaluable in cases of extraluminal, *i.e.*, positioned in an abscess or deeply embedded stones. With the consistent implementation of sialendoscopy and related minimally invasive procedures, we can significantly reduce the need for sialoadenectomies in patients with obstructive salivary gland disease.

## References

- Marchal F, Dulguerov P, Becker M, Barki G, Disant F, Lehmann W. Specificity of parotid sialendoscopy. *Laryngoscope* 2001; **111**: 264-71. doi: 10.1097/00005537-200102000-00015
- Marchal F, Dulguerov P, Becker M, Barki G, Disant F, Lehmann W. Submandibular diagnostic and interventional sialendoscopy: new procedure for ductal disorders. *Ann Otol Rhinol Laryngol* 2002; **111**: 27-35. doi: 10.1177/000348940211100105
- Ardekian L, Klein H, Al Abri R, Marchal F. Sialendoscopy for the diagnosis and treatment of juvenile recurrent parotitis. *Rev Stomatol Chir Maxillofac Chir Orale* 2014; **115**: 17-21. doi: 10.1016/j.revsto.2013.12.005
- Carroll WW, Walvekar RR, Gillespie MB. Transfacial ultrasound-guided gland-preserving resection of parotid sialoliths. *Otolaryngol - Head Neck Surg* 2013; **148**: 229-34. doi: 10.1177/0194599812471514
- Caversaccio M, Zheng G, Nolte LP. [Computer-aided surgery of the paranasal sinuses and the anterior skull base]. [German]. *HNO* 2008; **56**: 376-82. doi: 10.1007/s00106-008-1705-2
- Lorenz KJ, Frühwald S, Maier H. [The use of the BrainLAB Kolibri navigation system in endoscopic paranasal sinus surgery under local anaesthesia. an analysis of 35 cases]. [German]. *HNO* 2006; **54**: 851-60. doi: 10.1007/s00106-006-1386-7
- Groselj A, Kos B, Cemazar M, Urbancic J, Kragelj G, Bosnjak M, et al. Coupling treatment planning with navigation system: a new technological approach in treatment of head and neck tumors by electrochemotherapy. *Biomed Eng Online* 2015; **14(Suppl 3)**: S2. doi: 10.1186/1475-925X-14-S3-S2
- Capaccio P, Bresciani L, Di Pasquale D, Gaffuri M, Torretta S, Pignataro L. CT navigation and sialendoscopy-assisted transfacial removal of a parotid stone: a technical note. *Laryngoscope* 2019; **129**: 2295-8. doi: 10.1002/lary.27621
- Pezier TF, Prasad S, Marchal F. Towards an international database of benign salivary disease. *Br J Oral Maxillofac Surg* 2016; **45**: 968-9. doi: 10.1016/j.bjoms.2016.01.015
- Aničin A, Urbancič J. Sialendoscopy, a minimally invasive diagnostic and interventional procedure for the management of salivary gland diseases. *Zdr Vestn* 2016; **86**: 92-8. doi: https://doi.org/10.6016/ZdravVestn.1469
- Rzymaska-Grala I, Stopa Z, Grala B, Gołębowski M, Wanyura H, Zuchowska A, et al. Salivary gland calculi - contemporary methods of imaging. *Polish J Radiol* 2010; **75**: 25-37. http://www.ncbi.nlm.nih.gov/pubmed/22802788
- Yousem DM, Kraut MA, Chalian AA. Major salivary gland imaging. *Radiology* 2000; **216**: 19-29. doi: 10.1148/radiology.216.1.r00j4519
- Goncalves M, Mantsopoulos K, Schapher M, Iro H, Koch M. Ultrasound supplemented by sialendoscopy: diagnostic value in sialolithiasis. *Otolaryngol - Head Neck Surg* 2018; **159**: 449-55. doi: 10.1177/0194599818775946
- Terraz S, Poletti PA, Dulguerov P, Dfouni N, Becker CD, Marchal F, et al. How reliable is sonography in the assessment of sialolithiasis? *Am J Roentgenol* 2013; **201**: W104-9. doi: 10.2214/AJR.12.9383
- Madani G, Beale T. Inflammatory conditions of the salivary glands. *Semin Ultrasound CT MR* 2006; **27**: 440-51. doi: 10.1053/j.sult.2006.09.005
- Avrahami E, Englander M, Chen E, Shabtay D, Katz R, Harell M. CT of submandibular gland sialolithiasis. *Neuroradiology* 1996; **38**: 287-90. doi: 10.1007/BF00596550
- Becker M, Marchal F, Becker CD, Dulguerov P, Georgakopoulos G, Lehmann W, et al. Sialolithiasis and salivary ductal stenosis: diagnostic accuracy of MR sialography with a three-dimensional extended-phase conjugate-symmetry rapid spin-echo sequence. *Radiology* 2000; **217**: 347-58. doi: 10.1148/radiology.217.2.r00oc02347
- Luers JC, Stenner M, Schinke M, Helmstaedt V, Beutner D. Tolerability of sialendoscopy under local anesthesia. *Ann Otol Rhinol Laryngol* 2012; **121**: 269-74. doi: 10.1177/000348941212100413
- Koch M, Iro H, Zenk J. Combined endoscopic-transcutaneous surgery in parotid gland sialolithiasis and other ductal diseases: reporting medium- to long-term objective and patients' subjective outcomes. *Eur Arch Oto-Rhino-Laryngology* 2013; **270**: 1933-40. doi: 10.1007/s00405-012-2286-y
- Capaccio P, Torretta S, Ottavian F, Sambataro G, Pignataro L. Modern management of obstructive salivary diseases. *Acta Otorhinolaryngol Ital* 2007; **27**: 161-72. PMID: 17957846
- Koch M, Zenk J, Iro H. Algorithms for treatment of salivary gland obstructions. *Otolaryngol Clin North Am* 2009; **42**: 1173-92. doi: 10.1016/j.otc.2009.08.002
- Marchal F. A combined endoscopic and external approach for extraction of large stones with preservation of parotid and submandibular glands. *Laryngoscope* 2007; **117**: 373-7. doi: 10.1097/mlg.0b013e31802c06e9
- Llena-Puy C. The rôle of saliva in maintaining oral health and as an aid to diagnosis. *Med Oral Patol Oral Cir Bucal* 2006; **11**: E449-55. doi: 10.1097/mlg.0b013e31802c06e9
- Su YX, Xu JH, Liao GQ, Liang YJ, Chu M, Zheng GS, et al. Salivary gland functional recovery after sialendoscopy. *Laryngoscope* 2009; **119**: 646-52. doi: 10.1002/lary.20128

## research article

# Morphological features of breast cancer circulating tumor cells in blood after physical and biological type of isolation

Tanja Jesenko<sup>1,2</sup>, Ziva Modic<sup>1,2</sup>, Cvetka Grasic Kuhar<sup>2,3</sup>, Maja Cemazar<sup>1,4</sup>, Urska Matkovic<sup>1</sup>, Simona Miceska<sup>2,5</sup>, Jerneja Varl<sup>2,5</sup>, Anamarija Kuhar<sup>5</sup> and Veronika Kloboves-Prevodnik<sup>2,5</sup>

<sup>1</sup> Department of Experimental Oncology, Institute of Oncology Ljubljana, Ljubljana, Slovenia

<sup>2</sup> Faculty of Medicine, University of Ljubljana, Ljubljana, Slovenia

<sup>3</sup> Department of Medical Oncology, Institute of Oncology Ljubljana, Ljubljana, Slovenia

<sup>4</sup> Faculty of Health Sciences, University of Primorska, Izola, Slovenia.

<sup>5</sup> Department of Cytopathology, Institute of Oncology Ljubljana, Ljubljana, Slovenia

Radiol Oncol 2021; 55(3): 292-304.

Received 5 July 2021

Accepted 9 July 2021

Correspondence to: Assoc. Prof. Veronika Kloboves-Prevodnik, M.D., Ph.D., Department of Cytopathology, Institute of Oncology Ljubljana, Slovenia, email: vkloboves@onko-i.si, and Maja Čemazar, Department of Experimental Oncology, Institute of Oncology Ljubljana, Slovenia. E-mail: mcemazar@onko-i.si

Disclosure: No potential conflicts of interest were disclosed.

This is an open access article under the CC BY-NC-ND license (<http://creativecommons.org/licenses/by-nc-nd/4.0/>).

**Background.** Circulating tumor cells (CTCs) have become an important biomarker in breast cancer. Different isolation techniques based on their biological or physical features were established. Currently, the most widely used methods for visualization after their separation are based on immunofluorescent staining, which does not provide the information on the morphology.

**Materials and methods.** The aim of this study was to evaluate how two different separation techniques affect cell morphology and to analyse cell morphology with techniques used in routine cytopathological laboratory. A direct side-by-side comparison of physical (Parsortix®) and biological (MACS®) separation technique was performed.

**Results.** In the preclinical setting, both isolation techniques retained the viability and antigenic characteristics of MCF7 breast cancer cells. Some signs of degeneration such as cell swelling, cytoplasmic blebs, villous projections and vacuolization were observed. In metastatic breast cancer patient cohort, morphological features of isolated CTCs were dependent on the separation technique. After physical separation, CTCs with preserved cell morphology were detected. After biological separation the majority of the isolated CTCs were so degenerated that their identity was difficult to confirm.

**Conclusions.** Taken together, physical separation is a suitable technique for detection of CTCs with preserved cell morphology for the use in a routine cytopathological laboratory.

Key words: CTC; breast cancer; morphology; Parsortix®, MACS®; Giemsa

## Introduction

Circulating tumor cells (CTCs) have become an important biomarker in breast cancer as they can provide critical information about disease progression and response to therapy.<sup>1,2</sup> They represent an intermediate part of the metastatic cascade, therefore monitoring CTC levels in the blood has exceptional implications for the management of

cancer patients.<sup>3</sup> In the blood stream, CTCs are a heterogeneous cell population of tumor cells with different phenotypes. They show high level of epithelial-mesenchymal plasticity and can express an epithelial phenotype, mesenchymal phenotype or even a hybrid or partial epithelial/mesenchymal (E/M) phenotype in which cells express proteins of both phenotypes.<sup>4,5</sup>

Due to their heterogeneity, different isolation techniques from whole blood samples were established in order to separate them from the surrounding hematopoietic cells. Separation techniques can be based on CTC biological or physical properties. Biological separation techniques rely on the expression of cell markers and are usually based on epithelial cell markers positive selection or common leukocyte antigen CD45 negative selection. Currently the only FDA approved platform for enumeration of CTCs CELLSEARCH (Menarini Silicon Biosystems) is based on biological properties, which enables the detection of CTCs of epithelial origin (CD45-, EpCAM+, and cytokeratins 8, 18+, and/or 19+) in whole blood by fluorescent staining and imaging of cells that are pulled to a single focal depth by a magnetic force.<sup>6</sup> An alternative technique that also relies on EpCAM positive selection and magnetic force is Magnetic Activated Cell Sorting (MACS®, Miltenyi Biotec).<sup>7</sup> This technique was evaluated in our previous study for the isolation of CTCs in early breast cancer patients.<sup>8</sup> It was demonstrated to be a simple and useful method for enrichment of EpCAM expressing cells in a preclinical study, however the isolated CTCs from early breast cancer patients were not morphologically preserved enough for their visualization by methods used in a routine cytopathology laboratory. The limitation of separation techniques based on biological properties is that only CTCs that express the epithelial cell markers can be detected. Due to this limitation, platforms exploiting physical properties such as cell size, density, electric charge and deformability are gaining more attention. With the Parsortix® system (ANGLE), CTCs are caught in the Parsortix® filtration cassette due to their larger size and lower compressibility than other blood components.<sup>9</sup> The isolated cells are viable, intact and can be used for further *in vitro* experimentation and characterization.<sup>9</sup>

Currently, most methods for visualization of CTCs after separation from whole blood are usually based on staining with fluorescent antibodies and dyes. Therefore, these methods lack the information on the CTC morphology that is crucial for their identification by light microscopy which is still the gold standard in cytopathological and histological examination of tumor cells. The identification of CTCs by their morphology is challenging as these cells are often severely degenerated due to the combination of physical stress (shear forces), immune surveillance and the lack of growth factors in the blood stream.<sup>3,10</sup> Furthermore, separation methods could also induce some additional dam-

age that can result in degeneration and cell death which change morphological features of CTCs and influence their proper identification.<sup>11</sup> Probably for these reasons, data regarding basic CTC morphology in breast cancer are limited and thus the selection of the appropriate separation method is of utmost importance for proper cytopathological identification.<sup>11-14</sup>

There are few published data how separation techniques affect CTCs morphology.<sup>13-16</sup> Therefore, we designed a study aimed to select the separation method that would allow the identification of CTCs based on their morphology that could be integrated in a routine cytopathology laboratory. The advantage of cytopathological analysis is that it is easily accessible in the clinical environment as cytopathologists are an integral part of cancer patient care. Two separation techniques were first evaluated in the preclinical setting by spiking of blood of healthy volunteers with MCF7 breast cancer cell line, which is the most studied human breast cancer cell line.<sup>17</sup> The preclinical evaluation was followed by a prospective clinical trial in metastatic breast cancer patients with the primary objective being a side-by-side comparison of both separation techniques. The aims of this study were i) to evaluate how two different separation techniques affect cell morphology and ii) to analyze cell morphology with techniques used in routine cytopathological laboratory.

## Materials and methods

### Ethic statement

The study was conducted at the Institute of Oncology Ljubljana, Slovenia and was reviewed and approved by the Institutional Ethical Review Committee (ref. nb. ERID-KSOPKR-0071/2020) and National Medical Ethics Committee at the Slovenian Ministry of Health (ref. nb. 0120-150-2019/4). All enrolled patients and healthy volunteers signed an informed consent. The study was conducted in accordance with the Declaration of Helsinki. Blood samples were collected during the patients' routine blood draw, which is a minimally invasive procedure.

### Patients and healthy volunteers

Thirty-three patients were recruited in the study, however only 30 patients donated their blood samples, therefore their identification numbers are in the range P1 to P33. Three healthy volunteers were

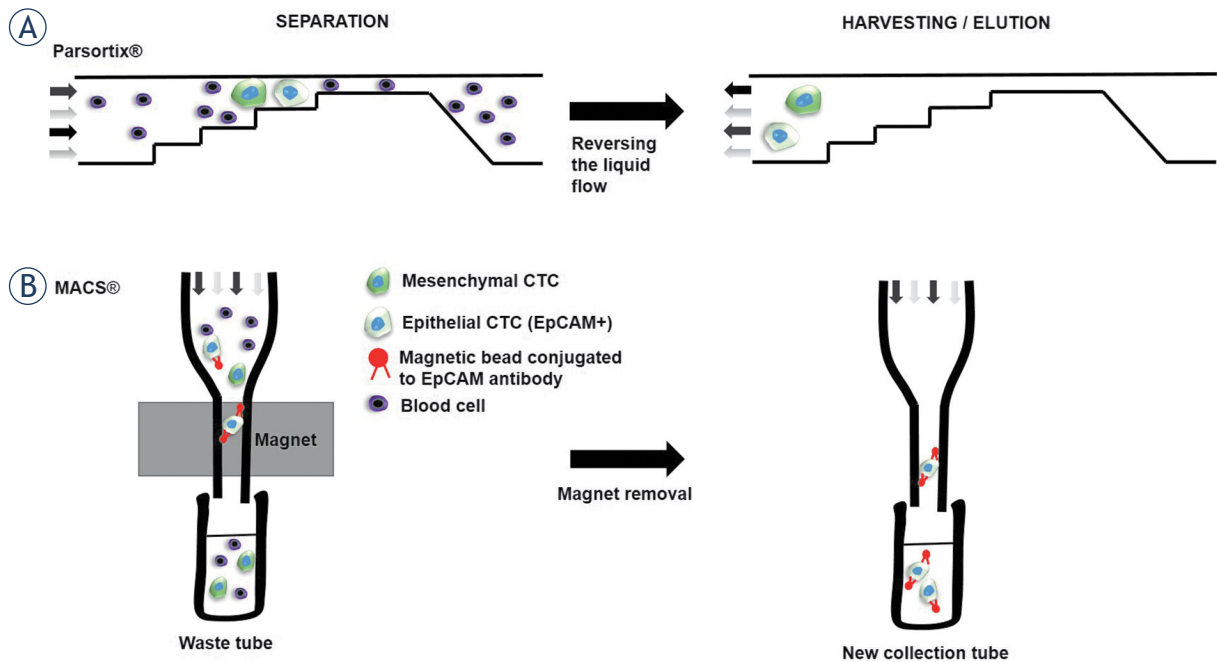


**FIGURE 1.** Schematic presentation of both separation techniques. **(A)** Parsortix® separation cassette contain a stepped structure, gradually narrowing in diameter until reaching a final gap of 6.5  $\mu\text{m}$ , therefore all of the cells that are larger than 6.5  $\mu\text{m}$  are retained and isolated while all smaller cells continue to flow through the cassette into a waste container. The technique enables the isolation of CTCs with different phenotypes. After the whole sample has been processed, the liquid flow is reversed and CTCs can be harvested. **(B)** MACS® separation column uses magnetic beads covered with anti-epithelial cell adhesion molecule (EpCAM) antibodies for positive selection of CTCs with epithelial origin. When magnetic bead labeled CTCs are passed through a dense magnetic column, they are retained by a strong magnetic field. Other non-labeled cells are passed through the column into the waste tube. After the whole sample has been passed through the column, the column is removed from the magnet and retained CTCs can be eluted.

also included in the study. Each patient or healthy volunteer donated two blood samples in a 10 ml EDTA collection tube (BD, Franklin Lakes, NJ, USA). The blood samples were processed within 1 h after collection to ensure the highest viability of the CTCs. One tube was used for Parsortix® and the other for MACS® separation. After separation, cytological slides were prepared as described below.

### Spiking of MCF7 cell line

Human epithelial breast cancer cell line MCF7 was obtained from ATCC (ATCC® HTB-22, ATCC, Manassas, VA, USA) and was cultured in Advanced MEM medium (Gibco, Thermo Fisher Scientific, Waltham, MA, USA) supplemented with 5% fetal bovine serum (Gibco), GlutaMAX (100x, Gibco) and Penicillin-Streptomycin solution (Sigma Aldrich, Merck, Darmstadt, Germany). The cells were cultured in a 5%  $\text{CO}_2$  humidified incubator at 37°C until they reached 80% confluence. Afterwards, the medium was removed, the cells were washed with phosphate buffered saline

(PBS) and detached from the surface with 0.25% trypsin/EDTA in Hank's buffer (Gibco). After collection, the cells were counted and  $5 \times 10^5$  cells were spiked into each blood collection tube and separated by Parsortix® or MACS®. For the purpose of retaining control non-separated cells, the same amount of MCF7 cells was seeded into a 24-well ultra-low attachment plate and incubated in a 5%  $\text{CO}_2$  humidified incubator at 37°C until the end of Parsortix® and MACS® separation.

### Separation techniques

Parsortix® separation was conducted by carefully following the manufacturer's instructions. Parsortix® separation cassette contains a stepped structure, gradually narrowing in diameter until reaching a final gap of 6.5  $\mu\text{m}$ , therefore all of the cells that are larger than 6.5  $\mu\text{m}$  are retained and isolated, while all smaller cells continue to flow through the cassette into a waste container (Figure 1A).<sup>18</sup> After the separation, retained cells were harvested into a 5 ml plain red-top BD vacutainer tube without a pre-harvest flush and re-

suspended in an in-house cell medium: 20% fetal bovine serum (Gibco), 5% EDTA (Sigma Aldrich) in PBS. MACS® separation was performed as previously described (Figure 1B) and harvested in MACS® Whole Blood Column Elution Buffer<sup>8</sup>. MACS® separation is not limited by the cell size.

### Preparation of cytological slides

For preclinical part of the study, three cytopspins were prepared using a cytocentrifuge (Thermo Scientific Shandon Cytospin R 4 Cytocentrifuge, Waltham, MA, USA) by centrifugation at 700 rpm for 4 min at room temperature (RT). The first cytopspin was stained with Giemsa (Sigma Aldrich, Merck) for microscopic evaluation, the second one was fixed in Delaunay (2500mL acetone, 2500 mL absolute ethanol and 2,5 mL 1 M trichloroacetic acid) and stained with Papanicolaou (PAP), which was subsequently stained for pancytokeratin AE1/AE3. The third one was fixed in methanol for estrogen receptor immunocytochemical staining. For clinical part of the study two cytopspins were made, one for Giemsa staining for morphological evaluation and the second for PAP staining and subsequent dual AE1/AE3 and vimentin immunocytochemical staining.

### Staining

For Giemsa staining, the slide was air dried for at least 30 minutes at room temperature and stained with Giemsa. The second cytopspin was fixed (Delaunay, 2 hours or overnight) and stained PAP using an automated stainer Leica Multistainer ST5020 (Leica Microsystems, Buffalo Grove, IL, United States).

Immunocytochemical staining of CK AE1/AE3 and estrogen receptor (ER) was performed with our routine immunocytochemical staining protocols. All protocols included manually performed endogenous peroxidase activity inhibition with 5% H<sub>2</sub>O<sub>2</sub>-methanol solution for 10 min at RT. After the incubation was done, slides were washed once 1x PBS and once with Reaction Buffer (Ventana, Roche Diagnostics). The presence of the antigens was detected with iView detection kit on Ultra autostainer (Ventana, Roche Diagnostics). Enzymatic detection was accomplished when a streptavidin enzyme (streptavidin-HRP) conjugates with the biotin-bound secondary antibody. Chromogen was deposited by a reaction with hydrogen peroxide in the presence of diaminobenzidine (DAB) and copper sulfate, producing brown

precipitate. External positive controls were used in all batches.

Immunocytochemical staining of the CK AE1/AE3 and vimentin was performed as dual staining on the same PAP stained cytopspin. The CK AE1/AE3 staining was performed with anti CK monoclonal antibody (CK AE1/AE3, ref. nr. M3515, dilution 1:100, Agilent, Santa Clara, CA, United States). The vimentin immune staining was performed after the CK AE1/AE3 staining was done, with anti-vimentin antibody (V9, ref. nr. M0725, dilution 1:500, Agilent, Santa Clara, CA, United States). The presence of vimentin was detected with ultraView Universal Alkaline Phosphatase Red Detection Kit (Ventana, Roche Diagnostics), enzymatic detection was accomplished with an alkaline phosphatase and chromogen Fast Red, producing red precipitate.

For ER staining, methanol fixed cytopspin was stained with anti ER monoclonal antibody (ER, ref. nr. NCL-L-ER-6F11, dilution 1:25, Novocastra, Leica Biosystems, United Kingdom). ER protocol included additional manual antigen retrieval step with previously boiled 1x TRIS-EDTA buffer solution (pH 9) for 3 min.

### Evaluation of cytological slides

Giemsa slides were evaluated by an experienced cytopathologist (VKP) and images of the cells on slides were captured with a DP72 CCD camera connected to a BX-51 microscope (Olympus, Hamburg, Germany). In the preclinical part, morphological features were quantified in 100 cells from each experimental group. Cell diameter, nuclear diameter and thickness of the cytoplasm were measured using ImageJ software.<sup>19</sup> Other morphological features that were analyzed were cytoplasmic and nuclear chromasia, degeneration characteristics (cytoplasmic blebs, cytoplasmic villous projections and vacuolization), regularity of plasma membrane and nuclear membrane and chromatin features. These morphological features were quantified by counting the cells that displayed these characteristics. In the clinical part of the study, the slides were evaluated by the cytopathologist and CTCs were identified by their cytomorphological features. Based on their morphological appearance, they were categorized as morphologically “preserved” or “unpreserved”. Criteria for the preserved CTCs were: cells with morphological features of malignancy such as large nuclei, high nuclear to cytoplasmic (N/C) ratio, scant cytoplasm, visible chromatin structure or presence of mitotic figures. Criteria for identifica-

tion of morphologically unpreserved CTCs were: cells with morphological features of malignancy such as large nuclei, high N/C ratio, scant cytoplasm and loss of chromatin structure and nuclear membrane integrity. All of the identified CTCs were imaged and their diameter was measured.

### Flow cytometry

Cell viability and type of cell death of MCF7 cells was determined by FITC Annexin V Apoptosis Detection Kit with 7-AAD (BioLegend, San Diego, CA, USA) according to manufacturer's instructions. Within 1 hour after separation, Annexin V and 7AAD were added to the cells and the measurements were performed on at least 100,000 cells per sample using FACSCanto II flow cytometer (BD Biosciences, San Jose, CA). Data were analyzed using FlowJo software.

### Statistical analysis

The values in this study are represented by median with interquartile range, mean  $\pm$  standard error of the mean (SE) or mean with 95% confidence interval and are defined in the figure legends. The patient's categorical characteristics were presented as frequencies and percentages. Age was presented as median and range. The comparison of means of more than two groups was statistically evaluated by one-way ANOVA followed by a Dunnett's multiple comparisons test. The comparison of medians of more than two groups was evaluated by Kruskal–Wallis one-way ANOVA followed by Dunn's multiple comparisons test. Fisher's exact test was used to determine the significance between two categorical variables. A P-value of  $<0.05$  was considered to be statistically significant. A sample size (n) for each experiment is stated in the figure legend. For statistical analysis and preparation of graphs, GraphPad Prism 8 (La Jolla, CA, USA) was used.

## Results

### Hydropic degeneration after Parsortix® and MACS® separation

In the first part of the study, the effect of both separation techniques on cell morphology was evaluated on Giemsa stained cytological slides of intact (non-separated) MCF7 cells vs. Parsortix® or MACS® isolated MCF7 cells. In comparison to the intact MCF7 cells (Figure 2A, No separation),

the Parsortix® and MACS® separated MCF7 cells showed signs of cell swelling *i.e.* hydropic degeneration (Figure 2A, Parsortix® and MACS®). Also high background of blood cells was observed after MACS® separation protocol (Figure 2A, MACS®).

Preservation of antigenic epitopes for immunocytochemical staining was determined by immunocytochemical staining of AE1/AE3 cytokeratin and estrogen receptor, as these stainings are usually used in the cytopathological detection of breast cancer cells. Both separation techniques retained the epitopes for immunocytochemical staining. All MCF7 cells presented with strong cytoplasmic AE1/AE3 cytokeratin positive staining (Figure 2B) in all experimental groups. Nuclear estrogen receptor staining was positive in around 70% of MCF7 cells either in non-separated cells or after Parsortix® or MACS® separation (Figure 2C).

Cell swelling was quantified based on the measurements of cell diameter, nuclear diameter and thickness of the cytoplasm (Figure 2D). Both separation techniques induced similar statistically significant enlargement of the cell diameter (Figure 2E), nuclear diameter (Figure 2F) and thickness of the cytoplasm (Figure 2G). Due to the increase in the thickness of cytoplasm and size of nucleus, cytoplasmic staining was significantly altered. Dark basophilic staining was statistically significantly reduced after both separation techniques (Figure 2H). Contrary, pale basophilic staining increased in the opposite manner, with MACS® separated cells having the highest fraction of pale basophilic cytoplasmic staining (Figure 2H). The plasma membrane was intact after both separation techniques (Figure 2A). The nuclear features such as chromatin structure and nucleoli were preserved after both separation techniques (Figure 1A). Nuclear staining was mostly hyperchromatic (Figure 2A). Chromatin was mostly coarsely granular (Figure 2D). The nuclear membrane was intact with some irregularities observed after both separation techniques (Figure 2A).

### Degenerative cytoplasmic changes and cell viability after Parsortix® and MACS® separation

Increased fraction of cells with degenerative cytoplasmic changes were observed in Giemsa stained MCF7 cells after both separation techniques. Morphologically non-degenerated cells were presented with homogenous cytoplasm and intact smooth plasma membrane (Figure 3A). Degenerative changes that were observed more

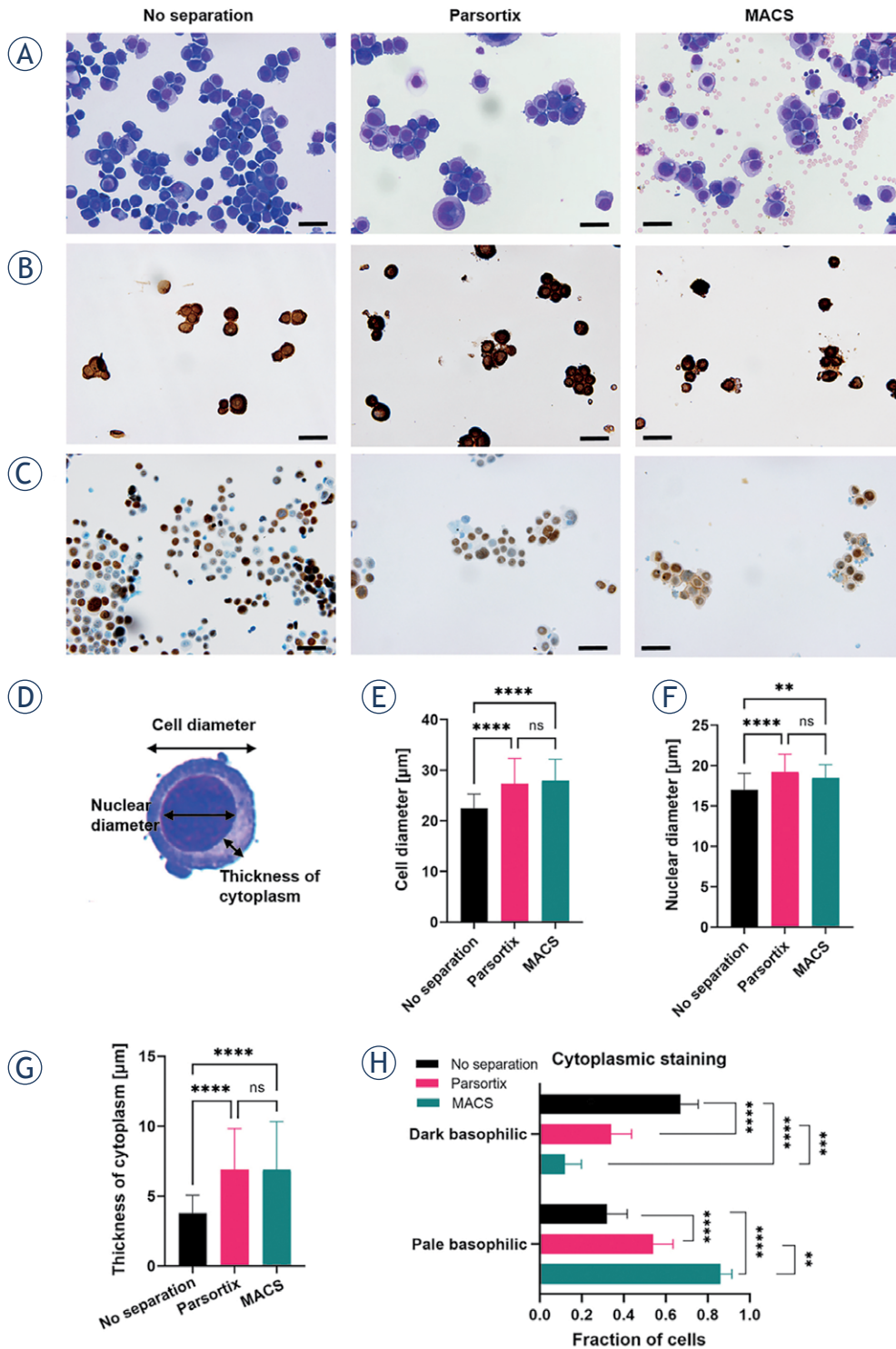


**FIGURE 2.** Parsortix® and MACS® separation techniques induced hydropic degeneration of cells. **(A)** Giemsa stained, **(B)** AE1/AE3 cytochrome stained and **(C)** estrogen receptor stained non-separated MCF7 cells (No separation) and separated MCF7 cells by Parsortix® (Parsortix®) or MACS® (MACS®). Scale bar represents 50 μm. Note that estrogen receptor stain is nuclear therefore cells appear smaller due to the poor contrasting of the cytoplasm. **(D)** Presentation of measured and evaluated cell sizes. Non-separated and Parsortix® or MACS® separated **(E)** cell diameter of, n=100 cells, **(F)** nuclear diameter, n=100 cells and **(G)** thickness of cytoplasm, n=100 cells. **(H)** Cytoplasmic staining of non-separated MCF7 cells and Parsortix® or MACS® separated cells, n=100 cells. Values in **(E, F, G)** represent median with interquartile range and **(H)** mean with 95% confidence interval. Statistical significance was determined by Kruskal–Wallis one-way ANOVA followed by Dunn’s multiple comparisons test for **(E, F, G)** and by Fisher’s exact test for **(H)**.

\*\* = p < 0.01; \*\*\* = p < 0.001; \*\*\*\* = p < 0.0001; ns = not significant

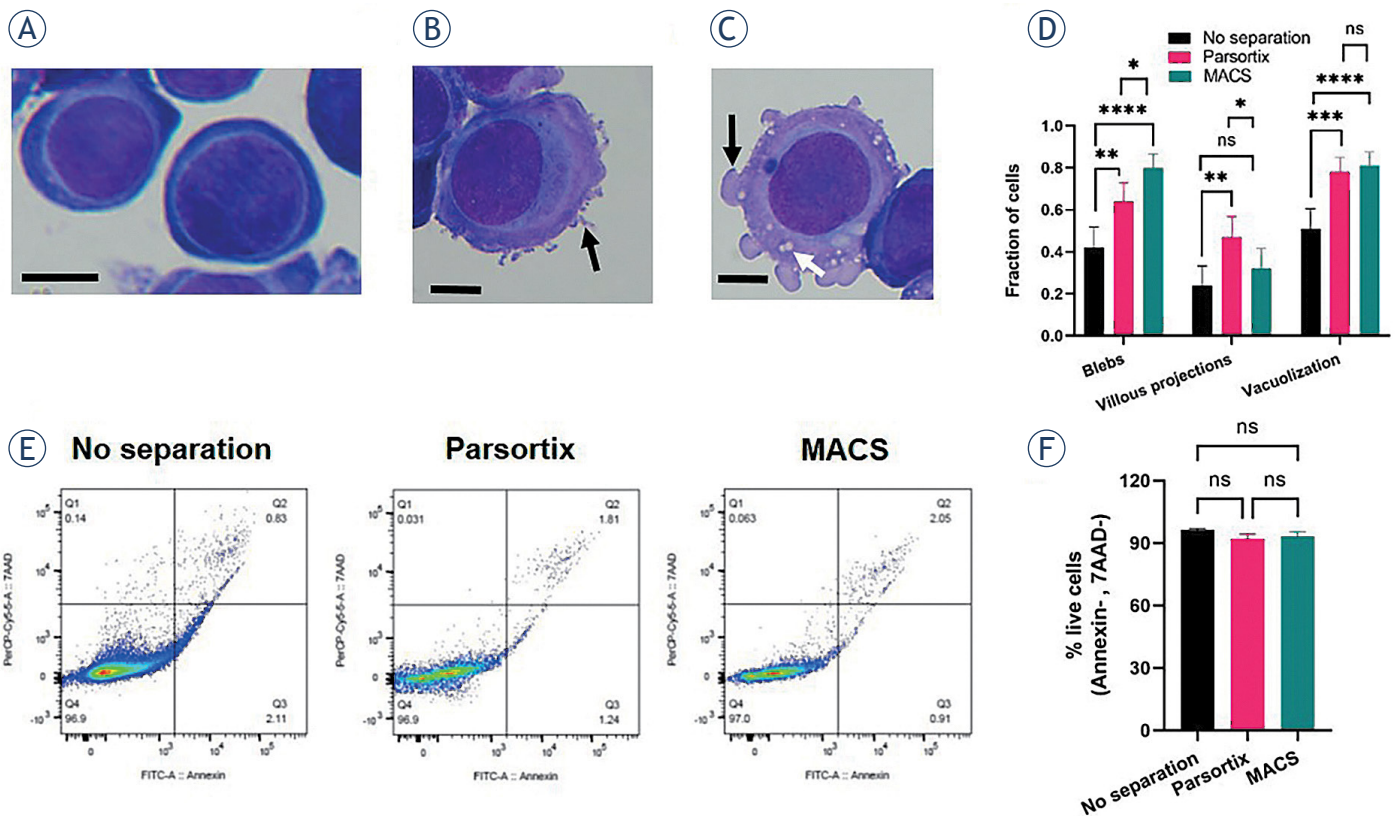


**FIGURE 3.** Parsortix® and MACS® separation techniques induced degenerative cytoplasmic changes but retained the viability of MCF7 cells. **(A)** Morphologically non-degenerated cells presented with homogenous cytoplasm and intact smooth plasma membrane. Scale bar represents 10  $\mu$ m. **(B)** Cytoplasmic villous projections as observed degenerative changes are indicated by black arrow. Scale represents 10  $\mu$ m. **(C)** Membrane blebbing (indicated by black arrow) and cytoplasmic vacuolization (indicate by white arrow) as observed degenerative changes. Scale represents 10  $\mu$ m. **(D)** Fraction of cells with villous projections, blebs or vacuolization. Values represent mean with 95% confidence interval, n = 100 cells. Statistical significance was determined by Fisher's exact test. \* = p<0.05, \*\* = p<0.01, \*\*\* = p<0.001, \*\*\*\* = p<0.0001, ns = not significant. **(E)** Representative dot plots of Annexin V and 7AAD staining in non-separated cells and Parsortix and MACS separated cells **(F)** Percent of live cells (Annexin V-, 7AAD-), n=3. The values represent mean  $\pm$  (SE), n = number of biological replicates. Statistical significance was determined by one-way ANOVA followed by a Dunnett's multiple comparisons test; ns- not significant.

frequently after both separation protocols were cytoplasmic villous projections (Figure 3B, black arrow), membrane blebbing (Figure 3C, black arrow) and cytoplasmic vacuolization (Figure 3C, white arrow). Quantification of the observed changes demonstrated that MACS® separation induced the highest increase in the fraction of cells with cytoplasmic blebs (Figure 3D). Villous projections were more frequent in Parsortix® separated cells (Figure 3D). Increased fraction of cells with cytoplasmic vacuoles was observed after both separation techniques (Figure 3D).

However, although degenerative changes were observed after both separation techniques, the separated cells retained their viability. Flow cytometric analysis of Annexin V (apoptosis) and 7AAD (necrosis) demonstrated that MCF7 cells remained their viability after both separation techniques (Figure 3E). The quantification demonstrated that

the percentage of live cells (Annexin V-, 7AAD-) remained unchanged following both separation techniques (Figure 3F). No significant changes were observed in the percentage of cells in early apoptosis (Annexin V+, 7AAD), late apoptosis (Annexin V+, 7AAD+) and necrosis (Annexin V-, 7AAD+) among the groups (Figure 3E).

### Evaluation of both separation techniques for isolation of CTCs in metastatic breast cancer

Both separation techniques were also evaluated in clinical setting in metastatic breast cancer patients. Patient characteristics are presented in Table 1. The median age of the patients was 58.1 years (min 39.5, max 79.3).

CTCs were isolated side-by-side by Parsortix® and MACS® separation, each from 10 ml of whole

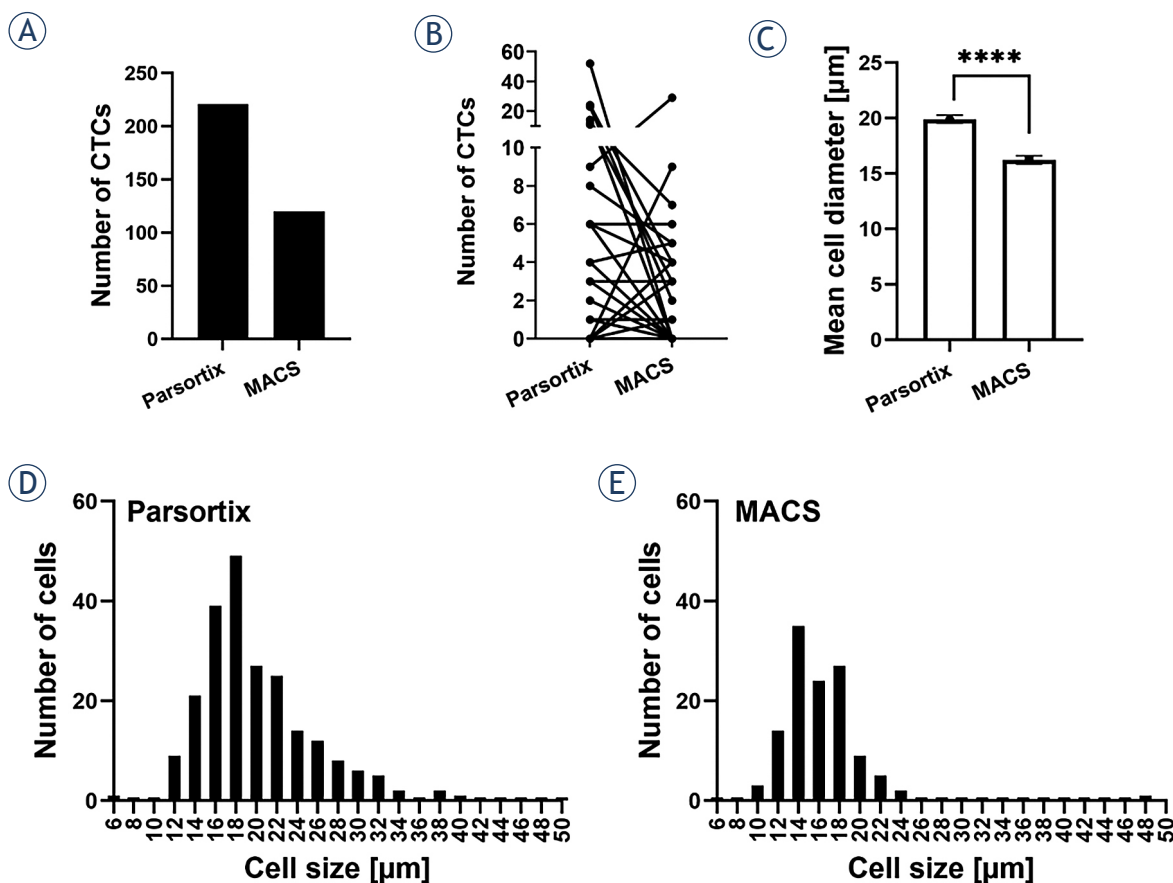


**FIGURE 4.** Parsortix® separation enabled identification of more CTCs and their size was larger compared to MACS® separation. **(A)** Total number of identified CTCs in the patient cohort. **(B)** Number of identified CTCs for each individual patient after Parsortix® or MACS® separation. **(C)** Mean cell diameter of CTCs after Parsortix® or MACS® separation. **(D)** Histogram showing CTC size distribution after Parsortix® separation and **(E)** MACS® separation.

\*\*\*\* =  $p < 0.0001$ ;  $n$  = total number of cells

blood collected through the same blood draw. CTCs were identified and enumerated based on their cytomorphological features such as their size (CTCs larger than 6.5  $\mu\text{m}$ ), round or oval shape, large nucleus, scant cytoplasm and a high N/C ratio. In some cases, mitoses were observed which were suggestive of CTCs since mitosis is not typically observed in normal blood cells. After Parsortix® separation, higher numbers of CTCs were identified. In total, Parsortix® separation resulted in identification of 221 CTCs and MACS® separation in 120 CTCs altogether (Figure 4A). In 58% of the patients, more CTCs were identified after Parsortix® separation, in 27% of patients more CTCs were identified after MACS® separation and in 15% equal numbers of CTCs were identified after both separation techniques (Figure 4B). The identified CTCs were diverse in their size. CTC mean diameter was significantly larger in CTCs after

Parsortix® separation (Figure 4C). Histograms of CTC sizes demonstrating that smaller CTCs were identified after MACS® separation are presented in Figure 4D and Figure 4E.

Besides cell size, different separation techniques also affected the morphology of CTCs. The identified CTCs were classified as morphologically “preserved” and “unpreserved” based on their morphological characteristics. After Parsortix® separation, the majority of identified CTCs were presented with preserved morphology with only 2 CTCs being identified as unpreserved (Figure 5A). Contrary, the majority of CTCs after MACS® separation were presented with unpreserved morphology, only one preserved CTC was identified after this separation technique (Figure 5B). The preserved CTCs were presented as cells with morphological features of malignancy and blast morphology such as large nuclei, high N/C ratio,

scant basophilic cytoplasm and finely granular chromatin structure (Figure 5C). Nucleoli were not visible. CTCs also presented signs of degeneration such as cytoplasmic blebs and cytoplasmic villous projections (Figure 5C). Some of the cells were in a state of active mitosis, which is also a characteristic of tumor cells (Figure 5C). After Parsortix® separation routine cytokeratin AE1/AE3 (CK) immunocytochemical staining was positive in 2 out of 30 patients that were morphologically identified as preserved CTCs (Figure 5C, CK). Vimentin staining was not confirmed in any of the samples due to the suboptimal ICC reaction. The external controls displayed a strong positive reaction, however internal controls (lymphocytes) did not stain properly. Therefore, the staining was not considered valid and further optimization steps are warranted. Morphologically unpreserved CTCs were presented as cells with morphological features of malignancy such as scant eosinophilic cytoplasm with vacuoles and eosinophilic inclusions, large nuclei, high N/C ratio, and irregular nuclear contours with loss of chromatin structure (Figure 5C). After MACS® isolation, unpreserved CTCs were positive for routine cytokeratin AE1/AE3 staining in 2 out of 30 patients.

### CTC polymorphism in metastatic breast cancer is dependent on the isolation protocol

In this metastatic breast cancer patient cohort, highly polymorphic CTCs with blast morphology were identified. CTCs isolated by Parsortix® from the same blood sample varied in size (Figure 6). Numerous CTCs presented villous projections or cytoplasmic blebs, however, plasma membrane of some CTCs was smooth (Figure 6). Cytoplasm was predominantly scant and in some cells, it was almost not visible (Figure 6). MACS® separation from a parallel blood sample collected in the same blood draw resulted in predominantly unpreserved CTCs that also varied in size (Figure 6). Their size was generally smaller (Figure 4C and Figure 6), sometimes the size of a lymphocyte.

## Discussion

In the preclinical part of study, we demonstrated that Parsortix® and MACS® isolation techniques retained the viability and antigenic characteristics of MCF7 breast cancer cells. Hydropic and some other signs of degeneration such as cytoplasmic

TABLE 1. Patient characteristics

Characteristics	Frequency N (%)
<b>Histology</b>	
Invasive ductal carcinoma	28 (93.3)
Invasive lobular carcinoma	2 (6.7)
<b>Tumor stage</b>	
T1	5 (16.7)
T2	18 (60.0)
T3	7 (23.3)
<b>N stage</b>	
N0	5 (16.7)
N1	9 (30.0)
N2	3 (10.0)
N3	7 (23.3)
Unknown	6 (20.0)
<b>Grade</b>	
Grade I	1 (3.3)
Grade II	9 (30.0)
Grade III	19 (63.3)
Unknown	1 (3.3)
<b>Hormone receptor</b>	
Estrogene receptor positive	24 (80.0)
Estrogene receptor negative	6 (20.0)
Progesterone receptor positive	21 (70.0)
Progesterone receptor negative	9 (30.0)
<b>HER2 status</b>	
Positive	4 (13.3)
Negative	26 (86.7)
<b>Molecular subtype</b>	
Luminal A-like	8 (25.8)
Luminal-B like HER2 negative	13 (43.3)
Luminal-B like HER2 positive	3 (10.0)
HER2 positive	1 (3.3)
Triple negative	5 (16.7)

blebs, villous projections and vacuolization were observed after separation with both techniques, however these changes were not severe, and the cells retained their viability. Parsortix® separation induced lower levels of degeneration compared to MACS® in some of the evaluated morphological features. MACS® samples also contained high background of remaining hematopoietic cells. In the clinical setting in metastatic breast cancer patient cohort, we demonstrated that morphologically preserved CTCs were detected by Parsortix® method only. On the contrary, after MACS® separation the majority of detected CTCs were morphologically unpreserved. Furthermore, we demonstrate that CTCs from metastatic breast cancer show a high degree of polymorphism, even within the same patient. Taken together, morphological features of isolated CTCs are dependent on the separation technique and also to some degree to the *in vivo* degeneration in the blood stream. Parsortix® separation was demonstrated to be a

suitable technique for detection of CTCs with preserved cell morphology in metastatic breast cancer for their identification by routine cytopathological techniques.

In our metastatic breast cancer patient cohort, Parsortix® separation was in general superior to MACS® in terms of the quantity and quality of identified CTCs. However, in some samples, MACS samples contained higher numbers of CTCs. When comparing both methods, it should be kept in mind that the successful CTC isolation is not dependent only on the separation technique, but also on the blood sample. In our case, both blood samples were taken during the same blood draw, however in two separate 10 ml blood collection tubes. Therefore, due to the fast blood flow it cannot be expected that both samples will contain equal numbers of CTCs, as CTC numbers in blood can depend on dynamics of CTC shedding from the tumor and also their distribution in the blood stream. Similar discrepancies in CTC numbers were observed also in the study of Xu *et al.*, comparing three isolation platforms.<sup>20</sup>

Higher number of identified CTCs by Parsortix® separation can be to some extent attributed to its higher sensitivity. The sizes of CTCs isolated in our study were all larger than 6.5 µm (gap size in the Parsortix® cassette), therefore the Parsortix® isolation capacity was retained. High recovery rates of different cell lines were reported also when directly compared to EpCAM positive selection techniques.<sup>9,18,21</sup> In the study of Maertens *et al.*, the median recovery rate of the Parsortix® system was 66% compared to 23% for EpCAM based separation (Epithelial Enrich Dynabeads, Invitrogen) after spiking of different cell lines.<sup>21</sup> The advantage of Parsortix® size exclusion separation is also that it enables the capture of CTCs of different phenotypes, therefore higher capture capacity can be expected. Parsortix® separation was demonstrated to identify significantly more mesenchymal human CTCs compared to the clinical CellSearch system.<sup>22</sup> Contrary, MACS® separation is limited by the capture of CTCs of epithelial phenotype, as was already confirmed in our previous study in spiking experiments of human fibroblasts into the buffy coat, demonstrating 0% recovery rate for mesenchymal cell line.<sup>8</sup> CTCs found in the blood of cancer patients are a heterogeneous population as epithelial, mesenchymal and hybrid E/M phenotypes were detected in different cancer types.<sup>23–25</sup> Detection of mesenchymal phenotype was shown to be associated with distant metastasis in breast cancer patients, therefore detection of CTCs with

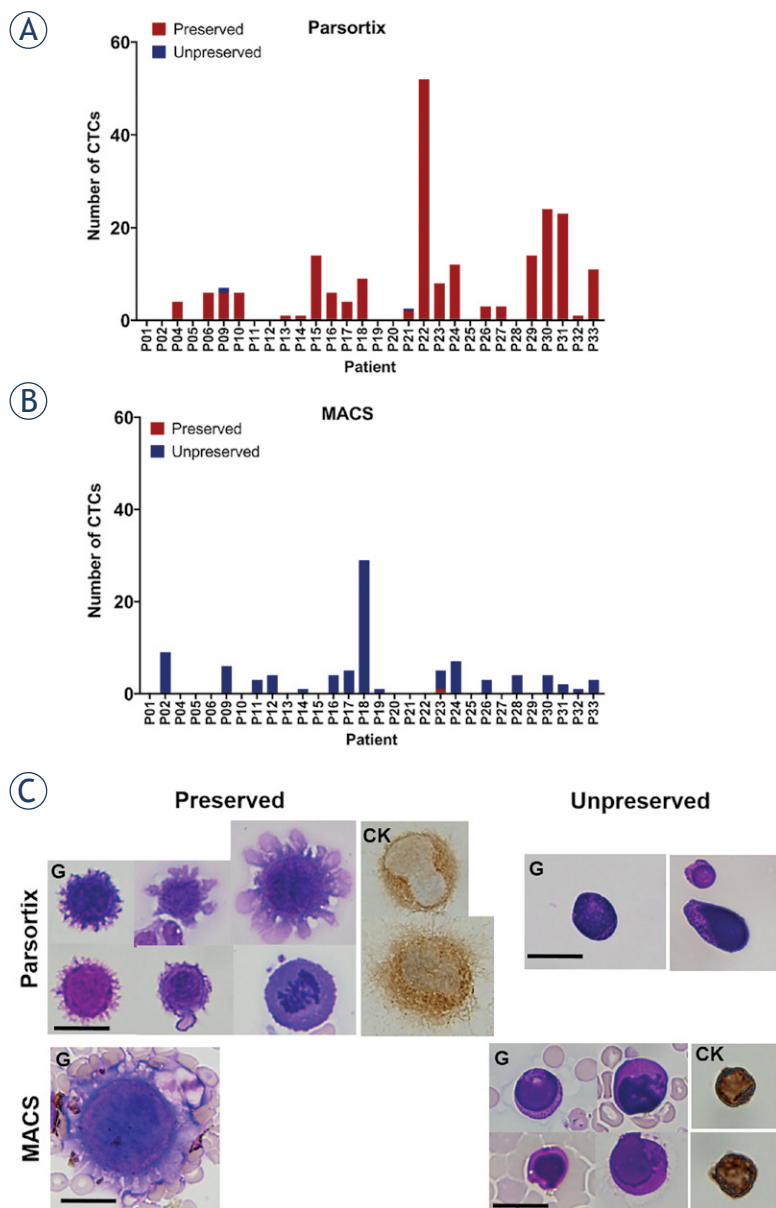


**FIGURE 5.** Effect of separation techniques on morphology of breast cancer CTCs. (A) Number of morphologically preserved or unpreserved CTCs after Parsortix® separation. (B) Number of morphologically preserved or unpreserved CTCs after MACS® separation. (C) Images of CTCs with preserved or unpreserved morphology after both separation techniques. Scale bar represents 20 µm. Cells were stained with Giemsa (G) and cytokeratin AE1/AE3 (CK).

this phenotype seems to be of utmost importance.<sup>24</sup> In our study we detected only 2 out of 30 patients with advanced metastatic disease with epithelial phenotype. CTCs presented with blast morphology, however unfortunately we could not confirm their mesenchymal phenotype due to the problems with our routine vimentin ICC staining, which seems to be suboptimal for CTC slides ob-

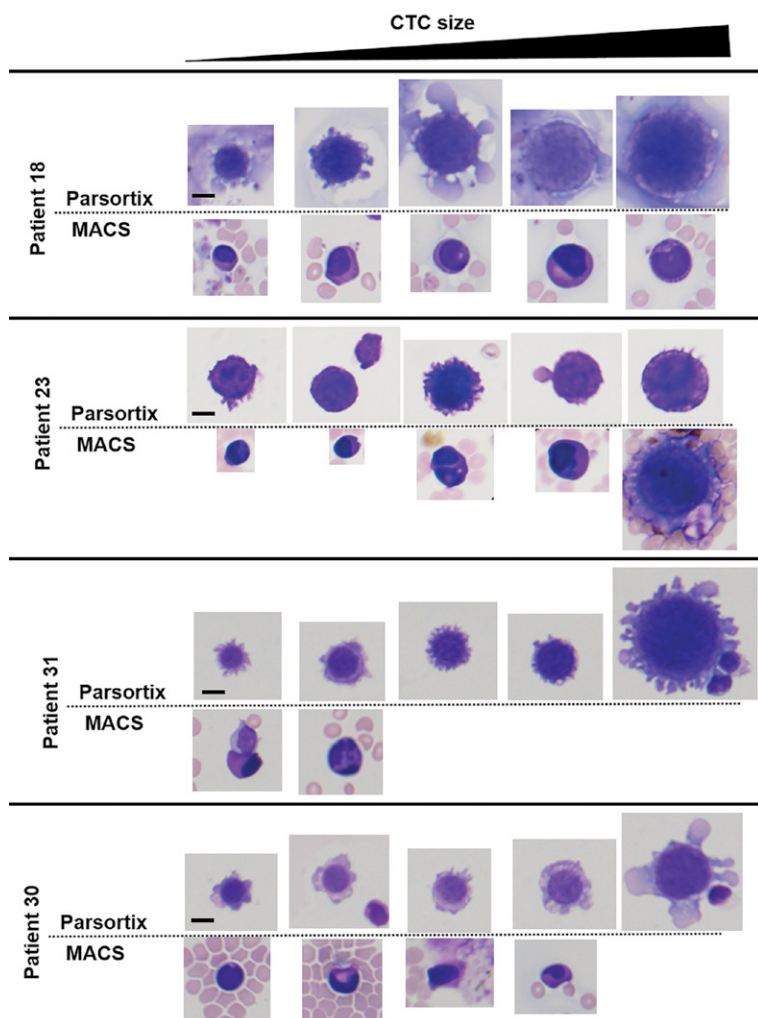


**FIGURE 6.** Morphological polymorphism of CTCs. Images of identified CTCs on a single patient level in four patients (patient 18, 23, 30, 31) are presented following Parsortix® or MACS® separation from blood obtained in a single blood draw. CTCs varied in size and their morphological characteristics. Scale bar represents 10  $\mu$ m.

tained in our study protocol. Further optimization steps for fixation and ICC staining are warranted.

Parsortix® separation was demonstrated to preserve the morphological properties of CTCs much better than MACS® separation. Both blood samples were taken during the same blood draw in the same type of collection tube and both separations were started at the same time, therefore the CTCs were retained at the same environmental conditions until the separation. Separation that followed was different. Parsortix® separation is based on microfluidic system that retain larger cells in the cassette with 6.5  $\mu$ m size gap. In MACS® separation, blood is passed through a dense magnetic column and cells are retained by a strong magnetic

field. After both separations, cells were harvested and cytological slides were prepared by the same protocol. For Parsortix®, harvest (elution) was performed directly from the instrument into the in-house washing buffer. For MACS®, elution of cells from the column was made by MACS® Whole Blood Column Elution Buffer of undisclosed composition. Therefore, the differences in cytomorphology of separated cells can arise from the separation technique itself and also the use of different recommended buffers for separation and elution.

A majority of patient' CTCs presented with the signs of morphological degeneration such as cytoplasmic blebs and villous projections after Parsortix® separation. Compared to our preclinical morphological evaluation of MCF7 cells, CTCs isolated from patient samples were more degenerated, displayed loss of chromatin structure with invisible nucleoli. The higher level of degeneration could be attributed to *in vivo* degeneration in the blood stream. After MACS® separation, degeneration was more severe and the cells displayed the characteristics of cell death such as loss of plasma membrane and nuclear membrane integrity, loss of chromatin structure, vacuoles and cytoplasmic eosinophilic inclusions. CTCs with the similar morphological characteristics were identified in our previous study in early breast cancer patient cohort and were presented as canonical and non-canonical.<sup>8</sup> CTCs were termed canonical if malignant morphological features as well as cytokeratin positivity were observed and non-canonical if malignant morphological features were observed but there was no cytokeratin expression.<sup>8</sup> In the current study, we were unable to use the same criteria as Parsortix® separation enables the isolation of CTCs with various phenotypes, therefore cytokeratin positive staining could not be considered as an identification criterion. Therefore, we focused exclusively on morphological features of cells, which are still a gold standard in cytopathology.<sup>26</sup> For more precise characterization of CTCs further immunochemical studies of their phenotype are required. Our routine cytokeratin AE1/AE3 staining resulted in positive staining in 2 out of 30 patients and routine vimentin staining was not positive in neither of the patients. Despite the fact that this staining performs well in the routine work, the staining is most probably not optimal for the CTCs from clinical samples as the signal of the staining was poor. Same was confirmed for vimentin staining, which could not be properly detected. The external controls displayed positive reaction, however internal controls (lymphocytes) did not

stain properly, therefore the staining was not considered valid. Therefore, we believe that optimization of the routine immunocytochemical staining of CTCs is needed in order to stain these delicate group of cells. Therefore, our next study is aimed at optimization of immunocytochemical and immunofluorescent staining protocols for breast cancer CTCs taking in mind the distinct phenotypes and other markers used for identification in breast cancer cells.

The discrepancy in cytomorphological changes after both separation techniques in preclinical in clinical setting could imply on the fact that patient' CTCs are more sensitive and susceptible to degeneration as cell lines. CTCs in the blood are exposed to the shear stress of blood flow, lack of growth factors and immune surveillance, which can degenerate a large proportion of CTCs.<sup>10</sup> These *in vivo* degenerated CTCs can also be more susceptible to subsequent stress during the separation. Furthermore, in our protocol, their degeneration can be enhanced also by centrifugation in a cyto-centrifuge when preparing the cytological slides.

To the best of our knowledge, our study is one of the few studies investigating detailed morphological features of breast cancer CTCs with routine cytopathological techniques. A direct comparison to other studies of CTC morphology in distinct cancer types cannot be made as the protocols for separation and visualization are different. Therefore, a comparison can be made only based on the published images. In the study of Hattori *et al.* in breast cancer and Tsutsuyama *et al.* in colorectal patients, morphologically preserved single or clustered CTCs were obtained.<sup>14,15</sup> The cells showed no sign of hydropic degeneration and the nuclear structure was preserved, as the samples were fixed in formalin prior to cytological slides preparation. Both studies utilized Optnics Precision Co. filtration device, which therefore also seems suitable for cytology-based detection of CTCs. In a case study of Marrinnuci *et al.*, 659 CTCs were identified in a single 10 ml blood sample in metastatic breast cancer patient following the fiber-optic array scanning technology (FAST) cytometry.<sup>13</sup> Similar to our study, they found that the patient's CTCs exhibit a high degree of polymorphism with CTCs exhibiting early and late apoptotic changes.<sup>13</sup> In the study of Kuvendjiska *et al.* in non-metastatic esophageal adenocarcinoma, different types of CTCs were identified based on their morphological features after ISET filtration.<sup>16</sup> Small and large single-CTCs, cluster CTCs and circulating cancer-associated macrophage-like cells (CAML) were identified.

CTCs presented with increased N/C ratio, enlarged and hyperchromatic nuclei, loss of chromatin structure, irregular nuclear borders and sometimes multilobulated nuclei, therefore, their morphology was to our opinion not sufficiently preserved.<sup>16</sup>

This study was a preliminary study, aimed at side-by-side comparison of two available separation techniques in order to identify which of the two methods is more appropriate for integration into our routine clinical cytopathology laboratory. The integration of this method to our laboratory will allow us to conduct subsequent clinical studies, which will be aimed at investigation of the clinical relevance of the CTC number and their preserved morphology in different tumor types.

In conclusion, Parsortix® technology is straightforward technology for CTC isolation, which enables the preservation of cell morphology and can be easily integrated into a routine cytopathology laboratory. Cytopathological analysis and microscopic examination of cells is still the gold standard in cytopathology and histology in cancer management. The advantage of cytopathological analysis is that it is easily accessible in the clinical environment as cytopathologists are an integral part of cancer patient care. Therefore, the analysis can be done without the use of special techniques and instruments such as flow cytometry or single cell next generation sequencing (NGS), which require substantial financial and human resources.

## Acknowledgments

We would like to thank all patients participating in this study. We would also like to thank ANGLE plc. for providing the Parsortix® instrument for evaluation in our lab with special thanks to Adam Giles, Michael O'Bri-en and Lara Stevenato for a detailed training and their valuable advice. We acknowledge the financial support of Slovenian Research Agency (grant no. P3-0003, P3-0289 and P3-0321).

## References

1. Bilani N, Elson L, Liang H, Elimimian EB, Arteta-Bulos R, Nahleh Z. Prognostic and predictive value of circulating and disseminated tumor cells in breast cancer: A National Cancer Database (NCDB) analysis. *Technol Cancer Res Treat* 2020; **19**: 1533033820980107. doi: 10.1177/1533033820980107
2. Theil G, Fornara P, Bialek J. Position of circulating tumor cells in the clinical routine in prostate cancer and breast cancer patients. *Cancers* 2020; **12**: 3782. doi: 10.3390/cancers12123782
3. Lozar T, Gersak K, Cemazar M, Grasic Kuhar C, Jesenko T. The biology and clinical potential of circulating tumor cells. *Radiol Oncol* 2019; **53**: 131–47. doi: 10.2478/raon-2019-0024

4. Grosse-Wilde A, Fouquier d'Hérouël A, McIntosh E, Ertaylan G, Skupin A, Kuestner RE, et al. Stemness of the hybrid epithelial/mesenchymal state in breast cancer and its association with poor survival. *PLoS One* 2015; **10**: e0126522. doi: 10.1371/journal.pone.0126522
5. Jolly MK, Boareto M, Huang B, Jia D, Lu M, Ben-Jacob E, et al. Implications of the hybrid epithelial/mesenchymal phenotype in metastasis. *Front Oncol* 2015; **5**:155. doi: 10.3389/fonc.2015.00155
6. Riethdorf S, Fritsche H, Muller V, Rau T, Schindlbeck C, Rack B, et al. Detection of circulating tumor cells in peripheral blood of patients with metastatic breast cancer: a validation study of the CellSearch System. *Clin Cancer Res* 2007; **13**: 920–8. doi: 10.1158/1078-0432.CCR-06-1695
7. Hu XC, Wang Y, Shi DR, Loo TY, Chow LWC. Immunomagnetic tumor cell enrichment is promising in detecting circulating breast cancer cells. *Oncology* 2003; **64**: 160–5. doi: 10.1159/000067776
8. Lozar T, Jesenko T, Kloboves Prevodnik V, Cemazar M, Hosta V, Jericevic A, et al. Preclinical and clinical evaluation of magnetic-activated cell separation technology for CTC isolation in breast cancer. *Front Oncol* 2020; **10**: 554554. doi: 10.3389/fonc.2020.554554.
9. Miller MC, Robinson PS, Wagner C, O'Shannessy DJ. The Parsortix™ cell separation system — a versatile liquid biopsy platform. *Cytometry A* 2018; **93**: 1234–9. doi: 10.1002/cyto.a.23571
10. Huang Q, Hu X, He W, Zhao Y, Hao S, Wu Q, et al. Fluid shear stress and tumor metastasis. *Am J Cancer Res* 2018; **8**: 763–777. PMID: 29888101
11. Lowe AC, Pignon JC, Carvo I, Drage MG, Constantine NM, Jones N, et al. Young investigator challenge: application of cytologic techniques to circulating tumor cell specimens: detecting activation of the oncogenic transcription factor STAT3. *Cancer Cytopathol* 2015; **123**: 696–705. doi: 10.1002/cnc.21640
12. Kamal M, Macall L, Horton C, Hills N, Davis R, Nguyen R, et al. Cytopathologic identification of circulating tumor cells (CTCs) in breast cancer: Application of size-based enrichment. *Clin Diagnostic Pathol* 2019; **3**: 1–5. doi: 10.15761/CDP.1000S1001
13. Marrinucci D, Bethel K, Bruce RH, Curry DN, Hsieh B, Humphrey M, et al. Case study of the morphologic variation of circulating tumor cells. *Hum Pathol* 2007; **38**: 514–9. doi: 10.1016/j.humpath.2006.08.027
14. Hattori M, Nakanishi H, Yoshimura M, Iwase M, Yoshimura A, Adachi Y, et al. Circulating tumor cells detection in tumor draining vein of breast cancer patients. *Sci Rep* 2019; **9**: 18195. doi: 10.1038/s41598-019-54839-y
15. Tsutsuyama M, Nakanishi H, Yoshimura M, Oshiro T, Kinoshita T, Komori K, et al. Detection of circulating tumor cells in drainage venous blood from colorectal cancer patients using a new filtration and cytology-based automated platform. *PLoS One* 2019; **14**: e0212221. doi: 10.1371/journal.pone.0212221
16. Kuvendjiska J, Pitman MB, Martini V, Braun C, Grebe K, Timme S, et al. Cytopathological heterogeneity of circulating tumor cells in non-metastatic esophageal adenocarcinoma. *Anticancer Res* 2020; **40**: 5679–85. doi: 10.21873/anticancer.14582
17. Lee AV, Oesterreich S, Davidson NE. MCF-7 cells - changing the course of breast cancer research and care for 45 years. *J Natl Cancer Inst* 2015; **107**: djv073. doi: 10.1093/jnci/djv073
18. Koch C, Joosse SA, Schneegans S, Wilken OJW, Janning M, Loreth D, et al. Pre-analytical and analytical variables of label-independent enrichment and automated detection of circulating tumor cells in cancer patients. *Cancers* 2020; **12**: 442. doi: 10.3390/cancers12020442
19. Schneider CA, Rasband WS, Eliceiri KW. NIH Image to ImageJ: 25 years of image analysis. *Nature Methods* 2012; **9**: 671–5. doi: 10.1038/nmeth.2089
20. Xu L, Mao X, Imrali A, Syed F, Mutsvangwa K, Berney D, et al. Optimization and evaluation of a novel size based circulating tumor cell isolation system. *PLoS One* 2015; **10**: e0138032. doi: 10.1371/journal.pone.0138032
21. Maertens Y, Humberg V, Erlmeier F, Steffens S, Steinestel J, Bögemann M, et al. Comparison of isolation platforms for detection of circulating renal cell carcinoma cells. *Oncotarget*, 2017; **8**: 87710–7. doi: 10.18632/oncotarget.21197
22. Kitz J, Goodale D, Postenka C, Lowes LE, Allan AL. EMT-independent detection of circulating tumor cells in human blood samples and pre-clinical mouse models of metastasis. *Clin Exp Metastasis* 2021; **38**: 97-108. doi:10.1007/s10585-020-10070-y.
23. Pan L, Yan G, Chen W, Sun L, Wang J, Yang J. Distribution of circulating tumor cell phenotype in early cervical cancer. *Cancer Manag Res* 2019; **11**: 5531–5536. doi: 10.2147/CMAR.S19839.
24. Zhang S, Wu T, Peng X, Liu J, Liu F, Wu S, et al. Mesenchymal phenotype of circulating tumor cells is associated with distant metastasis in breast cancer patients. *Cancer Manag Res* 2017; **9**: 691–700. doi: 10.2147/CMAR.S149801
25. Messaritakis I, Politaki E, Kotsakis A, Dermizaki EK, Koinis F, Lagoudaki E, et al. Phenotypic characterization of circulating tumor cells in the peripheral blood of patients with small cell lung cancer. *PLoS One* 2017; **12**: e0181211. doi: 10.1371/journal.pone.0181211
26. Dey P. Routine staining in cytology laboratory. In: *Basic and advanced laboratory techniques in histopathology and cytology*. Singapore: Springer; 2018. p. 133–8.

research article

# Simvastatin is effective in killing the radioresistant breast carcinoma cells

Bertram Aschenbrenner<sup>1,2,3</sup>, Giulia Negro<sup>1,2,3</sup>, Dragana Savic<sup>1,2,3</sup>, Maxim Sorokin<sup>3,4,5,6</sup>, Anton Buzdin<sup>3,6,7,8</sup>, Ute Ganswindt<sup>1</sup>, Maja Cemazar<sup>3,9</sup>, Gregor Sersa<sup>9</sup>, Sergej Skvortsov<sup>1,2</sup>, Ira Skvortsova<sup>1,2,3</sup>

<sup>1</sup> Medical University of Innsbruck, Therapeutic Radiology and Oncology, Innsbruck, Austria

<sup>2</sup> Tyrolean Cancer Research Institute, Innsbruck, Austria

<sup>3</sup> EORTC PathoBiology Group

<sup>4</sup> Institute of Personalized Medicine, Sechenov First Moscow State Medical University, Moscow, Russia

<sup>5</sup> Omicsway Corp., Walnut, USA

<sup>6</sup> Shemyakin-Ovchinnikov Institute of Bioorganic Chemistry, Moscow, Russia

<sup>7</sup> Oncobox Ltd., Moscow, Russia

<sup>8</sup> World-Class Research Center “Digital Biodesign and Personalized Healthcare”, Sechenov First Moscow State Medical University, Moscow, Russia

<sup>9</sup> Institute of Oncology Ljubljana, Department of Experimental Oncology, Ljubljana, Slovenia

Radiol Oncol 2021; 55(3): 305-316.

Received 10 March 2021

Accepted 2 April 2021

Correspondence to: Prof. Ira Skvortsova, Laboratory for Experimental and Translational Research on Radiation Oncology (EXTRO-Lab), Department of Therapeutic Radiology and Oncology, Medical University of Innsbruck, Anichstr. 35, A-6020 Innsbruck, Austria.  
E-mail: Ira.Skvortsova@i-med.ac.at

Disclosure: No potential conflicts of interest were disclosed.

This is an open access article under the CC BY-NC-ND license (<http://creativecommons.org/licenses/by-nc-nd/4.0/>).

**Background.** Statins, small molecular 3-hydroxy-3-methylglutaryl-coenzyme A reductase inhibitors, are widely used to lower cholesterol levels in lipid-metabolism disorders. Recent preclinical and clinical studies have shown that statins exert beneficial effects in the management of breast cancer by increasing recurrence free survival. Unfortunately, the underlying mechanisms remain elusive.

**Materials and methods.** Simvastatin, one of the most widely prescribed lipophilic statins was utilized to investigate potential radiosensitizing effects and an impact on cell survival and migration in radioresistant breast cancer cell lines.

**Results.** Compared to parental cell counterparts, radioresistant MDA-MB-231-RR, T47D-RR and Au565-RR cells were characterized by upregulation of 3-hydroxy-3-methylglutaryl-coenzyme A reductase (HMGCR) expression accompanied by epithelial-to-mesenchymal transition (EMT) activation. Radioresistant breast cancer cells can be killed by simvastatin via mobilizing of a variety of pathways involved in apoptosis and autophagy. In the presence of simvastatin migratory abilities and vimentin expression is diminished while E-cadherin expression is increased.

**Conclusions.** The present study suggests that simvastatin may effectively eradicate radioresistant breast carcinoma cells and diminish their mesenchymal phenotypes.

Key words: breast cancer cells; cancer stem cells; radiotherapy; migration; simvastatin

## Introduction

Breast cancer is the most diagnosed malignant tumor in women. It is estimated over 355,000 cases in the European Union will be registered in 2020 that corresponds to 13.3% of all diagnosed malignan-

cies.<sup>1</sup> Therapeutic management of breast cancer is markedly changed during last 20 years. Thus, after breast-conserving surgery, all patients receive either partial or whole-breast radiation therapy.<sup>2</sup> This strategy allows to significantly reduce the risk of local breast cancer recurrences and breast can-

cer-related mortality.<sup>3,4</sup> However, ipsilateral local recurrences still occur in locally and systemically treated breast cancer patients. Current clinical classification requires to determine whether an ipsilateral relapsed tumor is a true recurrence or a second primary tumor.<sup>5,6</sup> The relapsed tumors and second primary tumors are distinct in their localization and molecular features. It was also found that recurrence-free and overall survival rates for true recurrences are significantly shorter than for the second primary tumors.<sup>7</sup> We, therefore, assumed that true recurrences usually occur from surviving breast carcinoma cells after primary treatment using radiotherapy with or without chemotherapeutics, antihormonal or targeted agents. The cells recovered after their exposure to anti-cancer therapeutic approaches may possess a treatment resistant phenotype characterized by enhancement of pro-survival mechanisms protecting them from cytotoxic or cytostatic agents. It is logical to suggest that carcinoma cells comprising the tumor recurrences can demonstrate radiation resistance due to their abilities to survive and further proliferate within the irradiated field. To have a therapeutic benefit from re-irradiation, the radiation dose should be markedly increased to effectively kill radioresistant breast carcinoma cells. Unfortunately, due to the problem of tissue tolerance, the required dose can usually not be achieved<sup>3</sup>, and a lower dose of re-irradiation is not able to successfully eradicate radioresistant carcinoma cells and can even increase the molecular characteristics underlying radiation resistance.

Since therapy resistant carcinoma cells can also possess an augmentation of their metastatic capacities, true local breast cancer recurrences are often accompanied by distant metastasis.<sup>8,9</sup> These metastatic lesions can also be treated by radiotherapy. However, an efficacy of this therapeutic approach might be diminished due to radiation resistance of breast carcinoma cells spreading to distant organs and tissues. Therefore, it is logical to suggest the use of systemic treatment to improve radiation response and combat metastatic spread of radioresistant breast carcinoma cells.

Systemic treatment of cancer can include a variety of different agents. Our research group has focused on the lipid-lowering drug simvastatin, which is often used by breast cancer patients independently from their cancer diagnose. Simvastatin as other statins is a competitive inhibitor of 3-hydroxy-3-methylglutaryl-coenzyme A reductase (HMGCR). Although anti-cancer activity of statins is described in literature<sup>10</sup>, there is still no agree-

ment whether statins generally and simvastatin particularly can be used to improve therapy response of radioresistant breast carcinoma cells, and which molecular properties of carcinoma cells make them susceptible to simvastatin treatment.

Therefore, the main aim of this study was to determine the sensitivities of radioresistant breast carcinoma cells to simvastatin and mechanisms underlying the cellular responses to the drug alone or in combination with ionizing radiation.

## Materials and methods

### Cell culture and treatment with ionizing radiation

MDA-MB-231 (triple-negative type: estrogen, progesterone and HER2 receptor negative (ER-, PR-, HER2-), T47D (luminal A type: ER+, PR+, HER2-) and Au565 (Her2-positive type: ER-, PR-, HER2/neu+) cells were purchased from the American Type Culture Collection. All cell lines were grown in RPMI1640 medium supplemented with 2 mM L-glutamine, 50 U/mL penicillin, 50 µg/mL streptomycin (Thermo Fisher Scientific, Vienna, Austria), and 10% fetal bovine serum (FBS) (HyClone™) (Thermo Fisher Scientific, Vienna, Austria). T47D cells were maintained in medium containing 10 µg/ml bovine insulin (Sigma Aldrich, Millipore Merck, Vienna, Austria). Cell cultures were incubated in a 5% CO<sub>2</sub> humidified atmosphere at 37°C.

Radiation-resistant cells, MDA-MB-231-RR, T47D-RR and Au565-RR (RR cells), were obtained from parental breast cancer cells after repetitive exposure to ionizing radiation (10 Gy) (16 MV x-rays) using an Elekta Precise Linear Accelerator (Elekta Oncology Systems, UK) at a dose rate of approximately 1.8 Gy/min. The cells were irradiated every 2 weeks when breast cancer cells recovered from their exposure to ionizing radiation. Cells which survived after irradiation (total dose of 100 Gy) were collected for further experiments. The newly received cell lines maintained resistance to ionizing radiation independently from a number of passages.

Simvastatin was purchased from Calbiochem (Merck Millipore, Vienna, Austria). Simvastatin was dissolved in dimethyl sulfoxide (DMSO, Sigma Aldrich, Merck Millipore, Vienna, Austria) and used at a final clinically relevant concentration of 8 µM.

Cells were irradiated at single doses of 2, 4, 6, and 8 Gy to determine radiation response of parental and RR breast carcinoma cells, and at a single

clinically relevant dose of 2 Gy for all other experiments using an Elekta Precise Linear Accelerator (Elekta Oncology Systems, UK).

### 3D tomographic microscopy

Parental and radioresistant MDA-MB-231, T47D, and Au565 cells were seeded into the glass-bottom dishes with a diameter of 35 mm (Ibidi, Switzerland), and cells were incubated for 24 hours at 37°C and 5% CO<sub>2</sub> humidified atmosphere. Next, cells were analysed for their morphology using 3D tomographic microscope with a 60x objective (3D Cell Explorer-FLUO, Nanolive SA, Switzerland), and 3D tomographic images (z-stacks) were collected.

### Apoptosis assay

Investigated breast carcinoma cells (parental and radioresistant MDA-MB-231, T47D and Au565) were seeded and cultured overnight in 6-well plates at  $1.0 \times 10^5$  cells/well. Cells were exposed to ionizing radiation at single doses of 0, 2, 4, 6, and 8 Gy. After being cultured for 72 hours, irradiated cells were collected for apoptosis assay. Briefly, the cells were trypsinized and then pelleted by centrifugation at 300 g for 10 minutes at 4°C. The supernatant was discarded, and the pellet was washed once with cold PBS and further resuspended in Annexin-V binding buffer containing Annexin-V-APC and propidium iodide (PI) (AnxA100PI Kit, MabTag, Friesoythe, Germany). Cells were stained in darkness for 15 minutes, and the same volume (100 µL) of Annexin-V binding buffer was added to each sample and the prepared samples were analyzed by flow cytometry (BD FACSCanto™ II). The percentage of Annexin-V and PI positive cells was evaluated using the FlowJo\_V10.6.2 software. Three independent experiments in duplicates were performed.

### Cell death development and Sub-G1 evaluation

Breast carcinoma cells were seeded in 6-well plates and treated either with DMSO alone as a vehicle control, simvastatin (8 µM) alone, irradiation alone (2 Gy) or combination treatment using cell pretreatment with simvastatin (8 µM) for 24 hours followed by irradiation (2 Gy). Cell death development was studied during 72 hours after simvastatin treatment and different time points of 24 hours, 48 hours and 72 hours were selected for analysis.

To evaluate the induction of cell death, samples were analyzed as previously described.<sup>11</sup> Briefly, all cells were harvested at the indicated time points followed by centrifugation for 10 minutes (300 g) at 4°C. The pellets were washed with cold PBS and resuspended in hypotonicfluorochrome solution (50 µg/mL propidium iodide (PI), 0.1% sodium citrate, 0.1% Triton X-100). The samples were stained in darkness for 30 minutes at 4°C followed by flow cytometry (BD FACSCanto™ II) analysis. To determine DNA fragmentation, PI fluorescence of individual nuclei was evaluated with an excitation wavelength of 488 nm and an emission wavelength of 670 nm. Gating was done on single nuclei to exclude doublets and debris from the analysis. Cell cycle analysis was performed using FlowJo\_V10.6.2 software, and the Sub-G1 fraction was determined.

### Western blot analysis

Western blot was performed as published previously<sup>12,13</sup> using E-cadherin, caspase-3, caspase-7, caspase-8, caspase-9, PARP-1, cytochrome C, XIAP, AIF, beclin-1, LC3 A/B rabbit monoclonal antibody (Cell Signaling Technology, Inc., Beverly, MA, USA), HMGCR rabbit monoclonal antibody (Abcam, UK), Vimentin, Smac/DIABLO mouse (Cell Signaling Technology, Inc., Beverly, MA, USA). Loading control was evaluated using  $\alpha$ -tubulin rabbit monoclonal antibody (Cell Signaling Technology, Inc., Beverly, MA, USA). For evaluation of protein expression, X-ray films (GE Healthcare, Chicago, IL, USA) were scanned and analyzed by the Image Studio™ Lite 5.0 (LI-COR Biotechnology, Lincoln, NB, USA). The Integrated Density Value (IDV) was obtained as a ratio of normalized protein band densities in parental and radioresistant RR cells after background correction.

### Migration assay

Scratch assay or wound healing assay was performed to evaluate two-dimensional cancer cell migration. Parental and radioresistant breast carcinoma cells were grown to confluence in 6-well plates. A scratch was made on the monolayer using a sterile 200 µL-pipette tip. The monolayer was rinsed three times with PBS and placed in the appropriate complete medium with either simvastatin dissolved in DMSO (8 µM) or DMSO as a vehicle control. Phase contrast images were made during 20 hours at a magnification of 4x (Lionheart Live Cell Microscope, BioTek, Bad Friedrichshall,

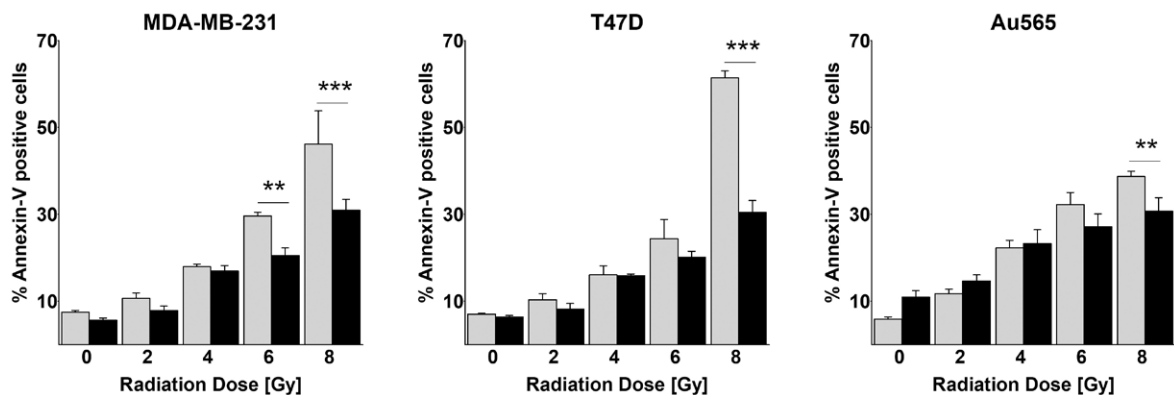


**FIGURE 1.** Radiation-induced apoptosis in breast carcinoma cells. Radiation sensitivity of the investigated parental and radioresistant breast carcinoma cells was determined using apoptosis assay as described in the section Materials and methods. Grey bars represent parental cells and black bars the radioresistant cells. All experiments were performed at least three times in duplicates; \* =  $p < 0.05$ ; \*\* =  $p < 0.01$ ; \*\*\* =  $p < 0.001$ .

Germany), and the gap width was measured using the Gen5 (V. 3.08) software. The percentage of the gap width which remained after 20 hours of cell incubation was plotted.

### Statistical analysis

GraphPad Prism software was used to plot the graphs and for statistical evaluation. All the values are represented as the means  $\pm$  standard error of the mean. Statistical comparisons were performed by one-way analysis of variance (ANOVA) followed by Bonferroni post-hoc comparisons to analyze the differences between each group. Statistical significance was defined as: \* =  $P \leq 0,05$ , \*\* =  $P \leq 0,01$ , \*\*\* =  $P \leq 0,001$  and \*\*\*\* =  $P \leq 0,0001$ .

## Results

### Radiation resistance of breast carcinoma cells

To confirm that newly received breast carcinoma cells (RR cells) possess radiation resistance, parental and RR cells were exposed to different doses of ionizing radiation and their susceptibility to apoptosis was determined. As it is seen in Figure 1, all three MDA-MB-231-RR, T47D-RR, and Au565-RR cells were less sensitive to irradiation than their parental counterparts. Although there are no significant differences in apoptosis development in parental and RR cells irradiated at lower single doses (2 and 4 Gy), cell exposure to ionizing radiation at higher doses of 6 and 8 Gy was accompanied by more pronounced cell death in parental cells. Thus,

irradiation at a dose of 8 Gy induced  $30.93 \pm 2.47\%$  AnnexinV-PI-positive cells in MDA-MB-231-RR,  $30.46 \pm 2.71\%$  in T47D-RR, and  $30.75 \pm 3.08\%$  in Au565-RR cells versus  $46.15 \pm 7.67\%$ ,  $61.40 \pm 1.60\%$ , and  $38.69 \pm 1.22\%$  in parental MDA-MB-231, T47D, and Au565 breast carcinoma cells, respectively.

### HMGCR expression in breast carcinoma cells

Since HMGCR is a target for simvastatin, its expression was evaluated in parental and RR breast carcinoma cells (Figure 2A). It was found that triple-negative MDA-MB-231-RR and hormone receptor positive T47D-RR cells were characterized by up-regulation of HMGCR in comparison with their parental counterparts. It is necessary to note that parental T47D breast carcinoma cells did not express HMGCR whereas T47D-RR cells showed HMGCR overexpression. Surprisingly, Her2-positive Au565-RR demonstrated slight downregulation of HMGCR compared to the parental Au565 cells.

Administration of simvastatin alone at a clinically relevant doses of 8  $\mu\text{M}$  resulted in significant downregulation of HMGCR in all investigated breast carcinoma cells (Figure 2B). Cell exposure to the clinically relevant single dose of irradiation of 2 Gy led to the substantial increase of HMGCR expression especially at 24 hours after the treatment. Simvastatin-pretreated parental and RR breast carcinoma cells were protected from radiation-induced HMGCR upregulation, which did not significantly differ from those in cells treated with simvastatin alone.

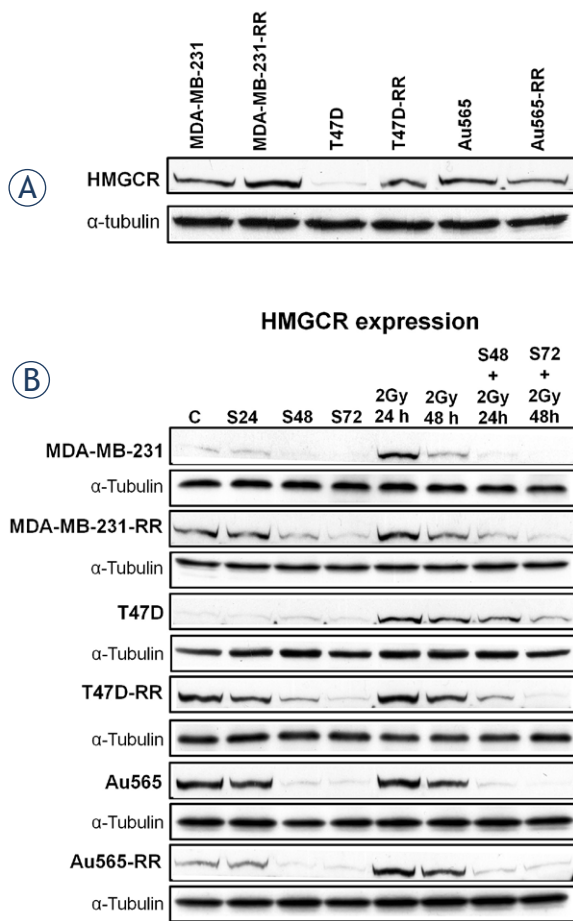


**FIGURE 2.** HMGR expression in breast carcinoma cells. **(A)** Constitutive 3-hydroxy-3-methylglutaryl-coenzyme A reductase (HMGR) expressions in parental and radioresistant breast carcinoma cells. Protein extracts from total cell lysates were subjected to Western blot analysis, and constitutive levels of HMGR were determined in all investigated breast carcinoma cells; **(B)** Simvastatin-caused modulation of HMGR expression in parental and radioresistant breast carcinoma cells was confirmed using Western blot analysis.

### Simvastatin-caused modulation of migratory abilities of breast carcinoma cells

Next, we have investigated whether RR breast carcinoma cells are altered in their migratory capacities (Figure 3A, 3B). Triple-negative MDA-MB-231-RR and hormone receptor-positive T47D-RR breast carcinoma cells showed increased migratory properties compared to their parental counterparts. Using scratch assay, it was observed that MDA-MB-231-RR cells were able to close the gap within 20 hours, whereas parental MDA-MB-231 cells demonstrated  $51.62 \pm 2.55\%$  of the original gap width left at this time point. Very similar data

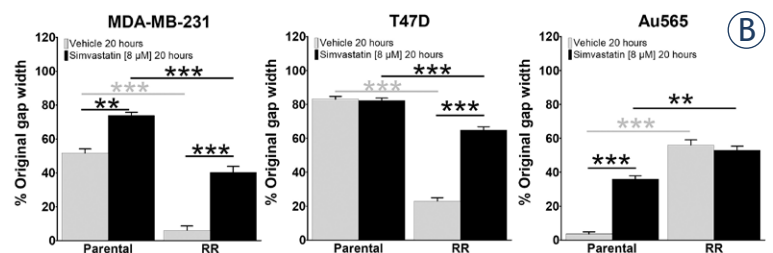
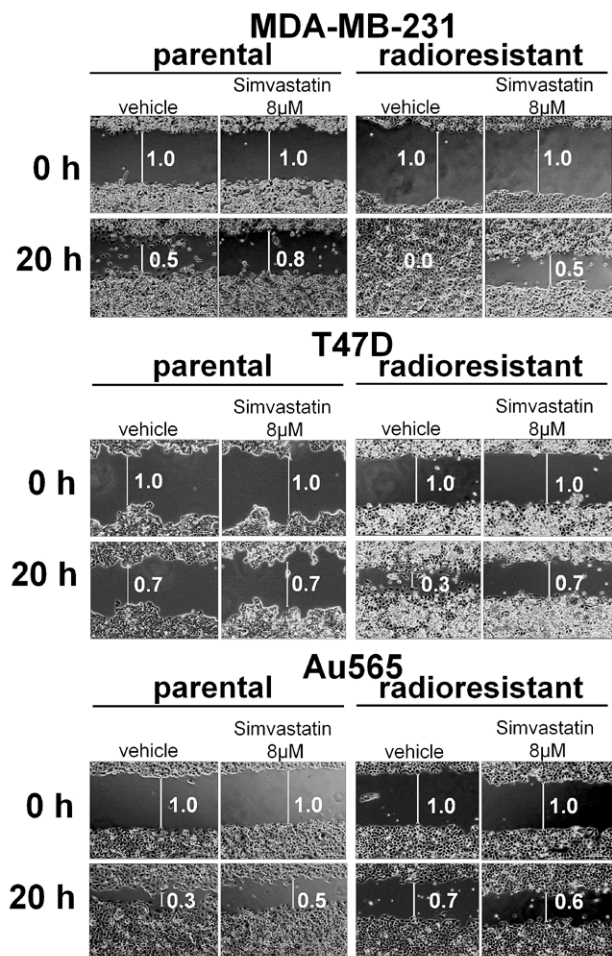


**FIGURE 3.** Simvastatin-regulated breast carcinoma cell migration. **(A)** Wound healing assay was used to determine how simvastatin affected breast carcinoma cell migration. Cell migration was assayed at a magnification of 4x (Lionheart Live Cell Microscope, BioTek, Bad Friedrichshall, Germany). The cell migration rates were determined as a ratio between the gap width at indicated time point and initial gap width at 0 hours; **(B)** Statistical evaluation of the gap width in breast carcinoma cells. Gap width was measured using the Gen5 (V. 3.08) software and the percentage of the gap width remained after 20 hours of cell incubation in presence of DMSO as a vehicle control or simvastatin (8  $\mu$ M) was plotted. All experiments were performed at least three times in duplicates; \* =  $p < 0.05$ ; \*\* =  $p < 0.01$ ; \*\*\* =  $p < 0.001$ .

were received when migratory capacities of T47D-RR breast carcinoma cells were compared with those in parental T47D cells. Thus, parental T47D cells had  $83.08 \pm 1.71\%$  of the gap open 20 hours

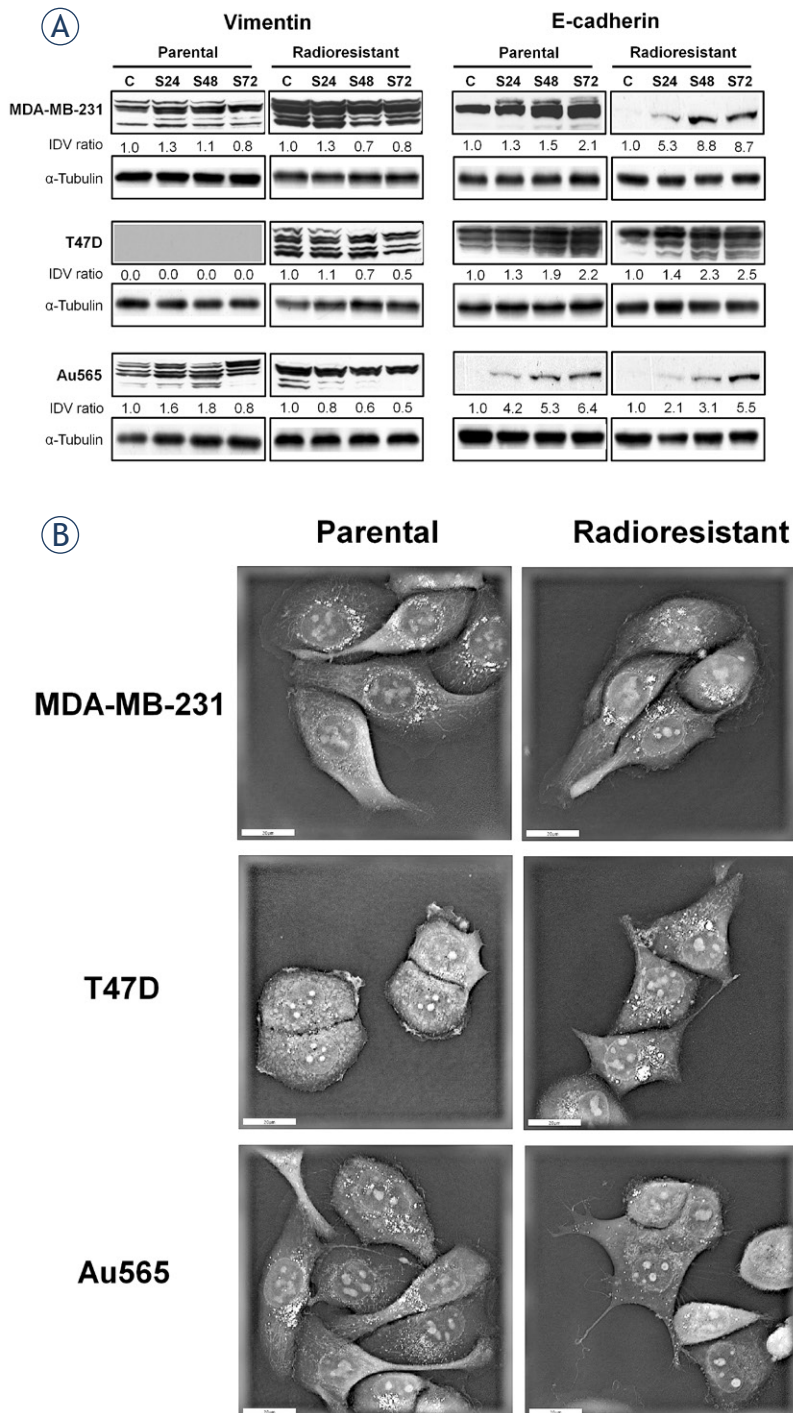


**FIGURE 4.** Mesenchymal and epithelial markers in breast carcinoma cells treated with simvastatin. **(A)** Simvastatin-dependent regulation of vimentin and E-cadherin expressions in parental and radioresistant breast carcinoma cells were evaluated using Western blot analysis as described in the section Materials and Methods. IDV was calculated for each protein band and normalized to the  $\alpha$ -tubulin band density after background correction. IDV ratio means fold-change of vimentin or E-cadherin band densities in simvastatin-treated compared to the vehicle-treated breast carcinoma cells. **(B)** 3D holographic breast cancer cell microscopy. Parental and radioresistant MDA-MB-231, T47D, and Au565 cells were analyzed for their morphology using 3D Nanolive Explorer-FLUO as described in the Materials and Methods.

after scratching, whereas radioresistant T47D-RR cells demonstrated only  $22.97 \pm 2.05\%$  of the original gap width open. In contrast, parental Her2-neu-positive Au565 cells were more migratory than their radioresistant Au565-RR counterparts with the gap closure of more than  $\sim 95\%$  and  $\sim 60\%$ , respectively.

Simvastatin significantly reduced migratory abilities of parental and radioresistant MDA-MB-231-RR, radioresistant T47D-RR, and parental Au565 breast carcinoma cells. The most prominent inhibition of cell migration was observed in radioresistant MDA-MB-231-RR and T47D-RR cells ( $\sim 5$ -fold simvastatin-caused reduction of migration in MDA-MB-231-RR cells versus  $\sim 1.6$ -fold in parental MDA-MB-231 cells, and  $\sim 3$ -fold simvastatin-induced reduction of migration in T47D-RR cells versus no effect observed in simvastatin-treated parental T47D cells). Surprisingly, radioresistant Au565-RR cells were not affected in their migratory capacities by simvastatin, and the gap was equally closed by the untreated and treated Au565-RR cells.

#### Simvastatin-regulated expression of epithelial and mesenchymal markers in breast carcinoma cells

Considering that radioresistant breast carcinoma cells were affected in their sensitivity to ionizing radiation and altered in their migratory capacities, we next analyzed the levels of expression of mesenchymal (vimentin) and epithelial (E-cadherin) markers in the investigated carcinoma cells (Figure 4A). It was found that all radioresistant breast carcinoma cells acquired a more mesenchymal phenotype compared to parental cells. Interesting to note that radioresistant MDA-MB-231-RR cells lost E-cadherin expression accompanied by up-regulation of vimentin. Parental T47D cells had a pure epithelial phenotype with overexpression of E-cadherin with no sign of vimentin expression, and radioresistant T47D-RR cells showed a switch toward mixed epithelial and mesenchymal phenotype characterized by overexpression of both epithelial and mesenchymal markers. Parental Au565 cells and radioresistant Au565-RR cells were equal in their mesenchymal phenotype with vimentin overexpression and lack of E-cadherin expression. Cell treatment with simvastatin resulted in the time-dependent down-regulation of vimentin and up-regulation of E-cadherin in all investigated breast carcinoma cells. Even the cells lacking E-cadherin revealed a simvastatin-induced up-regulation of the epithelial marker. Epithelial-

to-mesenchymal transition of radioresistant breast carcinoma cells was accompanied by morphological changes characterized by the membrane ruffling, filopodia and lamellipodia formation resulting in the increased cellular surfaces (Figure 4B).

### Cell death development in breast carcinoma cells treated with simvastatin and ionizing radiation

As previously mentioned, radioresistant breast carcinoma cells are affected in the susceptibility to apoptosis caused by ionizing radiation. Since apoptosis represents only one type of cell death, we decided to be focused on the evaluation of the total treatment-induced cell killing using Nicoletti staining.

Cell death development was determined in all investigated breast cancer cells after their exposure to simvastatin alone, irradiation alone, and their combination. It was observed that among all investigated breast carcinoma cell lines only parental T47D cells were not sensitive to simvastatin (Figure 5). All other parental and radioresistant breast carcinoma cells demonstrated time-dependent cell death development in response to cell exposure to simvastatin at a clinically relevant dose of 8  $\mu$ M. Thus, parental MDA-MB-231, radioresistant MDA-MB-231-RR and radioresistant T47D-RR cells showed equal cell death development with  $46.35 \pm 4.38\%$ ,  $43.78 \pm 3.19\%$ , and  $51.35 \pm 2.96\%$  at 96 hours, respectively. Parental and radioresistant Au565 breast carcinoma cells were less susceptible to simvastatin with cell death of  $41.96 \pm 9.05\%$  for parental Au565 cells and  $27.50 \pm 6.03\%$  for radioresistant Au565-RR cells at 96 hours after simvastatin treatment.

Breast cancer cell exposure to the clinically relevant single dose of irradiation of 2 Gy did not result in the substantial cell death in all investigated breast carcinoma cell lines. Parental and radioresistant Au565 cells were the most radiation sensitive among other cell lines, and radiation-caused cell death was  $17.43 \pm 2.58\%$  in parental Au565 cells and  $14.23 \pm 1.38\%$  in Au565-RR cells. Unfortunately, combination of simvastatin and irradiation did not lead to the enhancement of cell death compared to simvastatin alone in all parental and radioresistant breast carcinoma cells.

### Simvastatin activates different types of cell death

To understand which types of cell death are induced by simvastatin, we have performed Western

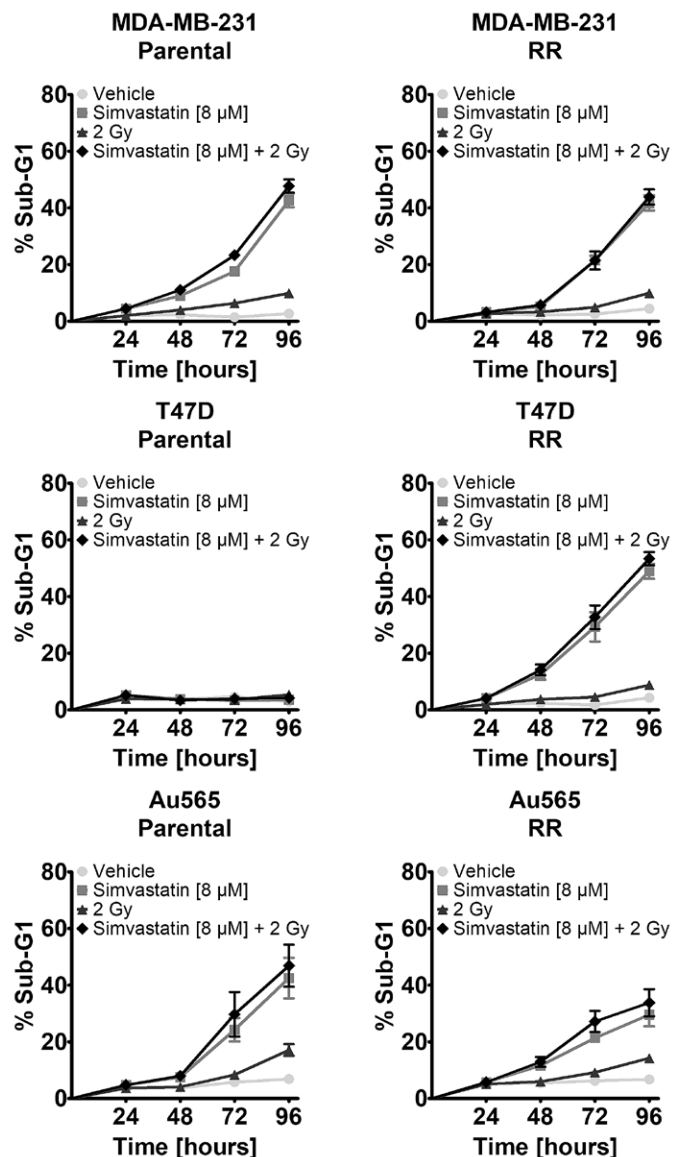


**FIGURE 5.** Cell death development in breast carcinoma cells treated with simvastatin or irradiation or their combination. At indicated time points, analysis of sub-G1 cell fraction was evaluated in the samples collected after treatment of parental and radioresistant breast carcinoma cells with simvastatin (8  $\mu$ M) alone, irradiation (2 Gy) alone or combination of simvastatin (8  $\mu$ M) and irradiation (2 Gy). All experiments were performed at least three times in duplicates; \* =  $p < 0.05$ ; \*\* =  $p < 0.01$ ; \*\*\* =  $p < 0.001$ .

blot analysis for the key regulators of caspase-dependent, caspase-independent apoptosis and autophagy (Figure 6). Interesting to note that parental and radioresistant triple-negative MDA-MB-231, hormone receptor-positive T47D, and Her2neu-positive Au565 breast carcinoma cells demonstrated different mechanisms of cell death development. Both intrinsic and extrinsic apoptosis pathways were implicated in simvastatin-triggered

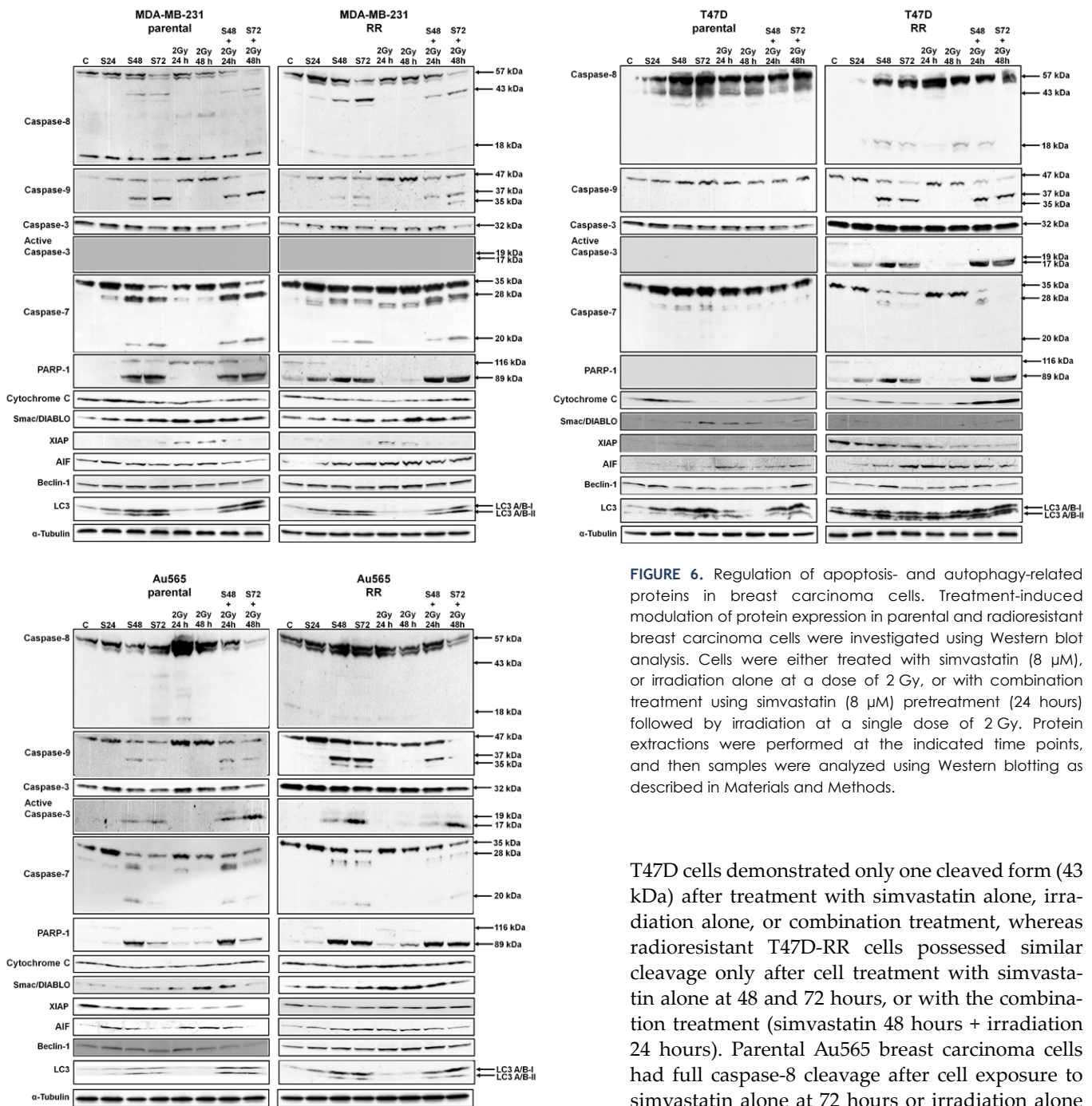


**FIGURE 6.** Regulation of apoptosis- and autophagy-related proteins in breast carcinoma cells. Treatment-induced modulation of protein expression in parental and radioresistant breast carcinoma cells were investigated using Western blot analysis. Cells were either treated with simvastatin (8  $\mu$ M), or irradiation alone at a dose of 2 Gy, or with combination treatment using simvastatin (8  $\mu$ M) pretreatment (24 hours) followed by irradiation at a single dose of 2 Gy. Protein extractions were performed at the indicated time points, and then samples were analyzed using Western blotting as described in Materials and Methods.

T47D cells demonstrated only one cleaved form (43 kDa) after treatment with simvastatin alone, irradiation alone, or combination treatment, whereas radioresistant T47D-RR cells possessed similar cleavage only after cell treatment with simvastatin alone at 48 and 72 hours, or with the combination treatment (simvastatin 48 hours + irradiation 24 hours). Parental Au565 breast carcinoma cells had full caspase-8 cleavage after cell exposure to simvastatin alone at 72 hours or irradiation alone at 24 hours. Radioresistant Au565-RR cells did not reveal a pronounced caspase-8 cleavage after any kind of treatment.

cell death in all investigated breast carcinoma cells. First, it was seen that initiator caspase-8 belonging to the extrinsic apoptosis pathway was activated in parental and radioresistant MDA-MB-231 cells independently from the kind of cell treatment, and both cleaved forms (43 kDa and 18 kDa) were observed. In contrast, all other cell lines were deficient in full caspase-8 cleavage. Thus, parental

Activation of the intrinsic apoptosis pathway was characterized by caspase-9 cleavage. In comparison with parental breast carcinoma cells, their radioresistant counterparts revealed a more pronounced caspase-9 cleavage after simvastatin-based treatments. It was manifested either in a more pronounced expression of the cleaved form

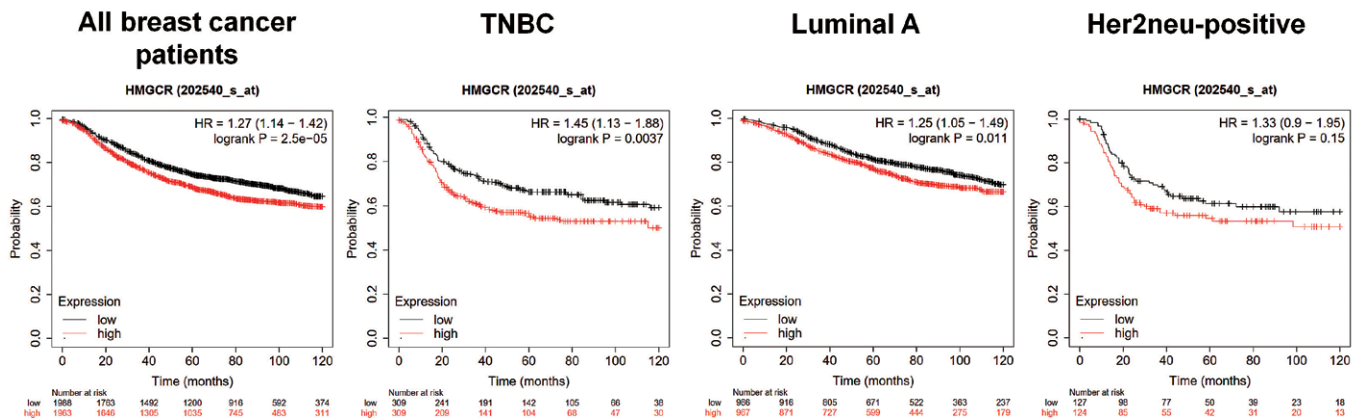


**FIGURE 7.** 3-hydroxy-3-methylglutaryl-coenzyme A reductase (*HMGCRC*) expression and recurrence free survival in breast cancer patients. Prognostic value of the *HMGCRC* expression at the mRNA level in breast cancer patients was evaluated using the KMplot database (<http://kmplot.com/analysis/>), and the results indicate that higher *HMGCRC* expression was associated with worse overall survival in all cohorts of patients.

of 37 kDa in T47D-RR cells or in caspase-9 cleavage accompanied by formation of a 37 and 35 kDa form in MDA-MB-231-RR and Au565-RR cells. Additionally, release of cytochrome C correlated with caspase-9 activation in the investigated parental and radioresistant breast carcinoma cells. Thus, there were very weak differences in cytochrome C expression in parental and radioresistant MDA-MB-231 cells that resulted in the similar caspase-9 activation with slightly more pronounced cleavage in radioresistant cells. Very low constitutive cytochrome C expression in the parental T47D cells was upregulated at 24 hours after simvastatin treatment only. Radioresistant T47D-RR cells were characterized by more stable release of cytochrome C after treatment with simvastatin alone, irradiation alone, and especially after combination treatment. Although cytochrome C expressions were not altered by any kind of treatment in parental and radioresistant Au565 breast carcinoma cells, radioresistant Au565-RR cells demonstrated higher cytochrome C expression compared to their parental counterparts.

Simvastatin-induced activation of initiator caspases 8 and 9 resulted in the modulation of expression of the executioner caspases 3 and 7. Although both parental and radioresistant MDA-MB-231 cells showed high expression of the total caspase-3, they were deficient in caspase-3 cleavage after all kinds of cell treatment with simvastatin alone, irradiation alone or their combination. Parental T47D breast carcinoma cells revealed comparable results as parental and radioresistant MDA-MB-231 cells. In contrast, radioresistant T47D-RR cells, parental Au565 and radioresistant Au565-RR cells demonstrated very pronounced simvastatin-induced cas-

pase-3 cleavage at 48 and 72 hours after treatment with simvastatin. Irradiation alone was unable to induce cleavage caspase-3, however combination of simvastatin and irradiation led to equal caspase-3 cleavage as observed in simvastatin-treated breast carcinoma cells. Another executioner caspase-7 was fully cleaved in parental and radioresistant MDA-MB-231 and Au565 cells after treatment with simvastatin alone or its combination with irradiation. Since neither caspase-3 nor caspase-7 cleavages were observed in the parental T47D cells, PARP-1 cleavage was also not observed in these cells after any kind of treatment. In contrast, activation of caspases executioners was accompanied by PARP-1 cleavage in parental and radioresistant MDA-MB-231 and Au565 cells, and radioresistant T47D-RR cells after application of simvastatin alone, irradiation alone, and their combination. It is necessary to note that PARP-1 was even cleaved in the cells treated with irradiation alone, though activation of caspases initiators and executioners was not detected. This led to the hypothesis that other mechanisms of cell death such as caspase-independent apoptosis and autophagy could be implicated in cell killing after cell exposure to irradiation alone or its combination with simvastatin.

Indeed, AIF and Smac/DIABLO expressions were modified by the treatment with simvastatin, irradiation, and their combination. Upregulation of AIF was more pronounced in radioresistant breast carcinoma cells than in their parental counterparts after administration of all treatments. Smac/DIABLO was weakly expressed in parental and radioresistant T47D cells, but it was increased by simvastatin, irradiation, or their combination in parental and radioresistant MDA-MB-231 and Au565

cells. Constitutive expression of the apoptosis inhibitor XIAP was enhanced in all radioresistant breast carcinoma cells. However, simvastatin alone or its combination with irradiation decreased XIAP expression. Although XIAP was up-regulated in parental and radioresistant MDA-MB-231 cells after their exposure to ionizing radiation, combination of simvastatin and irradiation did not result in the augmentation of XIAP expression.

Autophagy-related proteins beclin-1 and LC3 A/B were also analyzed for their constitutive and treatment-modulated expressions in parental and radioresistant breast carcinoma cells. Beclin-1 did not show any significant dysregulation in response to all treatment approaches. Although LC3 A/B was activated and cleaved after application of simvastatin alone or its combination with irradiation in parental and radioresistant MDA-MB-231 and Au565 cells, parental and radioresistant T47D cells were characterized by LC3 A/B cleavage after cell exposure to all kinds of cell treatment. It is necessary to note that the most prominent up-regulation of LC3 A/B expression and enhancement of its cleavage were detected in radioresistant MDA-MB-231-RR and T47D-RR breast carcinoma cells after simvastatin-containing treatment. Thus, LC3 A/B-II/LC3 A/B-I ratio in parental MDA-MB-231 and radioresistant MDA-MB-231-RR cells was  $\sim 0,6$  and  $\sim 0,5$  after simvastatin treatment at 72 hours, and  $\sim 0,6$  and  $\sim 0,8$  after combination treatment, respectively; for parental T47D and radioresistant T47D-RR cells:  $\sim 0,3$  and  $\sim 0,8$  after simvastatin treatment at 72 hours, and  $\sim 0,3$  and  $\sim 0,8$  after combination treatment, respectively; for parental Au565 and radioresistant Au565-RR cells:  $\sim 0,2$  and  $\sim 0,4$  after simvastatin treatment at 72 hours, and  $\sim 0,5$  and  $\sim 0,4$  after combination treatment, respectively.

## Discussion

Radiotherapy is an important therapeutic approach used in the management of breast cancer. Although radiotherapy techniques are markedly improved, the problem of radiation resistance of the primary or secondary (relapsed) tumors still exists.<sup>4,14</sup> It is currently known that radiation resistance can be supported by activated pro-survival intracellular pathways and microenvironmental factors.<sup>15,16</sup> A Western diet containing a lot of fat links not only increased levels of cholesterol in blood but can also be associated with the formation of more aggressive malignant breast tumors in women.<sup>15,17</sup> Tumor aggressiveness is characterized by reduced cancer

cell sensitivity to currently existing therapeutic approaches and inclination for metastatic spread.<sup>18-20</sup> Since high cholesterol levels could be related to the diminished therapy response and metastatic progression of breast cancer<sup>21-23</sup>, it is assumed that administration of statins can help to improve tumor sensitivity to anti-cancer treatment and attenuate the metastatic cancer cell capabilities.

Simvastatin is one of the widely used statins inhibiting the HMGCR and reducing hypercholesterolemia in patients. Since cholesterol levels can be regulated by the HMGCR, and cholesterolemia can be linked to more aggressive behavior of breast tumors, it is hypothesized that HMGCR can be upregulated in breast cancers with unfavorable clinical outcomes. Indeed, analysis of correlation between HMGCR expression and overall survival in breast cancer patients<sup>24</sup> has shown that HMGCR overexpression can be associated with reduced overall survival in breast cancer patients independently from the molecular subtypes of the tumors (Figure 7). Accordingly, our data have clearly demonstrated that breast carcinoma cells with confirmed radiation resistance possessed an augmentation of HMGCR expression. It was previously established that HMGCR is implicated in radiation response of melanoma cells, and lipophilic HMGCR inhibitor pitavastatin (Livalo) causes a delay in DNA repair resulting in the persistence of double strand breaks and development of senescence in malignant cells.<sup>23</sup> Although radiosensitizing and additional anti-tumor effects of the lipophilic statins are previously described<sup>22,23,25-29</sup>, there is only one report demonstrating that simvastatin can sensitize esophageal carcinoma cells to ionizing radiation via inhibition of PI3/Akt pathway.<sup>30</sup> To our knowledge, there are no publications showing a simvastatin efficacy on cell death and survival of radioresistant breast carcinoma cells. In this study, we have found that simvastatin-caused cytotoxic effects were observed in breast carcinoma cells expressing HMGCR, and the levels of their radiation responses did not play the significant roles. While irradiation alone resulted in the HMGCR up-regulation in all parental and radioresistant breast carcinoma cells independently from the constitutive HMGCR levels, combination treatment with simvastatin and ionizing radiation was not accompanied by enhancement of HMGCR in the majority of the investigated carcinoma cells. Only parental hormone receptor-dependent T47D cells lacking constitutive HMGCR expression did not show simvastatin-dependent downregulation of radiation-caused HMGCR expression in the ir-

radiated cells. We assume that simvastatin was not able to prevent radiation caused HMGR expression due to the constitutive lack of the target for simvastatin.

Interesting to note, there were no significant differences in cytotoxic cell responses to simvastatin alone and its combination with a clinically relevant dose of irradiation of 2 Gy. Simvastatin alone was equally effective as a combination treatment in both parental and radioresistant breast cancer cells if they expressed HMGR. However, radiation-caused HMGR up-regulation in the parental T47D cells did not influence the cytotoxic activities of simvastatin in combination with irradiation. We also cannot exclude that combination of simvastatin with a higher dose of irradiation can more effectively kill breast cancer cells than drug or ionizing radiation alone.

As expected, radioresistant breast carcinoma cells revealed an enhancement of metastasis-associated properties, such as increased migratory abilities and acquisition of more mesenchymal phenotype. Simvastatin treatment caused phenotypic transition of tumor cells between mesenchymal and epithelial states, which was accompanied by the reduction in migratory capabilities of breast carcinoma cells. Hence, it is possible to speculate that metastatic potential of radioresistant cells can be affected by the use of simvastatin.

Although there are several publications reporting on the inhibitory activities of statins on the epithelial-to-mesenchymal transition (EMT)<sup>30-34</sup>, our data additionally provide new evidence that simvastatin can effectively kill radioresistant breast carcinoma cells possessing a mesenchymal phenotype. We, therefore, hypothesize that radioresistant cells can be eliminated by simvastatin from local and/or distant recurrences. This assumption agrees with a clinical observation that statins cannot prevent breast cancer formation but can reduce cancer-related mortality in metastatic breast cancer patients.<sup>33</sup> It was also shown that lipophilic statins, including simvastatin, can improve a recurrence-free survival in breast cancer patients.<sup>33,34</sup> We, therefore, suppose that statins alter therapy-resistant breast carcinoma cells and affect carcinoma cell recovery after treatment.

In our study, simvastatin induced cell death in HMGR-expressing breast carcinoma cells, and we have detected activation of extrinsic, intrinsic, and caspase-independent apoptotic pathways, and autophagy. Although HMGR-positive breast carcinoma cells demonstrated comparable simvastatin-induced cell death development, apoptosis was

differently regulated either with more pronounced involvement of caspase-dependent or caspase-independent pathways. Interesting to note that simvastatin enhanced the expression of autophagy-related proteins beclin-1 and LC3 in HMGR-negative and simvastatin-resistant parental T47D cells. However, LC3 activation and cleavage was not very pronounced in parental cells as it was observed in radioresistant T47D cells. Therefore, we suppose that parental cells can be protected from cell death via weak activation of autophagy.<sup>35</sup> Since we have observed a variety of mechanisms regulating different types of cell death in simvastatin-treated carcinoma cells, it was impossible to detect any unique scenario of breast cancer cell killing after simvastatin treatment. In our opinion, it opens the wider perspectives to use simvastatin as a therapeutic approach to treat breast carcinomas possessing different capabilities for activation of apoptosis or autophagy.

We conclude, radioresistant breast carcinoma cells possessing HMGR expression accompanied by EMT activation can be successfully killed by simvastatin via mobilizing of a variety of pathways involved in apoptosis and autophagy.

## Acknowledgement

This study was supported by Austrian Science Fund (FWF P29457; FWF I4140), Anniversary Fund of Austrian National Bank (ÖNB 17620), Ingrid Shaker-Nessmann Cancer Research Foundation. Anton Buzdin and Maksim Sorokin were financed by the Russian Foundation for Basic Research Grant 19-29-01108. The research was supported also by the Slovenian Research Agency (ARRS) grant number P3-0003.

## References

1. EU Science Hub. 2020 Cancer incidence and mortality in EU-27 countries. [Internet]. [cited 2021 Jan 22]. Available at: <https://ec.europa.eu/jrc/en/news/2020-cancer-incidence-and-mortality-eu-27-countries>
2. Thomas MA, Ochoa LL, Zygmunt TM, Matesa M, Altman MB, Garcia-Ramirez JL, et al. Accelerated partial breast irradiation: a safe, effective, and convenient early breast cancer treatment option. *Mo Med* 2015; **112**: 379-84. PMID: 26606820
3. Merino T, Tran WT, Czarnota GJ. Re-irradiation for locally recurrent refractory breast cancer. *Oncotarget* 2015; **6**: 35051-62. doi: 10.18632/oncotarget.6036
4. Siglin J, Champ CE, Vakhnenko Y, Anne PR, Simone NL. Radiation therapy for locally recurrent breast cancer. *Int J Breast Cancer* 2012; **2012**: 571946. doi: 10.1155/2012/571946

5. Fredriksson I, Liljegren G, Arnesson L-G, Emdin SO, Palm-Sjövall M, Fornander T, et al. Local recurrence in the breast after conservative surgery – a study of prognosis and prognostic factors in 391 women. *Eur J Cancer* 2002; **38**: 1860-70. doi: 10.1016/s0959-8049(02)00219-8
6. Alpert TE, Kuerer HM, Arthur DW, Lannin DR, Haffty BG. Ipsilateral breast tumor recurrence after breast conservation therapy: outcomes of salvage mastectomy vs. salvage breast-conserving surgery and prognostic factors for salvage breast preservation. *Int J Radiat Oncol Biol Phys* 2005; **63**: 845-51. doi: 10.1016/j.ijrobp.2005.02.035
7. Huang E, Buchholz TA, Meric F, Krishnamurthy S, Mirza NQ, Ames FC, et al. Classifying local disease recurrences after breast conservation therapy based on location and histology: new primary tumors have more favorable outcomes than true local disease recurrences. *Cancer* 2002; **95**: 2059-67. doi: 10.1002/cncr.10952
8. Bedwinek J. Natural history and management of isolated local-regional recurrence following mastectomy. *Semin Radiat Oncol* 1994; **4**: 260-9. doi: 10.1053/SRA000400260
9. Belkacemi Y, Hanna NE, Besnard C, Majdoul S, Gligorov J. Local and regional breast cancer recurrences: salvage therapy options in the new era of molecular subtypes. *Front Oncol* 2018; **8**: 112. doi: 10.3389/fonc.2018.00112
10. Matuszewicz L, Czogalla A, Sikorski AF. Attempts to use statins in cancer therapy: an update. *Tumor Biol* 2020; **42**: 1010428320941760. doi: 10.1177/1010428320941760
11. Skvortsova I, Skvortsov S, Popper BA, Haidenberger A, Saurer M, Gunkel AR, et al. Rituximab enhances radiation-triggered apoptosis in Non-Hodgkin's lymphoma cells via caspase-dependent and-independent mechanisms. *J Radiat Res* 2006; **47**: 183-96. doi: 10.1269/jrr.47.183
12. Skvortsova I, Skvortsov S, Haidenberger A, Devries A, Nevinny-Stickel M, Saurer M, et al. Effects of paclitaxel and docetaxel on EGFR-expressing human carcinoma cells under normoxic versus hypoxic conditions in vitro. *J Chemother* 2004; **16**: 372-80. doi: 10.1179/joc.2004.16.4.372
13. Skvortsov S, Sarg B, Lindner H, Lukas P, Hilbe W, Zwierzina H, et al. Cetuximab inhibits thymidylate synthase in colorectal cells expressing epidermal growth factor receptor. *Proteomics Clin Appl* 2008; **2**: 908-14. doi: 10.1002/prca.200780034
14. Choi J, Yoon YN, Kim N, Park CS, Seol H, Park I-C, et al. Predicting radiation resistance in breast cancer with expression status of phosphorylated S6K1. *Sci Rep* 2020; **10**: 641. doi: 10.1038/s41598-020-57496-8
15. Garcia-Estevez L, Moreno-Bueno G. Updating the role of obesity and cholesterol in breast cancer. *Breast Cancer Res* 2019; **21**: 35. doi: 10.1186/s13058-019-1124-1
16. Hirata E, Sahai E. Tumor microenvironment and differential responses to therapy. *Cold Spring Harb Perspect Med* 2017; **7**: a026781. doi: 10.1101/cshperspect.a026781
17. Bjarnadottir O, Feldt M, Inasu M, Bendahl PO, Elebro K, Kimbung S, et al. Statin use, HMGR expression, and breast cancer survival - The Malmo Diet and Cancer Study. *Sci Rep* 2020; **10**: 558. doi: 10.1038/s41598-019-57323-9
18. Arnold CR, Mangesius J, Skvortsova II, Ganswindt U. The role of cancer stem cells in radiation resistance. *Front Oncol* 2020; **10**: 164. doi: 10.3389/fonc.2020.00164
19. Steinbichler TB, Dudás J, Skvortsov S, Ganswindt U, Riechelmann H, Skvortsova I-I. Therapy resistance mediated by cancer stem cells. *Semin Cancer Biol* 2018; **53**: 156-67. doi: 10.1016/j.semcancer.2018.11.006
20. Steinbichler TB, Savic D, Dudás J, Kvitsaridze I, Skvortsov S, Riechelmann H, et al. Cancer stem cells and their unique role in metastatic spread. *Semin Cancer Biol* 2020; **60**: 148-56. doi: 10.1016/j.semcancer.2019.09.007
21. Wu QJ, Tu C, Li YY, Zhu J, Qian KQ, Li WJ, et al. Statin use and breast cancer survival and risk: a systematic review and meta-analysis. *Oncotarget* 2015; **6**: 42988-3004. doi: 10.18632/oncotarget.5557
22. Efimova E V, Ricco N, Labay E, Mauceri HJ, Flor AC, Ramamurthy A, et al. HMG-CoA reductase inhibition delays DNA repair and promotes senescence after tumor irradiation. *Mol Cancer Ther* 2018; **17**: 407-18. doi: 10.1158/1535-7163.MCT-17-0288
23. Longo J, van Leeuwen JE, Elbaz M, Branchard E, Penn LZ. Statins as anti-cancer agents in the era of precision medicine. *Clin Cancer Res* 2020; **26**: 5791-800. doi: 10.1158/1078-0432.CCR-20-1967
24. Kaplan-Meier Plotter. Breast cancer. [Internet]. [cited 2021 Jan 22]. Available at: <https://kmplot.com/analysis/>
25. Ricco N, Flor A, Wolfgeher D, Efimova EV, Ramamurthy A, Appelbe OK, et al. Mevalonate pathway activity as a determinant of radiation sensitivity in head and neck cancer. *Mol Oncol* 2019; **13**: 1927-43. doi: 10.1002/1878-0261.12535
26. Wolfe AR, Debeb BG, Lacerda L, Larson R, Bambhroliya A, Huang X, et al. Simvastatin prevents triple-negative breast cancer metastasis in pre-clinical models through regulation of FOXO3a. *Breast Cancer Res Treat* 2015; **154**: 495-508. doi: 10.1007/s10549-015-3645-3
27. Wolfe AR, Woodward WA. Breast cancer stem cell correlates as predictive factors for radiation therapy. *Semin Radiat Oncol* 2015; **25**: 251-9. doi: 10.1016/j.semradonc.2015.05.009
28. Van Wyhe RD, Rahal OM, Woodward WA. Effect of statins on breast cancer recurrence and mortality: a review. *Breast Cancer* 2017; **9**: 559-65. doi: 10.2147/BCTT.S148080
29. Rahal OM, Woodward WA. Cholesterol and radiosensitivity. *Curr Breast Cancer Rep* 2016; **8**: 32-9. doi: 10.1007/s12609-016-0202-y
30. Jin Y, Xu K, Chen Q, Wang B, Pan J, Huang S, et al. Simvastatin inhibits the development of radioresistant esophageal cancer cells by increasing the radiosensitivity and reversing EMT process via the PTEN-PI3K/AKT pathway. *Exp Cell Res* 2018; **362**: 362-9. doi: 10.1016/j.yexcr.2017.11.037
31. Xie F, Liu J, Li C, Zhao Y. Simvastatin blocks TGF- $\beta$ 1-induced epithelial-mesenchymal transition in human prostate cancer cells. *Oncol Lett* 2016; **11**: 3377-83. doi: 10.3892/ol.2016.4404
32. Kato S, Liberona MF, Cerda-Infante J, Sánchez M, Henríquez J, Bizama C, et al. Simvastatin interferes with cancer "stem-cell" plasticity reducing metastasis in ovarian cancer. *Endocr Relat Cancer* 2018; **25**: 821-36. doi: 10.1530/ERC-18-0132
33. Ahern TP, Pedersen L, Tarp M, Cronin-Fenton DP, Garne JP, Silliman RA, et al. Statin prescriptions and breast cancer recurrence risk: a Danish nationwide prospective cohort study. *J Natl Cancer Inst* 2011; **103**: 1461-8. doi: 10.1093/jnci/djr291
34. Manthravadi S, Shrestha A, Madhusudhana S. Impact of statin use on cancer recurrence and mortality in breast cancer: a systematic review and meta-analysis. *Int J cancer* 2016; **139**: 1281-8. doi: 10.1002/ijc.30185
35. Bhutia SK, Mukhopadhyay S, Sinha N, Das DN, Panda PK, Patra SK, et al. Autophagy: cancer's friend or foe? *Adv Cancer Res* 2013; **118**: 61-95. doi: 10.1016/B978-0-12-407173-5.00003-0

research article

# Five-year follow-up and clinical outcome in euthyroid patients with thyroid nodules

Katica Bajuk Studen<sup>1,2</sup>, Simona Gaberscek<sup>1,2</sup>, Edvard Pirnat<sup>1,2</sup>, Katja Zaletel<sup>1,2</sup>

<sup>1</sup> Department of Nuclear Medicine, University Medical Centre Ljubljana, Slovenia

<sup>2</sup> Faculty of Medicine, University of Ljubljana, Slovenia

Radiol Oncol 2021; 55(3): 317-322.

Received 5 December 2020

Accepted 15 April 2021

Correspondence to: Katica Bajuk Studen, Department of Nuclear Medicine, University Medical Centre Ljubljana, Slovenia.  
E-mail: katica.bajuk@kclj.si

Disclosure: No potential conflicts of interest were disclosed.

This is an open access article under the CC BY-NC-ND license (<http://creativecommons.org/licenses/by-nc-nd/4.0/>).

**Background.** Thyroid nodule diagnosis has become increasingly frequent. Defining optimum surveillance intervals for patients with unsuspected thyroid nodules remains a challenge. This was a single centre cohort study in which patients diagnosed with unsuspected thyroid nodules in whom no treatment was indicated were invited for re-evaluation 5 years after the diagnosis. The primary end point of the study was to estimate the change in nodule size with thyroid ultrasound (US) and the secondary end point was to assess the need for clinical management 5 years after the diagnosis.

**Patients and methods.** Baseline patient parameters and ultrasound characteristics of the nodules were retrospectively collected. At follow-up, thyroid ultrasound was performed.

**Results.** A hundred and eighteen (107 women / 11 men, aged  $56.8 \pm 13.4$  years) patients were included in the study having 203 nodules at baseline, with mean largest nodule diameter  $10.5 \pm 7.4$  mm. After 5 years, 58 (28.6%) nodules significantly increased in size, 27 (13.3%) decreased, and for 104 (51.2%) of nodules, no change in size was noted. Fourteen (6.9%) nodules disappeared. Additional 26 new nodules (mean largest diameter  $7.7 \pm 5.0$  mm) in 16 patients were identified at follow-up. Regarding the clinical outcome, no new thyroid cancers were found. For 107 (90.7%) patients no further management was indicated. Five (4.2%) patients were referred to thyroidectomy because of the growth of the nodules. Two (1.7%) patients were treated for hyperthyroidism. Four (3.4%) patients did not complete the study.

**Conclusions.** We report a single centre experience of the natural history of unsuspected thyroid nodules. Our results showed that 71.4% of such nodules remained stable in size, decreased or even disappeared and that the vast majority of the patients remained clinically stable with no need for treatment 5 years after the diagnosis.

Key words. thyroid, nodule, goiter

## Introduction

Thyroid nodules are discrete lesions within the thyroid gland that are morphologically distinct from the surrounding thyroid parenchyma.<sup>1</sup> Currently, thyroid nodule diagnosis has become increasingly frequent due to incidental findings in different imaging tests performed for reasons unrelated to thyroid pathology.<sup>2,3</sup> The prevalence of thyroid nodules detected by thyroid ultrasound

(US) in unselected populations was reported to be of up to 50% in adult females and 30% in adult males.<sup>4</sup>

The initial evaluation of patients with thyroid nodules consists of careful clinical, imaging and laboratory assessment, often aided by US-guided fine needle aspiration biopsy (FNAB). It should identify a small subgroup of nodules that either harbour thyroid cancer (approx. 10%), cause compressive symptoms (approx. 5%) or progress

to functional disease (approx. 5%) and therefore need further clinical management.<sup>1,5,6</sup> The rest of the nodules can safely be managed with a surveillance program. However, since the knowledge of the natural history of thyroid nodules is incomplete, defining optimum surveillance intervals still remains a challenge with goals not to miss out a clinically significant change of the nodule and not to overburden medical facilities and patients with unnecessary follow-up examinations. At present, long-term follow-up recommendations are mainly based on expert opinion consensus since there is no reliable method to identify patients likely to experience clinically significant nodule growth or change to malignancy.<sup>1,6</sup>

The purpose of our study was to establish a natural history of thyroid nodules in a cohort of euthyroid patients diagnosed with unsuspecting thyroid nodules. The primary end point of the study was to estimate the change in nodule size with thyroid US and the secondary end point was to assess the need for clinical management five years after the diagnosis.

## Patients and methods

The study was carried out in 2015–2017 as a 5-year follow-up of patients diagnosed with thyroid nodules at the Outpatient Thyroid Department of the University Medical Centre Ljubljana in the years 2010–2012. Only patients with unsuspecting nodules in whom at the time of diagnosis no treatment was indicated and who did not have autoimmune thyroid disease were included in the study. None of the patients was receiving levothyroxine therapy. Five years after the initial diagnosis, patients were invited by mail for clinical and US re-evaluation. The study was performed in an iodine sufficient area.<sup>7</sup> It was approved by the Republic of Slovenia National Medical Ethics Committee (No. 0120-721/2015-2). A written informed consent was obtained by all patients included in the study.

At baseline, a complete thyroid gland examination was performed, including clinical examination, thyroid US and measurement of thyrotropin (TSH), free thyroxine (fT<sub>4</sub>), free triiodothyronine (fT<sub>3</sub>), thyroid peroxidase antibodies (TPOAb), thyroglobulin antibodies (TgAb) and thyroglobulin (Tg). If the largest diameter of thyroid nodules exceeded 1 cm, thyroid scintigraphy was performed. To rule out malignancy, US-guided FNAB was performed in hypofunctioning thyroid nodules with suspicious US features.

At follow-up, the evaluation included clinical examination and thyroid US. If a significant increase of one or more thyroid nodules was confirmed or new nodules larger than 5 mm were detected, the patient was advised to proceed to a further complete thyroid gland examination that was scheduled at a separate visit. The complete thyroid gland examination included clinical examination, thyroid US, TSH and Tg measurement, FNAB for nodules with suspicious ultrasound appearance, and re-evaluation of the need for treatment.

All laboratory measurements were performed at the biochemical laboratory of the Department of Nuclear Medicine of the University Medical Centre Ljubljana. Serum concentration of TSH, fT<sub>4</sub>, fT<sub>3</sub>, TPOAb and TgAb was measured by ADVIA Centaur System (Siemens Medical Solutions Diagnostics). Reference values for TSH were 0.35–5.5 mIU/L, for fT<sub>4</sub> 11.5–22.7 pmol/L, for fT<sub>3</sub> 3.5–6.5 pmol/L, and for TPOAb and TgAb less than 60 kIU/L. Thyroglobulin was measured by Kryptor platform (Brahms), based on TRACETM (time-resolved amplified cryptate emission) method with reference values between 0.5–58 µg/L.

Thyroid US was performed by 1 of 2 experienced thyroid specialists using an US machine (SSD-4000; Aloka Co, Ltd, Tokyo, Japan) with a 7.5-MHz linear transducer. The number of the nodules was recorded as well as their size in three dimensions. Multinodularity was defined as having more than 1 nodule. The volume of the nodules was calculated by the formula width × length × thickness ×  $\pi/6$ . Suspicious ultrasound features were defined as at least one of the following: hypoechogenicity, irregular margins, taller-than-wide shape, and microcalcifications. A significant change in the size of thyroid nodule was defined as the increase or decrease that involved at least 2 nodule dimensions, each amounting to at least 2 mm and representing at least 20% of the baseline diameter.<sup>1,9</sup> Thyroid autoimmunity was defined as hypoechoic US pattern and/or increased level of TPOAb and/or TgAb.

Thyroid scintigraphy was performed using a gamma camera equipped with a pinhole collimator (Siemens BASICAM) after intravenous administration of 100 MBq of Tc-99m pertechnetate.

Cytology results of FNAB were reported using the Bethesda system.<sup>8</sup> Only patients with unsuspecting cytology results were included in the study (Bethesda category 2 as well as cysts, categorized as Bethesda 1).

The statistical analysis was performed with IBM SPSS Statistics Version 25 Software. Values are expressed as mean ± standard deviation (SD).

TABLE 1. Basic characteristics of patients included in the study (N = 118)

Parameter	All patients (N = 118)	Nodule Growth			New nodules detected		
		Without (N = 72)	With (N = 46)	P	Without (N = 102)	With (N = 16)	P
Age (years)	51.6 ± 13.4	51.8 ± 13.6	51.2 ± 13.2	0.81	51.2 ± 13.6	53.9 ± 11.9	0.46
TSH (mIU/L)	1.64 ± 0.85	1.73 ± 0.83	1.49 ± 0.85	0.07	1.63 ± 0.83	1.72 ± 1.00	0.80
Tg (µg/L)	42.4 ± 184.9	51.3 ± 237.2	28.8 ± 33.4	0.08	43.7 ± 196.6	33.2 ± 70.5	0.68
Maximum diameter of the largest nodule (mm)	12.2 ± 8.2	11.7 ± 8.4	12.9 ± 7.7	0.11	12.2 ± 8.3	12.2 ± 7.6	0.86
Volume of the largest nodule (mL)	1.4 ± 2.4	1.4 ± 2.6	1.4 ± 2.1	0.17	1.4 ± 2.5	1.2 ± 1.4	0.70
Multinodularity (%)	55 (46.6%)	27 (37.5%)	28 (60.9%)	<b>0.02</b>	48 (47.1%)	7 (43.8%)	1.0

Tg = thyroglobulin; TSH = thyrotropin;

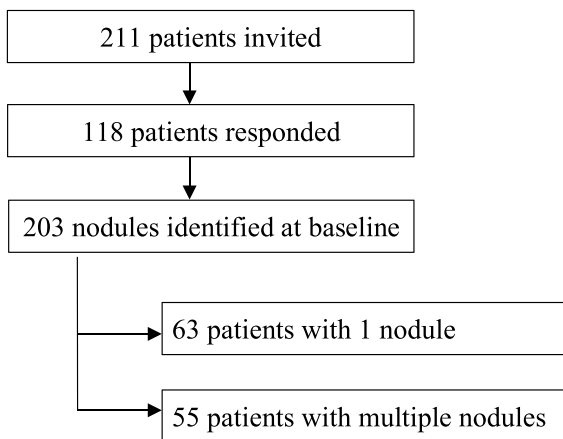


FIGURE 1. Flowchart explaining the recruitment process and the number of included patients and thyroid nodules.

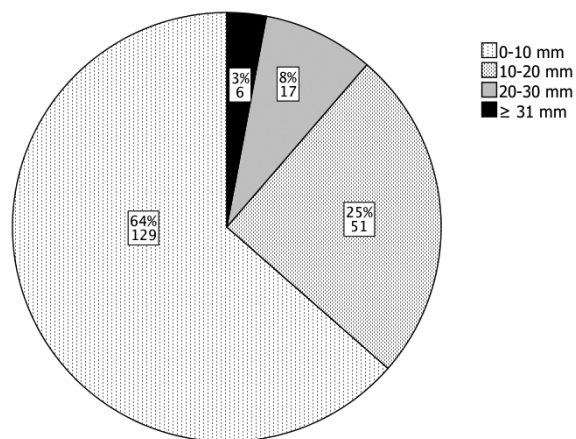


FIGURE 2. Nodule largest diameter distribution at baseline (N = 203).

For categorical baseline characteristics, differences between subgroups of patients were assessed by Pearson chi-square test. For continuous baseline characteristics, correlations with subgroup classification were assessed using Spearman's rho test. Correlations of growth indicative variables with baseline parameters were calculated by using the Pearson correlation test (Pearson correlation coefficient,  $r$ ).  $p$ -value below 0.05 was considered statistically significant.

## Results

The recruitment process is summarized in Figure 1. One hundred and eighteen patients were included in the study, with 203 thyroid nodules identified at baseline. One hundred and seven (90.7%) of the included patients were females and 11 (9.3%) were males. Basic characteristics of the included patients

and the two subgroups with or without nodule growth are depicted in Table 1.

Mean baseline largest diameter of the nodules was  $10.5 \pm 7.4$  mm and mean baseline volume  $1.1 \pm 2.2$  mL, with nodule baseline largest diameter distribution shown in Figure 2. In 55 nodules, FNAB was performed. The result of FNAB was Bethesda category 2 for 38 nodules and Bethesda category 1 (cyst) for 17 nodules.

After 5 years, 58 nodules significantly increased in size, 27 nodules significantly decreased in size; whereas for 104 of nodules, no significant change in size was noted (Figure 3). Furthermore, 14 of them disappeared. Twenty-six new nodules (mean largest diameter  $7.7 \pm 5.0$  mm, mean volume  $0.4 \pm 0.8$  mL) in 16 patients were found. The presence of multiple nodules was found to be significantly associated with nodule growth (Table 1).

The parameters of 58 nodules that significantly increased in size were further analyzed.

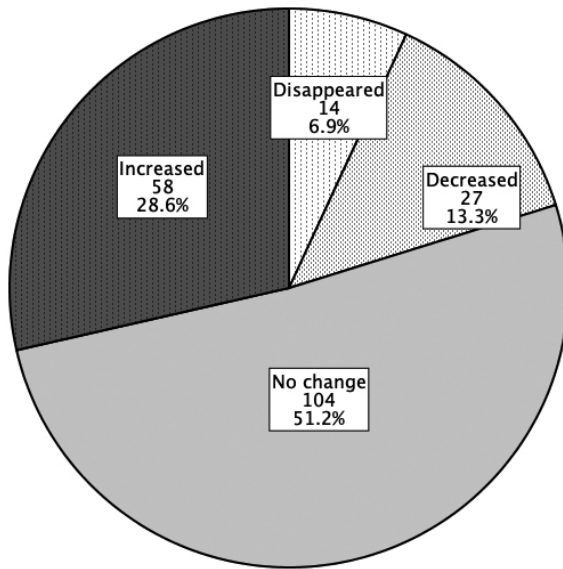


**FIGURE 3.** Growth status of the nodules after 5 years (N = 203). A significant change in the size of a thyroid nodule was defined as the increase or decrease that involved at least 2 nodule dimensions, each amounting to at least 2 mm and representing at least 20% of the baseline diameter.

Correlations between baseline parameters (baseline age, baseline Tg, baseline largest nodule diameter and baseline nodule volume) and changes in the largest nodule diameter and nodule volume are depicted in Figure 4. Baseline TSH level was not found to correlate with changes in the largest nodule diameter nor nodule volume,  $r = -0.119$ ,  $p = 0.37$  and  $r = -0.082$ ,  $p = 0.60$ , respectively (not shown in Figure 4). Baseline Tg level, baseline largest nodule diameter as well as baseline nodule volume positively and significantly correlated with nodule growth ( $p = 0.03$ ,  $p = 0.011$  and  $p < 0.001$ , respectively).

### Clinical outcome after five years

No new thyroid cancers were found. For 107 (90.7%) patients no further management was indicated. Five (4.2%) patients were referred to thyroidectomy because of the growth of the nodules. Two (1.7%) patients were treated for hyperthyroidism (one received radioiodine treatment because of toxic multinodular goiter, another was treated

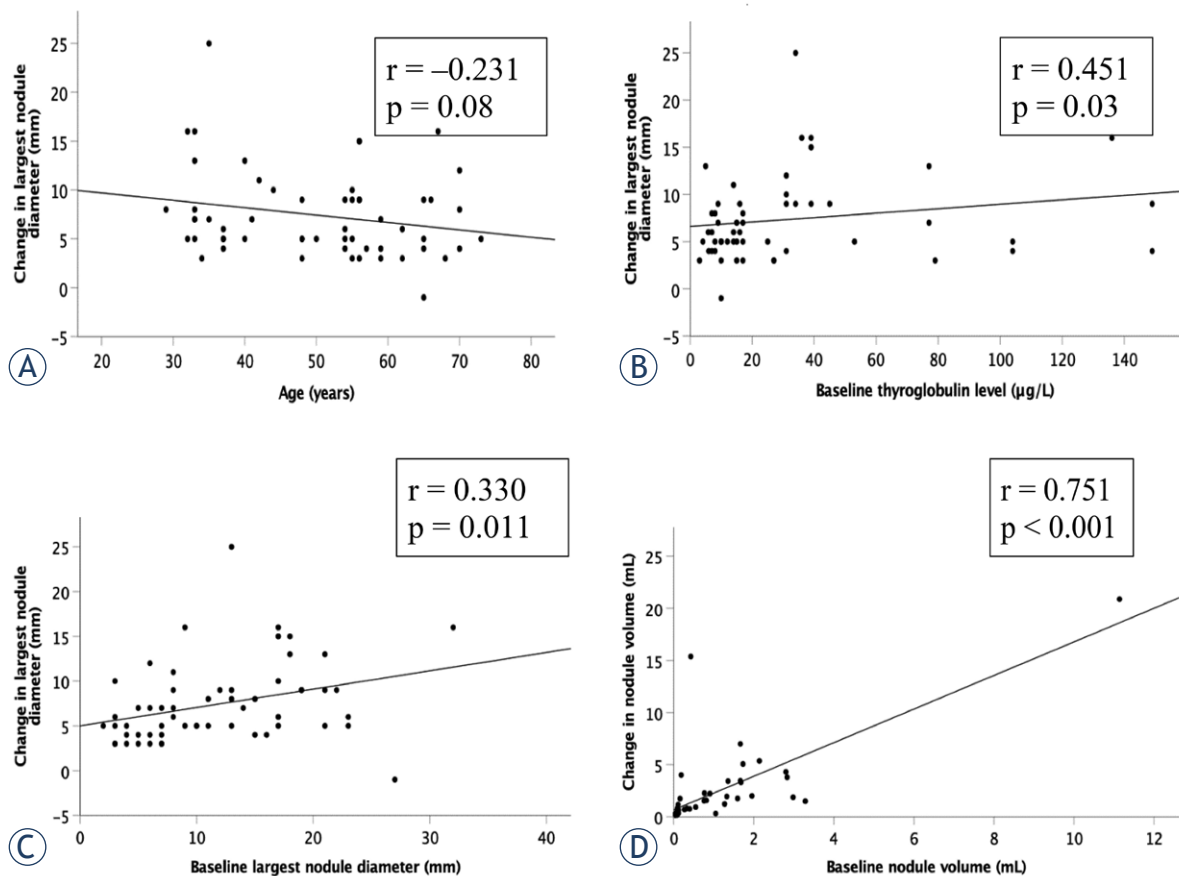


**FIGURE 4.** Correlations of baseline parameters with change in the largest nodule diameter and change in the nodule volume in nodules that significantly increased in size at the five-year follow-up (N = 58).

with anti-thyroid drugs because of newly occurred Graves' disease). Four (3.4%) included patients who were advised to proceed to a complete thyroid gland examination did not decide to do so for unknown reasons and were lost to follow-up.

## Discussion

In our study, we report a single center experience of the natural history of unsuspected thyroid nodules in euthyroid patients for whom no treatment was indicated at the time of diagnosis. Our results show that 71.4% of such nodules remain stable in size, decrease or even disappear and that the vast majority of the patients remain clinically stable with no treatment indication five years after the diagnosis. The presence of multiple nodules in patients is associated with nodule growth. For nodules that grow, nodule's growth positively correlates with the baseline Tg level, baseline largest nodule diameter as well as with the baseline nodule volume.

Previous studies have reported conflicting results regarding the natural course of thyroid nodules.<sup>10,11,12</sup> These results could be due to the methodological problems – different, often short follow-up intervals and different cut-offs of change in nodule size were used, which are not easily reproducible. In our study, the size change of the nodule was considered significant if a change of 20% or more was recorded in at least 2 nodule diameters, with a minimum increase of 2 mm. This approximates a nodule volume change of 50% which represents the minimal significant and reproducible change in nodule size suggested to be applied in clinical investigations and practice.<sup>1,6,9</sup> Our finding that after five years, most of the nodules remained stable, decreased or even disappeared is in agreement with a previously published study applying the same strict cut-off measure for a significant change in nodule size.<sup>13</sup>

Our finding that nodule growth was positively associated with the baseline largest nodule diameter and nodule volume as well as with the presence of multiple nodules is also in agreement with a previous report.<sup>13</sup> As expected, no association of baseline TSH level with nodule growth was found in our study since only patients with TSH within normal limits were included.

The pathogenesis of thyroid nodules as well as their growth are influenced by genetic and environmental factors. Among environmental factors, iodine supply is probably the most important risk

factor with nodular goiter being more prevalent in iodine deficient areas.<sup>14</sup> Our study was conducted in an area that was iodine-sufficient for more than ten years before baseline evaluation of the patients.<sup>7</sup> Therefore, the change in size of thyroid nodules reported in our study can be attributed to genetic and non-iodine related factors.<sup>15</sup> However, firm data of relative contributions and causality of those factors is lacking and should be elucidated by future research.

Our finding that more than 90% of the patients five years after initial diagnosis did not need any further management of thyroid nodules supports our approach of a thorough first examination, which enables identifying a subgroup of patients who need treatment (due to malignancy, thyroid autonomy or compressive symptoms). It seems that such approach is more important than planning different follow-up strategies. Of note, patients with autoimmune thyroid disease with possible increasing TSH levels over time, patients with suspicious US features of thyroid nodules and those with inconclusive cytology reports were not included in the study. In such patients, follow-up is indicated.<sup>1,6</sup>

## Conclusions

In conclusion, our results support the approach that after a thorough first examination the majority of patients with unsuspected thyroid nodules do not need frequent follow-up. Further research should elucidate the genetic determinants and biological characteristics of thyroid nodules that grow in time.

## Acknowledgement

This work was supported by the national project funded by Slovenian Research agency (Project number J3-1760).

## References

1. Haugen BR, Alexander EK, Bible KC, Doherty GM, Mandel SJ, Nikiforov YE, et al. 2015 American thyroid association management guidelines for adult patients with thyroid nodules and differentiated thyroid cancer: the American thyroid association guidelines task force on thyroid nodules and differentiated thyroid cancer. *Thyroid* 2016; **26**: 1-133. doi: 10.1089/thy.2015.0020
2. Russ G, Leboulleux S, Leenhardt L, Hegedüs L. Thyroid incidentalomas: epidemiology, risk stratification with ultrasound and workup. *Eur Thyroid J* 2014; **3**: 154-63. doi: 10.1159/000365289

3. Jamsek J, Zagar I, Gabersček S, Grmek M. Thyroid lesions incidentally detected by (18)F-FDG PET-CT – a two centre retrospective study. *Radiol Oncol* 2015; **49**: 121-7. doi: 10.2478/raon-2014-0039
4. Hegedüs L. Clinical practice. The thyroid nodule. *N Engl J Med* 2004; **351**: 1764-71. doi: 10.1056/NEJMcp031436
5. Russ G, Bonnema SJ, Erdogan MF, Durante C, Ngu R, Leenhardt L. European thyroid association guidelines for ultrasound malignancy risk stratification of thyroid nodules in adults: the EU-TIRADS. *Eur Thyroid J* 2017; **6**: 225-37. doi: 10.1159/000478927
6. Durante C, Grani G, Lamartina L, Filetti S, Mandel SJ, Cooper DS. The diagnosis and management of thyroid nodules. *JAMA* 2018; **319**: 914. doi: 10.1001/jama.2018.0898
7. Zaletel K, Gaberšček S, Pirnat E, Krhin B, Hojker H. Ten-year follow-up of thyroid epidemiology in Slovenia after increase in salt iodization. *Croat Med J* 2011; **52**: 615-21. doi: 10.3325/cmj.2011.52.615
8. Cibas ES, Ali SZ. The Bethesda system for reporting thyroid cytopathology. *Thyroid* 2009; **19**: 1159-65. doi: 10.1089/thy.2009.0274
9. Brauer VFH, Eder P, Miehle K, Wiesner TD, Hasenclever H, Paschke R. Interobserver variation for ultrasound determination of thyroid nodule volumes. *Thyroid* 2005; **15**: 1169-75. doi: 10.1089/thy.2005.15.1169
10. Quadbeck B, Pruellage J, Roggenbuck U, Hirche H, Janssen OE, Mann K, et al. Long-term follow-up of thyroid nodule growth. *Exp Clin Endocrinol Diabetes* 2002; **110**: 348-54. doi: 10.1055/s-2002-34992
11. Alexander EK, Hurwitz S, Heering JP, Benson CB, Frates MC, Doubilet PM, et al. Natural history of benign solid and cystic thyroid nodules. *Ann Intern Med* 2003; **138**: 315-8. doi: 10.7326/0003-4819-138-4-200302180-00010
12. Erdogan MF, Gursoy A, Erdogan G. Natural course of benign thyroid nodules in a moderately iodine-deficient area. *Clin Endocrinol* 2006; **65**: 767-71. doi: 10.1111/j.1365-2265.2006.02664.x
13. Durante C, Costante G, Lucisano G, Bruno R, Meringolo D, Paciaroni A, et al. The natural history of benign thyroid nodules. *JAMA* 2015; **313**: 926-35. doi: 10.1001/jama.2015.0956
14. Carlé A, Kreibjerg A, Laurberg P. Epidemiology of nodular goitre. Influence of iodine intake. *Best Pract Res Clin Endocrinol Metabol* 2014; **28**: 465-79. doi: 10.1016/j.beem.2014.01.001
15. Knudsen N, Brix TH. Genetic and non-iodine-related factors in the aetiology of nodular goitre. *Best Pract Res Clin Endocrinol Metabol* 2014; **28**: 495-506. doi: 10.1016/j.beem.2014.02.005

research article

# The importance of flaps in reconstruction of locoregionally advanced lateral skull-base cancer defects: a tertiary otorhinolaryngology referral centre experience

Domen Vozel<sup>1,2</sup>, Peter Pukl<sup>1</sup>, Ales Groselj<sup>1,2</sup>, Aleksandar Anicin<sup>1,2</sup>, Primoz Strojan<sup>2,3</sup>, Saba Battelino<sup>1,2</sup>

<sup>1</sup> Department of Otorhinolaryngology and Cervicofacial Surgery, University Medical Centre Ljubljana, Ljubljana, Slovenia

<sup>2</sup> Faculty of Medicine, University of Ljubljana, Ljubljana, Slovenia

<sup>3</sup> Institute of Oncology Ljubljana, Ljubljana, Slovenia

Radiol Oncol 2021; 55(3): 323-332.

Received 14 January 2021  
Accepted 17 February 2021

Correspondence to: Assoc. Prof. Saba Battelino, M.D., Ph.D., Head of Audiology and Otosurgery, Department of Otorhinolaryngology and Cervicofacial Surgery, University Medical Centre Ljubljana, Zaloška 2, SI-1000 Ljubljana, Slovenia; E-mail: saba.battelino@kclj.si

Disclosure: No potential conflicts of interest were disclosed.

This is an open access article under the CC BY-NC-ND license (<http://creativecommons.org/licenses/by-nc-nd/4.0/>).

**Background.** The aim of the study was to identify the value of extensive resection and reconstruction with flaps in the treatment of locoregionally advanced lateral skull-base cancer.

**Patients and methods.** The retrospective case review of patients with lateral skull-base cancer treated surgically with curative intent between 2011 and 2019 at a tertiary otorhinolaryngology referral centre was made.

**Results.** Twelve patients with locoregionally advanced cancer were analysed. Lateral temporal bone resection was performed in nine (75.0%), partial parotidectomy in six (50.0%), total parotidectomy in one (8.3%), ipsilateral selective neck dissection in eight (66.7%) and ipsilateral modified radical neck dissection in one patient (8.3%). The defect was reconstructed with anterolateral thigh free flap, radial forearm free flap or *pectoralis major* myocutaneous flap in two patients (17.0%) each. Mean overall survival was 3.1 years (SD = 2.5) and cancer-free survival rate 100%. At the data collection cut-off, 83% of analysed patients and 100% of patients with flap reconstruction were alive.

**Conclusions.** Favourable local control in lateral skull-base cancer, which mainly involves temporal bone is achieved with an extensive locoregional resection followed by free or regional flap reconstruction. Universal cancer registry should be considered in centres treating this rare disease to alleviate analysis and multicentric research.

Key words: temporal bone; microsurgery; parotid region; free tissue flaps; neoplasm staging; ear

## Introduction

Lateral skull-base cancer, which principally involves temporal bone is a rare pathology with an estimated annual incidence of approximately 0.8–6 per 1 million inhabitants.<sup>1,2</sup> It presents about 0.2% of all head and neck cancers.<sup>3</sup> Metastatic lesions of the lateral skull-base are less frequent than primary tumours and most commonly originate from the breast, pulmonary and renal primaries.

Previous radiotherapy of skull-base (*e.g.*, due to nasopharyngeal cancer), chronic otitis media, human papillomavirus infection, and chlorinated disinfectants are possible risk factors. However, there is a lack of scientific evidence.<sup>2,4</sup> Lateral skull-base cancer can arise *de-novo* or result from a malignant transformation of pre-existing benign tumours, such as chondroma to chondrosarcoma.<sup>5</sup>

Despite the advancement of surgical and non-surgical treatment modalities, the prognosis re-

mains poor since the reported mean overall survival time does not exceed five years.<sup>6</sup>

### Classification of lateral skull-base cancer

Lateral skull-base cancer can be classified according to the anatomical site into five categories (an adaptation of Homer *et al.*<sup>3</sup>):

- advanced skin cancer of external ear (aEEC); including auricle, concha or periauricular skin,
- advanced parotid cancer (aPC),
- infratemporal fossa and temporomandibular joint cancer,
- primary external auditory canal cancer (EACC) and
- primary middle ear cancer (MEC).

The cancer histological type depends upon the abovementioned site.<sup>3</sup> Regardless the site, the squamous cell carcinoma is the most common type which accounts for more than 40% of all primary lateral skull-base cancers, followed by basal cell carcinoma in 10%, adenoid cystic carcinoma in 8–10% and melanoma is less than 5%.<sup>7</sup>

### Clinical presentation of lateral skull-base cancer

The clinical presentation of lateral skull-base cancer is not pathognomonic since it can mimic the chronic inflammatory diseases, such as chronic otitis media, chronic otitis externa, necrotising otitis externa or vasculitis (*e.g.*, granulomatosis with polyangiitis). For that reason, bloody otorrhoea, hearing loss, bleeding, chronic otalgia, facial swelling or palsy and mass should be attributed to the lateral skull-base cancer until proven otherwise. Granulation tissue, nonhealing ulcer or erosion should be elucidated by histopathological examination. In case of progressive pain in the temporomandibular joint area, trismus, facial pain and fullness or subtle mass immediately above zygoma, suspicion of infratemporal fossa cancer should be raised.<sup>3</sup>

### Diagnosis of lateral skull-base cancer

Diagnosis of lateral skull-base cancer mainly comprises histopathological or cytopathological verification, high-resolution computed tomography (CT) and magnetic resonance imaging (MRI) of skull-base and adjacent structures (*i.e.* parotid region, neck), neck CT or ultrasonography (US) and further evaluation of signs of systemic cancer spread (*e.g.*, abdominal CT/US, chest CT/x-ray, positron emission tomography-CT).<sup>3</sup>

TABLE 1. Modified Pittsburgh staging system<sup>8,9</sup>

T assessment	
T1	Tumour limited to external auditory canal without bony erosion or evidence of soft tissue involvement
T2	Tumour with limited external auditory canal bone erosion (not full thickness) or limited (<0.5 cm) soft-tissue involvement
T3	Tumour eroding osseous external auditory canal (full thickness) with limited (<0.5 cm) soft tissue involvement or tumour involving the middle ear and/or mastoid
T4	Tumour eroding cochlea, petrous apex, medial wall of the middle ear, carotid canal, jugular foramen or dura, or with extensive soft tissue involvement (>0.5 cm) such as involvement of temporomandibular joint or styloid process, or evidence of facial paresis
N assessment	
N0	No regional lymph node metastasis
N1	Regional lymph node metastasis
M assessment	
M0	No distant metastasis
M1	Distant metastasis
Stage group	
I	T1N0M0*
II	T2N0M0*
III	T3N0M0†, T1N1M0†
IV	T4N0M0‡, T2–4N1M0‡, T1–4N0–1M1‡

The TNM assessment is based on the clinical examination and imaging findings. This staging system has been applied to assess primary external auditory canal cancer and primary middle ear cancer.<sup>1</sup> Middle ear cancer is assessed as at least T3, therefore always locoregionally advanced.

T = tumour; N = regional lymph node metastasis; M = distant metastasis; \* = localised cancer; † = locoregionally advanced cancer; ‡ = systemically advanced cancer

The clinical examination and diagnostic procedures enable the assessment of tumour stage according to the TNM classification system. Primary tumour (T), regional lymph node metastases (N) and distant metastases (M) can be assessed according to the primary tumour site: *e.g.* for skin carcinoma of the head and neck, major salivary glands, malignant melanoma of the skin, tumours of bone and soft tissue. EACC and MEC deserve particular emphasis in T, N and M assessment as the AJCC and UICC grading systems do not include these cancer types. EACC should be graded with the modified Pittsburgh staging system (Table 1)<sup>8,9</sup>, which has the highest prognostic accuracy.<sup>10</sup> This staging system should be used in pathological TNM staging also.<sup>11</sup> MEC has been graded with many staging systems including modified Pittsburgh staging system<sup>18,9</sup> and Stell and McCormick grading system.<sup>12</sup>

## Treatment of lateral skull-base cancer

After the diagnosis has been established, the patient should be presented at the multidisciplinary tumour board to determine the treatment modalities and goals.<sup>3</sup> In our tertiary referral centre, the board, usually consists of an otorhinolaryngologist subspecialised in otologic and lateral skull-base surgery, otorhinolaryngologist subspecialised in head and neck surgery and free flap reconstruction, radiation oncologist and medical oncologist.

The best prognosis of lateral skull-base cancer is achieved with the radical surgical treatment, which depends on the tumour's extent and presence of regional lymph node metastasis.<sup>7</sup> Therefore, it can include for an example wide local excision of the tumour, temporal bone resection (lateral, subtotal or total), parotidectomy (superficial or total), neck dissection (selective, modified radical, radical) and temporomandibular joint resection. When the histopathological examination of the resected specimen implies an increased risk of local/regional tumour re-appearance, adjuvant treatment must be considered. Other non-surgical treatment modalities (*i.e.*, radiotherapy, systemic therapy), when indicated, can significantly improve the rate of local and/or regional control.<sup>7</sup>

Since the extensive surgery of locoregionally advanced lateral skull-base cancer results in large tissue defects, the reconstruction should be planned immediately. An assortment of free flaps can be considered to aid the reconstruction such as radial forearm free flap (RFFF), deep inferior epigastric perforator flap, latissimus dorsi free flap and anterolateral thigh free flap (ALT).<sup>3</sup> ALT is considered a workhorse in lateral skull-base reconstruction since it provides an adequate tissue bulk to fill the tissue defect. Additionally, the donor site (*i.e.*, thigh wound) can be used to harvest *fascia lata* to reconstruct dural defect or statically suspend the oral commissure if the facial nerve has been sacrificed. Moreover, ALT can be harvested as chimaeric, *i.e.* incorporating the lateral cutaneous femoral nerve, which can be used as interposition nerve graft in facial nerve reanimation. It is recommended that facial nerve reanimation should be initiated at primary surgery. However, in certain circumstances (*i.e.*, peripheral arterial occlusive disease, head and neck scarring after the previous radiotherapy) free flaps cannot be used or have failed to reconstruct the defect.<sup>3</sup> For that reason, regional flaps such as the pectoralis major myocutaneous flap (PM) should be harvested.<sup>3,13,14</sup>

The treatment of lateral-skull base cancer should be reserved for highly specialised centres. This manuscript aims to provide an experience of a single tertiary otorhinolaryngology referral centre in the treatment of this pathology, emphasising the role of regional and free flaps in reconstruction after resection of locoregionally advanced lateral skull-base cancer.

## Patients and methods

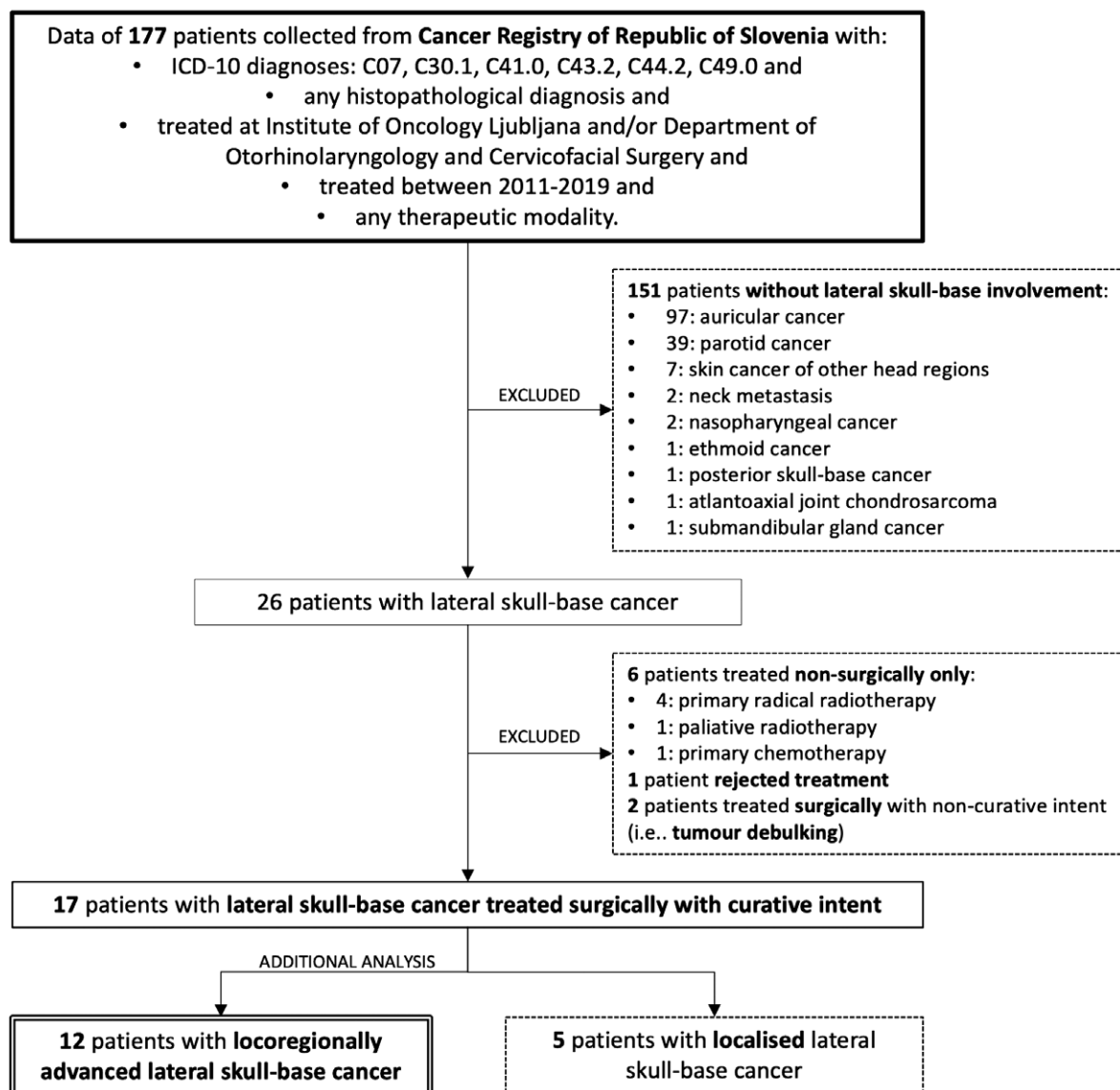
The study protocol was approved by the Institutional Committee for Medical Ethics and the Protocol Review Board (ERIDNPVO-0012/2020, 29.7.2020). The study was performed according to the ethical standards of the responsible institutional review board on human experimentation and with the Helsinki Declaration. Patients provided written, informed consent at the admission.

### Patients' data acquisition

A retrospective case review of patients treated at the Institute of Oncology Ljubljana, Slovenia and/or Department of Otorhinolaryngology and Cervicofacial Surgery, University Medical Centre, Ljubljana, Slovenia was performed. Inclusion criteria were:

- time of cancer diagnosis between the January 1<sup>st</sup> 2011 and December 31<sup>st</sup> 2019,
- international classification of diseases, 10<sup>th</sup> revision (ICD-10) diagnoses:
  - C07 (lat. *neoplasma malignum glandulae parotidae*),
  - C30.1 (lat. *neoplasma malignum auris mediae*),
  - C41.0 (lat. *neoplasma malignum ossium cranii et faciei*),
  - C43.2 (lat. *melanoma malignum auris et meatus acustici externi*),
  - C44.2 (lat. *neoplasma malignum cutis auris et meatus acustici externi*) or
  - C49.0 (lat. *neoplasma malignum textus connexivi et mollis capitis, faciei et colli*).
- surgical treatment with curative intent.

The data were collected from the Cancer Registry, Slovenia, databases of Department of Otorhinolaryngology and Cervicofacial Surgery, University Medical Centre Ljubljana, Slovenia and Institute of Oncology Ljubljana, Slovenia.



ICD = International statistical classification of diseases and related Health problems 10<sup>th</sup> revision

**FIGURE 1.** Data acquisition flowchart of patients with lateral skull-base cancer. Data of 177 patients were thoroughly analysed using Cancer Registry of the Republic of Slovenia and databases of Department of Otorhinolaryngology and Cervicofacial Surgery, University Medical Centre Ljubljana, Slovenia and Institute of Oncology Ljubljana, Slovenia. The majority of excluded patients suffered from auricular or parotid cancer without lateral skull-base involvement. Additional analysis was performed on the data of locoregionally advanced cancer.

### Patients' data analysis

Included patients were analysed for the gender, age, symptoms at presentation, date of cancer diagnosis, ICD-10 diagnosis, histology, clinical and pathological TNM stage (utilising the University of Pittsburgh TNM staging system (Table 1) for EACC and MEC or 8th edition of UICC staging system for aEEC and aPC), tumour localisation according to the abovementioned classification, preoperative

head and neck imaging modalities and preoperative pure tone audiometry. Pure tone average was calculated for the affected ear (for bone and air conduction) as an average of hearing levels of pure tone audiometry at speech frequencies (*i.e.*, 500 Hz, 1000 Hz, 1500 Hz, 2000 Hz, 3000 Hz and 4000 Hz). The average air-bone gap was calculated from pure tone average for bone and air conduction.

Moreover, date of surgery, treatment modalities employed (*i.e.*, surgery, radiotherapy, systemic

therapy), residual tumour classification according to the UICC staging system (*i.e.*, R0 no residual tumour, R1 microscopic residual tumour and R2 macroscopic residual tumour), and date of the last recorded check-up or date and reason of death were analysed. Cancer recurrence was defined as the re-appearance of cancer in the surgical bed after the treatment was completed, and cancer was considered cured.

Listed data was used to analyse age at the cancer diagnosis, age at death, postoperative follow-up period and survival. Local control and overall survival crude rates and estimates using the Kaplan-Meier method were determined. Patients were considered cancer-free if there was no cancer recorded at five years after the surgery.

Statistical analysis was performed using Microsoft Excel for Mac (version 16 and later, Microsoft Corporation, Redmond, Washington) and SPSS (version 23, IBM Corp., Armonk, New York). Basic descriptive statistics were reported with means (*M*) and standard deviations (*SD*) and a *p*-value (*p*) below 0.05 was considered statistically significant.

## Results

### Study flowchart, demographics and clinical presentation

Data collection was cut off on September 14<sup>th</sup> 2020. Initially, 177 patients were included in the study. Seventeen (10%) patients with lateral skull-base cancer were treated with curative intent between 2011 and 2019, and in 12 of them, the tumour was locally advanced (Table 2).

At the admission, 12 (71%) patients reported discharge, 10 (59%) crusting or nonhealing lesion, 10 (59%) pain, 6 (35%) bleeding, 5 (29%) hearing loss and 2 (12%) itching. A patient (6%) with aPC extending to the lateral skull-base reported the unilateral facial muscle weakness. None reported vertigo or other symptoms related to other cranial nerves involvement.

### Tumour characteristics and localisation

There was no left to right predominance (53% left and 47% right). Seven patients (41%) had an aEEC. Basal cell carcinoma was present in four (57%) and squamous cell carcinoma in three (43%) patients (Table 2).

Six patients (35%) suffered from EACC. The latter was classified as C44.2 in 100%. The cancer was

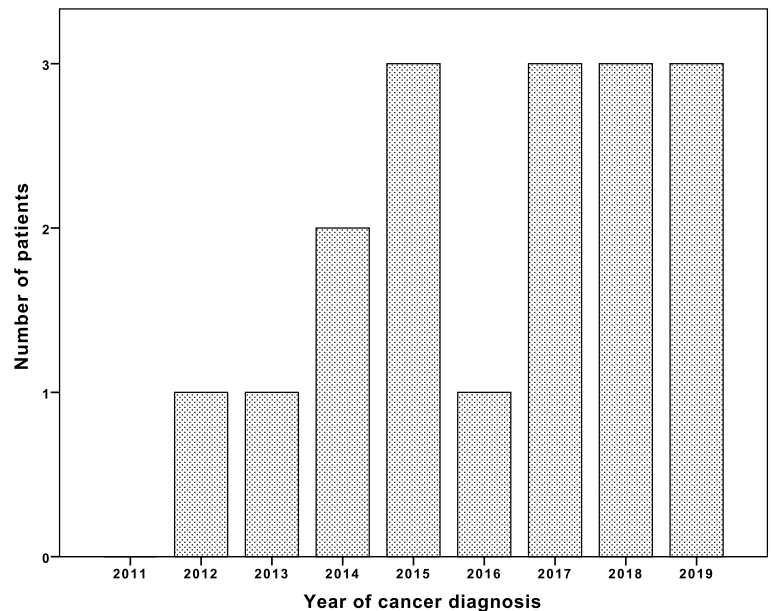


FIGURE 2. Bar chart of seventeen patients with lateral skull-base cancer treated with curative intent between 2011 and 2019.

squamous cell carcinoma in three (50%), basal cell carcinoma in two (33%) and adenoid cystic carcinoma in one patient (17%).

Both (12%) MECs were squamous cell carcinoma and two (12%) aPCs were mucoepidermoid carcinoma (50%) and adenocarcinoma (50%).

Disregarding the tumour localisation squamous cell carcinoma was the most common type (8 patients, 47%), followed by basal cell carcinoma (6 patients, 35%), and others (adenoid cystic carcinoma (6%), mucoepidermoid carcinoma (6%) and adenocarcinoma (6%).

### Locoregionally advanced lateral skull-base cancer

In twelve patients (71%), the tumour was locoregionally advanced (*i.e.*, grades III and IV). Preoperative skull-base imaging (*i.e.*, CT or MRI) was performed in all of them. Pure tone average for air and bone conduction and air-bone gap could be calculated in eight patients (67%). Average value of pure tone average was 69 dB (*SD* = 39 dB) for air conduction, 43 dB (*SD* = 19 dB) for bone conduction and average air-bone gap was 26 dB (*SD* = 20 dB).

The primary surgery was the only treatment modality in five patients (42%) patients. Other treatment modalities employed were salvage surgery in three (25%) patients (*i.e.*, one after radiotherapy, one after radiotherapy and electrochemotherapy,

TABLE 2. Dataset of patients with lateral skull-base cancer treated between 2011 and 2019

Age	Year	Site	ICD-10	HP	Clinical TNM staging				Preoperative imaging	PTA	Treatment modalities	Otosurgical resection	Parotidectomy	Neck dissection	TMJ resection	Reconstruction	RTC	Survival
					cT	cN	cM	Grade										
80 <sup>M</sup>	2012	aEEC <sup>R</sup>	C44.2	SCC	cT4 <sup>a</sup>	cN1 <sup>a</sup>	cM0 <sup>a</sup>	IV <sup>P</sup>	CT <sub>sb</sub> , US <sub>N</sub>	yes	SURG→RT	WLE	partial	iSND	none	PM	R1	8.1
79 <sup>M</sup>	2014	EACC <sup>R</sup>	C44.2	BCC	cT1 <sup>P</sup>	cN0 <sup>P</sup>	cM0 <sup>P</sup>	I <sup>P</sup>	CT <sub>sb</sub>	none	SURG	WLE	none	none	yes	skin graft	R0	6.9
52 <sup>M</sup>	2014	EACC <sup>L</sup>	C44.2	SCC	cT4 <sup>P</sup>	cN0 <sup>P</sup>	cM0 <sup>P</sup>	IV <sup>P</sup>	MRI <sub>sb</sub> , CT <sub>sb</sub> , US <sub>N</sub>	yes	SURG	LTBR	partial	iSND	none	primary closure	R0	5.7
90 <sup>F</sup>	2015	EACC <sup>L</sup>	C44.2	SCC	T3 <sup>P</sup>	cN0 <sup>P</sup>	cM0 <sup>P</sup>	III <sup>P</sup>	CT <sub>sb</sub> , US <sub>N</sub>	yes	SURG	LTBR	none	none	none	primary closure	R0	5.5
59 <sup>M</sup>	2017	EACC <sup>L</sup>	C44.2	ACC	cT4 <sup>P</sup>	cN0 <sup>P</sup>	cM0 <sup>P</sup>	IV <sup>P</sup>	MRI <sub>sb</sub> , CT <sub>sb</sub> , US <sub>N</sub>	yes	SURG→RT	LTBR	partial	iSND	none	primary closure	R1	5.2
50 <sup>M</sup>	2017	EACC <sup>L</sup>	C44.2	BCC	cT <sup>P</sup>	cN0 <sup>P</sup>	cM0 <sup>P</sup>	I <sup>P</sup>	MRI <sub>sb</sub>	none	ECT→SURG	WLE	partial	none	none	primary closure	R0	4.5
85 <sup>F</sup>	2017	aEEC <sup>R</sup>	C44.2	BCC	cT2 <sup>a</sup>	cN0 <sup>a</sup>	cM0 <sup>a</sup>	II <sup>a</sup>	US <sub>N</sub>	none	SURG	WLE	none	none	none	primary closure	R0	2.9 (†88)
75 <sup>M</sup>	2018	aEEC <sup>L</sup>	C44.2	BCC	cT1 <sup>a</sup>	cN0 <sup>a</sup>	cM0 <sup>a</sup>	I <sup>a</sup>	none	none	SURG	WLE	none	none	none	skin graft	R0	2.8 (†78)
79 <sup>M</sup>	2018	MEC <sup>R</sup>	C30.1	SCC	cT3 <sup>P</sup>	cN0 <sup>P</sup>	cM0 <sup>P</sup>	III <sup>P</sup>	MRI <sub>sb</sub> , CT <sub>sb</sub> , MRI <sub>N</sub>	yes	SURG	LTBR	none	none	none	primary closure	R1	0.4 (†80)
67 <sup>M</sup>	2018	aEEC <sup>R</sup>	C44.2	BCC	cT4a <sup>a</sup>	cN0 <sup>a</sup>	cM0 <sup>a</sup>	IVa <sup>a</sup>	MRI <sub>sb</sub> , CT <sub>sb</sub>	yes	SURG	LTBR <sup>a</sup>	partial	iSND	none	RFFF	R0	2.3
66 <sup>F</sup>	2019	EACC <sup>L</sup>	C44.2	SCC	cT1 <sup>P</sup>	cN1 <sup>P</sup>	cM0 <sup>P</sup>	III <sup>P</sup>	MRI <sub>sb</sub> , CT <sub>sb</sub>	yes	SURG	WLE	none	iSND	none	secondary intention	R0	2.0
76 <sup>M</sup>	2019	aEEC <sup>R</sup>	C44.2	SCC	cT3 <sup>a</sup>	cN0 <sup>a</sup>	cM0 <sup>a</sup>	III <sup>a</sup>	MRI <sub>sb</sub> , CT <sub>sb</sub>	yes	RT→SURG	LTBR <sup>a</sup>	partial	iSND	none	PM	R0	2.4
85 <sup>M</sup>	2012	MEC <sup>R</sup>	C30.1	SCC	cT3 <sup>P</sup>	cN0 <sup>P</sup>	cM0 <sup>P</sup>	III <sup>P</sup>	CT <sub>sb</sub> , US <sub>N</sub>	yes	SURG→RT	LTBR	none	none	none	primary closure	R0	0.5 (†85)
73 <sup>F</sup>	2014	aEEC <sup>L</sup>	C44.2	BCC	cT4a <sup>a</sup>	cN0 <sup>a</sup>	cM0 <sup>a</sup>	IVa <sup>a</sup>	MRI <sub>sb</sub> , CT <sub>sb</sub> , US <sub>N</sub>	yes	RT→ECT→SURG	LTBR <sup>a</sup>	partial	iSND	none	RFFF	R0	1.6
58 <sup>F</sup>	2014	aPC <sup>S</sup>	C07	MC	cT4a <sup>a</sup>	cN0 <sup>a</sup>	cM0 <sup>a</sup>	IVa <sup>a</sup>	MRI <sub>sb</sub> , CT <sub>sb</sub>	yes	SURG→RT→SURG	LTBR <sup>a</sup>	performed previously	iSND	none	ALT	R0	0.6
85 <sup>F</sup>	2015	aPC <sup>S</sup>	C07	AC	cT4a <sup>a</sup>	cN2b <sup>a</sup>	cM0 <sup>a</sup>	IVa <sup>a</sup>	CT <sub>sb</sub>	yes	SURG→RT	MWLE	total	IMRND	none	ALT	R0	0.3
84 <sup>M</sup>	2017	aEEC <sup>L</sup>	C44.2	SCC	cT2 <sup>a</sup>	cN0 <sup>a</sup>	cM0 <sup>a</sup>	II <sup>a</sup>	US <sub>N</sub>	none	SURG→RT	WLE	partial	iSND	none	secondary intention	R0	0.8

Locoregionally advanced cancer is shown in bold. Age and survival are depicted in years

AC = adenocarcinoma; ACC = adenoid cystic carcinoma; aEEC = advanced skin cancer of external ear (including auricle, concha or periauricular skin); Age = age at the time of cancer diagnosis; ALT = anterolateral thigh free flap; aPC = advanced parotid cancer; BCC = basal cell carcinoma; CT<sub>sb</sub> = skull-base computed tomography; EACC = primary external auditory canal cancer; ECT = electrochemotherapy; ECT→SURG = ECT was performed with primary curative intent and surgery as salvage; F = female; HP = histopathological diagnosis; ICD-10 = international classification of diseases, 10<sup>th</sup> revision; IMRND = ipsilateral modified radical neck dissection; iSND = ipsilateral selective neck dissection; L = left; LTBR = lateral temporal bone resection; LTBR<sup>a</sup> = lateral temporal bone resection with wide local excision; M = male; MWLE = mastoidectomy with wide local excision; MC = mucoepidermoid carcinoma; MEC = primary middle ear cancer; MRI<sub>N</sub> = neck magnetic resonance imaging; MRI<sub>sb</sub> = skull-base MRI; P = modified Pittsburgh staging system; PM = pectoralis major myocutaneous flap; PTA = pure tone audiometry performed prior surgery; R = right; R0 = no residual tumour; R1 = microscopic residual tumour; RFFF = radial forearm free flap; RT = radiotherapy; RTC = residual tumour classification according to the UICC staging system; SCC = squamous cell carcinoma; SURG = surgery; SURG→RT = combined surgery and postoperative radiotherapy; TMJ = temporomandibular joint; US<sub>N</sub> = neck ultrasound; WLE = wide local excision; Year = year of cancer diagnosis; † = Union for International Cancer Control (UICC) staging system for skin carcinoma of the head and neck †† = UICC staging system for major salivary glands; † with a number = an age at death

one after surgery and radiotherapy) and postoperative radiotherapy in four patients (33%) (Table 2). None received postoperative chemotherapy.

Wide local excision only was performed in two (16.7%), mastoidectomy in one (8.3%) and lateral temporal bone resection with obliteration in nine patients (75%). Additional partial parotidectomy was performed in six (50%), total parotidectomy in one (8.3%), ipsilateral selective neck dissection of regions II–IV in eight (66.7%) and ipsilateral modified radical neck dissection including resection of the sternocleidomastoid muscle in one patient (8.3%).

The post-resection lateral skull-base defect was reconstructed with primary closure in five (41.7%) and flap in six (50%) patients with locoregionally advanced cancer. The wound was left to heal by

secondary intention in one (8.3%) patient with T1N1M0 (stage III) EACC.

Reconstruction with ALT (Figure 3), RFFF (Figure 4) and PM (Figure 5) was performed in two patients each. There was no flap failure. In five patients (83%) with flap reconstruction, the resection was R0. Postoperative photon radiotherapy with a dose of 60 Gy and 64 Gy in 2 Gy daily fractions was performed in two patients, including the one with R1 resection.

### Local control and survival after locoregionally advanced lateral skull-base cancer resection

The mean follow-up time (*i.e.*, the mean overall survival time) of twelve patients after locoregion-

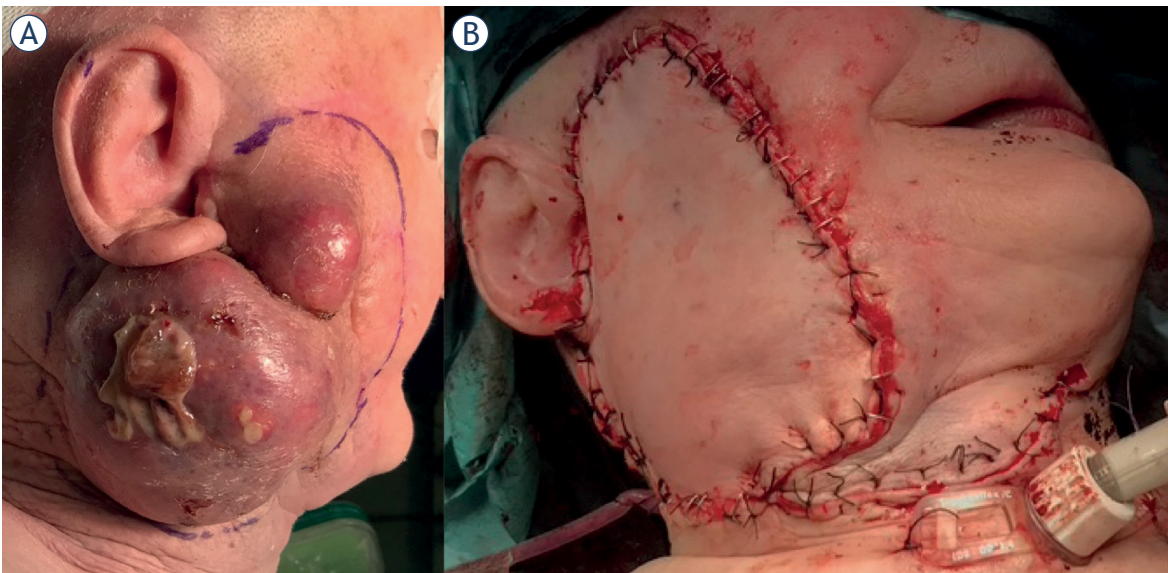


**FIGURE 3.** 85-year old female with locoregionally advanced parotid adenocarcinoma (i.e., parotid metastasis after incomplete temporal skin adenocarcinoma cancer resection) extending to the right external auditory canal and lateral skull-base. The resection margin is outlined (A). Primary surgery involving mastoidectomy with wide local excision, total parotidectomy, modified radical neck dissection, temporary tracheostomy, static suspension of oral commissure with fascia lata and anterolateral thigh free flap reconstruction were performed (B).

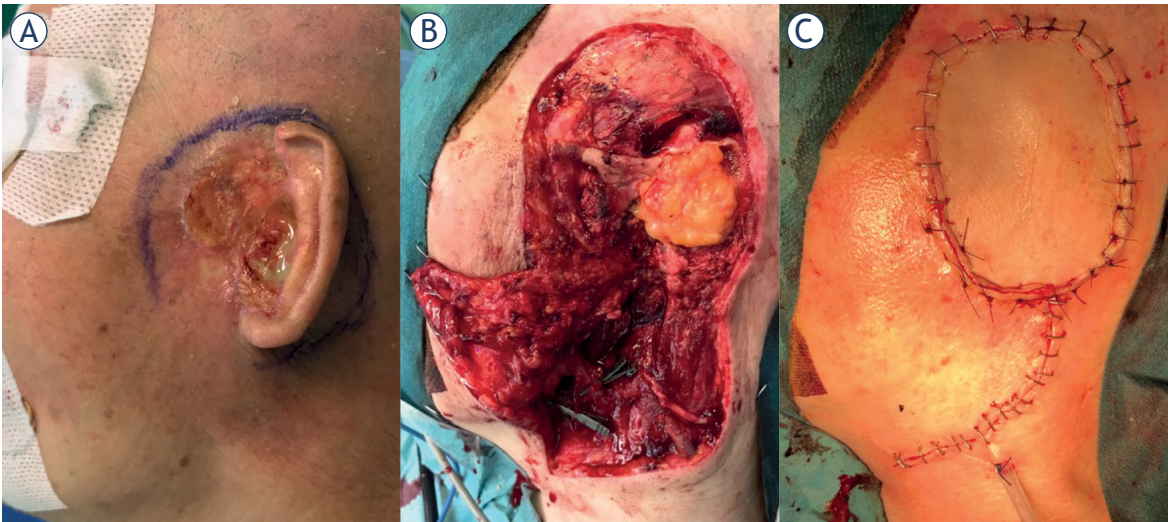


**FIGURE 4.** 73-year old female with locoregionally advanced external ear basal cell carcinoma extending to the left lateral skull-base. The resection margin is outlined (A). Salvage surgery (i.e., after primary radical radiotherapy and electrochemotherapy) involving lateral temporal bone resection with fat obliteration, with wide local excision, partial parotidectomy, ipsilateral selective neck dissection (B) and radial forearm free flap reconstruction (C) were performed.

ally advanced lateral skull-base cancer resection was 2.9 years ( $SD = 2.6$  years, range: 0.3 years – 8.1 years). At the data collection cut-off date, ten of these patients (83%) were alive and had no cancer recurrence (Table 2) (Figure 6A). Two patients (27%) died, but no recurrence was detected. One patient died with MEC since the resection was R1,

and the patient did not receive planned postoperative radiotherapy due to generalised weakness. One patient after R0 resection of MEC died due to comorbidities. The survival was 100% in patients treated with flap reconstruction and 67% in patients treated with other reconstruction modalities (Figure 6B).

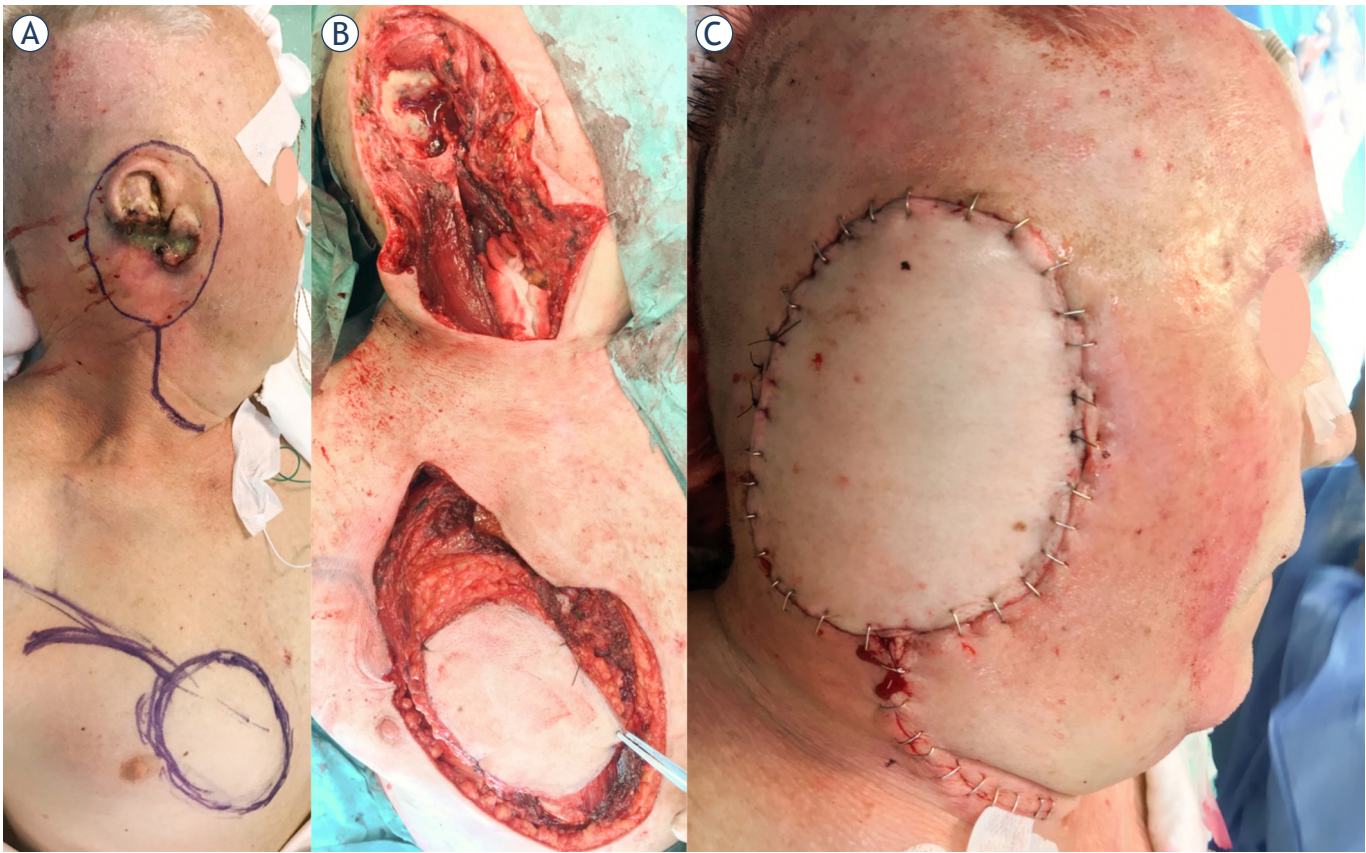


**FIGURE 5.** 76-year old male with locoregionally advanced external ear squamous cell carcinoma extending to the right lateral skull-base. The resection margin is outlined (A). Salvage surgery (*i.e.*, after primary radical radiotherapy) involving lateral temporal bone resection with wide local excision, partial parotidectomy, ipsilateral selective neck dissection and pectoralis major myocutaneous flap reconstruction (due to recipient vessel insufficiency) were performed (B, C).

## Discussion

Our study presents 17 patients treated surgically with curative intent in 9 years at Slovenia's two main healthcare centres dealing with surgical and non-surgical head and neck cancer treatment. As many as 12 patients (71%) had locoregionally advanced disease at the time of surgery.

The percentage (10%) of patients included in the final analysis (17 patients) among initially collected data (177 patients) confirms that the lateral skull-base cancer is a rare entity, and data acquisition is arduous. The main reason is that this cancer can be classified under various ICD-10 diagnoses. Middle ear cancer is the only lateral skull-base cancer with a universal ICD-10 code (C30.1). Our study presents only the minority of lateral skull-base cancer; therefore, other ICD-10 diagnoses should be included. Despite the efforts, the list of included diagnoses in our study is possibly not exhaustive, and some cases with lateral skull-base involvement

may have been diagnosed under other diagnoses (*i.e.*, C44.3). As already proposed<sup>1,3</sup>, the establishment of the universal lateral skull-base cancer registry should be encouraged, which would overcome obstacles in prospective data analysis and alleviate multicentric research in this rare type of cancer.

Male predominance (65%) and discharge as the most common initial symptom (71%) in our group are consistent with the literature. Nevertheless, the average age at the cancer diagnosis ( $M = 74$   $SD = 13$ ) was higher in our study.<sup>6</sup>

Set of histopathological types recorded in our patients are consistent with the literature which reports the predominance of squamous cell carcinoma.<sup>6</sup> Nonetheless, its predominance over other cancer types is not as significant as reported in other studies.<sup>1</sup> This is perchance due to the predominance (57%) of basal cell carcinoma classified as aEEC, which present the majority (41%) of cases in our study.

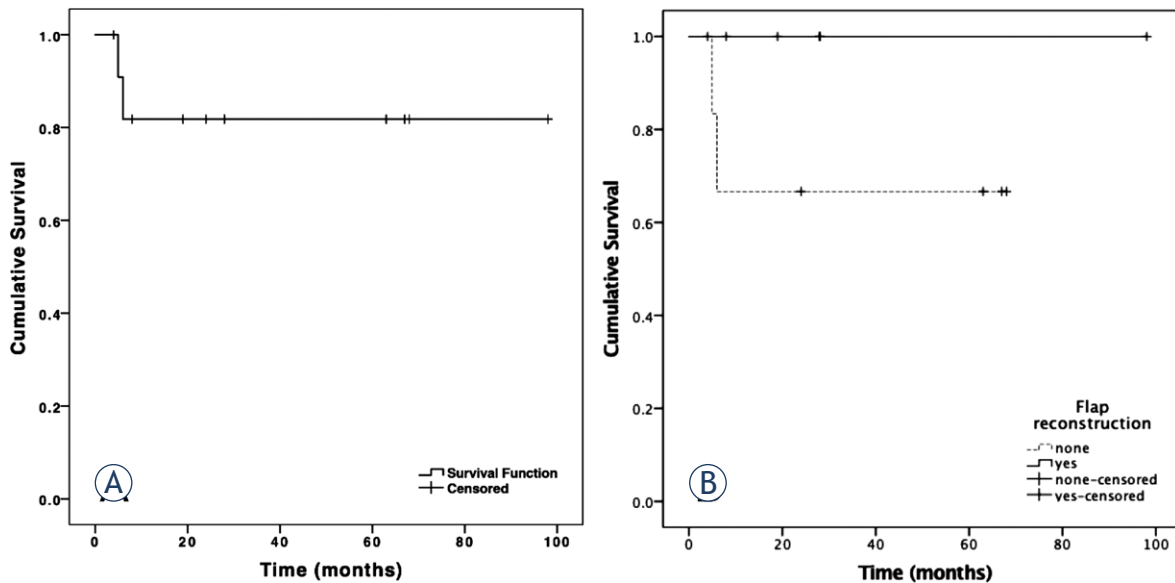


**FIGURE 6.** Kaplan-Meier analysis of overall survival of 12 patients with locoregionally advanced lateral skull-base cancer treated surgically with curative intent. **(A)** Kaplan-Meier analysis of 12 patients regardless of the reconstruction modality. Cumulative survival remained at 83% after six months. **(B)** Kaplan-Meier analysis of 6 patients treated with flap reconstruction and six patients with other reconstruction modalities. Cumulative survival remained at 67% after six months.

The study focused on analysing surgically treated locoregionally advanced lateral skull-base cancer (*i.e.*, TNM grades III and IV), which presented the vast majority of all cancers (71%). These patients suffered from a severe mixed (*i.e.*, sensorineural and conductive) hearing loss according to the hearing level measurements. Mostly, the extensive radical surgery was performed such as lateral temporal bone resection with obliteration (66.7%), ipsilateral neck dissection (66.7% selective, 8.7% modified radical) and parotidectomy (50% partial, 8.3% total). In all patients with locoregionally advanced skin cancer of external ear (3 patients) and parotid cancers (2 patients), the extensive radical resection including skin prompted the tissue defect reconstruction with a major regional or free flap. Combination of extensive radical resection and flap reconstruction proved efficient since all of these patients are still alive. According to our experiences, ALT, RFFF, and PM can be harvested simultaneously while performing the lateral skull-base resection, which shortens surgery time but requires two surgical teams. None of our ALT, RFFF and PM failed, despite postoperative radiotherapy in 2 of these patients, consistent with the literature.<sup>15</sup> Primary closure was the reconstruction of choice after resection of EACC or MEC since there was no large skin defect (*i.e.*, blind sac external auditory canal closure and no pinna amputation).

Results show that our patients' local control and survival with locoregionally advanced cancer were high, especially in patients treated with flap reconstruction (Figure 6). The cancer-free survival rate of 100% was calculated on only four patients since others were not followed-up for at least five years. 83% of alive patients at data collection cut-off confirms the favourable treatment outcome. This percentage is higher than the information collected in the pertinent literature (58.7%), although our patients were considerably older than in other reports.<sup>1</sup>

Our study has certain limitations inherent to other retrospective studies. The calculation of the annual incidence of lateral skull-base cancer in our country could not be performed since the data involve only patients treated in a single tertiary otorhinolaryngology referral centre. Moreover, our study does not present patients treated with non-surgical modalities only. Namely, for a comprehensive overview of the field, it would be essential to consider other treatment modalities such as primary radio(chemo)therapy<sup>3</sup> and also electrochemotherapy.<sup>16</sup>

## Conclusions

Extensive radical resection of the tumour, adjacent tissues and structures of lateral skull-base should

be planned in locoregionally advanced skin cancer of external ear and locoregionally advanced parotid cancer. The tissue defect should be reconstructed with tissue flap; therefore, otorhinolaryngologist treating this cancer should be experienced in free and regional flap elevation such as ALT, RFFF and PM. This surgical approach enables a high survival rate.

In locoregionally advanced primary external auditory canal cancer, the high survival rate is allowed with lateral temporal bone resection, obliteration and blind sac external auditory canal closure without amputation of the pinna, which offers the best chances for durable local control.

MEC is always locoregionally advanced if modified Pittsburgh staging system is applied, and the risk of tumour re-appearance is high despite extensive surgery and adjuvant treatment.

Collaboration within otorhinolaryngology subspecialists and oncologists is vital to treat lateral skull-base cancer. It is imperative to establish universal lateral skull-base cancer registry in tertiary healthcare centres involved in treating this disease.

## Acknowledgements

To Tina Žagar and Aleš Matos for data collection and distribution. The study was financially supported by the Slovenian Research Agency (programme no. P3-0307).

## References

1. Wierzbicka M, Niemczyk K, Bruzgielewicz A, Durko M, Klatka J, Kopeć T, et al. Multicenter experiences in temporal bone cancer surgery based on 89 cases. *PLoS One* 2017; **12**: e0169399. doi: 10.1371/journal.pone.0169399
2. da Silva AP, Breda E, Monteiro E. Malignant tumors of the temporal bone - our experience. *Braz J Otorhinolaryngol* 2016; **82**: 479-83. doi: 10.1016/j.bjorl.2015.09.010
3. Homer JJ, Lesser T, Moffat D, Slevin N, Price R, Blackburn T. Management of lateral skull base cancer: United Kingdom national multidisciplinary guidelines. *J Laryngol Otol* 2016; **130**(Suppl 2): S119-24. doi: 10.1017/S0022215116000542
4. Masterson L, Rouhani M, Donnelly NP, Tysome JR, Patel P, Jefferies SJ, et al. Squamous cell carcinoma of the temporal bone: clinical outcomes from radical surgery and postoperative radiotherapy. *Otol Neurotol* 2014; **35**: 501-8. doi: 10.1097/MAO.0000000000000265
5. Raghu M, Moumoulidis I, De R, Moffat D. Chondrosarcomas of the temporal bone: presentation and management. *J Laryngol Otol* 2004; **118**: 551-5. doi: 10.1258/0022215041615272
6. Sinha S, Dedmon MM, Naunheim MR, Fuller JC, Gray ST, Lin DT. Update on surgical outcomes of lateral temporal bone resection for ear and temporal bone malignancies. *J Neurol Surg Part B Skull Base* 2017; **78**: 37-42. doi: 10.1055/s-0036-1584310
7. Mehta GU, Muellemann TJ, Brackmann DE, Gidley PW. Temporal bone resection for lateral skull-base malignancies. *J Neurooncol* 2020; **150**: 437-44. doi: 10.1007/s11060-020-03445-4
8. Moody SA, Hirsch BE, Myers EN. Squamous cell carcinoma of the external auditory canal: an evaluation of a staging system. *Am J Otol* 2000; **21**: 582-8. doi: 10.1055/s-2007-994290
9. Hirsch BE. Staging system revision. *Arch Otolaryngol Neck Surg* 2002; **128**: 93-4. PMID: 11784271
10. Morita S, Mizumachi T, Nakamaru Y, Sakashita T, Kano S, Hoshino K, et al. Comparison of the University of Pittsburgh staging system and the eighth edition of the American Joint Committee on Cancer TNM classification for the prognostic evaluation of external auditory canal cancer. *Int J Clin Oncol* 2018; **23**: 1029-37. doi: 10.1007/s10147-018-1314-3
11. Gupta R, Sandison A, Wenig BM, Thompson LDR. Data set for the reporting of ear and temporal bone tumors: explanations and recommendations of the guidelines from the International Collaboration on Cancer Reporting. *Arch Pathol Lab Med* 2019; **143**: 593-602. doi: 10.5858/arpa.2018-0415-SA
12. Stell PM, McCormick MS. Carcinoma of the external auditory meatus and middle ear. Prognostic factors and a suggested staging system. *J Laryngol Otol* 1985; **99**: 847-50. doi: 10.1017/s0022215100097796
13. Wei W, Qiu Y, Fang Q, Jia Y. Pectoralis major myocutaneous flap in salvage reconstruction following free flap failure in head and neck cancer surgery. *J Int Med Res* 2019; **47**: 76-83. doi: 10.1177/0300060518795530
14. Moncrieff MD, Hamilton SA, Lamberty GH, Malata CM, Hardy DG, Macfarlane R, et al. Reconstructive options after temporal bone resection for squamous cell carcinoma. *J Plast Reconstr Aesthetic Surg JPRAS* 2007; **60**: 607-14. doi: 10.1016/j.jbjs.2006.11.005
15. Trojanowski P, Szymański M, Trojanowska A, Andrzejczak A, Szczepanek D, Klatka J. Anterolateral thigh free flap in reconstruction of lateral skull base defects after oncological resection. *Eur Arch Otorhinolaryngol* 2019; **276**: 3487-94. doi: 10.1007/s00405-019-05627-x
16. Bonadies A, Bertozzi E, Cristiani R, Govoni FA, Migliano E. Electrochemotherapy in skin malignancies of head and neck cancer patients: clinical efficacy and aesthetic benefits. *Acta Derm Venereol* 2019; **99**: 1246-52. doi: 10.2340/00015555-3341

## research article

# State of the art in breast intraoperative electron radiation therapy after intraoperative ultrasound introduction

Cristiana Vidali<sup>1</sup>, Mara Severgnini<sup>2</sup>, Gabriele Bellio<sup>3</sup>, Fabiola Giudici<sup>4</sup>, Vittorino Milan<sup>5</sup>, Zaira Pellin<sup>3</sup>, Sara Savatovic<sup>6</sup>, Serena Scomersi<sup>3</sup>, Gerd Fastner<sup>7</sup>, Antonella Ciabattoni<sup>8</sup>, Marina Bortul<sup>3</sup>

<sup>1</sup> Department of Radiation Oncology, Azienda Sanitaria Universitaria Integrata di Trieste, Trieste, Italy

<sup>2</sup> Department of Medical Physics, Azienda Sanitaria Universitaria Giuliano-Isontina, Trieste, Italy

<sup>3</sup> Department of Surgery, Azienda Sanitaria Universitaria Giuliano-Isontina Trieste, Italy.

<sup>4</sup> Unit of Biostatistics, Epidemiology and Public Health, Department of Cardiac, Thoracic, Vascular Sciences and Public Health, University of Padua, Padua, Italy

<sup>5</sup> Department of Radiation Oncology, Azienda Sanitaria Universitaria Giuliano-Isontina, Trieste, Italy

<sup>6</sup> Department of Physics, University of Trieste, Trieste, Italy

<sup>7</sup> Department of Radiotherapy and Radio-Oncology, Paracelsus Medical University, University Hospital Salzburg, Landeskrankenhaus, Salzburg, Austria

<sup>8</sup> Department of Radiotherapy, San Filippo Neri Hospital, ASL Roma1, Rome, Italy

Radiol Oncol 2021; 55(3): 333-340.

Received 12 November 2020

Accepted 6 April 2021

Correspondence to: Dr. Cristiana Vidali, former Senior Assistant Department of Radiation Oncology, Azienda Sanitaria Universitaria Integrata di Trieste, Trieste, Italy. E-mail: cristiana.vidali@libero.it

Disclosure: No potential conflicts of interest were disclosed.

This is an open access article under the CC BY-NC-ND license (<http://creativecommons.org/licenses/by-nc-nd/4.0/>).

**Background.** Breast intraoperative electron radiation therapy (B-IOERT) can be used in clinical practice both as elective irradiation (partial breast irradiation – APBI) in low risk breast cancer patients, and as an anticipated boost. The procedure generally includes the use of a shielding disk between the residual breast and the pectoralis fascia for the protection of the tissues underneath the target volume. The aim of the study was to evaluate the role of intraoperative ultrasound (IOUS) in improving the quality of B-IOERT.

**Patients and methods.** B-IOERT was introduced in Trieste in 2012 and its technique was improved in 2014 with IOUS. Both, needle and IOUS were used to measure target thickness and the latter was used even to check the correct position of the shielding disk. The primary endpoint of the study was the evaluation of the effectiveness of IOUS in reducing the risk of a disk misalignment related to B-IOERT and the secondary endpoint was the analysis of acute and late toxicity, by comparing two groups of patients treated with IOERT as a boost, either measured with IOUS and needle (Group 1) or with needle alone (Group 2). Acute and late toxicity were evaluated by validated scoring systems.

**Results.** From the institutional patients who were treated between June 2012 and October 2019, 109 were eligible for this study (corresponding to 110 cases, as one patients underwent bilateral conservative surgery and bilateral B-IOERT). Of these, 38 were allocated to group 1 and 72 to group 2. The target thickness measured with the IOUS probe and with the needle were similar (mean difference of 0.1 mm,  $p = 0.38$ ). The percentage of patients in which the shield was perfectly aligned after IOUS introduction increased from 23% to more than 70%. Moreover, patients treated after IOUS guidance had less acute toxicity (36.8% vs. 48.6%,  $p = 0.33$ ) from radiation therapy, which reached no statistical significance. Late toxicity turned out to be similar regardless of the use of IOUS guidance: 39.5% vs. 37.5% ( $p = 0.99$ ).

**Conclusions.** IOUS showed to be accurate in measuring the target depth and decrease the misalignment between collimator and disk. Furthermore there was an absolute decrease in acute toxicity, even though not statistically significant, in the group of women who underwent B-IOERT with IOUS guidance.

Key words: breast cancer; intraoperative electron radiation therapy; ultrasound; whole breast radiotherapy

## Introduction

Breast cancer is the most common malignant disease among women and about 53 000 new cases were estimated in Italy in 2019.<sup>1</sup> It still represents the first cause of death for cancer among women, even though there is a downward trend in the mortality in recent years (0.8%/year), due to the spread of screening programs and to therapeutic progress.<sup>2</sup>

Adjuvant radiotherapy (RT) after breast conservative surgery is currently considered the standard treatment for early breast cancer and plays an important role to reduce local recurrences (LR) and to improve disease-free and overall survival.<sup>3</sup>

Traditionally whole breast radiation therapy (WBRT) consisted of a total dose of 50–50.4 Gy in 25–28 fractions. In recent years moderate hypofractionated WBRT has become the preferred dose-fractionation scheme, with a total dose of 40 Gy in 15 fractions or 42.50 Gy in 16 fractions, as loco-regional and survival endpoint analyses have demonstrated no inferiority compared to a conventionally fractionated schedule in several meta-analyses.<sup>4,5</sup>

The use of an additional external boost, of 10–16 Gy to the tumor bed can reduce the local failure rate from 10.2% to 6.2% ( $p < 0.0001$ ).<sup>6</sup> This effect could be observed in all age-classes whereas the absolute gain is greatest in the group below 40 years. So far the impact of the boost has not yet been explicitly investigated in hypofractionation trials.<sup>4,5</sup>



**FIGURE 1.** First case of breast intraoperative electron radiation therapy (B-IOERT) in Trieste using the dedicated electron beam accelerator Mobetron by IntraOp® Company.

Intraoperative electron beam radiotherapy (IOERT) in the treatment of early-stage breast cancer was introduced into the clinical practice at the end of the 1990s, when dedicated mobile linear accelerators (Linacs) became available.<sup>6</sup> It can be used both as elective RT to the partial breast as accelerated partial breast irradiation (APBI) and as an anticipated boost.<sup>6–8</sup> In this case, it shortens the total radiation treatment time by 1–1.5 weeks and improves the precision of dose delivery to the tumor bed, which provides high local in-breast control rates for patients allocated to every risk group.<sup>8</sup>

Clinical data and technical details for both possible types of IOERT application, as a boost and as APBI, were summarized and discussed extensively within recently published ESTRO-guidelines.<sup>9</sup>

Beside others, in breast intraoperative electron radiation therapy (B-IOERT) the protection of the tissues underneath the target volume, as the heart, lungs, and bony structures, is obtained by positioning a shielding disk between the residual breast and the pectoralis muscle. The two main criticalities in this step of the procedure are the misalignment and the wrong orientation of the disk.<sup>10,11</sup>

B-IOERT was introduced in the “Azienda Sanitaria Universitaria Integrata” of Trieste in 2012 using the Mobetron® (IntraOp Medical, Inc. Santa Clara, CA), a “dedicated” electron beam accelerator, that produces electrons with nominal energies of 6, 9, and 12 MeV at dose rates up to approximately 10 Gy/min (Figure 1). Initially it was used as an anticipated boost in the treatment of early breast cancer and since March 2018 also as APBI in selected patients, according to the international recommendations.<sup>12</sup> Its technique was improved in 2014 with IOUS. Both needle and IOUS were used to measure target thickness; the latter was used even to check the correct position of the shielding disk.

The primary endpoint of this retrospective study was the evaluation of the role of IOUS in reducing the risk of the disk misalignment related to B-IOERT and the secondary endpoint was the analysis of acute and late toxicity, by comparing two groups of patients treated with IOERT as a boost, whose target was measured either with IOUS and needle (Group 1) or with needle alone (Group 2).

## Patients and methods

This is a retrospective cohort analysis of prospectively recorded data involving patients who underwent B-IOERT as an anticipated boost between

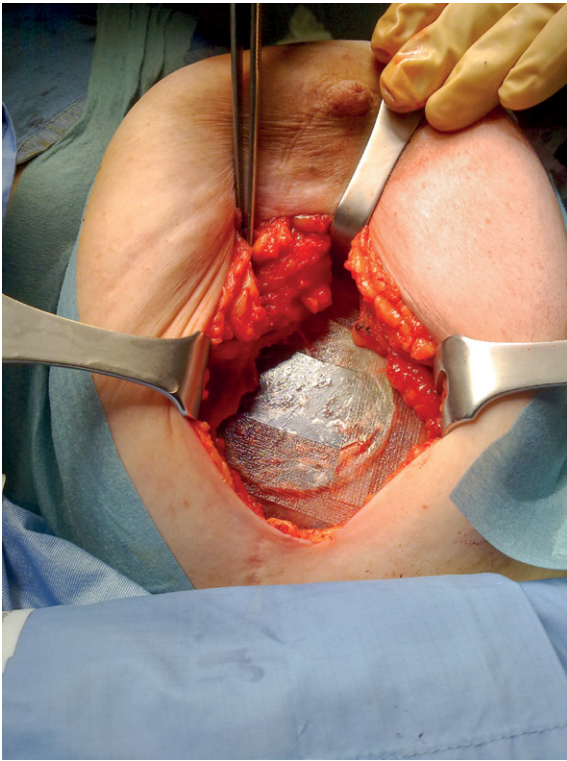


**FIGURE 2A.** The shielding disk positioned beneath the tumor bed during the operation.

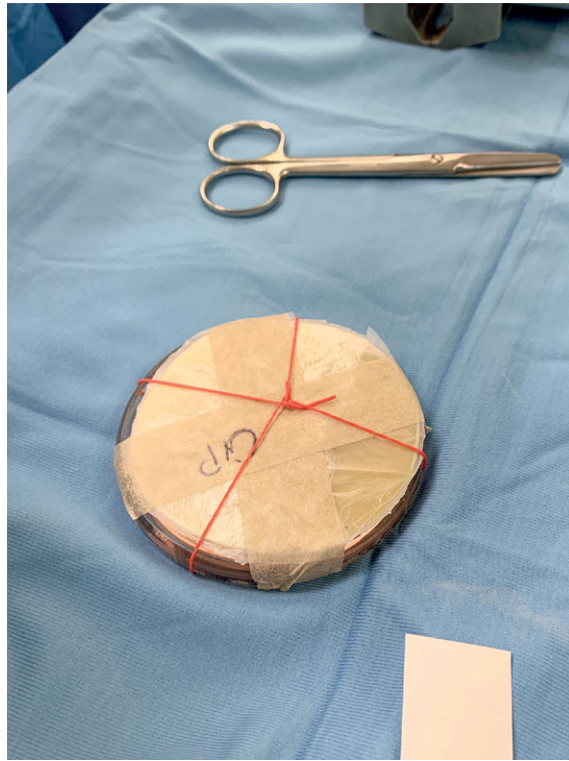


**FIGURE 2B.** The disk provided by IntraOp® Company, made up of three stacked layers.

June 2012 and November 2019 in the “Azienda Sanitaria Universitaria Integrata di Trieste”.

B-IOERT boost dose prescription was 10 Gy specified as maximum dose; the planning target volume (PTV) should be encompassed by 90% of the prescribed dose (*i.e.* 9 Gy); dose inhomogeneity: -10% within the target volume was allowed. It was followed by conventionally fractionated WBRT with a total dose of 50 Gy (2 Gy/25 fr.).

Since November 2014 we have taken part in the HIOB protocol (Hypofractionated Whole-Breast Irradiation preceded by Intra-Operative Radiotherapy with Electrons as anticipated Boost – Prospective one-armed multi-center-trial), after the approval of the Regional Ethics Committee.

The anticipated IOERT boost dose was 11,10 Gy, specified at the point of maximum dose on the central axis depth dose curve, and it was followed by hypofractionated WBRT with a total dose of 40,5 Gy in 15 fractions, 2,7 Gy/fr.<sup>13</sup> First clinical results on treatment tolerance (toxicity and cosmetic outcome) were published in 2020.<sup>14</sup>

In the whole series before starting IOERT (either as a boost or as the unique radiation treatment), a shielding disk was positioned beneath the tumor bed on the pectoralis muscle (Figure 2A). A disk

provided by IntraOp® Company was employed, made by stacking a 5 mm polymethyl methacrylate (PMMA) layer, a 3 mm copper layer and 2 mm PMMA layer (Figure 2B).<sup>15</sup>

The optimum size of the shielding disk depends upon the electron applicator chosen for the treatment. As described in our research and in some recent studies, the set-up of normal tissue protection and applicator placement are closely correlated with two very relevant risks in IOERT treatments: misalignment and wrong orientation of the shielding disk.<sup>11,16,17</sup> The low accuracy in the alignment of the disk would cause the delivery of an excess of dose to the underlying normal tissues. The surrounding healthy gland was sutured above the shielding disk.

Initially target depth was measured with a needle in 5 different points of the tumor bed and the average value was assumed in order to select the proper electron energy. Since the end of 2014, when HIOB Protocol was introduced, both needle and IOUS were used in a certain number of cases, to obtain 5 measures of the target thickness and the latter was used even to check the correct position of the shielding disk. An Esaote MyLab™One/Touch equipment with SL 3332 linear probe was applied.

The effectiveness of the correct localization by IOUS was verified employing “in vivo dosimetry”. A properly calibrated EBT3 radiochromic film can be fixed on both faces of the disk, allowing to obtain two images that provide a detailed bidimensional dose distribution. From the first image, obtained just below the target, it is possible to measure the absolute entrance dose in that position. Moreover, the visual analysis acquired within the prepared target tissue can provide the surgeon with an effective feedback about the actual homogeneity acquired in the reconstruction of the target. From the second image positioned beyond the shielding disk, it is possible to evaluate the fraction of the dose passing through the disk and arriving at the underlying healthy tissue.<sup>15</sup>

The post-processing analysis of the dose distribution measured on the films provides a quantitative estimate of the misalignment between the collimator and the disk.

In order to investigate possible differences in the target thickness between needle and IOUS, which could alter the results, we compared preliminarily these measures in a sample of 23 patients.

Between June 2012 and October 2019 a total of 109 women (corresponding to 110 cases, as one patient underwent bilateral conservative surgery and bilateral B-IOERT for two different cancers on both breasts) underwent B-IOERT as an anticipated boost and 35 of them entered the HIOB trial.<sup>13,14</sup> In 38 cases both needle and IOUS were used (Group 1) and in 72 only the needle (Group 2).

Acute toxicity was rated according to the Radiation Therapy Oncology Group (RTOG) criteria<sup>18</sup> and late toxicity to the LENT-SOMA score, respectively.<sup>19</sup>

This study was approved by the Institutional Review Boards of the Hospital and all patients signed preoperatively a specific informed consent.

### Statistical analysis

The statistical analysis was performed by R software (version 3.5.0). Shapiro-Wilk test was applied to quantitative (continuous) variables to check for distribution normality. Continuous variables were reported as median with range (minimum-maximum). Qualitative (categorical) variables were reported as absolute frequencies and/or percentages. Measures of target thickness (in mm) between needle and IOUS were compared by paired student's *t* test for every patients and overall. Moreover, Lin's concordance correlation coefficient ( $\rho_c$ ) was calculated to evaluate the agreement on target thick-

ness obtained by the two methods.  $\rho_c$  ranges from 0 to 1, with perfect agreement at 1 while values near to 0 indicates no agreement. The value of  $\rho_c$  was interpreted according to the Mc-Bride classification (< 0.90: poor; 0.90–0.95: moderate; 0.95–0.99: substantial; > 0.99: almost perfect). Categorical variables were compared by Chi-square test or Fischer's exact test whenever appropriate. All p-values were calculated from 2-sided tests using 0.05 as the significance level.

## Results

### Description of the population

Information on patient characteristics and adjuvant systemic treatments of the whole population and of the two groups are summarized in Table 1. Baseline characteristics are similar between treatment groups. The median age of the entire cohort of patients was 67 years (range: 43–85).

Two patients (one belonged to Group 1 and the other to Group 2) refused adjuvant radiotherapy and one (Group 2) performed it elsewhere.

Of note, two patients did not receive the allocated systemic therapy: one was discouraged for endocrine therapy due to severe osteoporosis and the second refused chemotherapy without compensating it by another oncological relevant medication.

With a median follow-up of 52 months (range: 5–87), 3 patients died of breast cancer and 4 of other causes; one patient is alive with progressive disease and another one was treated for a contralateral tumor and is disease-free at the last follow-up.

### Effect of IOUS

The target thickness detected preliminarily with IOUS in a sample of 23 patients turned out to be completely in agreement with the measures obtained with the needle, with Lin's concordance coefficient  $\rho_c = 0.98$ , 95%CI: 0.96:0.99 and with a negligible average difference of 0.1 mm (range 0.1–1.2 mm) ( $p = 0.38$ ) as described in Supplementary Table 1.

The EBT3 “in vivo dosimetry” showed that IOUS guidance achieved a reduction in the misalignment with an electron field area outside the shielding disk reduction from 5.6 cm<sup>2</sup> to 2.6 cm<sup>2</sup>.

After IOUS introduction, the percentage of patients in whom the shield was perfectly aligned, defined as a field totally inside the shield, increased from 23% to more than 70%. The proper

TABLE 1. Description of the population

Variables	All cohort (n = 110)	Group 1 (n = 38)	Group 2 (n = 72)	p-value
Age (years) Median (range)	67 (43–85)	67 (48–80)	67 (43–85)	p = 0.51
Clinical stage				
cT1a N0	2 (1.8%)	1 (2.6%)	1 (1.4%)	p = 0.42
cT1b N0	47 (42.8%)	20 (52.6%)	27 (37.5%)	
cT1c N0	59 (53.6%)	17 (44.8%)	42 (58.3%)	
cT1b N1	1 (0.9%)	0 (0.0%)	1 (1.4%)	
cT2 N0	1 (0.9%)	0 (0.0%)	1 (1.4%)	
Histological type				
Ductal carcinoma in situ (DCIS)	1 (0.9%)	1 (2.6%)	0 (0.0%)	p = 0.46
Invasive ductal carcinoma	70 (63.6%)	26 (68.4%)	44 (61.1%)	
Invasive lobular carcinoma	19 (17.3%)	5 (13.2%)	14 (19.45%)	
Others	20 (18.2%)	6 (15.8%)	14 (19.45%)	
Multifocal disease	6 (5.4%)	4 (10.5%)	2 (2.8%)	p = 0.21
Pathological Stage pT				
pTis	1 (0.9%)	1 (2.6%)	0 (0.0%)	p=0.40
pT1a	3 (2.7%)	0 (0.0%)	3 (4.2%)	
pT1b	41 (37.3%)	16 (42.1%)	25 (34.7%)	
pT1c	59 (53.6%)	20 (52.6%)	39 (54.2%)	
pT2	6 (5.5%)	1 (2.6%)	5 (6.9%)	
Pathological Stage pN				
pN0	88 (80.0%)	32 (84.2%)	56 (77.8%)	p=0.71
pN1mi	7 (6.4%)	3 (7.9%)	4 (5.6%)	
pN1a	14 (12.7%)	3 (7.9%)	11 (15.3%)	
pN3	1 (0.9%)	0 (0.0%)	1 (1.4%)	
Grading				
G1	15 (13.7%)	7 (18.4%)	8 (11.1%)	p = 0.67
G2	68 (61.8%)	24 (63.2%)	44 (61.1%)	
G3	21 (19.1%)	6 (15.8%)	15 (20.8%)	
Gx	6 (5.4%)	1 (2.6%)	5 (7%)	
Adjuvant therapy*				
None	2 (1.8%)	0 (0.0%)	2 (2.8%)	p = 0.92
Chemotherapy	6 (5.5%)	2 (5.4%)	4 (5.6%)	
Endocrine therapy	85 (78%)	29 (78.4%)	56 (77.7%)	
Chemotherapy + Endocrine therapy	12 (11%)	4 (10.8%)	8 (11.1%)	
Chemotherapy + Trastuzumab	4 (3.7%)	2 (5.4%)	2 (2.8%)	

\* Calculated on 109 patients

alignment with IOUS improved the absolute dose accuracy and tripled the number of patients without disk misalignment. The results of post processing analysis of the dose distribution measured on film, the collimator used, the estimated dose, the area outside the shielding disk and the dose map distribution are presented in Figure 3.

In the whole series acute toxicity, detected 4 weeks after WBRT, occurred in 49 patients (44.5%): G1 in 36 (32.7%) and G2 in 13 (11.8%) of them. The most common acute reaction was erythema due to postoperative WBRT. As perioperative complications the occurrence of seroma (one case), hematoma (2 cases) and lymphocele (2 cases) were identified. With regard to clinical collateral effects, patients allocated to group 1 developed less radiation induced acute toxicity compared to group 2 (36.8%

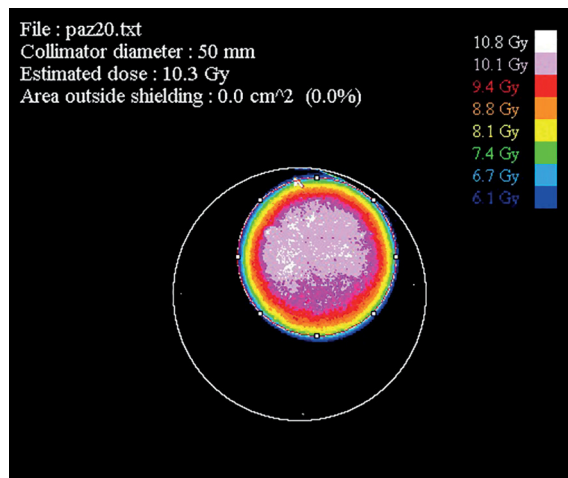


FIGURE 3. Post processing analysis of the dose distribution measured on film.

TABLE 2. Acute toxicity of radiotherapy in the two groups

	Group 1 (n = 38)	Group 2 (n = 72)	Total (n = 110)
Grade 0	23 (60.5%)	36 (50%)	59 (53.6%)
Grade 1	8 (21.1%)	28 (38.9%)	36 (32.7%)
Grade 2	6 (15.8%)	7 (9.7%)	13 (11.8%)
Grade X	1 (2.6%)	1 (1.4%)	2 (1.9%)
Grade 1-2	14 (36.8%)	35 (48.6%)	49 (44.5%)

Group 1 = cases treated with breast intraoperative electron radiation therapy (B-IOERT) as a boost in which both needle and intraoperative ultrasound (IOUS) were used; Group 2 = cases treated with B-IOERT as a boost in which only the needle was used

TABLE 3. Late toxicity of radiotherapy in the two groups

	Group 1 (n = 38)	Group 2 (n = 72)	Total (n = 110)
Grade 0	22 (57.9%)	43 (59.7%)	65 (59.1%)
Grade 1	12 (31.6%)	24 (33.3%)	36 (32.7%)
Grade 2	3 (7.9%)	3 (4.2%)	6 (5.5%)
Grade X	1 (2.6%)	2 (2.8%)	3 (2.7%)
Grade 1-2	15 (39.5%)	27 (37.5%)	42 (38.2%)

Group 1 = cases treated with breast intraoperative electron radiation therapy (B-IOERT) as a boost in which both needle and intraoperative ultrasound (IOUS) were used; Group 2 = cases treated with B-IOERT as a boost in which only the needle was used

vs 48.6%), which turned out as not statistically significant ( $p = 0.33$ ) (Table 2).

Late toxicity, evaluated at the last follow-up, was observed in 42 patients (Grade 1: 36 cases; Grade 2: 6 cases). There was a negligible difference in the two groups of patients: 39.5% (Group 1) vs. 37.5% (Group 2) ( $p = 0.99$ ). (Table 3). The most common type of sequelae were: fibrosis/fat necrosis (G1/2: 21.8%) and breast edema (G1/2: 6.4%). In the whole population no Grade 3 acute and late toxicity occurred.

Detailed results for late toxicity according to LENT-SOMA score are summarized in Supplementary Table 2. As regards the different WBRT schedules, no significant differences were detected for acute and late toxicity (Supplementary Table 3A, 3B).

## Discussion

The primary objective of this analysis was to evaluate the role of IOUS in improving the quality and in reducing the risks related to B-IOERT.

We could demonstrate that IOERT is a safe treatment modality; the target thickness measures

performed with the needle were comparable with those obtained with IOUS. Moreover IOUS contributed considerably to optimize the alignment of the shielding disk.

At present, a commercially available treatment planning system (TPS) for IOERT, which allows to accurately illustrate a dose distribution within the target as well as the surrounding tissues, is used only by a small number of Centers.<sup>20</sup> The process leading to intraoperative radiation treatment, without TPS, is mostly the result of a sequence of manually handled actions involving the Surgeon, the Radiation Oncologist, the Medical Physicist, the Technicians and the Nurses of the operating room.<sup>9,11</sup>

Some papers examined the importance of risk assessment analysis applied to IOERT procedure: in the Italian publications a dedicated mobile Linac was used, while in the Spanish analysis the irradiation was performed with a conventional Linac.<sup>11,16,17</sup> In all of the studies the highest risk was associated with the alignment of the shielding disk, as it was observed in our experience.

The low accuracy in the alignment of the disk would cause the delivery of an excess of dose to the underlying normal tissues and is mainly related to the lack of direct visual disk control.<sup>11</sup> Selecting a plate much larger than the applicator size and fixing it to the pectoralis fascia is some effective corrective actions. The introduction of intraoperative ultrasound allows to check the position of the shielding disk as well as to better define the target thickness and is an important strategy for reducing the risk of shield misalignment and incorrect thickness measures.

The secondary endpoint of the study was the evaluation of early and late toxicity in the whole series with the comparison between the group of patients who underwent IOUS examination vs. the group who underwent only needle measures.

The target volume with IOERT boost is smaller than the volume with conventional EBRT boost. This leads to a reduction in the radiation exposure of the subcutaneous tissues and intra-thoracic organs (i.e. lungs and heart). Besides it avoids the irradiation of the skin and of the contralateral mammary gland, reducing both the short-term and long-term sequelae correlated with RT and resulting in good cosmesis.<sup>9</sup>

To date various papers have been published on IOERT boost in the treatment of early-stage breast cancer, with the largest deriving from a pooled analysis of the International Society of Intraoperative Radiation Therapy (ISIRT)

Europe, which was updated for the Salzburg cohort with a 10 year follow-up in 2018.<sup>21,22</sup> Excellent local control was reported in all the studies and side effects were generally low and acceptable. Merrick *et al.* reported 11% delayed fibrosis around the tumor bed and late breast or arm pain in 8% of patients; Lemanski *et al.* Grade 2 subcutaneous fibrosis in 14% and late breast or arm pain in 8% of patients.<sup>23,24</sup> In the Salzburg experience less than 2% of patients developed G3 late toxicity.<sup>8</sup> In the prospective study by Wong *et al.*, there was no G3 acute toxicity; two patient developed G3 late toxicity (3.8%) and 5 patients (9.6%) fat necrosis.<sup>25</sup> In these studies conventionally fractionated WBRT (total dose: 50–56 Gy/25–28 fr.) was delivered. In a retrospective German study 14 of 157 patients (8.9%) were treated with hypofractionated WBRT; the whole acute skin toxicity was evaluable in 153 patients: G1 in 75.2%; G2 in 15.7% and G3 in 4.6%, 6–8 weeks after WBRT.<sup>26</sup>

In three prospective investigations, IOERT boost was combined with hypofractionated WBRT. In the report by Ivaldi *et al.* G1 and G2 acute toxicity were found in 79/132 (59.8%) and in 22/132 (16.7%) respectively, and G3 in 3/132 (2.3%) patients one month after the end of WBRT.<sup>27</sup> The recorded late skin toxicity was Grade 4 in one patient, Grade 3 in another one and Grade 2 or less in 106/108 cases (98.2%) with a median follow-up of 11 months. In the study by Bhandari *et al.* only 24 patients underwent IOERT as a boost; after a short follow-up (12 months), G1 and G2 acute toxicity was present in 47.8% and 4.4% of the cases, respectively; late toxicity in 40% (G1) and in 10% (G2) of the cases.<sup>28</sup> In the recent paper from HIOB prospective multicenter trial, G0–1 acute effects were noted in 92% of patients and G3 in one patient, 4 weeks after the end of WBRT; G0–1 late toxicity in 93%, G2 in 4.3% and G3–4 in 2.7% of cases at 4 years.<sup>14</sup>

Our results are similar to the data reported in the other series and even better than the results of the early published reports. Additionally the effectiveness of IOUS application during IOERT procedure was analyzed and less acute toxicity, even if not statistically significant, was observed in the group of women who underwent B-IOERT with IOUS guidance. As regards G1–G2 late toxicity, no differences in the two groups of patients were detected. No grade 3 and 4 acute and late toxicity were present in both treatment groups.

To our knowledge no other studies evaluated shielding disk misalignment and possible correlations with acute or late toxicity in B-IOERT procedure. However, these results should be taken with

caution. First of all this is a retrospective study; besides the analysis was carried out on a small series of patients and median follow-up is rather short. A longer follow-up is advisable, to monitor the incidence of late toxicity.

## Conclusions

In this study, IOUS turned out to be an excellent intraoperative imaging modality that allows to measure the thickness of the tumor bed, to optimize the position of the shielding disk and it possibly contributes to decrease adverse effects in term of acute toxicity. Its application is advisable also in other areas of intraoperative radiation treatments.

## References

1. AIOM-AIRTum. [The number of cancer in Italy 2019]. [Italian]. Brescia: Intermedia Editore; 2019. Available at: [www.medineews.it](http://www.medineews.it)
2. AIOM Linee guida. [Breast neoplasms, 2019]. [Italian]. [internet]. 2019. [cited 2020 Oct 14]. Available at: <https://www.aiom.it/linee-guida-aiom-neoplasie-della-mammella-2019>
3. Early Breast Cancer Trialists' Collaborative Group (EBCTCG). Effect of radiotherapy after breast-conserving surgery on 10-year recurrence and 15-year breast cancer death: meta-analysis of individual patient data for 10,801 women in 17 randomized trials. *Lancet* 2011; **378**: 1707-16. doi: 10.1016/S0140-6736(11)61629-2
4. Hickey BE, James ML, Lehman M, Hider PN, Jeffery M, Francis DP, et al. Fraction size in radiation therapy for breast conservation in early breast cancer. *Cochrane Database Syst Rev*, 2016; **7**: CD003860. doi: 10.1002/14651858.CD003860.pub4.
5. Valle LF, Agarwal S, Bickel KE, Herceck HA, Nalepinski DC, Kapadia NS. Hypofractionated whole breast radiotherapy in breast conservation for early-stage breast cancer: a systematic review and meta-analysis of randomized trials. *Breast Cancer Res Treat* 2017; **162**: 409-17. doi: 10.1007/s10549-017-4118-7
6. Veronesi U, Orecchia R, Maisonneuve P, Viale G, Rotmensz N, Sangalli C, et al. Intraoperative radiotherapy versus external radiotherapy for early breast cancer (ELIOT): a randomised controlled equivalence trial. *Lancet Oncol* 2013; **14**: 1269-77. doi: 10.1016/S1470-2045(13)70497-2
7. Maluta S, Dall'Oglio S, Goer DA, Marciai N. Intraoperative electron radiotherapy (IOERT) as an alternative to standard whole breast irradiation: only for low-risk subgroups? *Breast Care* 2014; **9**: 102-6. doi: 10.1159/000362392
8. Sedlmayer F, Reitsamer R, Wenz F, Sperk E, Fussl C, Kaiser J, et al. Intraoperative radiotherapy (IORT) as boost in breast cancer. *Radiat Oncol* 2017; **12**: 23. doi: 10.1186/s13014-016-0749-9
9. Fastner G, Gaisberger C, Kaiser J, Scherer P, Ciabattioni A, Petoukhova A, et al. ESTRO IORT Task Force/ACROP recommendations for intraoperative radiation therapy with electrons (IOERT) in breast cancer. *Radiother Oncol* 2020; **149**: 150-15. doi: 10.1016/j.radonc.2020.04.059
10. Russo G, Casarino C, Arnetta G, Candiano G, Stefano A, Alongi F, et al. Dose distribution changes with shielding disc misalignments and wrong orientations in breast IOERT: a Monte Carlo-GEANT<sub>4</sub> and experimental study. *J Appl Clin Med Phys* 2012; **13**: 74-92. doi: 10.1120/jacmp.v13i5.3817
11. Vidali C, Severgnini M, Urbani M, Toscano L, Perulli A, Bortol M. FMECA application to intraoperative electron beam radiotherapy procedure as a quality method to prevent and reduce patient's risk in conservative surgery for breast cancer. *Front Med* 2017; **4**: 138. doi: 10.3389/fmed.2017.00138

12. Correa C, Harris EE, Leonardi MC, Smith BD, Taghian AG, Thompson AM, et al. Accelerated partial breast irradiation: executive summary for the update of an ASTRO evidence-based consensus statement. *Pract Radiat Oncol* 2017; **7**: 73-9. doi: 10.1016/j.prro.2016.09.007
13. Sedlmayer F, Fastner G, Sedlmayer F. Intra-operative electron boost and hypofractionated whole-breast irradiation during breast-conserving treatment (BCT) (HIOB). *ClinicalTrials.gov Identifier: NCT01343459*. [internet]. [cited 2020 Oct 13]. Available at: <https://clinicaltrials.gov/ct2/show/NCT01343459>
14. Fastner G, Reitsamer R, Urbanski B, Kopp P, Murawa D, Adamczyk B, et al. Toxicity and cosmetic outcome after hypofractionated whole breast irradiation and boost-IOERT in early stage breast cancer (HIOB): first results of a prospective multicenter trial (NCT01343459). *Radiother Oncol* 2020; **146**: 136-42. doi: 10.1016/j.radonc.2020.02.001
15. Severgnini M, de Denaro M, Bortol M, Vidali C, Beorchia A. In vivo dosimetry and shielding disk alignment verification by EBT3 GAFCHROMIC film in breast IOERT treatment. *J Appl Clin Med Phys* 2015; **16**: 112-20. doi: 10.1120/jacmp.v16i1.5065
16. Ciocca, M, Cantone MC, Veronese I, Cattani F, Pedroli G, Molinelli S, et al. Application of failure mode and effects analysis to intraoperative radiation therapy using mobile electron linear accelerators. *Int J Radiat Oncol Biol Phys* 2012; **82**: e305-11. doi: 10.1016/j.ijrobp.2011.05.010
17. López-Tarjuelo J, Bouché-Babiloni A, Santos-Serra A, Morillo-Macias V, Calvo FA, Kubyshev Y, et al. Failure mode and effect analysis oriented to risk-reduction interventions in intraoperative electron radiation therapy: the specific impact of patient transportation, automation, and treatment planning availability. *Radiother Oncol* 2014; **113**: 283-9. doi: 10.1016/j.radonc.2014.11.012
18. Cox JD, Stetz J, Pajak TF. Toxicity criteria of the Radiation Therapy Oncology Group (RTOG) and the European Organization for Research and Treatment of Cancer (EORTC). *Int J Radiat Oncol Biol Phys* 1995; **31**: 1341-6. doi: 10.1016/0360-3016(95)00060-C
19. Rubin P, Constine LS, Fajardo LF, Phillips TF, Wasserman TH. RTOG Late Effects Working Group. Overview of late effects of normal tissues (LENT) scoring system. *Int J Radiat Oncol Biol Phys* 1995; **31**: 1041-2. doi: 10.1016/0360-3016(95)00057-6
20. Valdivieso-Casique MF, Rodríguez R, Rodríguez-Bescós S, Lardies D, Guerra P, Ledesma MJ, et al. RADIANCE – a planning software for intra-operative radiation therapy. *Transl Cancer Res* 2015; **4**: 196-209. doi: 10.3978/j.issn.2218-676X.2015.04.05
21. Fastner G, Sedlmayer F, Merz F, Deutschmann H, Reitsamer R, Menzel C, et al. IOERT with electrons as boost strategy during breast conserving therapy in limited stage breast cancer: long term results of an ISIOR pooled analysis. *Radiother Oncol* 2013; **108**: 279-86. doi: 10.1016/j.radonc.2013.05.031
22. Kaiser J, Reitsamer R, Kopp P, Gaisberger C, Kopp M, Fischer T, et al. Intraoperative electron radiotherapy (IOERT) in the treatment of primary breast cancer. *Breast Care* 2018; **13**: 162-7. doi: 10.1159/000489637
23. Merrick HW 3rd, Hager E, Dobelbower RR Jr. Intraoperative radiation therapy for breast cancer. *Surg Oncol Clin N Am* 2003; **12**: 1065-78. doi: 10.1016/s1055-3207(03)00098-x
24. Lemanski C, Azria D, Thezenas S, Gutowski M, Saint-Aubert B, Rouanet P, et al. Intraoperative radiotherapy given as a boost for early breast cancer: long-term clinical and cosmetic results. *Int J Radiat Oncol Biol Phys* 2006; **64**: 1410-5. doi: 10.1016/j.ijrobp.2005.10.025
25. Wong WW, Pockaj BA, Vora SA, Halyard MY, Gray RJ, Schild SE. Six-year outcome of a prospective study evaluating tumor bed boost with intraoperative electron irradiation followed by whole-breast irradiation for early-stage breast cancer. *Breast J* 2014; **20**: 125-30. doi:10.1111/tbj.12235
26. König L, Lang K, Heil J, Golatta M, Major G, Krug D, et al. Acute toxicity and early oncological outcomes after intraoperative electron radiotherapy (IOERT) as boost followed by whole breast cancer patients – first clinical results from a single center. *Front Oncol* 2019; **9**: 384. doi: 10.3389/fonc.2019.00384
27. Ivaldi GB, Leonardi MC, Orecchia R, Zerini D, Morra A, Galimberti V, et al. Preliminary results of electron intraoperative therapy boost and hypofractionated external beam radiotherapy after breast-conserving surgery in premenopausal women. *Int J Radiat Oncol Biol Phys* 2008; **72**: 485-93. doi: 10.1016/j.ijrobp.2007.12.038
28. Bhandari T, Babaran W, Forouzannia A, Williams V, Harness J, Carpenter M, et al. A prospective phase I comparison of toxicity and cosmesis outcomes of single-fraction IOERT and hypofractionated radiotherapy with IOERT boost in early-stage breast cancer. *Brachytherapy* 2017; **16**: 1232-1238.e2. doi: 10.1016/j.brachy.2017.09.002

research article

# Preoperative serum CA-125 level as a predictor for the extent of cytoreduction in patients with advanced stage epithelial ovarian cancer

Sebastjan Merlo<sup>1,2</sup>, Nikola Basic<sup>2,3</sup>, Eva Drmota<sup>2</sup>, Nina Kovacevic<sup>1,2,4</sup>

<sup>1</sup> Department of Gynaecological Oncology, Institute of Oncology Ljubljana, Ljubljana, Slovenia

<sup>2</sup> Faculty of Medicine, University of Ljubljana, Ljubljana, Slovenia

<sup>3</sup> Department of Surgical Oncology, Institute of Oncology Ljubljana, Ljubljana, Slovenia

<sup>4</sup> Faculty of Health Care Angele Boškin, Jesenice, Slovenia

Radiol Oncol 2021; 55(3): 341-346.

Received 25 November 2020

Accepted 9 February 2021

Correspondence to: Assist. Nina Kovačević M.D., Ph.D., Department of Gynaecological Oncology, Institute of Oncology Ljubljana, Zaloška cesta 2, SI-1000 Ljubljana, Slovenia. Phone: + 386 41 277 602; E-mail: nkovacevic@onko-i.si

Disclosure: No potential conflicts of interest were disclosed.

This is an open access article under the CC BY-NC-ND license (<http://creativecommons.org/licenses/by-nc-nd/4.0/>).

**Background.** Ovarian cancer is the seventh most common cancer in women worldwide and the eighth most common cause of cancer death. Due to the lack of effective early detection strategies and the unspecific onset of symptoms, it is diagnosed at an advanced stage in 75% of cases. The cancer antigen (CA) 125 is used as a prognostic marker and its level is elevated in more than 85% of women with advanced stages of epithelial ovarian cancer (EOC). The standard treatment is primary debulking surgery (PDS) followed by adjuvant chemotherapy (ACT), but the later approach is neoadjuvant chemotherapy (NACT) followed by interval debulking surgery (IDS). Several studies have been conducted to find out whether preoperative CA-125 serum levels influence treatment choice, surgical resection and survival outcome. The aim of our study was to analyse experience of single institution as Cancer comprehensive center with preoperative usefulness of CA-125.

**Patients and methods.** At the Institute of Oncology Ljubljana a retrospective analysis of 253 women with stage FIGO IIIc and IV ovarian cancer was conducted. Women were divided into two groups based on their primary treatment. The first group was the NACT group (215 women) and the second the PDS group (38 women). The differences in patient characteristics were compared using the Chi-square test and ANOVA and the Kaplan-Meier method was used for calculating progression-free survival (PFS) and overall survival (OS).

**Results.** The median serum CA-125 level was higher in the NACT group than in the PDS group, 972 IU/ml and 499 IU/ml, respectively. The PFS in the NACT group was 8 months (95% CI 6.4–9.5) and 18 months (95% CI 12.5–23.4) in the PDS group. The median OS was lower in the NACT group than in the PDS group, 25 months (95% CI 20.6–29.5) and 46 months (95% CI 32.9–62.1), respectively.

**Conclusions.** Preoperative CA-125 cut off value of 500 IU/ml is a promising threshold to predict a successful PDS.

Key words: ovarian cancer; tumour marker; CA-125; primary debulking surgery; neoadjuvant chemotherapy

## Introduction

Ovarian cancer is the seventh most common cancer in women around the world, with approximately 240,000 new cases diagnosed each year. Epithelial ovarian cancer (EOC) is a very aggressive disease and is the eighth leading cause of cancer death with five-year survival rates below 45%.<sup>1</sup> Of all

patients diagnosed with EOC, approximately 15% of patients will have germline BRCA1 or BRCA2 mutation present. The cumulative ovarian cancer risk to age of 80 is 36–53% in BRCA1 mutation and 11–25% in BRCA2 mutation. Cumulative ovarian risk to age of 80 in population without BRCA mutation is 1–2%.<sup>2,3</sup>

Due to the lack of effective screening strategies and the unspecific onset of symptoms, EOC is detected in 75% of cases at an advanced stage.<sup>4</sup> The initial symptoms are persistent or frequent, non-specific and mainly include abdominal distension or flatulence, pelvic or abdominal pain, bloating, loss of appetite, unexplained weight loss, fatigue or changes in bowel habits. About 36% of women with unspecific clinical symptoms make several visits to their general practitioner before being diagnosed with ovarian cancer.<sup>5</sup>

CA-125, also known as mucin 16 or MUC16, is a large membrane glycoprotein belonging to the wide mucin family, encoded by the homonymous MUC16 gene.<sup>6</sup> It can be very useful and highly specific as a prognostic maker, but not as a diagnostic tool due to lack of sensitivity.<sup>7</sup> CA-125 level is increased in more than 85% of women with an advanced stage EOC but is only increased in 50% of stage I cancers.<sup>7,8</sup> CA-125 level may also be increased in almost 6% of women without ovarian cancer due to adenomyosis, endometriosis, retrograde menstrual bleeding or other non-malignant diseases.<sup>7</sup>

For decades the standard treatment for EOC has been primary debulking surgery (PDS) followed by platinum- and taxane-based adjuvant chemotherapy (ACT). A more contemporary approach is neoadjuvant chemotherapy (NACT) followed by interval debulking surgery (IDS), but, opinions on the optimal treatment are still divided.<sup>9</sup> Despite different treatment approaches, the prognosis is mainly influenced by the residual disease after surgical cytoreduction. Patients benefit most from complete gross resection or optimal cytoreduction (residual lesions with a diameter of 1 cm or less). Suboptimal cytoreduction with residual disease of more than 1 cm is associated with poorer survival.<sup>10</sup> Many studies have attempted to assess different scoring systems which include preoperative serum CA-125 to determine the patient selection where optimal primary cytoreduction might be achievable but results and recommendations are inconsistent.<sup>11-16</sup>

The aim of our study was to analyse experience of single institution as Cancer comprehensive centre with preoperative usefulness of CA-125.

## Patients and methods

### Study design

A retrospective observational study was conducted at the Institute of Oncology Ljubljana, from January

2005 to December 2014. The data collection and its analysis were approved by Institutional Ethical committee.

### Patients

Two hundred and fifty-three women with advanced stage ovarian cancer were enrolled in the study. All women had histologically confirmed FIGO stage IIIC and IV EOC. Women were divided into two groups based on their initial treatment. The first group consisted of 215 women receiving NACT (based on carboplatin and paclitaxel), followed by IDS. The second group consisted of 38 women treated with PDS, followed by ACT (3 courses of the same regimen as NACT). The selection of women for the specific treatment was based on the ability to perform a complete gross resection or to achieve a residual disease of 1 cm or less. This decision was based on preoperative imaging studies (abdominal and thoracic CT) and/or diagnostic laparoscopy in 173 patients. Levels of preoperative CA-125 did not influence the decision about primary treatment modality. When option to achieve complete gross or at least optimal cytoreduction was considered low, NACT was selected. Patients were assessed as inoperable (low probability of < 1cm residual disease) if the tumour penetrated the pelvic wall, if carcinosis of the intestine, intestinal serosa or mesentery was present or if imaging studies showed tumour spread to distant organs. The time from NACT to IDS was 4–6 weeks and the interval from PDS to ACT was 3–4 weeks for all included women.

Progression-free survival (PFS) was defined as the time from the date of completion of treatment to the first radiological evidence of progression. An increase of CA-125 serum level without clinical signs of recurrence was not counted as progression, but triggered further radiological examinations. Overall survival (OS) was defined as the interval between the date of diagnosis and the date of death. The surviving patients were censored at the time of the last follow-up.

The extent of residual disease was based on the diameter of the largest single lesion. At complete gross resection there were no macroscopic lesions, at optimal resection the lesions had a diameter of 1 cm or less and at suboptimal resection the lesions were larger than 1 cm. The study excluded women with a history of other malignant tumours or chemotherapy, FIGO stage I or II ovarian cancer, or non-epithelial histology of ovarian cancer.

## Data collection

Patients enrolled in the study were selected using the prospective clinical database of the Institute of Oncology Ljubljana. Clinical variables were collected from electronic hospital records, paper documentation and pathology reports to determine eligibility for the study, general characteristics of the patients, FIGO stage, tumour classification and histological type. Vital status was determined by analysing electronic medical records. Data were collected on the patient's age, body mass index (BMI), menopause status, preoperative CA-125, duration of follow-up and residual disease after surgery.

## Statistical analysis

For demographic data, descriptive statistics were used. The median survival of the two groups was calculated based on the non-normal distribution. The differences in patient characteristics were compared using the Chi-square test and ANOVA. ROC analysis was performed to determine cutoff values of serum CA-125 levels. PFS and OS were estimated using the Kaplan-Meier method, and the rates in the two groups were compared using the log-rank test.  $P < 0.05$  indicated that the difference between the groups was statistically significant. The statistical software SPSS for Windows version 26 was used for statistical analysis.

## Results

A retrospective analysis of 253 patients with advanced stage EOC treated at the Institute of Oncology Ljubljana between January 2005 and December 2014 was performed. There were 215 (84.9%) women enrolled in the NACT group and 38 (15.1%) women in the PDS group. The characteristics of the patients are shown in Table 1. Patients in the PDS group were statistically significantly younger (53.7 vs. 62.2 years), with lower disease stage (FIGO IIIC 89.5% vs. 66.6%) and had lower CA-125 levels (499 IU/ml vs. 972 IU/ml).

In patients with NACT, 57.6% (124/215) had complete gross resection, 14.0% (30/215) had optimal resection and 28.4% (61/215) had suboptimal resection ( $p = 0.002$ ; Table 1).

In women with PDS, 23.7% (9/38) had complete gross resection, 18.4% (7/38) had optimal resection and 57.9% (22/38) had suboptimal resection. Patients with complete gross resection had low-

TABLE 1. Clinical characteristics (N = 253)

Characteristic	PDS (N = 38)	NACT (N = 215)	P value
<b>Age-years</b>			
Median	53.7	62.2	< 0.001
Range	29–84	39–85	
<b>BMI-kg/m<sup>2</sup></b>			
Median	24.5	23.8	0.210
Range	17.4–45.2	18.2–32.1	
<b>Parity-number</b>			
Median	2	2	0.080
Range	0–5	0–4	
<b>Menopause-years</b>			
Median	50	51.5	0.340
Range	37–60	45–58	
<b>ASA score</b>			
1	7 (18.4)	23 (10.7)	0.780
2	22 (57.9)	141 (65.6)	
3	9 (23.7)	49 (22.8)	
4	0 (0)	2 (0.9)	
<b>WHO performance status</b>			
0	26 (68.4)	96 (44.7)	0.130
1	8 (21.0)	85 (40.0)	
2	4 (10.6)	26 (12.1)	
3	0 (0)	5 (2.3)	
4	0 (0)	3 (1.4)	
<b>FIGO stage</b>			
IIIC	34 (89.5)	143 (66.6)	0.010
IV	4 (10.5)	72 (33.4)	
<b>Histologic type</b>			
Serous	32 (84.2)	202 (94.0)	0.100
Endometrioid	6 (15.8)	8 (3.7)	
Mucinous	0 (0)	3 (1.4)	
Clear-cell	0 (0)	2 (0.9)	
<b>Preoperative CA-125- IU/ml</b>			
Median	499	972	0.058
Range	59–5739	10–31481	
<b>Surgical outcome</b>			
Complete gross resection	9 (23.7)	124 (57.6)	0.002
Optimal visible residual ( $\leq 1$ cm)	7 (18.4)	30 (14.0)	
Suboptimal ( $> 1$ cm)	22 (57.9)	61 (28.4)	
<b>Hospitalisation time-days</b>			
Median	10	9	0.555
Range	7–28	5–59	

ASA = American Society of Anesthesiologist; BMI = body mass index; FIGO = International Federation of Gynecology and Obstetrics; NACT = neoadjuvant chemotherapy; PDS = primary debulking surgery; WHO = World Health Organization

**TABLE 2.** Median and range CA-125 levels in different surgical outcomes in primary debulking surgery (PDS) and = neoadjuvant chemotherapy (NACT) group

Surgical outcomes	PDS (N = 38)	NACT (N = 215)	P value
<b>CA-125 at diagnosis IU/ml</b>			
Complete gross resection	359 59–5739	943 10–12803	0.006
Optimal resection	512 85–11117	1006 48–24824	
Suboptimal resection	1522 200–3569	1063 28–31481	
<b>CA-125 post NACT IU/ml</b>			
Complete gross resection		25 5–2074	0.020
Optimal resection		36 15–2180	
Suboptimal resection		68 9–2657	

CA-125 = cancer antigen 125

est CA-125 level at the time of diagnosis, 359 IU/ml respectively. Highest CA-125 level was found in the group with suboptimal resection, 1522 IU/ml, respectively.

CA-125 level in NACT group with complete gross resection at the time of diagnosis was 943 IU/mL and after NACT 25 IU/ml (97.3% decline). CA-125 level in NACT group with optimal resection at the time of diagnosis was 1006 IU/ml and after NACT 36 IU/ml (96.4% decline). Serum CA-125 level in NACT group with suboptimal resection at the time of diagnosis was 1063 IU/ml and after NACT 68 IU/ml (93.6% decline) (Table 2).

Cut off values of serum CA-125 levels and sensitivity to obtain complete gross or optimal cytoreduction are shown in Table 3. If CA-125 preoperative serum level is 250 IU/ml, there is 74 % chance to obtain at least optimal cyoreduction (Table 3).

PFS in the NACT group was 8 months (95% CI: 6.4–9.5) and 18 months (95% CI: 12.5–23.4) in the PDS group (P = 0.008).

The median OS in the NACT group was 25 months (95% CI: 20.6–29.5) and 46 months (95% CI: 32.9–62.1) in the PDS group (p = 0.009).

## Discussion

PDS followed by platinum- and taxane-based ACT was the standard treatment for patients with advanced stage EOC until 2016, when the American Society of Clinical Oncology (ASCO) and the Society of Gynecologic Oncology (SGO) developed new clinical practice guidelines.<sup>17</sup>

**TABLE 3.** Statistical cut off values of serum CA-125 level and probability to obtain complete gross or optimal cytoreduction

CA-125 level (IU/ml)	Sensitivity (%)	Number and percentage of patients
50	96.5	9 3.5 %
100	86.5	33 13.0 %
250	74.0	66 26.1 %
500	58.0	98 38.7 %
750	50.0	128 50.6 %
1000	42.0	150 59.3 %

CA-125 = cancer antigen 125

According to these guidelines in patients with high likelihood of achieving cytoreduction with residual disease < 1cm (ideally no visible disease) with acceptable morbidity, PDS is recommended over NACT. For women with high perioperative risk or a low likelihood of achieving a cytoreduction with residual disease < 1cm (ideally no visible disease) NACT is the treatment of choice. For women who are fit for PDS but cytoreduction with residual disease < 1cm (ideally no visible disease) is unlikely, NACT is also the treatment of choice. IDS should be performed after three to six cycles of NACT for women who respond to chemotherapy or with stable disease.<sup>9,17</sup> Patients with disease progression during NACT have a poor prognosis. Options include alternative chemotherapy regimens, inclusion in clinical trials and/or discontinuation of active cancer therapy and initiation of palliative supportive care. The role of surgery in palliative care is limited.<sup>18,19</sup>

There were studies published before year 2016 which showed non-inferiority of NACT compared to PDS.<sup>20–23</sup> Therefore also at our institute patients were treated with NACT where low chances to achieve at least optimal PDS were expected.

We studied the use of preoperative serum CA-125 levels to predict the likelihood of achieving at least optimal PDS or IDS in patients with advanced stage EOC.

Many studies have attempted to assess the ability of preoperative serum CA-125 level and various scoring systems to determine the patient selection where optimal primary cytoreduction can be achieved.

As expected, our results confirmed that the higher the CA-125 level is, the lower is probability to achieve optimal cytoreduction. At the preoperative CA-125 cut off value of 500 IU/ml the probability of achieving complete gross or at least

optimal cytoreduction in patients with advanced stage EOC was 58%. The probability increased to 74% at the cut off value of 250 IU/ml. These results add further data on usefulness of CA-125 levels as predictive factor for type of resection and are consistent with results published by other authors.<sup>12,13</sup>

Vorgias *et al.*<sup>12</sup> and Kang *et al.*<sup>13</sup> showed that CA-125 level above 500 IU/ml correlates with a more complex and radical surgical procedure and a worse outcome. Cut off value of 500 IU/ml had sensitivity ranging from 49% to 78% and specificity ranging from 59% to 77%. They reported that CA-125 levels above 500 IU/ml were strongly correlated with a suboptimal cytoreduction and poorer overall survival in patients with advanced EOC.

Furthermore, Arab *et al.*<sup>11</sup> established a model for predicting optimal surgical outcome, in which a CA-125 value of 420 IU/ml or less, the absence of massive ascites and liver metastases were shown to be significant factors in achieving optimal cytoreduction.

However, Chi *et al.*<sup>14</sup> reported that preoperative CA-125 value of more than 500 IU/ml had no predictive usefulness on the surgical outcome after an extensive upper abdominal surgery. A preoperative value of CA-125 above 500 IU/ml was associated with a probability of only 22% for optimal cytoreduction, but when extensive upper abdominal surgery was performed, the rate of optimal cytoreduction increased to 75% and the preoperative CA-125 value was no longer an independent predictor of surgical outcome.<sup>14</sup>

If optimal PDS is not achievable or patients are not suitable for extensive surgery, NACT and IDS are indicated. These patients usually have higher preoperative CA-125 levels and a higher disease burden than patients treated with a PDS. This was also the case in our patients where patients with NACT and IDS had higher disease stage (FIGO IV 33.4% *vs.* 10.5%) and higher preoperative CA-125 levels (972 IU/ml *vs.* 499 IU/ml).

Rodriguez *et al.*<sup>15</sup> reported that a preoperative CA-125 level of less than 100 IU/ml may be a suitable predictor of complete gross resection rather than optimal cytoreduction. According to our results preoperative CA-125 levels of less than 100 IU/ml can be expected in only 13% of patients. At an arbitrary cut off value of 250 IU/ml the probability to obtain complete gross or optimal cytoreduction is 75% and roughly one fourth (26.1%) of all patients with EOC belong to this group. If we increase the cut off value to 500 IU/ml about one third (38.7%) of patients will be included and the probability to obtain complete gross or optimal cytoreduction will be 58%.

After NACT the role of CA-125 to predict complete gross or optimal cytoreduction is even more complex. Pelissier *et al.*<sup>16</sup> found out that a preoperative CA-125 level of less than 75 IU/ml after the third cycle of NACT predicted a complete IDS. CA-125 of less than 200 IU/ml can be an independent predictor of complete gross IDS and also a predictor of chemosensitivity according to Zeng *et al.*<sup>24</sup>. However, after NACT the percentage of reduction is probably even more important than the absolute decrease in the CA-125 value. A reduction of at least 90% indicates a better response of the tumour to treatment and therefore correlates with a better surgical outcome and better overall survival.<sup>25</sup>

Our study showed that patients with CA-125 serum reduction of more than 96.4% achieved higher complete gross and optimal IDS rate in comparison to patients with lower reduction of serum CA-125 level. It is well established that CA-125 serum level represents the tumour burden in most patients with advanced stage EOC. Sharp CA-125 serum level reduction during NACT might reflect the chemosensitivity of the tumour. This might be a predictive factor for surgical outcome. However, we cannot predict in advance the reduction of CA-125 level and therefore cannot predict the benefit of NACT.

A study published by Gupta *et al.*<sup>26</sup> showed that a 95% reduction of CA-125 levels and an absolute preoperative CA-125 level of 100 IU/ml or less predicted complete gross resection after NACT.

Kessous *et al.*<sup>27</sup> think that the regression coefficient is impractical for clinical daily routine and found out that an early reduction of CA-125 levels by the third cycle of NACT can best predict surgical outcome and patients overall survival.

Our study showed that NACT group had shorter OS and PSF compare to PDS group. The median PFS and OS for patients in the NACT group was 8 and 25 months, compared to 25 and 49 months in the PDS group, respectively. This is consistent with data published by Mueller *et al.*<sup>28</sup> but in contrast to EORTC/NCIC and CHORUS study.<sup>20,29</sup> The explanation for our results is that women treated with NACT had a higher disease burden, a higher FIGO stage, a higher CA-125 level at time of diagnosis and were older in comparison to PDS group.

Patients included in before mentioned three studies were of comparable age, FIGO stage and had comparable preoperative CA-125 levels.

According to Maner and Machida NACT can be associated with lower peri- and postoperative morbidity and mortality and shorter hospital stay but PDS may offer a better chance of survival in

selected patients.<sup>30,31</sup> Median hospital stay in our patients treated with IDS (9 days) was not different from patients treated with PDS (10 days,  $p = 0.555$ ) which is consistent with the study published by du Bois.<sup>32</sup> However, patients treated with PDS had better survival as already mentioned.

There are limitations to our study among which are its retrospective nature and that there were no generally accepted selection criteria at that time for which patients are candidates for PDS or NACT.

## Conclusions

Preoperative CA-125 cut off value of 500 IU/ml is a promising threshold to predict a successful PDS. After NACT a decline of CA-125 of more than 96.4% predicts at least optimal cytoreduction of IDS.

## References

- Momenimovahed Z, Tiznobaik A, Taheri S, Salehiniya H. Ovarian cancer in the world: epidemiology and risk factors. *Int J Womens Health* 2019; **11**: 287-99. doi: 10.2147/IJWH.S197604
- Kuchenbaecker KB, Hopper JL, Barnes DR, Phillips K-A, Mooij TM, Roos-Bloom MJ, et al. Risks of breast, ovarian, and contralateral breast cancer for BRCA1 and BRCA2 mutation carriers. *JAMA* 2017; **317**: 2402-16. doi: 10.1001/jama.2017.7112
- Neff RT, Senter L, Salani R. BRCA mutation in ovarian cancer: testing, implications and treatment considerations. *Ther Adv Med Oncol* 2017; **9**: 519-31. doi: 10.1200/JCO.2003.01.068
- Bast RC Jr. Status of tumor markers in ovarian cancer screening. *J Clin Oncol* 2003; **21**(10 Suppl): 200s-5s. doi: 10.1200/JCO.2003.01.068
- Yawn BP, Barrette BA, Wollan PC. Ovarian cancer: the neglected diagnosis. *Mayo Clin Proc* 2004; **79**: 1277-82. doi: 10.4065/79.10.1277
- Bottoni P, Scatena R. The role of CA 125 as tumor marker: biochemical and clinical aspects. *Adv Exp Med Biol* 2015; **867**: 229-44. doi: 10.1007/978-94-017-7215-0\_14
- Yang WL, Lu Z, Bast RC. The role of biomarkers in the management of epithelial ovarian cancer. *Expert Rev Mol Diagn* 2017; **17**: 577-91. doi: 10.1080/14737159.2017
- Sundar S, Neal RD, Kehoe S. Diagnosis of ovarian cancer. *BMJ* 2015; **351**: h4443. doi: https://doi.org/10.1136/bmj.h4443
- Elies A, Rivière S, Pouget N, Becette V, Dubot C, Donnadiou A, et al. The role of neoadjuvant chemotherapy in ovarian cancer. *Expert Rev Anticancer Ther* 2018; **18**: 555-66. doi: 10.1080/14737140.2018.1458614
- du Bois A, Reuss A, Pujade-Lauraine E, Harter P, Ray-Coquard I, Pfisterer J. Role of surgical outcome as prognostic factor in advanced epithelial ovarian cancer: a combined exploratory analysis of 3 prospectively randomized phase 3 multicenter trials: by the Arbeitsgemeinschaft Gynaekologische Onkologie Studiengruppe Ovarialkarzinom (AGO-OVAR) and the Groupe d'Investigateurs Nationaux Pour les Etudes des Cancers de l'Ovaire (GINECO). *Cancer* 2009; **115**: 1234-44. doi: 10.1002/cncr.24149
- Arab M, Jamdar F, Sadat Hosseini M, Ghodssi-Ghasemabadi R, Farzaneh F, Ashrafjanjoe T. Model for prediction of optimal debulking of epithelial ovarian cancer. *Asian Pac J Cancer Prev* 2018; **19**: 1319-24. doi: 10.22034/APJCP.2018.19.5.1319
- Vorgias G, Iavazzo C, Savvopoulos P, Myriokefalitaki E, Katsoulis M, Kalinoglou N, et al. Can the preoperative Ca-125 level predict optimal cytoreduction in patients with advanced ovarian carcinoma? A single institution cohort study. *Gynecol Oncol* 2009; **112**: 11-5. doi: 10.1016/j.ygyno.2008.09.020
- Kang S, Kim TJ, Nam BH, Seo SS, Kim BG, Bae DS, et al. Preoperative serum CA-125 levels and risk of suboptimal cytoreduction in ovarian cancer: a meta-analysis. *J Surg Oncol* 2010; **101**: 13-7. doi: 10.1002/jso.21398
- Chi DS, Zivanovic O, Palayekar MJ, Eisenhauer EL, Abu-Rustum NR, Sonoda Y, et al. A contemporary analysis of the ability of preoperative serum CA-125 to predict primary cytoreductive outcome in patients with advanced ovarian, tubal and peritoneal carcinoma. *Gynecol Oncol* 2009; **112**: 6-10. doi: 10.1016/j.ygyno.2008.10.010
- Rodriguez N, Rauh-Hain JA, Shoni M, Berkowitz RS, Muto MG, Feltmate C, et al. Changes in serum CA-125 can predict optimal cytoreduction to no gross residual disease in patients with advanced stage ovarian cancer treated with neoadjuvant chemotherapy. *Gynecol Oncol* 2012; **125**: 362-6. doi: 10.1016/j.ygyno.2012.02.006
- Pelissier A, Bonneau C, Chéreau E, de La Motte Rouge T, Fourchotte V, Daraï E, et al. CA125 kinetic parameters predict optimal cytoreduction in patients with advanced epithelial ovarian cancer treated with neoadjuvant chemotherapy. *Gynecol Oncol* 2014; **135**: 542-6. doi: 10.1016/j.ygyno.2014.09.005
- Wright AA, Bohlke K, Armstrong DK, Bookman MA, Cliby WA, Coleman RL, et al. Neoadjuvant chemotherapy for newly diagnosed, advanced ovarian cancer: Society of Gynecologic Oncology and American Society of Clinical Oncology clinical practice guideline. *J Clin Oncol* 2016; **34**: 3460-73. doi: 10.1200/JCO.2016.68.6907
- Orr B, Edwards RP. Diagnosis and treatment of ovarian cancer. *Hematol Oncol Clin North Am* 2018; **32**: 943-64. doi: 10.1016/j.hoc.2018.07.010
- Eisenhauer EA. Real-world evidence in the treatment of ovarian cancer. *Ann Oncol* 2017; **28**(Suppl 8): viii61-5. doi: 10.1093/annonc/mdx443
- Vergote I, Tropé CG, Amant F, Kristensen GB, Ehlen T, Johnson N, et al. Neoadjuvant chemotherapy or primary surgery in stage IIIC or IV ovarian cancer. *N Engl J Med* 2010; **363**: 943-53. doi: 10.1056/NEJMoa0908806
- Schwartz PE. Neoadjuvant chemotherapy for the management of ovarian cancer. *Best Pract Res Clin Obstet Gynaecol* 2002; **16**: 585-96. doi: 10.1053/beog.2002.0304
- Morice P, Dubernard G, Rey A, Atallah D, Pautier P, Pomel C, et al. Results of interval debulking surgery compared with primary debulking surgery in advanced stage ovarian cancer. *J Am Coll Surg* 2003; **197**: 955-63. doi: 10.1016/j.jamcollsurg.2003.06.004
- Pecorelli S, Odicino F, Favalli G. Interval debulking surgery in advanced epithelial ovarian cancer. *Best Pract Res Clin Obstet Gynaecol* 2002; **16**: 573-83. doi: 10.1053/beog.2002.0302
- Zeng J, Yin J, Song X, Jin Y, Li Y, Pan L. Reduction of CA125 levels during neoadjuvant chemotherapy can predict cytoreduction to no visible residual disease in patients with advanced epithelial ovarian cancer, primary carcinoma of fallopian tube and peritoneal carcinoma. *J Cancer* 2016; **7**: 2327-32. doi: 10.7150/jca.16761
- Mahdi H, Maurer KA, Nutter B, Rose PG. The impact of percent reduction in CA-125 levels on prediction of the extent of interval cytoreduction and outcome in patients with advanced-stage cancer of Müllerian origin treated with neoadjuvant chemotherapy. *Int J Gynecol Cancer* 2015; **25**: 823-9. doi: 10.1097/IGC.0000000000000434
- Gupta M, Patel SM, Arora R, Tiwari R, Dave P, Desai A, et al. Does preoperative CA-125 cutoff value and percent reduction in CA-125 levels correlate with surgical and survival outcome after neoadjuvant chemotherapy in patients with advanced-stage ovarian cancer? – Our experience from a tertiary cancer institute. *South Asian J Cancer* 2020; **9**: 30. doi: 10.4103/sajc.sajc\_53\_17
- Kessous R, Wissing MD, Piedimonte S, Abitbol J, Kogan L, Laskov I, et al. CA-125 reduction during neoadjuvant chemotherapy is associated with success of cytoreductive surgery and outcome of patients with advanced high-grade ovarian cancer. *Acta Obstet Gynecol Scand* 2020; **99**: 933-40. doi: 10.1111/aogs.13814
- Mueller JJ, Zhou QC, Iasonos A, O'Ceirbhail RE, Alvi FA, El Haraki A, et al. Neoadjuvant chemotherapy and primary debulking surgery utilization for advanced-stage ovarian cancer at a comprehensive cancer center. *Gynecol Oncol* 2016; **140**: 436-42. doi: 10.1016/j.ygyno.2016.01.008
- Kehoe S, Hook J, Nankivell M, Jayson GC, Kitchener H, Lopes T, et al. Primary chemotherapy versus primary surgery for newly diagnosed advanced ovarian cancer (CHORUS): an open-label, randomised, controlled, non-inferiority trial. *Lancet* 2015; **386**: 249-57. doi: 10.1016/S0140-6736(14)62223-6
- Mahner S, Trillsch F, Chi D, Harter P, Pfisterer J, Hilpert F, et al. Neoadjuvant chemotherapy in ovarian cancer revisited. *Ann Oncol* 2016; **27**(Suppl 1): i30-2. doi: 10.1093/annonc/mdw092
- Machida H, Tokunaga H, Matsuo K, Matsumura N, Kobayashi Y, Tabata T, et al. Survival outcome and perioperative complication related to neoadjuvant chemotherapy with carboplatin and paclitaxel for advanced ovarian cancer: a systematic review and meta-analysis. *Eur J Surg Oncol* 2020; **46**: 868-75. doi: 10.1016/j.ejso.2019.11.520
- du Bois A, Baert T, Vergote I. Role of neoadjuvant chemotherapy in advanced epithelial ovarian cancer. *J Clin Oncol* 2019; **37**: 2398-405. doi: 10.1200/JCO.19.00022

research article

# Predictive impact of the inflammation-based indices in uveal melanoma liver metastases treated with transarterial hepatic chemoperfusion

Johannes M. Ludwig<sup>1</sup>, Johannes Haubold<sup>1</sup>, Sebastian Bauer<sup>2</sup>, Heike Richly<sup>2</sup>, Jens T. Siveke<sup>3,4</sup>, Julia Wimmer<sup>1</sup>, Lale Umutlu<sup>1</sup>, Benedikt M. Schaarschmidt<sup>1</sup>, Jens M. Theysohn<sup>1</sup>

<sup>1</sup> Department of Diagnostic and Interventional Radiology and Neuroradiology, University Hospital Essen, University of Duisburg-Essen, Essen, Germany

<sup>2</sup> Department of Medical Oncology, Sarcoma Center, West German Cancer Center, University of Duisburg-Essen, Essen, Germany

<sup>3</sup> Institute for Developmental Cancer Therapeutics, West German Cancer Center, University Hospital Essen, Essen, Germany

<sup>4</sup> Division of Solid Tumor Translational Oncology, German Cancer Consortium (DKTK, partner site Essen) and German Cancer Research Center, DKFZ, Heidelberg, Germany

Radiol Oncol 2021; 55(3): 347-353.

Received 17 January 2021

Accepted 12 April 2021

Correspondence to: Prof. Dr. med. Jens M. Theysohn, Department of Diagnostic and Interventional Radiology and Neuroradiology, University Hospital Essen, University of Duisburg-Essen, Hufelandstr. 55, 45147 Essen, Germany. E-mail: jens.theysohn@uk-essen.de

Disclosure: No potential conflicts of interest were disclosed.

This is an open access article under the CC BY-NC-ND license (<http://creativecommons.org/licenses/by-nc-nd/4.0/>).

**Background.** The aim of the study was to evaluate pretreatment inflammatory markers as prognostic factors in patients with unresectable uveal melanoma liver metastases treated with transarterial hepatic chemoperfusion.

**Patients and methods.** 54 patients (44% male, median age: 61 years) were retrospectively assessed. A median of 3 (range: 1–11) treatment sessions were performed with melphalan (92%) or fotemustin (8%). Inflammatory indices were calculated as follows: neutrophils/nl to lymphocytes/nl ratio (NLR), systemic immune-inflammation index ( $[\text{platelets/nl} \times \text{neutrophils/nl}] / [\text{lymphocytes/nl}]$ ; SII), and platelets/nl to lymphocytes/nl ratio (PLR). The cut-off for dichotomization purposes was set at the median (inflammatory indices, hepatic tumor burden) or the upper level of normal. Kaplan Meier analysis was performed for median overall survival (OS) in months, and Cox proportional hazard model for uni- (UVA) and multivariate (MVA) hazard ratio (HR, 95%CI) analyses were performed.

**Results.** Median OS of the study cohort was 7.7 (6.3–10.9) months. In UVA OS was prolonged for low C reactive protein (CRP) (13.5 vs. 5.2;  $p = 0.0005$ ), low SII (10.8 vs. 5.6;  $p = 0.0005$ ), low NLR (11.1 vs. 6.3;  $p = 0.0045$ ), low aspartate aminotransferase (AST) (11.5 vs. 5.6;  $p = 0.015$ ), alanine aminotransferases (ALT) (11.5 vs. 5.6;  $p = 0.01$ ), and tumor burden  $\leq 50\%$  (8.2 vs. 4.8;  $p = 0.007$ ). MVA confirmed low CRP (HR: 0.29, 0.11–0.7;  $p = 0.005$ ), low SII (HR: 0.19, 0.11–0.7;  $p = 0.008$ ), and low ALT (HR: 0.13, 0.02–0.63;  $p = 0.011$ ) as independent predictors for prolonged OS. Patients with  $\leq 1, 2, 3$  elevated significant MVA-factors survived a median of 14.9, 7.7, and 3.9 months, respectively ( $p = 0.0001$ ).

**Conclusions.** Pretreatment inflammatory markers (CRP, SII) and AST were independent prognostic survival markers in patients with uveal melanoma liver metastases treated with transarterial hepatic chemoperfusion. A combination of factors may help to identify patients potentially benefitting from treatment.

Key words: uveal melanoma; liver metastases; transarterial hepatic chemoperfusion; melphalan; inflammatory markers

## Introduction

Uveal melanoma is the most common primary ocular malignancy in adults accounting for around 5% of all melanomas.<sup>1,2</sup> Although local tumors are usually treated aggressively, about 50% of all patients will eventually develop metastases, with in 60.5% of cases involvement of the liver at the time of diagnosis of metastatic disease.<sup>3</sup> In patients with predominant and unresectable hepatic disease, we routinely perform transarterial hepatic chemoperfusion (THC) as a palliative treatment option demonstrating prolonged progression-free survival and fewer hematological severe adverse events compared to intravenous chemotherapy.<sup>4</sup>

Setting expectations for treatment benefit and life expectancy is crucial for informed clinical decision-making and may guide patients and their families to set expectations. To date, few pretreatment prognostic factors on treatment outcomes, including but not limited to tumor burden, lactate dehydrogenase (LDH), and gamma-glutamyl transferase (GGT) serum values have been reported.<sup>5,6</sup>

The role of inflammation has long been acknowledged as a hallmark during cancerogenesis and tumor progression in malignant disease.<sup>7,8</sup> In the context of tumor-associated inflammation, the systemic inflammatory response is linked with poorer outcomes and as of significant prognostic relevance in various cancer types.<sup>9,10</sup> This systemic inflammatory response is usually measured in the peripheral blood with numbers of differential blood cell counts (lymphocytes, neutrophils, platelets) as well as serum proteins (C-reactive protein, albumin). Here, the inflammation-based indices of differential cell counts, the neutrophil to lymphocyte ratio (NLR), the platelet to lymphocyte ratio (PLR), and the systemic immune-inflammation index (SII) have been proven as significant prognostic factors in several cancer types.<sup>11</sup>

The purpose of this study was to evaluate inflammatory markers routinely assessed before THC as pretreatment prognostic factors in patients with unresectable uveal melanoma liver metastases.

## Patients and methods

### Study population

This study is a retrospective single-center database analysis that has been approved by the local institutional review board with waived informed consent (IRB#: 20-9799-BO). All procedures performed in studies involving human participants were in ac-

cordance with the ethical standards of the institutional and/or national research committee and with the 1964 Helsinki declaration and its later amendments or comparable ethical standards. The decision to perform transarterial chemoperfusion was based on multidisciplinary tumor board meetings.

Fifty-four consecutive patients first treated in the years 2014 and 2015 were included in this study. Inclusion criteria were as follows: I) At least 18-years of age, II) imaging or biopsy-proven uveal melanoma liver metastases, and III) treatment of liver metastases with THC. Patient data were obtained from the medical record system, including disease history and laboratory testing results before treatment.

### Treatment

Transarterial hepatic chemoperfusion was performed by gaining access via the femoral artery by inserting a 5 Fr catheter sheath and placing a microcatheter into the hepatic arteries, either in the proper hepatic artery or consecutively in the left, right, and/or accessory hepatic arteries. Chemoperfusion of the liver was performed for 45–60 minutes. If the dose was infused into two lobes, a median of 30% for the left and 70% for the right lobe of the total dose were administered. All patients started with 40 mg of melphalan. In case of progression, either the melphalan dose was escalated (45 mg, 50 mg), or the chemotherapeutic agent was switched to fotemustin.

### Data collection

Laboratory blood test values were measured within thirty days before the first THC: Alanine aminotransferases (ALT; normal: < 35 U/L), aspartate aminotransferase (AST, normal: < 35 U/L), alkaline phosphatase (AP, normal: 20–100 U/L), gamma-glutamyl transpeptidase (GGT, normal <35 U/L), lactate dehydrogenase (LDH, normal 120–247 U/L). Furthermore, absolute neutrophils (ANC, normal: 1.7–6.2/nl), lymphocytes (ALC, normal: 1.0–3.4/nl), and platelets (APC, normal: 180–380/nl) counts were obtained for calculating inflammatory indices. The neutrophil to lymphocyte ratio (NLR) was defined as the ratio of ANC/ALC, the platelet to lymphocyte ratio (PLR) as the ratio of APC/ALC, and the SII as the platelet count  $\times$  ANC/ALC. For dichotomization purposes, the cut-off values were set at the upper level of normal (ULN) for laboratory values, at the median for inflammatory indices and tumor burden, or according to categorical

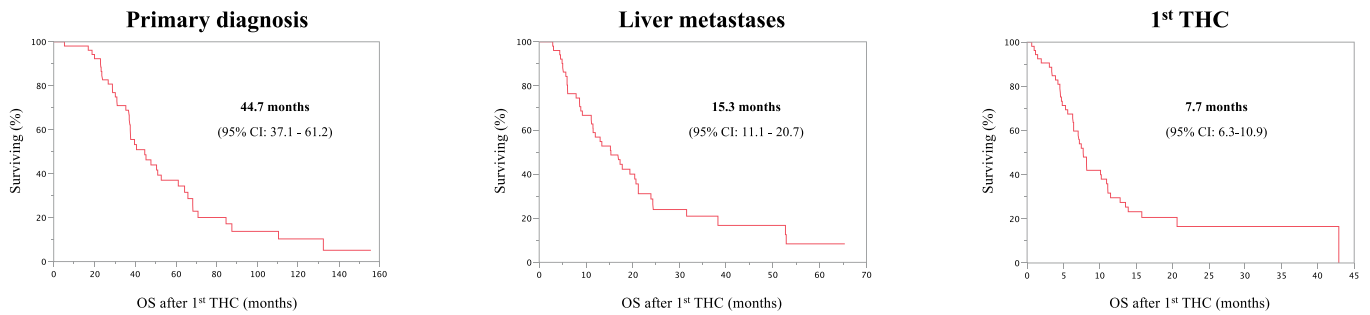


**FIGURE 1.** Overall survival of the entire study cohort. Estimated overall survival (OS) after diagnosis of primary, diagnosis of liver metastases, and after 1<sup>st</sup> transarterial chemoperfusion (THC).

status. Analysis of albumin and bilirubin have not been performed due to inconsistent and low numbers of reporting. The date of death was obtained regardless of etiology.

### Statistics

The Kaplan-Meier method (log-rank test) was applied for estimating the overall survival (OS) with 95% confidence intervals (95%CI). Uni- (UVA) & multivariate (MVA) analyses for determining the hazard ratios (HR), including the 95% CI were calculated utilizing the Cox proportional hazards model. Factors statistically significant in UVA were included in MVA. For correlation analysis, the Spearman analysis was performed. Contingency testing was calculated using Pearson's chi-squared test. Calculations were performed using JMP Pro 13.2.1 for Windows (SAS Institute Inc.). P-values < 0.05 were considered statistically significant.

## Results

### Patient baseline and treatment characteristics

The study consisted of fifty-four patients (44% male, 100% Caucasians, median age: 61 years; range: 26–81 years). Death was recorded in 42 patients, and 12 patients were lost to follow-up with a median follow-up of 15.8 months (95% CI: 2.3–24 months). The median time between primary diagnosis and occurrence of hepatic metastases was 24.4 months (range: 0–122 months). The first THC session was performed after a median of 4.6 months following diagnosis of liver metastases (range: 0.3–38.7 months) with a median of 3 (range: 1–11) THC sessions/patient. The median time between treatments was 1.6 months (range 0.9 – 6.2). In total, 198 THC sessions were performed with melphalan

**TABLE 1.** Overview of patient baseline characteristics

Characteristics	Number of patients (%) / median values
Total number of patients	54
Gender (male).	24 (44%)
Median age in years at 1 <sup>st</sup> THC (range)	61 (26–81)
<b>Prior systemic/liver-directed therapies</b>	
Prior systemic therapy	29 (53.7%)
Sorafenib	25 (46.3)
MEK and PKC inhibitors	3 (5.6%)
Ipilimumab	1 (1.9%)
Conventional chemotherapy	5 (9%)
Prior liver resection	4 (7.4%)
Prior ablation	1 (1.9%)
Further therapy after last transarterial chemoperfusion	18 (33.3%)
Limited extrahepatic metastases at the time of 1 <sup>st</sup> THC	20 (37%)
Median maximal tumor size in cm (range)	5.9 (1.3–19.8)
<b>Lobar tumor involvement</b>	
Bilobar	54 (96.4%)
Unilobar	2 (3.6%)
<b>Hepatic tumor burden</b>	
0–25%	23 (46%)
> 25–50%	12 (24%)
> 50–75%	9 (18%)
> 75%	6 (12%)
<b>ECOG</b>	
0	43 (80%)
1	6 (11%)
2	2 (4%)
Unknown	3 (6%)
<b>Karnofsky Index</b>	
100	4 (7%)
90	33 (61%)
80	7 (13%)
< 80	3 (6%)
Unknown	7 (13%)

MEK = mitogen-activated protein kinase enzymes MEK1 and/or MEK2; PKC = protein kinase C; THC = transarterial hepatic chemoperfusion

TABLE 2. Uni- and multivariate analysis of overall survival (OS)

Subgroups		Median OS in months (95% CI)	Univariate analysis		Multivariate analysis	
			HR (95% CI)	p-value	HR (95% CI)	p-value
NLR	≤ median (3.58)	11.1 (7.1–20.6)	0.39 (0.2–0.75)	<b>0.0045</b>	0.73 (0.25–2.2)	0.57
	> median (3.58)	6.3 (3.5–7.8)	1		1	
SII	≤ median (1076)	10.8 (7.2–20.6)	0.33 (0.17–0.65)	<b>0.0013</b>	0.19 (0.11–0.7)	<b>0.008</b>
	> median (1076)	5.6 (3.4–7.7)	1		1	
PLR	≤ median (203.8)	8.2 (5.6–15.8)	0.69 (0.37–1.27)	0.23	-	-
	> median (203.8)	7.5 (4.7–11.1)	1		-	
CRP	normal	13.5 (7.2–20.6)	0.3 (0.15–0.6)	<b>0.0005</b>	0.29 (0.11–0.7)	<b>0.005</b>
	> ULN	5.3 (3.9–7.8)	1		1	
Neutrophils	normal	8.2 (6.4–11.5)	0.6 (0.3–1.28)	0.18	-	-
	> ULN	6.3 (3.9–11.1)	1		-	
Thrombocytes	normal	8.2 (6.3–11.1)	0.8 (0.35–2.13)	0.62	-	-
	> ULN	7.5 (0.64–13.5)	1		-	
LDH	≤ ULN	12.8 (7.2–20.6)	0.54 (0.23–1.11)	0.1	-	-
	>ULN	7 (4.8–8.2)	1		-	
AST	≤ ULN	11.5 (7.2–20.6)	0.45 (0.22–0.85)	<b>0.015</b>	0.34 (0.07–1.44)	0.15
	> ULN	5.6 (4.5–8.2)	1		1	
ALT	≤ ULN	11.5 (7.5–15.8)	0.43 (0.2–0.8)	<b>0.01</b>	0.13 (0.02–0.63)	<b>0.011</b>
	> ULN	5.6 (4.2–7.8)	1		1	
GGT	≤ ULN	10.9 (7.2–15.8)	0.94 (0.32–2.2)	0.9	-	-
	> ULN	7.13 (5.3–10.2)	1		-	
AP	≤ ULN	10.94 (4.8–20.6)	0.54 (0.22–1.26)	0.15	-	-
	> ULN	6.3 (3.4–10.1)	1		-	
Hepatic tumor burden	≤ 50%	8.2 (7.12–11.5)	0.36 (0.18–0.74)	<b>0.007</b>	0.5 (0.17–1.6)	0.24
	> 50%	4.8 (1.2–7.8)	1		1	
Prior systemic treatment	Yes	8.2 (7.5–11.5)	0.78 (0.42–1.45)	0.43	-	-
	No	6.3 (4.5–11.1)	1		-	
Extrahepatic metastases	No	7.12 (4.6–10.1)	1.1 (0.59–2.17)	0.75	-	-
	Yes	10.2 (6.3–11.1)	1		-	

ALT = alanine aminotransferase; AP = alkaline phosphatase; AST = aspartate aminotransferase; CRP = C-reactive protein; GGT = gamma-glutamyl transpeptidase; HR = hazard ratio; LDH = lactate dehydrogenase; NLR = neutrophil to lymphocyte ratio; PLR = platelet to lymphocyte ratio; SII = systemic immune-inflammation index; ULN = upper level of normal

in 186 (median: 40 mg, range: 40–50 mg) and fote-mustin in 12 (median: 188 mg, range: 160–208 mg) cases. Eighteen patients (33%) received subsequent therapy after the last THC with systemic therapy in 13 Patients (8 patients received immune checkpoint inhibitors), radioembolization of liver metastases in 2 patients, and three patients received palliative external beam radiation of extrahepatic lesions for symptom control. Additional patient baseline characteristics are presented in Table 1.

### Survival analysis

Following the diagnosis of primary tumor median survival of all patients was estimated to be 44.7

months (95% CI: 37.1–61.2). After the diagnosis of liver metastases, the median overall survival of 15.3 months (95% CI: 11.1–20.7) was observed. Median OS following first THC therapy was 7.7 months (95% CI: 6.3–10.9) (Figure 1). 6 months, 1- and 2 years survival rates were 67.4% (95% CI: 53.7–78.8%), 29.5% (95% CI: 18.7–43.8), and 16.5% (95%CI: 8.0–31.7) respectively.

### Inflammatory prognostic factors

Median absolute cell counts were 5.13/nl for neutrophils (interquartile range [IQR]: 3.11–6.37), 1.36/nl for lymphocytes (IQR: 1.02–1.71), and 267/nl for platelets (IQR: 209–346). When dichotomized at the

median and upper level of normal, absolute cell counts were not significant regarding OS ( $p > 0.05$ ). Median values of inflammatory indices for the study cohort were 3.58 for NLR (IQR: 2.43–5.04), 1076 for SII (IQR: 539–1645), and 208.8 for PLR (IQR: 151.2–278). In Spearman's analysis, the correlation between inflammatory markers ranged from very good (SII & NLR, Spearman's  $\rho = 0.92$ ) to good (SII & PLR, Spearman's  $\rho = 0.72$ ; PLR & NLR, Spearman's  $\rho = 0.66$ ). Decreased NLR and SII, as well as non-elevated C reactive protein (CRP), were both associated with more prolonged median OS, whereas PLR was not (Table 2).

### Non-inflammatory prognostic factors

Patients with serum values of the liver enzymes ALT and AST within the normal range had prolonged overall survival in contrast to AP and GGT. Aside from laboratory markers, the tumor burden was identified as a significant factor with patients with  $\leq 50\%$  hepatic tumor burden doing significantly better. In contrast, pretreatment status (yes *vs.* no;  $p = 0.18$ ), presence of limited extrahepatic disease not considered life-limiting compared to liver metastases (yes *vs.* no;  $p = 0.3$ ), ECOG Status (ECOG 0 *vs.*  $\geq 1$ ;  $p = 0.99$ ), and Karnofsky Index (100–90% *vs.*  $< 90\%$ ;  $p = 0.44$ ) were not significant (Table 2). Of note, patients who received treatment after last chemoperfusion showed a significant longer survival (13.9 *vs.* 7.2 months,  $p = 0.01$ ; HR: 0.41; 95% CI: 0.21–0.83;  $p = 0.009$ ). There was no significant difference regarding the SII between the patients with and without further treatment in contingency testing ( $p = 0.11$ ).

### Results from the multivariate analysis

In multivariate analysis, the overall strongest predictor with the lowest hazard ratio for values below the median was found for ALT (HR: 0.13;  $p = 0.011$ ). SII proved as the strongest independent inflammatory predictor with a hazard ratio of 0.19 ( $p = 0.008$ ) followed by CRP (HR: 0.29,  $p = 0.005$ ). NLR and GOT were not identified as independent predictors for overall survival in this study population.

### Scoring with significant factors from the multivariate analysis

Yet, as none of the identified independent predictors for overall survival was clearly stronger than the others, an additive scoring was performed to

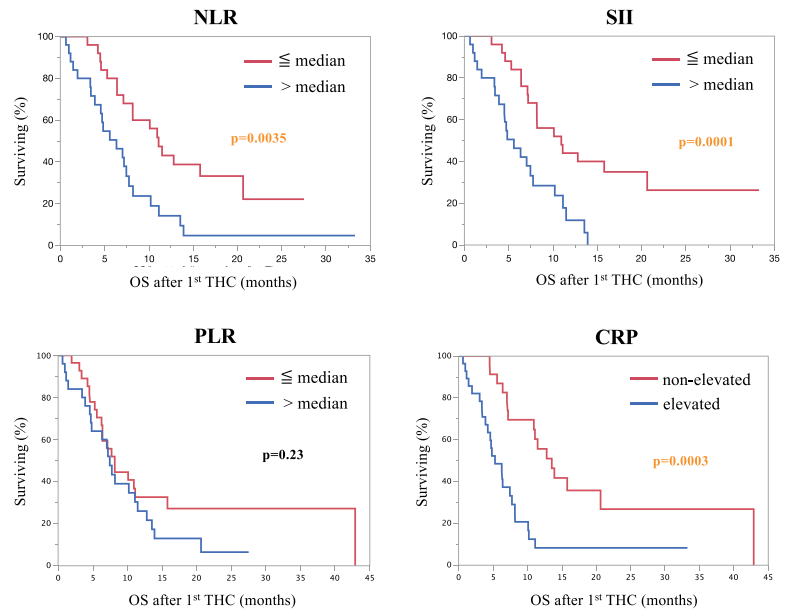


**FIGURE 2.** Pretreatment inflammation-based markers predict overall survival. Overall survival is stratified for low ( $\leq$  median) vs. high ( $>$  median) neutrophil to lymphocyte ratio (NLR), systemic immune-inflammation index (SII), platelet to lymphocyte ratio (PLR), and C-reactive protein (CRP).

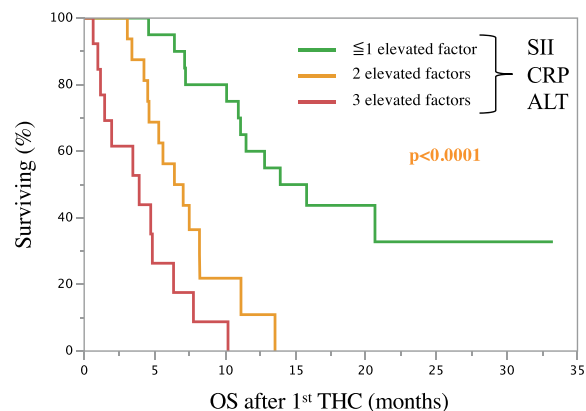


**FIGURE 3.** Scoring further improves overall survival estimation. Patients with zero to one elevated independent significant factors from multivariate analysis [C-reactive protein [CRP], systemic immune-inflammation index [SII], alanine aminotransferases [ALT]] had a significantly longer overall survival than patients with two or three elevated factors  $p < 0.0001$ .

test for an additional predictive value of significant parameters (Figure 3). Patients with an elevation of none to one elevated parameter (SII, CRP, or ALT) survived significantly longer with a median overall survival of 14.9 months (95% CI: 10.1–0.0) compared to patients with two (6.7 months, 95% CI: 4.5–8.2) and all three parameters elevated (3.9 months, 95% CI: 1.15–6.3);  $p < 0.0001$ . Performed

**TABLE 3.** Scoring with significant independent factors from multivariate analysis. The number of elevated CRP, SII, ALT in patients further helps to predict median overall survival

Group	Median OS in months (95% CI)	Hazard ratio (95% CI)	p-value
≤ 1 elevated factor	14.9 (10.1–0.0)	0.08 (0.3–0.2)	-
2 elevated factors	6.7 (4.5–8.2)	0.38 (0.17–0.86)	<b>0.0003</b>
3 elevated factors	3.9 (1.15–6.3)	1	<b>&lt; 0.0001*</b>

\* = The difference between the of 2 and 3 elevated factors groups was statistically significant in univariate analysis,  $p = 0.022$

univariate analysis demonstrated a statistical difference between each group (Table 3).

## Discussion

Uveal melanoma patients with liver metastases have a grim prognosis with a median overall survival of 4–6 months and a 1-year survival rate of 12–15% when left untreated.<sup>12</sup> Nowadays, thanks to treatment advances, the median overall survival after diagnosis of liver metastases is around 13.4 months, with a 2-year survival rate of 8%, which is similar to our study cohort.<sup>13–16</sup> As no treatment appears to be clearly superior over the others, identification of patients potentially benefitting from the treatment approach is vital for therapy allocation to provide the best care possible for each patient.<sup>17</sup>

Inflammatory cells in cancers have been thought to represent an antitumor response for many years. Nevertheless, there is a growing body of evidence that inflammation also plays a vital role in the initiation, malignization, and metastasis process of tumors driven by different immune cell subtypes.<sup>7,8,18</sup> In cancer patients, increased blood neutrophils and platelet counts have been associated with tumor progression and worse clinical outcomes in several solid tumors and can, therefore, be considered pro-tumorigenic.<sup>19,20</sup> Neutrophils achieve this by activating the endothelium and parenchymal cells through the secretion of soluble factors promoting adhesion to tumor cells at remote sites and thus promoting tumor spread.<sup>21–23</sup> Platelets, by gathering around and thus also shielding tumor cells, promote adhesion, metastatic spread, and prevent cancer cell death.<sup>20</sup>

In contrast, lymphocytes play a crucial role in immuno-monitoring cancer by hampering tumor cell proliferation and migration by causing cytotoxic cell death.<sup>24</sup> Thus, a high SII, comprising of elevated neutrophils and platelets and low counts

of lymphocytes, suggests greater pro- than anti-tumorigenic activity with more unsatisfactory outcomes for patients. Not only could SII be identified as an independent prognostic factor for overall survival in this study, but it was also found to be statistically relevant in a recent meta-analysis on solid tumors.<sup>25</sup>

Similar to SII, an increased NLR could also be identified as a prognostic factor for overall survival in metastatic uveal melanoma disease.<sup>26,27</sup> Although NLR significantly predicted overall survival in the univariate analysis, it could not be confirmed as an independent. Considering the significant overlap and high correlation between SII and NLR, it is not unsurprising that only one remained significant in multivariate analysis, potentially emphasizing the additive value of incorporating platelet counts on the overall survival. Additionally, neutrophils also seem to be a relevant factor, as PLR was not significant in this analysis.

CRP, an acute-phase reactant reflecting tissue injury and inflammation, has long been suggested as a prognostic marker in several cancer types.<sup>28,29</sup> In a systematic literature review, elevated CRP was associated with higher mortality in patients with solid tumors in 90% of studies underlining the general prognostic relevance.<sup>30</sup> In patients with metastatic uveal melanoma treated with immune checkpoint inhibitors showed that patients with high CRP had a significantly shorter survival in multivariate analysis (HR: 12.12;  $p = 0.001$ ).<sup>28</sup> Similarly, patients in this study succumbed significantly earlier when an elevated CRP before therapy was recorded.

Aside from immune markers, elevated Liver enzymes (AST and ALT) >ULN were identified as prognostic factors in univariate analysis for overall survival with ALT proving as independent as also by others in metastatic liver disease.<sup>31</sup> It may be speculated that ALT and/or AST rise due to “space-occupying effects” associated with higher tumor burden, which could be confirmed in this patient set.

When stratified according to the numbers of elevated independent factors (CRP, SII, ALT), an even more distinct risk-based survival estimation may be achieved than just considering single factors.

Several study limitations should be acknowledged as enrollment of patients was retrospectively and limited to one institution with a treatment protocol and patient cohort characteristics that may substantially differ from other institutions hampering comparability to different patient cohorts. Moreover, the sample size did not allow for a validation cohort to confirm the results.

## Conclusions

In Patients treated with uveal melanoma liver metastases treated with transarterial chemoperfusion, lower pretreatment values of CRP, SII and ALT were independent prognostic factors associated with prolonged overall survival suggesting a role of systemic inflammation in this setting. Moreover, as the benefit of low pretreatment CRP, SII & ALT act synergistically, an even more distinct outcome stratification can be achieved. As physicians aim to provide the best possible care, the results from this study may help to identify patients who may benefit most from treatment or how best to stratify patients based on clinical risk factors in future clinical trials. Nevertheless, future prospective studies are warranted to confirm the relevance of pretreatment inflammatory markers and ALT for patient selection.

## References

- Carvajal RD, Schwartz GK, Tezel T, Marr B, Francis JH, Nathan PD. Metastatic disease from uveal melanoma: treatment options and future prospects. *Br J Ophthalmol* 2017; **101**: 38-44. doi: 10.1136/bjophthalmol-2016-309034
- Singh AD, Turell ME, Topham AK. Uveal melanoma: trends in incidence, treatment, and survival. *Ophthalmology* 2011; **118**: 1881-5. doi: 10.1016/j.ophtha.2011.01.040
- Rietschel P, Panageas KS, Hanlon C, Patel A, Abramson DH, Chapman PB. Variates of survival in metastatic uveal melanoma. *J Clin Oncol* 2005; **23**: 8076-80. doi: 10.1200/JCO.2005.02.6534
- Leyvraz S, Piperno-Neumann S, Suciú S, Baurain JF, Zdzienicki M, Testori A, et al. Hepatic intra-arterial versus intravenous fotemustine in patients with liver metastases from uveal melanoma (EORTC 18021): a multicentric randomized trial. *Ann Oncol* 2014; **25**: 742-6. doi: 10.1093/annonc/mdt585
- Mariani P, Dureau S, Savignoni A, Rouic LL, Levy-Gabriel C, Piperno-Neumann S, et al. Development of a prognostic nomogram for liver metastasis of uveal melanoma patients selected by liver MRI. *Cancers* 2019; **11**. doi: 10.3390/cancers11060863
- Lorenzo D, Piulats JM, Ochoa M, Arias L, Gutierrez C, Catala J, et al. Clinical predictors of survival in metastatic uveal melanoma. *Jpn J Ophthalmol* 2019; **63**: 197-209. doi: 10.1007/s10384-019-00656-9
- Grivennikov SI, Greten FR, Karin M. Immunity, inflammation, and cancer. *Cell* 2010; **140**: 883-99. doi: 10.1016/j.cell.2010.01.025
- Hanahan D, Weinberg RA. Hallmarks of cancer: the next generation. *Cell* 2011; **144**: 646-74. doi: 10.1016/j.cell.2011.02.013
- Proctor MJ, Morrison DS, Talwar D, Balmer SM, O'Reilly DS, Foulis AK, et al. An inflammation-based prognostic score (mGPS) predicts cancer survival independent of tumour site: a Glasgow inflammation outcome study. *Br J Cancer* 2011; **104**: 726-34. doi: 10.1038/sj.bjc.6606087
- Jomrich G, Hollenstein M, John M, Baiert A, Paireder M, Kristo I, et al. The modified glasgow prognostic score is an independent prognostic indicator in neoadjuvantly treated adenocarcinoma of the esophagogastric junction. *Oncotarget* 2018; **9**: 6968-76. doi: 10.18632/oncotarget.24087
- Ohno Y. Role of systemic inflammatory response markers in urological malignancy. *Int J Urol* 2019; **26**: 31-47. doi: 10.1111/iju.13801
- Gragoudas ES, Egan KM, Seddon JM, Glynn RJ, Walsh SM, Finn SM, et al. Survival of patients with metastases from uveal melanoma. *Ophthalmology* 1991; **98**: 383-9; discussion 390. doi: 10.1016/s0161-6420(91)32285-1
- Krantz BA, Dave N, Komatsubara KM, Marr BP, Carvajal RD. Uveal melanoma: epidemiology, etiology, and treatment of primary disease. *Clin Ophthalmol* 2017; **11**: 279-89. doi: 10.2147/OPHT.S89591
- Diener-West M, Reynolds SM, Agugliaro DJ, Caldwell R, Cumming K, Earle JD, et al. Development of metastatic disease after enrollment in the COMS trials for treatment of choroidal melanoma: Collaborative Ocular Melanoma Study Group report No. 26. *Arch Ophthalmol* 2005; **123**: 1639-43. doi: 10.1001/archophth.123.12.1639
- Kujala E, Makitie T, Kivela T. Very long-term prognosis of patients with malignant uveal melanoma. *Invest Ophthalmol Vis Sci* 2003; **44**: 4651-9. doi: 10.1167/iovs.03-0538
- Kuk D, Shoushtari AN, Barker CA, Panageas KS, Munhoz RR, Momtaz P, et al. Prognosis of mucosal, uveal, acral, nonacral cutaneous, and unknown primary melanoma from the time of first metastasis. *Oncologist* 2016; **21**: 848-54. doi: 10.1634/theoncologist.2015-0522
- Yang J, Manson DK, Marr BP, Carvajal RD. Treatment of uveal melanoma: where are we now? *Ther Adv Med Oncol* 2018; **10**: 1758834018757175. doi: 10.1177/1758834018757175
- Bronkhorst IH, Jager MJ. Inflammation in uveal melanoma. *Eye* 2013; **27**: 217-23. doi: 10.1038/eye.2012.253
- Teramukai S, Kitano T, Kishida Y, Kawahara M, Kubota K, Komuta K, et al. Pretreatment neutrophil count as an independent prognostic factor in advanced non-small-cell lung cancer: an analysis of Japan Multinational Trial Organisation LC00-03. *Eur J Cancer* 2009; **45**: 1950-8. doi: 10.1016/j.ejca.2009.01.023
- Labelle M, Begum S, Hynes RO. Direct signaling between platelets and cancer cells induces an epithelial-mesenchymal-like transition and promotes metastasis. *Cancer Cell* 2011; **20**: 576-90. doi: 10.1016/j.ccr.2011.09.009
- Houghton AM, Rzymkiewicz DM, Ji H, Gregory AD, Egea EE, Metz HE, et al. Neutrophil elastase-mediated degradation of IRS-1 accelerates lung tumor growth. *Nat Med* 2010; **16**: 219-23. doi: 10.1038/nm.2084
- De Larco JE, Wuertz BR, Furcht LT. The potential role of neutrophils in promoting the metastatic phenotype of tumors releasing interleukin-8. *Clin Cancer Res* 2004; **10**: 4895-900. doi: 10.1158/1078-0432.CCR-03-0760
- Chen HC, Lin HC, Liu CY, Wang CH, Hwang T, Huang TT, et al. Neutrophil elastase induces IL-8 synthesis by lung epithelial cells via the mitogen-activated protein kinase pathway. *J Biomed Sci* 2004; **11**: 49-58. doi: 10.1007/bf02256548
- Mantovani A, Allavena P, Sica A, Balkwill F. Cancer-related inflammation. *Nature* 2008; **454**: 436-44. doi: 10.1038/nature07205
- Zhong JH, Huang DH, Chen ZY. Prognostic role of systemic immune-inflammation index in solid tumors: a systematic review and meta-analysis. *Oncotarget* 2017; **8**: 75381-8. doi: 10.18632/oncotarget.18856
- Nicholas MN, Khoja L, Atenafu EG, Hogg D, Quirt I, Butler M, et al. Prognostic factors for first-line therapy and overall survival of metastatic uveal melanoma: The Princess Margaret Cancer Centre experience. *Melanoma Res* 2018; **28**: 571-7. doi: 10.1097/CMR.0000000000000468
- Zhan H, Ma JY, Jian QC. Prognostic significance of pretreatment neutrophil-to-lymphocyte ratio in melanoma patients: A meta-analysis. *Clin Chim Acta* 2018; **484**: 136-40. doi: 10.1016/j.cca.2018.05.055
- Heppit MV, Heinzerling L, Kahler KC, Forschner A, Kirchner MC, Loquai C, et al. Prognostic factors and outcomes in metastatic uveal melanoma treated with programmed cell death-1 or combined PD-1/cytotoxic T-lymphocyte antigen-4 inhibition. *Eur J Cancer* 2017; **82**: 56-65. doi: 10.1016/j.ejca.2017.05.038
- Mahmoud FA, Rivera NI. The role of C-reactive protein as a prognostic indicator in advanced cancer. *Curr Oncol Rep* 2002; **4**: 250-5. doi: 10.1007/s11912-002-0023-1
- Shrotriya S, Walsh D, Bennani-Baiti N, Thomas S, Lorton C. C-Reactive Protein is an important biomarker for prognosis tumor recurrence and treatment response in adult solid tumors: A systematic review. *PLoS One* 2015; **10**: e0143080. doi: 10.1371/journal.pone.0143080
- Jiang Z, Li C, Zhao Z, Liu Z, Guan X, Yang M, et al. Abnormal liver function induced by space-occupying lesions is associated with unfavorable oncologic outcome in patients with colorectal cancer liver metastases. *Biomed Res Int* 2018; **2018**: 9321270. doi: 10.1155/2018/9321270

## research article

# Adverse events during immunotherapy in Slovenian patients with metastatic melanoma reveal a positive correlation with better treatment outcomes

Tanja Mesti<sup>1</sup>, Vid Ceplak Mencin<sup>1</sup>, Biljana Mileva Boshkoska<sup>3,4</sup>, Janja Ocvirk<sup>1,2</sup>

<sup>1</sup> Department of Medical Oncology, Institute of Oncology Ljubljana, Ljubljana, Slovenia

<sup>2</sup> Faculty of Medicine, University of Ljubljana, Ljubljana

<sup>3</sup> Faculty of information studies in Novo mesto, Novo mesto, Slovenia

<sup>4</sup> Department for Knowledge Technologies, Institute Jožef Stefan, Ljubljana Slovenia

Radiol Oncol 2021; 55(3): 354-361.

Received 24 November 2020

Accepted 16 March 2021

Correspondence to: Prof. Janja Ocvirk, M.D., Ph.D., Institute of Oncology Ljubljana, Zaloška 2, Ljubljana. E-mail: jocvirk@onko-i.si

Disclosure: No potential conflicts of interest were disclosed.

This is an open access article under the CC BY-NC-ND license (<http://creativecommons.org/licenses/by-nc-nd/4.0/>).

**Background.** Immunotherapy with CTLA-4 inhibitors and PD1 checkpoint inhibitors has initiated a breakthrough in the treatment and prognosis of patients with metastatic melanoma. The survival of these patients has increased from the expected survival time of less than 12 months to at least forty months. However, immunotherapy with either anti-CTLA-4 antibodies or PD1 inhibitors alone or in combination has a broad palette of significant immune-related adverse events. The aim of the study was to assess the correlation of immune-related adverse events with treatment outcomes defined as significant differences in the overall response rate (ORR) and progression-free survival (PFS) of patients, who developed immune-related adverse events during immunotherapy.

**Patients and methods.** A retrospective analysis of patients with metastatic melanoma treated with immunotherapy in 2020 at the Oncology Institute of Ljubljana was performed. Only patients with radiological evaluation of the immunotherapy response were included. The patients were divided into two cohorts: a cohort of patients with immune-related adverse events (irAE group) and a cohort of patients with no immune-related adverse events (NirAE group). Significantly better overall response and progression-free survival in the irAE cohort defined the primary aim of our study. To investigate the differences in progression-free survival between the irAE cohort and NirAE cohort, we used survival analysis. In particular, a Cox proportional hazards model with covariates of time to progression and adverse events was used for survival analysis. The Kruskal-Wallis H-test was applied, and a p-value of  $p \leq 0.05$  was considered the cut-off point for a statistically significant difference between the groups.

**Results.** Among the 120 patients treated with immunotherapy, radiological response evaluation was performed for 99 patients: 38 patients in the irAE cohort and 61 patients in the NirAE cohort. The ORRs for the irAE and NirAE cohorts were 57% and 37%, respectively. The PFS was significantly better for the irAE cohort (301.6 days) than for the NirAE cohort (247.29 days). The results of the survival regression analysis showed a significant increase in the survival probability from less than 60% for the NirAE cohort to almost 80% for the irAE cohort.

**Conclusions.** Patients with metastatic melanoma treated with immunotherapy who developed immune-related adverse events showed better treatment outcomes with longer times to disease progression and better overall response rates than patients treated with immunotherapy who did not develop immune-related adverse events, with a significant increase in the survival probability from less than 60% for the NirAE cohort to almost 80% for the irAE cohort.

Key words: immune related adverse events; immunotherapy; melanoma; metastases; response; survival

## Introduction

Ipilimumab, an anti-CTLA-4 antibody, was the first immunotherapy approved for the treatment of metastatic malignant melanoma and is associated with a median 5-year overall survival rate of 20 months.<sup>1</sup> Significantly longer response times were achieved with the checkpoint PD1 inhibitors pembrolizumab and nivolumab, with a 5-year overall survival rate of approximately 40 months.<sup>1-3</sup> Ipilimumab in combination with nivolumab results in an extension of the overall survival time to 60 months.<sup>1</sup>

Immunotherapy with either anti-CTLA-4 antibodies or PD1 inhibitors alone or in combination has a broad spectrum of significant immunologically related adverse events, such as immunologically related skin toxicity, pneumonitis, thyroid dysfunction and other endocrinopathies, hepatitis, and renal dysfunction.<sup>1-3</sup>

At the Institute of Oncology Ljubljana, a national centre for the treatment of patients with metastatic melanoma, we used immunotherapy on a daily basis. The PD1 inhibitors pembrolizumab and nivolumab are the main inhibitors used, as well as anti-CTLA-4 antibodies in combination with nivolumab, in accordance with the Slovenian national guidelines, based on the European Society for Medical Oncology (ESMO) and National Comprehensive Cancer Network (NCCN) guidelines for the treatment of metastatic melanoma.<sup>4-6</sup> The past years of work with patients on immunotherapy have led us to the unusual observation that patients who experience immune-related adverse events have a better treatment outcome in terms of time to relapse. Several recent studies from different melanoma centres and one meta-analysis showed that regardless of the cancer type, irAEs exhibited a positive correlation with ORR, PFS and OS.<sup>7-9</sup> The meta-analysis revealed that the ORR of irAE patients with melanoma was 37.67% but was 23.44% in NirAE patients. PFS and OS were significantly longer in the irAE population. In particular, the PFS for irAE ranged from 17.61 months to unreached and for NirAE ranged from 2.23 to 3 months. The OS for irAEs and NirAEs was 15.24 months and 8.94 months, respectively.<sup>9</sup> Hence, the aim of this study was to assess the correlation of immune-related adverse events and treatment outcomes defined as significant differences in the overall response rate (ORR) and progression-free survival (PFS) of patients who developed immune-related adverse events during immunotherapy treatment.

## Patients and methods

A retrospective analysis of patients with metastatic melanoma treated with immunotherapy from January to July 2020 was performed at the Institute of Oncology Ljubljana. Data were collected from the clinical database. The study included only metastatic melanoma patients with radiographic evaluations of immunotherapy treatment. The iRECIST (immune Response Evaluation Criteria in Solid Tumours) criteria were used to evaluate the tumour response. Patient characteristics, including age, sex, Eastern Cooperative Oncology Group (ECOG) performance status, systemic treatment prior to immunotherapy, stage of melanoma, histology type and location of primary melanoma, were recorded. The patients were divided into two cohorts: the cohort of patients with immune-related adverse events (irAE group) and the cohort of patients without immune-related adverse events (NirAE). The irAEs were evaluated by a clinician based on the findings of laboratory tests, clinical examinations, and imaging studies. The irAEs (with a potential immunologic cause) were graded according to the National Cancer Institute Common Terminology Criteria for Adverse Events, version 4.0.

The Python programming language was used for statistical calculations. The Kruskal-Wallis H-test was applied, and a p-value of  $p \leq 0.05$  was considered the threshold for statistical significance.

For survival analysis, we used the Cox proportional hazards model with the covariates time to progression and adverse events. For each patient, we considered the *length of time* from introduction of immunotherapy to the time the study analysis was performed. We considered *whether the patient remained alive* throughout the study duration and the *occurrence of an adverse event*. The hazard rate was assumed to be a Weibull distribution. Posterior survival probabilities were obtained by Monte Carlo simulation implemented in Python using the package `pymc3`.

The study was approved by the Institutional Review Board Committee and was carried out according to the Declaration of Helsinki.

## Results

From January to July 2020, 120 patients with metastatic melanoma were treated with immunotherapy. Seventy-six patients did not develop immune-related adverse events, and 44 patients developed

TABLE 1. Baseline characteristics of the cohorts

Characteristics		irAE cohort n (%)	NirAE cohort n (%)
Number		38 (38)	61 (62)
Age mean		67.4	61.6
Sex	Male	18 (47.4)	37 (60.7)
	Female	20 (52.6)	24 (39.3)
Treatment	Naive	34 (89.5)	51 (83.6)
	Previously treated	4 (10.5)	10 (16.4)
Immunotherapy	Pembrolizumab	34 (89.5)	52 (85.2)
	Nivolumab	2 (5.3)	5 (8.2)
	Nivolumab + ipilimumab	2 (5.3)	4 (6.6)
BRAF status	BRAF mutated	10 (26.3)	17 (27.9)
	BRAF wild type	21 (55.3)	27 (44.3)
	Not reported	7 (18.4)	17 (27.9)
M1a/b	Cohort a and b	22 (57.9)	35 (57.4)
M1c/d	Cohort c and d	16 (42.1)	26 (42.6)
LDH	increased	7 (18.4)	15 (24.6)
LDH	normal	31 (81.6)	46 (75.4)

irAE cohort = patients with metastatic melanoma who developed immune-related side effects during immunotherapy; LDH = lactate dehydrogenase; M1a/b = Distant metastasis to skin, soft tissue including muscle and/or nonregional lymph node and lungs; M1c/d = Distant metastasis to other visceral sites and to the central nervous system (CNS); NirAE cohort = patients with metastatic melanoma who did not develop immune-related side effects during immunotherapy

immune-related adverse events. Radiological evaluation (PET CT or CT) of the immunotherapy treatment response was performed for 99 out of 120 patients who were included in our study. The included patients were divided into two cohorts. The cohort of immunotherapy-treated patients who did not develop immune-related adverse events (NirAE cohort) included 61 (61, 62%) patients, and

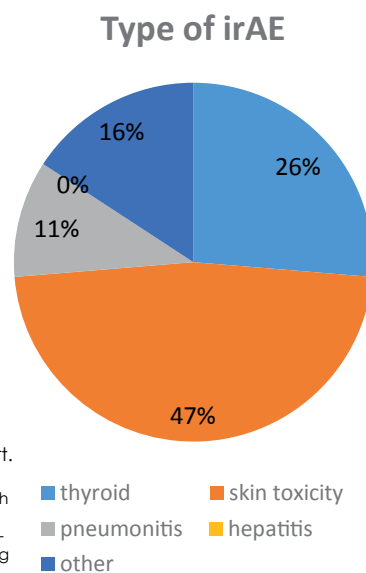


FIGURE 1. Distribution of immune-related adverse events by type in the irAE cohort.

the cohort of patients who developed immune-related side effects (irAE cohort) included 38 (38, 38%) patients. The baseline characteristics of both cohorts are presented in Table 1.

Of the 38 patients in the irAE cohort, 10 patients had thyroiditis (hyperthyroiditis/hypothyroiditis), 18 patients had skin toxicity (vitiligo, rash, itchy skin, dermatitis), 4 had pneumonitis, none had hepatitis, and 6 had other adverse events (arthritis, colitis, fatigue). The distribution of the immune-related adverse events of the immunotherapy in the irAE cohort is presented in Figure 1 below.

Most of the immune-related adverse events were grade 1 or 2. One patient developed grade 3 immune-related adverse events in the form of psoriasisiform dermatitis, and immunotherapy had to be discontinued. One patient with colitis presented with diarrhoea, and four patients with pulmonary toxicity presented with pneumonitis (Figure 2). No immune-related adverse events of grade 4 or 5 were present.

The radiological response evaluation was performed for 99 patients, 61 patients representing the NirAE cohort and 38 patients representing the irAE cohort. The overall response rates (ORRs) for the irAE and NirAE cohorts were 57% and 37%, respectively. Complete response was achieved in 14% of patients in the irAE cohort and in 4% of patients in the NirAE cohort. The irAE cohort had a higher rate of partial response (44%) than the NirAE cohort (34%). One-third (31%) of the NirAE cohort had progressive disease, and only 14% of

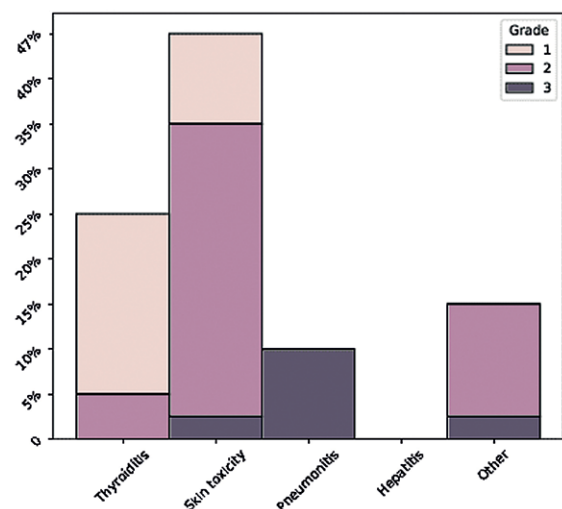
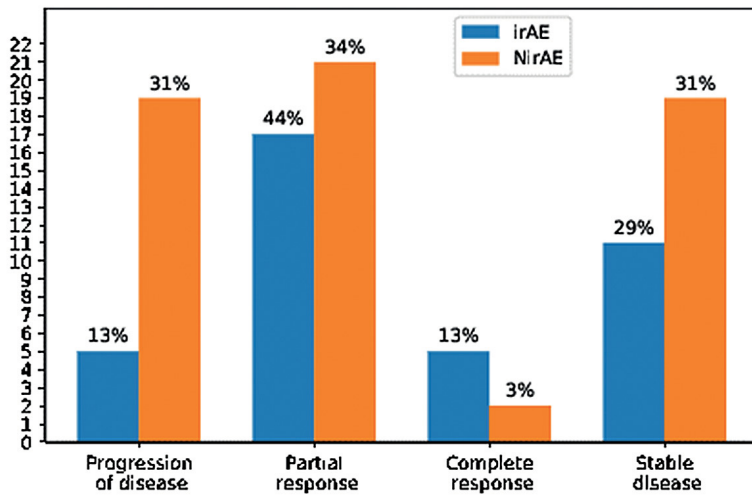


FIGURE 2. Distribution of immune-related adverse events by grade (1-3) regarding the type of immune-related adverse event in the irAE cohort presented as a percentage (%).

irAE cohort = patients with metastatic melanoma who developed immune-related side effects during immunotherapy



**FIGURE 3.** Distribution of the treatment response between the irAE and NirAE. The numbers above the bars represent the percentages with respect to its cohort, while the bar height is the absolute number of patients and is given on the Y axis.

irAE cohort = patients with metastatic melanoma who developed immune-related adverse events during immunotherapy; NirAE cohort = patients with metastatic melanoma who did not develop immune-related adverse events during immunotherapy

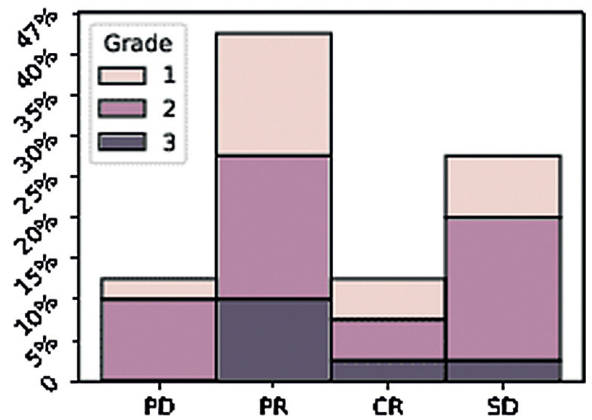


**FIGURE 4.** Correlation between the treatment response and the grade (1-3) of the immune-related side effect adverse events in the irAE cohort presented as a percentage (%).

CR = complete response; PD = partial response; PR = progression of disease; SD = stable disease

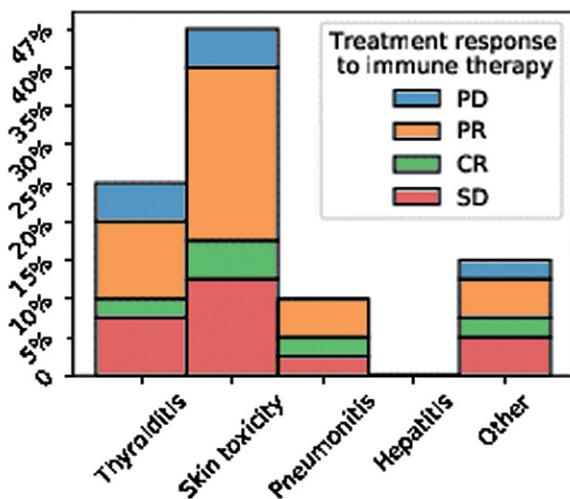


**FIGURE 5.** CORRELATION between the treatment response and the type of immune-related adverse events in the irAE cohort presented as percentages (%).

CR = complete response; PD = partial response; PR = progression of disease; SD = stable disease

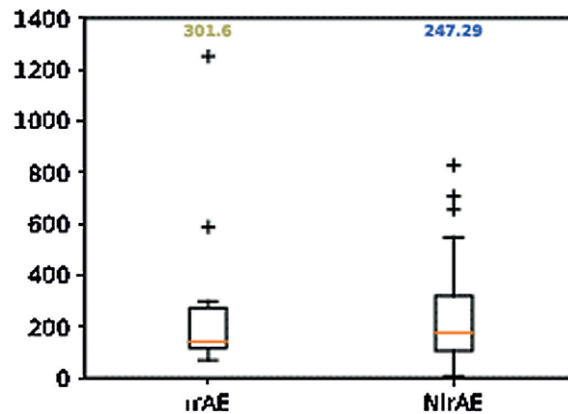


**FIGURE 6.** Progression-free survival difference in patients with metastatic melanoma between the two cohorts, cohort with immune-related adverse events (irAEs) and cohort with no immune-related adverse events (NirAEs), presented in days. The orange line indicates the median, while the patients who belong to the fourth quartile are represented with plus signs (“+”).

irAE cohort = patients with metastatic melanoma who developed immune-related adverse events during immunotherapy; NirAE cohort = patients with metastatic melanoma who did not develop immune-related adverse events during immunotherapy

the irAE cohort had progressive disease. The data are presented in Figure 3.

irAE cohort = patients with metastatic melanoma who developed immune-related adverse events during immunotherapy; NirAE cohort = patients with metastatic melanoma who did not develop immune-related adverse events during immunotherapy

Our data show that no patient who developed severe immune-related adverse events (grade 3), had progressive disease, as presented in Figure 4 below.

Grade 4 and 5 immune-related adverse events were not present. irAE cohort: patients with metastatic melanoma who developed immune-related adverse events during immunotherapy.

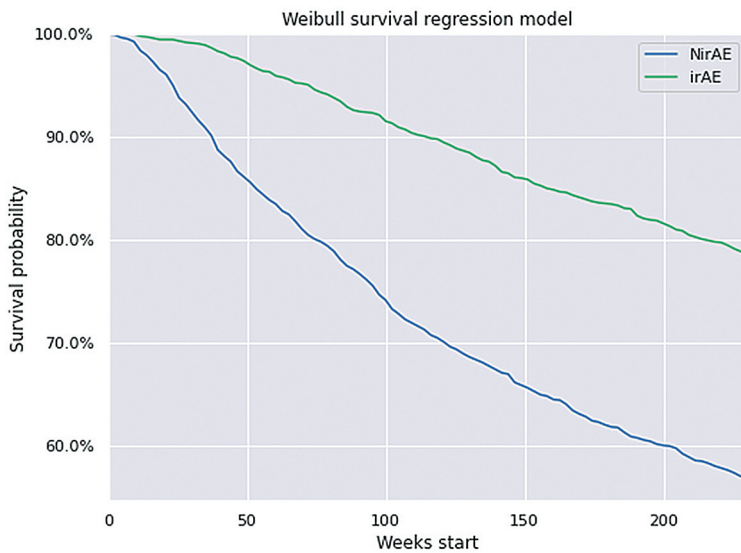


**FIGURE 7.** Difference in progression-free survival between the irAE and NirAE cohorts, with a significant increase in the survival probability from less than 60% for the NirAE cohort to almost 80% for the irAE cohort.

irAE cohort = patients with metastatic melanoma who developed immune-related adverse events during immunotherapy; NirAE cohort = patients with metastatic melanoma who did not develop immune-related adverse events during immunotherapy

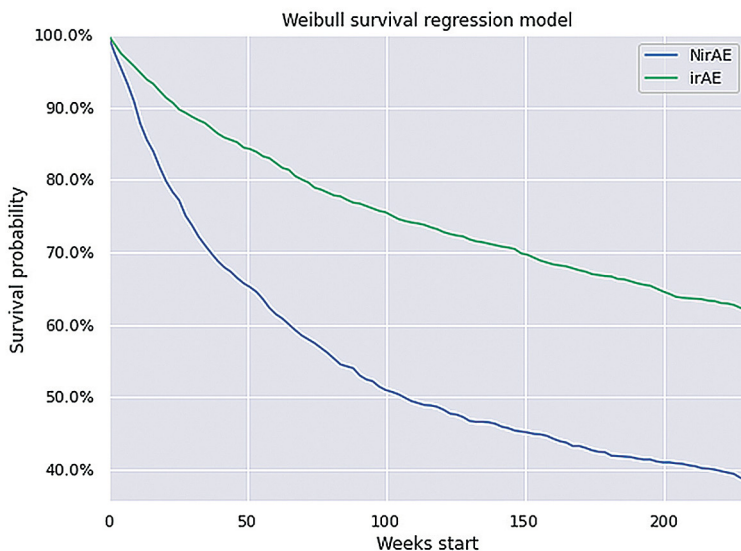


**FIGURE 8.** Difference in progression-free survival between the irAE and NirAE cohorts with increased LDH, with a significant increase in the survival probability from less than 40% for the NirAE cohort to more than 60% for the irAE cohort.

irAE cohort = patients with metastatic melanoma who developed immune-related adverse events during immunotherapy; NirAE cohort = patients with metastatic melanoma who did not develop immune-related adverse events during immunotherapy

No patient who developed immune-related pneumonitis had disease progression, as shown in Figure 5.

Grade 4 and 5 immune-related adverse events were not present; irAE cohort: patients with metastatic melanoma who developed immune-related adverse events during immunotherapy.

Finally, the time to progression of the disease in the cohort (Figure 6) that experienced immune-related adverse events was significantly longer than the time to progression in the cohort that did not experience immune-related adverse events ( $p = 0.001$ ). There was no significant difference between the time of progression and the severity of immune-related adverse events.

To investigate the differences in progression-free survival between the irAE cohort and NirAE cohort, we used survival analysis, which showed a significant increase in the survival probability from less than 60% for the NirAE cohort to almost 80% for the irAE cohort (Figure 7). This supports our study hypothesis that patients with immune-related adverse events due to immunotherapy treatment have better treatment outcomes (Figure 7).

A Cox proportional hazards model with covariates time to progression and AE was used for survival analysis. The hazard rate was assumed to be a Weibull distribution. The posterior survival probabilities were obtained through Monte Carlo simulation implemented in Python with the pymc3 package.

Furthermore, the irAE cohort with elevated LDH had better PFS with a 60% survival probability than the 40% survival probability for the NirAE cohort with elevated LDH (Figure 8). The same trend was present for the subgroup of patients with irAE stage M1a/b melanoma with a survival probability higher than 80% (Figure 9). For the cohort of patients with irAE stage M1c/d melanoma, the results were reversed, showing lower survival probability in comparison with the subgroup of NirAE patients with stage M1c/d melanoma. The survival probability for irAE stage M1c/d patients and NirAE stage M1c/d patients was 50% and 70%, respectively (Figure 10).

A Cox proportional hazards model with covariates time to progression and AE was used for survival analysis. The hazard rate was assumed to be a Weibull distribution. The posterior survival probabilities were obtained through Monte Carlo simulation implemented in Python with the pymc3 package.

Cox proportional hazards model with covariates time to progress and AE were used for sur-

vival analysis. The hazard rate was assumed to be a Weibull distribution. The posterior survival probabilities were obtained through Monte Carlo simulation implemented in Python with pymc3 package.

## Discussion

The main goal of the oncological treatment for metastatic melanoma is progression-free survival while obtaining good quality of life with as few adverse events as possible. Usually, the treatment of adverse events results in treatment delays, decreases quality of life and, consequently, results in loss of disease control and disease progression.

The introduction of immunotherapy in the treatment of metastatic melanoma has improved the prognosis of this disease, prolonging the survival time from less than a year to more than three years.<sup>1-3</sup> Additionally, recent data show evidence that immunotherapy is much more tolerable, with fewer adverse events than chemotherapy. A meta-analysis of 3450 patients suffering from non-small lung carcinoma and melanoma who were treated with the PD1 inhibitors nivolumab and pembrolizumab and the PDL1 inhibitor atezolizumab showed that compared to chemotherapy, the aforementioned drugs had a significantly lower risk of any all- and high-grade adverse events (fatigue, sensory neuropathy, diarrhoea, haematologic toxicities, anorexia, nausea, and constipation) and consequently a lower rate of treatment discontinuation.<sup>10</sup>

For more than a decade, it has been known that malignant melanoma has a unique immunogenic nature, and the presence of vitiligo in melanoma patients seems to improve the prognosis of melanoma in animals and humans, presenting effective strategy for antitumour immunity.<sup>15-17</sup>

Among immunotherapy drugs used in metastatic melanoma treatment, the CTLA4 inhibitor ipilimumab and the PD1 inhibitors pembrolizumab and nivolumab have immune-related adverse events. Ipilimumab is a fully humanized anti-CTLA-4 monoclonal antibody; pembrolizumab and nivolumab are humanized monoclonal anti-programmed cell death-1 (PD-1) antibodies.<sup>11-13</sup> With the use of CTLA4 inhibitors or anti-PD1 antibodies, also called checkpoint inhibitors, as monotherapy or in combination (nivolumab and ipilimumab), the increased risk of immune-related lung, intestinal, liver, kidney, skin, or endocrine adverse events persists.<sup>11-14</sup> Due to the severity of the ad-

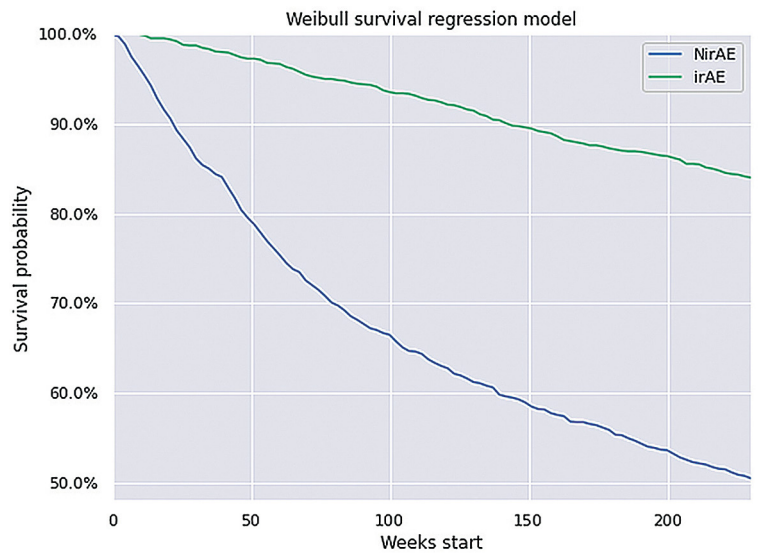


**FIGURE 9.** Difference in progression free survival between the irAE and NirAE cohort with M1a and M1b (M1a/b) patients, with a significant increase in the survival probability of approximately 50% for NirAE cohort to more than 80% for irAE cohort.

irAE cohort = patients with metastatic melanoma that developed immune-related adverse events during immunotherapy; M1a/b = distant metastasis to skin, soft tissue including muscle and/or nonregional lymph node and lungs; NirAE cohort = patients with metastatic melanoma that did not develop immune-related adverse events during immunotherapy;

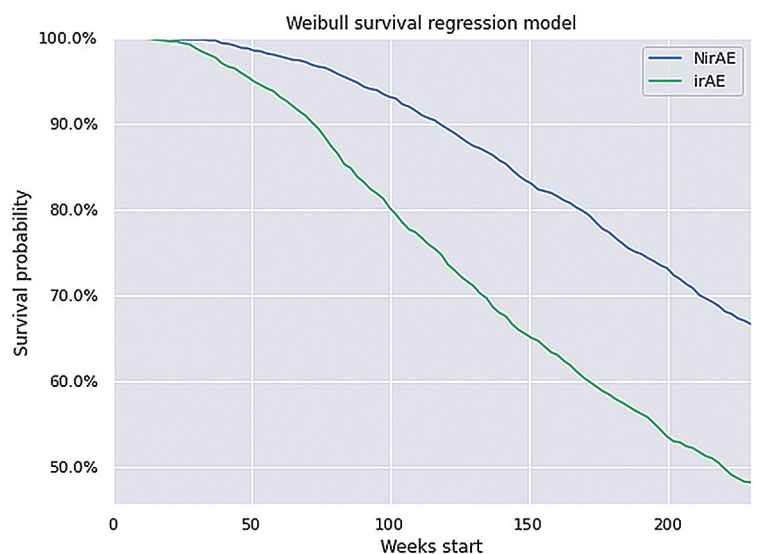


**FIGURE 10.** Difference in progression free survival between the irAE and NirAE cohort with M1c and M1d (M1c/d) patients, with a significant increase in the survival probability of almost 70% for NirAE cohort to less than 50% for irAE cohort.

irAE cohort = patients with metastatic melanoma that developed immune-related adverse events during immunotherapy; M1c/d = distant metastasis to other visceral sites than lungs and to the central nervous system (CNS); NirAE cohort = patients with metastatic melanoma that did not develop immune-related adverse events during immunotherapy

verse events caused by immunotherapy treatment, in some cases, discontinuation of the treatment is required. It has been shown that an early discontinuation of immunotherapy due to an adverse event does not negatively affect the long-term survival among these patients.<sup>1,3</sup>

The results of this study show that patients treated with immunotherapy who developed immune-related adverse events had better treatment outcomes than patients without immune-related adverse events. This retrospective study, performed on 99 patients with metastatic melanoma who were treated with immunotherapy, showed that patients with immune-related adverse events had an improved ORR in comparison to the ORR of patients without immune-related adverse events (75% vs. 37%). The PFS was significantly longer for the patients with immune-related adverse events, 301.6 days, compared to 247.29 days for patients without immune-related adverse events. Neither the severity nor the type of immune-related adverse events correlated with the ORR or PFS.

The presented data are in line with recent publications reporting a positive correlation between immune-related adverse events and survival.<sup>7-9</sup> A Dutch prospective study on 147 patients with metastatic melanoma treated with pembrolizumab showed that high-grade toxicity at any time during treatment was associated with higher objective response rate, progression-free survival, and overall survival.<sup>7</sup> A retrospective study on 144 metastatic melanoma patients treated with pembrolizumab showed similar results, as the development of any irAE (HR, 0.24,  $P < .001$ ) was significantly associated with longer OS times.<sup>8</sup>

The Cox proportional hazards regression analysis in this study shows a difference in progression-free survival between the irAE and NirAE cohorts, with a significantly increased survival probability from less than 60% for the NirAE cohort to almost 80% for the irAE cohort. Furthermore, the subgroup of patients with irAEs with elevated LDH, before the start of immunotherapy, had better PFS, with a 60% survival probability compared to the 40% survival probability for the subgroup of NirAE patients with elevated LDH. The same pattern was observed for the subgroup of patients with irAEs and stage M1a/b with a survival probability of greater than 80%. The findings were reversed for the subgroup of patients with irAEs and stage M1c/d melanoma, where the survival probability was lower than that of the subgroups of patients with NirAEs and stage M1c/d mel-

noma, with survival probabilities of 50% and 70%, respectively. There were only a few patients with increased LDH for each M1 stage; hence, we omitted these patients from multivariate analysis.

Elevated LDH is a poor prognostic marker for melanoma patients; however, LDH and immune-related side effects are widely used for the prognosis of immunotherapy outcomes.<sup>18</sup> Immunotherapy is effective for melanoma patients with dissemination locations indicating poor prognosis (M1c/d)<sup>19</sup>; however, there is a lack of data regarding the negative correlation in patients with immune-related side effects. As reported, developing immune-related adverse events correlates with better treatment outcomes.<sup>7-9,18</sup> Dissemination of melanoma in visceral organs other than the lungs and CNS, historically, is related to poor prognosis and outcome. The response rate of melanoma patients with brain metastases ranges from 26% with PD1 inhibitors to 55% with a combination of CTLA4 and PD1 inhibitors.<sup>20,21</sup> The expected time to response is longer, and the risk for hyperprogression in this subgroup of melanoma patients is higher.<sup>22,23</sup> Our data, though represented by a small group of patients, contribute to the possibility of new melanoma entities with worse immunotherapy outcomes—*i.e.*, the subgroup of irAE patients with stage M1c/d disease. Potentially, the small group of patients may lead to bias; hence, a broader retrospective analysis of patients with metastatic melanoma treated with immunotherapy at the Institute of Oncology Ljubljana is planned in the future.

## Conclusions

Our study indicates a positive correlation of the higher autoimmunogenicity caused by immunotherapy in patients with metastatic melanoma with the treatment outcome and thus improves knowledge about immunotherapy. In the present cohort, patients with immune-related adverse events during immunotherapy had better ORRs, OS and PFS than patients with metastatic melanoma without any immune-related adverse events. The Cox proportional hazards regression analysis showed a difference in PFS between the irAE and NirAE cohorts, with a significant increase in the survival probability from less than 60% for the NirAE cohort to almost 80% for the irAE cohort even in the presence of elevated LDH. This pattern was not observed for the group of patients with M1c/d disease, stipulating the need for further research.

## Acknowledgement

We thank Pavle Boškosi for his contribution to the survival regression model analysis. TM, VČM, JO acknowledges funding from the Slovenian Research Agency via program P3-0321. BMB acknowledges funding from the Slovenian Research Agency via program Complex Networks P1-0383.

## References

- Larkin J, Chiarion-Sileni V, Gonzalez R, Grob JJ, Rutkowski R, Lao CD, et al. Five-year survival with combined nivolumab and ipilimumab in advanced melanoma. *N Engl J Med* 2019; **381**: 1535-46. doi: 10.1056/NEJMoa1910836
- Hamid O, Robert C, Daud A, Hodi FS, Hwu WJ, Kefford R, et al. Five-year survival outcomes for patients with advanced melanoma treated with pembrolizumab in KEYNOTE-001. *Ann Oncol* 2019; **30**: 582-8. doi: 10.1093/annonc/mdz011
- Robert C, Hwu W-J, Hamid O, Ribas A, Weber JS, Daud AI, et al. Long-term safety of pembrolizumab monotherapy and relationship with clinical outcome: a landmark analysis in patients with advanced melanoma. *Eur J Cancer* 2021; **144**: 182-91. doi: 10.1016/j.ejca.2020.11.010
- Hocevar M, Strojan P, Ocvirk J, Peric B, Blatnik O, Luzar B, et al. [Recommendation for the treatment of patients with melanoma]. [Slovenian]. Rebersek M, editor. [cited 2020 Oct 15]. Ljubljana: Institute of Oncology Ljubljana; 2019. Available at: [https://www.onko-i.si/fileadmin/onko/datoteke/Strokovna\\_knjiznica/smernice/Priporocila\\_za\\_obravnavo\\_bolnikov\\_z\\_melanomom\\_2020.pdf](https://www.onko-i.si/fileadmin/onko/datoteke/Strokovna_knjiznica/smernice/Priporocila_za_obravnavo_bolnikov_z_melanomom_2020.pdf)
- Michielin O, van Akkooi ACJ, Ascierto PA, Dummer R, Keilholz U, on behalf of the ESMO Guidelines Committee. Cutaneous melanoma: ESMO Clinical Practice Guidelines for diagnosis, treatment and follow-up. *Ann Oncol* 2019; **30**: 1884-901. doi: 10.1093/annonc/mdz411
- NCCN Clinical Practice Guidelines in Oncology, Cutaneous melanoma. Version 4.2020. [cited 2020 Oct 14]. Available at: [https://www.nccn.org/professionals/physician\\_gls/pdf/cutaneous\\_melanoma.pdf](https://www.nccn.org/professionals/physician_gls/pdf/cutaneous_melanoma.pdf)
- Bisschop C, Wind TT, Blank CU, Koornstra RHT, Kapiteijn E, Van den Eertwegh AJM, et al. Association between pembrolizumab-related adverse events and treatment outcome in advanced melanoma: results from the Dutch Expanded Access Program. *J Immunother* 2019; **42**: 208-14. doi: 10.1097/CJI.0000000000000271
- Suo AE, Chan Y, Cheung WY, Monzon JG, Smylie M, Walker JWT, et al. Pembrolizumab-induced immune related adverse events and survival outcomes in advanced melanoma. [abstract]. *J Clin Oncol* 2018; **36** (15 Suppl): e21577. doi: 10.1200/JCO.2018.36.15\_suppl.e21577
- Hussaini S, Chehade R, Boldt RG, Raphael J, Blanchette P, Maleki Vareki S, et al. Association between immune-related side effects and efficacy and benefit of immune checkpoint inhibitors - a systematic review and meta-analysis. *Cancer Treat Rev* 2021; **92**: 102134. doi: 10.1016/j.ctrv.2020.102134
- Nishijima TF, Shachar SS, Nyrop KA, Muss HB. Safety and tolerability of PD-1/PD-L1 inhibitors compared with chemotherapy in patients with advanced cancer: a meta-analysis. *Oncologist* 2017; **22**: 470-9. doi: 10.1634/theoncologist.2016-0419
- EMA. Annex I. Summary of product characteristics. Ipilimumab (Yervoy) product information. [cited 2020 Oct 13]. Available at: [https://www.ema.europa.eu/en/documents/product-information/yervoy-epar-product-information\\_en.pdf](https://www.ema.europa.eu/en/documents/product-information/yervoy-epar-product-information_en.pdf)
- EMA. Annex I. Summary of product characteristics. Pembrolizumab (Keytruda) product information: [cited 2020 Oct 12]. [https://www.ema.europa.eu/en/documents/product-information/keytruda-epar-product-information\\_en.pdf](https://www.ema.europa.eu/en/documents/product-information/keytruda-epar-product-information_en.pdf)
- EMA. Annex I. Summary of product characteristics. Nivolumab (Opdivo) product information: [cited 2020 Oct 11]. [https://www.ema.europa.eu/en/documents/product-information/opdivo-epar-product-information\\_sl.pdf](https://www.ema.europa.eu/en/documents/product-information/opdivo-epar-product-information_sl.pdf)
- Hribernik N, Boc M, Ocvirk J, Knez-Arbeiter J, Mesti T, Ignjatovic M, et al. Retrospective analysis of treatment-naive Slovenian patients with metastatic melanoma treated with pembrolizumab – real-world experience. *Radiol Oncol* 2020; **54**: 119-27. doi: 10.2478/raon-2020-0003
- Bystryn JC. Serum antibodies in vitiligo patients. *Clin Dermatol* 1989; **7**: 136-45; doi: 10.1016/0738-081x(89)90063-1
- Oyarbide-Valencia K, van den Boorn JG, Denman CJ, Li M, Carlson JM, Hernandez C, et al. Therapeutic implications of autoimmune vitiligo T cells. *Autoimmun Rev* 2006; **5**: 486-92. doi: 10.1016/j.autrev.2006.03.012
- Hua C, Boussemart L, Mateus C, Routier E, Boutros C, Cazenave H, et al. Association of vitiligo with tumor response in patients with metastatic melanoma treated with pembrolizumab. *JAMA Dermatol* 2016; **152**: 45-51. doi: 10.1001/jamadermatol.2015.2707
- Dick J, Lang N, Slynko A, Kopp-Schneider A, Schulz C, Dimitrakopoulou-Strauss A, et al. Use of LDH and autoimmune side effects to predict response to ipilimumab treatment. *Immunotherapy* 2016; **8**: 1033-44. doi: 10.2217/imt-2016-0083
- Olson D, Luke JJ, Poklepovic AS, Bajaj M, Higgs E, Carll TC, et al. Significant antitumor activity for low-dose ipilimumab (IPI) with pembrolizumab (PEMBRO) immediately following progression on PD1 Ab in melanoma (MEL) in a phase II trial. [abstract]. *J Clin Oncol* 2020; **38** (Suppl 15): 10004. doi: 10.1200/JCO.2020.38.15\_suppl.10004
- Kluger HM, Chiang V, Mahajan A, Zito CR, Sznol M, Tran T, et al. Long-term survival of patients with melanoma with active brain metastases treated with pembrolizumab on a phase II trial. *J Clin Oncol* 2019; **37**: 52-60. doi: 10.1200/JCO.18.00204.
- Long GV, Atkinson V, Lo S, Sandhu S, Guminski AD, Brown MP, et al. Combination nivolumab and ipilimumab or nivolumab alone in melanoma brain metastases: a multicentre randomised phase 2 study. *Lancet Oncol* 2018; **19**: 672-81. doi: 10.1016/S1470-2045(18)30139-6
- Tawbi HA, Forsyth PA, Algazi A, Hamid O, Hodi FS, Moschos SJ, et al. Combined nivolumab and ipilimumab in melanoma metastatic to the brain. *N Engl J Med* 2018; **379**: 722-30. doi: 10.1056/NEJMoa1805453

## research article

# Breast cancer during pregnancy: retrospective institutional case series

Erika Matos<sup>1,2</sup>, Tanja Ovcaricek<sup>1</sup><sup>1</sup> Department of Medical Oncology, Institute of Oncology Ljubljana, Ljubljana, Slovenia<sup>2</sup> Faculty of Medicine, University of Ljubljana, Ljubljana, Slovenia

Radiol Oncol 2021; 55(3): 362-368.

Received 29 August 2020

Accepted 29 March 2021

Correspondence to: Assist. Prof. Erika Matos, M.D., Ph.D., Department of Medical Oncology, Institute of Oncology Ljubljana, Zaloska 2, SI-1000 Ljubljana, Slovenia. E-mail: ematos@onko-i.si

Disclosure: No potential conflict of interest were disclosed.

This is an open access article under the CC BY-NC-ND license (<http://creativecommons.org/licenses/by-nc-nd/4.0/>).

**Background.** Pregnancy associated breast cancer is a rare disease. It presents a unique entity of breast cancer with aggressive phenotype. The main aim was to evaluate how the international guidelines were followed in daily practice.

**Patients and methods.** Data concerning patients' and tumours' characteristics, management, delivery and maternal outcome were recorded from institutional electronic database. In this paper a case series of pregnant breast cancer patients treated at single tertiary institution between 2007 and 2019 are presented and the key recommendations on managing such patients are summarized.

**Results.** Fourteen patients met the search criteria. The majority of tumours were high grade, triple negative or HER2 positive, two patients were de novo metastatic. Treatment plan was made for each patient by multidisciplinary team. Eight patients were treated with systemic chemotherapy with no excess toxicity or severe maternal/fetal adverse effects. In all but two patients, delivery was on term and without major complications. Only one event, which was not in whole accordance with international guidelines, was identified. It was the use of blue dye in one patient.

**Conclusions.** Women with pregnancy associated breast cancer should be managed like non-pregnant breast cancer patients and should expect a similar outcome, without causing harm to the unborn child. To achieve a good outcome in pregnancy associated breast cancer, a multidisciplinary approach is mandatory.

Key words: breast cancer; pregnancy; clinical characteristics; prognosis; therapeutic strategy

## Introduction

Breast cancer is the most common malignancy among women in the developed world and is one of the most common cancer diagnosis during pregnancy.<sup>1,2</sup> Nevertheless, it is relatively rare, the reported incidence of pregnancy-associated breast cancer (PABC) is 15 to 35 breast cancer patients per 100,000 births.<sup>3,4</sup> Although rare, the incidence of PABC is increasing as women are delaying childbirth.<sup>5</sup> PABC is defined as breast cancer diagnosed during pregnancy or in the first postpartum year and it represents the second most common malignancy during pregnancy worldwide, second to cervical cancer.<sup>1,6</sup> Diagnostic and treatment recom-

mendations have been mainly based on evidence from retrospective single institutional or small case-control studies and expert consensus, as randomized trials on this entity are understandably lacking. In the present paper, we present a case series of patients diagnosed with breast cancer during pregnancy treated at Institute of Oncology Ljubljana between 2007 and 2019. The aim of the study was to evaluate the adherence of the management of PABC in daily clinical practice to the international clinical guidelines.

Diagnostic procedures for pregnant breast cancer patients should not significantly differ from those for non-pregnant women and the first step in treatment planning is to determine the extent of the

disease.<sup>6</sup> As in non-pregnant women, a pathomorphological characterisation of breast cancer is crucial for optimal decision about systemic treatment. Therefore, a core needle biopsy of the tumour has to be done.<sup>7</sup> The biology of PABC is considered different from that of non-pregnant women with usually more aggressive phenotype.<sup>8-12</sup> Recommended diagnostic procedures in pregnant woman with breast cancer are presented in Table 1.<sup>7</sup> Since the incidence of mutation in BRCA 1 or 2 gene is higher in younger breast cancer patients genetic testing should be offered to pregnant women with breast cancer.<sup>7,13</sup> Once a diagnosis of breast cancer has been made, it is important not to delay treatment. It is recommended that optimal treatment strategy for individual patient is planned by a multidisciplinary team.<sup>14</sup>

There is no epidemiological, clinical or prognostic evidence to suggest that pregnancy, or its termination, will alter the natural history of breast cancer or improve survival. Further, pregnancy by itself need not compromise effective breast cancer treatment, although the selection of and order of modalities need to consider fetal safety.<sup>6</sup> The most important decision upon diagnosis is thus selection of and order of modalities which need to consider fetal safety.<sup>6,14,15</sup> The decision about optimal treatment sequence should depend mainly on the extent of the disease and gestational age. Surgery is preferable in the 1<sup>st</sup> trimester, however, for patients in the 2<sup>nd</sup> or 3<sup>rd</sup> trimester, the treatment strategy should depend mainly on the extent of the disease.<sup>14</sup> Historically, a modified radical mastectomy was considered the standard of care for PABC because this approach eliminates the need for postoperative radiotherapy, and definitively managed the axillary region. However, breast conservation is a valid surgical option for many, although limited by the postoperative radiotherapy which is contraindicated during all trimesters of pregnancy.

Systemic treatment should not begin before the end of 1<sup>st</sup> trimester, upon completion of organogenesis, however chemotherapy in the 2<sup>nd</sup> and 3<sup>rd</sup> trimester is considered safe therapeutic options for the majority of patients with PABC and thus postponing treatment until after delivery is not advised since it was associated with a worse outcome of the malignant disease.<sup>7,16,17</sup> It is recommended to end with chemotherapy before the 36th week of gestation or within 3 weeks of planned delivery to avoid potential hematologic complications at the time of delivery.<sup>15</sup> The greatest experience of chemotherapy in pregnancy has been with anthracyclines and there is limited data on the use of taxanes in preg-

nancy and thus taxane use is not recommended during pregnancy but, if indicated, may be used after delivery.

Endocrine therapy is also not recommended during pregnancy. The literature regarding breast radiotherapy during pregnancy is scarce and according to current international guidelines, radiotherapy is not recommended during pregnancy.<sup>7</sup> Delivery should be scheduled on the estimated date of delivery. Early induction of delivery is not recommended unless so indicated for other medical reasons.<sup>15,18</sup> Table 2 presents recommended treatment modality according to gestational age.

Although in the past PABC was thought to have a poor prognosis recent studies showed that prognosis is comparable to non-pregnant patients when adjusted for age and disease stage.<sup>18,19</sup>

## Patients and methods

This is a retrospective case series of patients who were treated for breast cancer at Institute of

TABLE 1. Diagnostic procedures for pregnant breast cancer patients

Diagnostic procedures	Patients selection
Breast US with CNB	All patients
Mammography	All patients
Chest X-ray	All patients
CNB: tumor grade, ER, PR, HER2 status	All patients
Laboratory test (CBC, ALP, LFT, CA 15-3)	All patients
Liver US	Liver metastases suspected
Bone MRI	Bone metastases suspected

ALP = alkaline phosphatase; CBC = complete blood counts; CNB = core needle biopsy; ER = estrogen receptor; LFT = liver function tests; MRI = magnetic resonance imaging; PR = progesterone receptor; US = ultrasound

TABLE 2. Treatment of pregnant breast cancer patients

Gestational age	Surgery	Systemic treatment	Treatment after delivery
1 <sup>st</sup> trimester	Mastectomy + SNB/ALND	Adjuvant ChT beginning in 2 <sup>nd</sup> trimester	Adjuvant ET/anti-HER2 therapy (if indicated) + RT (if indicated)
2 <sup>nd</sup> and 3 <sup>rd</sup> trimester	Mastectomy/BCS + SNB/ALND	ChT (adjuvant/neo-adjuvant)	Adjuvant ET/anti-HER2 therapy (if indicated) + RT (if indicated)
Late 3 <sup>rd</sup> trimester	Mastectomy/BCS + SNB/ALND		Adjuvant ET/anti-HER2 therapy (if indicated) + RT (if indicated)

ALND = axillary lymph node dissection; BCS = breast conserving surgery; ChT = chemotherapy; ET = endocrine therapy; RT = radiotherapy; SNB = sentinel node biopsy

Oncology Ljubljana between 2007 and 2019 and were pregnant at the time of confirmed malignant disease. Data were recorded from institutional electronic database using the following search criteria: "breast cancer" and "pregnancy" and "gestational" or "breast cancer during pregnancy". Patients and tumours characteristics as well as data about treatment and delivery were collected from individual patient's charts.

Data were analysed applying descriptive statistics. SPSS version 19.0 was used for analysis (IBM, Armonk, NY).

The study was approved by the Institutional Review Board Committee and was carried out according to the Declaration of Helsinki.

## Results

Fourteen patients matched the search criteria in the period between January 1, 2007 and December 31, 2019. The average age of the patients was 33 (from 27 to 39) years. The gestational age upon diagnosis was between 6 and 40 weeks, with an average of 21 weeks. The details of the individual patients regarding the stages and histopathological characteristics of tumours and types of systemic and surgical treatment as well as radiotherapy are listed in Table 3. In almost half of the patients, the tumor was classified as triple-negative and most of the tumours were poorly differentiated. Almost half of the patients had HER2 positive tumours. All patients were offered genetic testing. Ten patients decided to do it. Out of them, four were found to be BRCA1 or BRCA2 gene mutation carriers.

Eight patients received chemotherapy during pregnancy. All were treated with anthracyclines in combination with cyclophosphamide, and only one received taxanes (paclitaxel). As part of supportive treatment, they mainly received antiemetic ondansetron and corticosteroids. Patients tolerated the treatment with no significant adverse effects. In addition to alopecia which was reported in all patients treated with chemotherapy, anaemia was the second most common adverse event, three patients had grade 2 anaemia.<sup>20</sup>

Two patients were diagnosed with primary metastatic breast cancer. In both cases, the disease was detected in the 3rd trimester; they continued with pregnancy and gave birth on term (more than 38 weeks of gestation). Primary metastatic disease was suspected based on symptoms (hip pain) and abnormal laboratory values. Both patients had high levels of tumour marker Ca 15-3 (1673, 157;

normal level below 30 kU/L) and elevated levels of alkaline phosphatase (ALP; 2.02, 2.91; normal level below 1.74 ukat/L) at presentation.

Most of deliveries occurred on the scheduled date, in most cases by vaginal delivery. One patient decided to terminate pregnancy at week 10 to start treatment, one patient gave birth prematurely at week 27 due to placenta praevia. In another patient delivery was induced at week 34 due to recommended adjuvant trastuzumab therapy.

No serious post-natal complications were reported. Twelve patients received systemic treatment (cytostatic, endocrine and/or antiHER2 treatment) post-partum. The median period from delivery to initiation of post-partum systemic treatment was 16 days (from 7 to 24 days). The median follow-up period was 64 months. Two patients died due to breast cancer, one of them was primary metastatic, in the second case, the patient died due to central nervous system relapse that occurred only two months after completion of neoadjuvant chemotherapy and surgery. At presentation there were no signs or symptoms of metastatic disease. All the others continue with regular follow-ups at Institute of Oncology Ljubljana.

## Discussion

In the present paper, we present 14 cases of breast cancer patients diagnosed during pregnancy. With regard to the primary aim of the study, which was to evaluate the adherence of the treatment of PABC in daily clinical practice to the international clinical guidelines, we found that most patients were treated accordingly.

Over the observed period 14 cases were identified. According to the incidences of PABC reported in the literature one would expect between one to five cases per year in Slovenia.<sup>2,4</sup> The number of cases in our study is low which may be due to case identification method and/or a fact that only patients who were pregnant at the time of diagnosis were included, which does not fit to the definition of PABC. For the purpose of this study, we focused on the management of pregnant women with newly diagnosed breast cancer.

Breast cancer diagnosed during pregnancy is most often detected as a palpable mass. This was true for all our 14 patients. Due to hormonal changes palpation of breasts during pregnancy and breastfeeding is often unreliable and this is one of the reasons why PABC is often diagnosed in more advanced stage in comparison to other patients.<sup>6,21</sup>

Diagnostic procedures should not significantly differ from those for non-pregnant women. Breast ultrasound (US) is considered the standard first line imaging modality with known high sensitivity, specificity and safety.<sup>22,23</sup> Due to the increased density of the breast tissue mammography is less sensitive in this population.<sup>24</sup> It is indicated for US confirmed solid lesions to determine the spread

of calcifications, which is important for surgical treatment planning. By adequate shielding of the abdomen, mammography exposes the fetus to a minimal dose of radiation (0.001-0.01 mGy).<sup>25,26</sup> Opinions on safety of breast magnetic resonance imaging (MRI) in pregnant women are contradictory.<sup>27</sup> According to the latest guidelines on the use of contrast agents in pregnant women by European

TABLE 3. Individual patients and tumours characteristics with details of treatment

Patient	Patient's age at BC diagnosis (years)	GA at BC diagnosis (weeks)	BC stage, tumor grade	HR HER2 BRCA	Systemic treatment during pregnancy	Mode of delivery	Complications at delivery, post-partum	Type of BC surgery	Post-partum treatment
1	34	28	T2N1M0 IIB G3	ER/PR neg HER2 poz BRCA pos	EC	Vaginal	-	MRM	Doce, trastuzumab RT
2	28	13	T2N0M0 IIA G3	ER/PR neg HER2 neg BRCA neg	EC	CS	Placenta praevia, delivery at 27 weeks of gestation	BCS and ALND	EC, pacli RT
3	37	32	T2N0M0 IIA G3	ER/PR neg HER2 neg BRCA neg	EC	Vaginal	-	BCS and SNB	EC, pacli RT
4	38	40	T3N1M0 IIIA G2	ER/PR pos HER2 pos BRCA neg	-	Vaginal	-	MRM	FEC, doce, trastuzumab, tamoxifen, RT
5	27	14	T1N0M0 IA G3	ER/PR neg HER2 neg BRCA pos	EC	Vaginal	-	Mastectomy and SNB and reconstruction (expander)	-
6	34	8	T2N0M0 IIA G3	ER/PR pos HER2 pos BRCA ND	-	NR	Pregnancy termination advised, 10 weeks of gestation	MRM	FEC, doce, trastuzumab, tamoxifen, RT
7	30	24	T3N0M0 IIB G3	ER/PR neg HER2 neg BRCA pos	AC, pacli	CS	-	Mastectomy and SNB and reconstruction (expander)	Cape, RT
8	32	26	T4dN2M1 IV G2	ER/PR pos HER2 pos BRCA ND	AC	Vaginal	-	No surgery	Doce, trastuzumab, tamoxifen, RT
9	39	13	T2N1M0 IIB G2	ER/PR pos HER2 neg BRCA ND	AC	Vaginal	-	MRM	Pacli, tamoxifen
10	32	30	T1cN0M0 IA G3	ER/PR pos HER2 neg BRCA pos	-	CS	Induced delivery, 35 weeks of gestation	Mastectomy and SNB	EC, tamoxifen
11	29	6	T2N2M0 IIIA G3	ER/PR neg HER2 pos BRCA neg	EC	Vaginal	-	MRM	Trastuzumab, RT
12	33	6	T1miN0M0 IA G3	ER/PR neg HER2 neg BRCA neg	-	Unknown	-	Mastectomy and SNB	-
13	31	38	T3N2M0 IIIA G3	ER/PR neg HER2 neg BRCA ND	-	Vaginal	-	MRM	FEC, doce, RT
14	38	36	T3N2M1 IV G3	ER/PR pos HER2 pos BRCA neg	-	Vaginal	-	No surgery	Doce, pertuzumab, trastuzumab, tamoxifen

AC = doxorubicin and cyclophosphamide; BC = breast cancer; BCS = breast conserving surgery; BRCA = BRCA status; Cape = capecitabine; CS = caesarean section; doce = docetaxel; EC = epidoxorubicin and cyclophosphamide; ER = estrogen receptor; FEC = 5-fluorouracil, epidoxorubicin and cyclophosphamide; GA = gestational age, HR = hormone receptor status; HER2 = HER2 status; MRM = modified radical mastectomy; ND = not done; NR = not relevant; pacli = paclitaxel; PR = progesterone receptor; RT = radiotherapy; SNB = sentinel lymph node biopsy

Society of Urogenital Radiology breast MRI using gadolinium-based contrast may be done in pregnant woman and no extra neonatal tests are proposed in these cases.<sup>28</sup> In none of our patients MRI was performed during pregnancy, however, all of them had breast US and mammography done.

Staging investigations are not routinely indicated in newly diagnosed operable PABC, although if they have symptoms suggestive of distant metastases, selective imaging can be performed, including chest radiograph and an abdominal US. When bone metastases are suspected, MRI is currently a preferred diagnostic modality.<sup>26</sup> In two of our patients primary metastatic disease was suspected at presentation based on elevated levels of tumour marker Ca 15-3 and abnormal values of ALP. In one patient abdominal US and lung X-ray were performed during pregnancy, both were normal. Although bone metastases were suspected due to reported pain in her left hip, skeletal MRI was not performed, since at that time it was not regarded as safe diagnostic procedure during pregnancy. However, bone scan, the standard diagnostic procedure for detection of bone metastases at that time, was postponed until after delivery when bone metastases were confirmed. In second patient breast cancer was diagnosed close to the end of pregnancy, therefore, staging of breast cancer was performed postpartum and included abdominal and thoracic CT. Liver metastases were diagnosed and were later on confirmed by fine needle aspiration biopsy.

As in non-pregnant women a pathomorphological characterisation of breast cancer is crucial for optimal decision about systemic treatment.<sup>7</sup> Core needle biopsy of the tumor was performed in all 14 patients from our series. The biology of PABC is considered different from that of non-pregnant women.<sup>8</sup> These tumours usually present with more aggressive phenotype. They are frequently poorly differentiated, estrogen-receptor negative, of either triple-negative or HER2 positive subtype. Therefore, the disease is often diagnosed at higher stage.<sup>9-12</sup> The majority of our patients had poorly differentiated tumours and almost half had a triple-negative breast cancer subtype, which is in concordance with other reports.<sup>7,11,12,14</sup> As per guidelines genetic testing has been offered to all patients since it is known that the incidence of mutation in BRCA 1 or 2 gene is higher in younger breast cancer patients and was performed in 10 patients, 4 of them were positive for germline BRCA mutations. In general, however, there is a lack of studies on this topic and its incidence in PABC is

unknown. Beside that it is unclear how the knowledge of germ line mutations in established PABC may affect treatment decisions, especially with regard to risk-reducing operative procedures and/or systemic treatments. On the other hand, genetic testing results may however affect the extent of breast surgery and regimen of further follow-up.<sup>7,13</sup>

Once a diagnosis of breast cancer has been made, it is important not to delay treatment. As recommended, the optimal treatment strategy for all of our 14 patients was planned by a multidisciplinary board, which consisted of surgical oncologist, medical oncologist, radiotherapist and gynaecologist.<sup>14</sup> Per guidelines surgery can be safely performed in all three trimesters. Mastectomy and breast-conservation surgery are both safe, while breast reconstruction surgery is not recommended during pregnancy.<sup>7,14,24,29</sup> The extent of axillary surgery should follow the same guidelines that apply to the rest of the breast cancer population.<sup>14,30,31</sup> In patients with clinically negative axillary lymph nodes, sentinel lymph node biopsy is the method of choice to minimize the likelihood of lymphedema. Data about the safety of this procedure in pregnant patients are limited, but mostly show that this approach is safe if used in modified manner.<sup>32,33</sup> The safety of radioactive tracer (eg technetium 99m sulphur colloid) during pregnancy was verified by measuring the uterine dose of radiation from lymphoscintigraphy. Doses were found to be much lower than teratogenic threshold. Therefore, some experts believe sentinel lymph node biopsy should be considered standard of care in clinically negative axilla.<sup>34</sup> On the contrary, the use of any dye is not permitted during pregnancy due to concern for maternal anaphylaxis and the possibility for teratogenicity.<sup>14,31,34</sup> We found that in regard of surgery our patients were mostly treated in accordance to current clinical guidelines, but some minor deviations were detected.<sup>7,14,24</sup> In one patient blue dye was used to detect the sentinel lymph node. Sentinel node biopsy was performed in five patients, in two of them also breast reconstruction with expanders placed during the initial mastectomy. Although according to current guidelines breast reconstruction surgery should not be performed during pregnancy small studies support the safety of immediate expander placement with improved psychologic and aesthetic outcomes.<sup>31,32,35</sup>

The literature regarding breast radiotherapy during pregnancy is scarce and radiotherapy is according to current international guidelines contraindicated during pregnancy. However, some authors believe that modern approaches, such as

3D-conformal radiotherapy (3DCRT) or intraoperative radiotherapy (IORT), can be considered during the first two trimesters in selected cases.<sup>36</sup> None of our patients received radiotherapy during pregnancy.

Eight of our patients received chemotherapy during pregnancy. According to guidelines systemic treatment should follow the recommendations that apply to the rest of the breast cancer population. It should not begin before the end of 1st trimester, upon completion of organogenesis.<sup>7,16</sup> Postponing treatment until after delivery may be associated with a worse outcome of the malignant disease and is therefore not advised.<sup>37,38</sup> The dosage is supposed to be calculated according to the patient's actual body weight and the intervals should remain the same as for non-pregnant patients.<sup>39</sup> Pregnancy is not a restraining factor for treatment with a dose-dense regimen supported by granulocyte growth factors. However, more frequent blood counts tests are advised due to the risk of anaemia and neutropenia.<sup>15,40</sup> Use of anthracyclines and cyclophosphamide during pregnancy was found to be safe, regarding the safety of other cytotoxic drugs during pregnancy data are scarce.<sup>41-43</sup> Most of the reports on taxanes relate to the safety of paclitaxel.<sup>44,45</sup> Use of trastuzumab is contraindicated during pregnancy due to increased occurrence of oligo and anhydramnion. The same applies to other anti-HER2 therapy.<sup>15,46</sup> Endocrine therapy is also not permitted during pregnancy due to many reported developmental abnormalities, particularly with tamoxifen treatment.<sup>15,47,48</sup>

Among anti-emetics, ondansetron is classified as group B drug in terms of safety during pregnancy and metoclopramide is also recognized to be safe.<sup>49,50</sup> Data regarding safety of glucocorticoids during pregnancy are conflicting, some favour the use of methylprednisolone.<sup>51</sup>

Systemic treatment of pregnant patients from our cohort was based on anthracyclines and did not start before the end of 1st trimester. One patient also received taxanes. Although some experts still warn about the routine use of taxanes in pregnant women, some case reports series suggest similar safety profiles of taxanes to doxorubicin.<sup>45</sup> Therefore, we do not consider this approach as guidelines violation. None of our patients received endocrine or anti-HER2 therapy during pregnancy.

In the past, PABC was thought to have a poor prognosis.<sup>18</sup> Multiple less extensive, retrospective cohort and case-control studies conducted in recent decades have demonstrated different findings. When adjusted for age, disease stage and morpho-

logical characteristics of the tumours many studies have failed to demonstrate a significantly worse outcome for women who were diagnosed with early and locally advanced breast cancer during pregnancy compared to non-pregnant patients.<sup>19</sup> On the contrary, prognosis of metastatic PABC is generally poor and the expected 5-year survival is only about 10%.

Although the median follow-up period in our case series is fairly short and the sample size small and thus is impossible to assess the impact of PABC on prognosis of these patients. However, no breast cancer relapse in initially non-metastatic patients was detected so far. This might suggest no significantly worse prognosis in our series of patients.

## Conclusions

Treatment of breast cancer diagnosed during pregnancy is a major professional and ethical challenge for all members of the multidisciplinary team. We found that the incidence of breast cancer diagnosed in pregnant women was low in the observed period. Patients were mostly treated in accordance with current international clinical guidelines. Only one event that was not in accordance was identified. It was the use of blue dye in one patient. The reason for this event is unknown.

## References

1. Bray F, Ferlay J, Soerjomataram I, Siegel RL, Torre LA, Jemal A. Global cancer statistics 2018: GLOBOCAN estimates of incidence and mortality worldwide for 36 cancers in 185 countries. *CA Cancer J Clin* 2018; **68**: 394-424. doi: 10.3322/caac.21492
2. Lee YY, Roberts CL, Dobbins T, Stavrou E, Black K, Morris J, et al. Incidence and outcomes of pregnancy-associated cancer in Australia, 1994-2008: a population-based linkage study. *Bjog* 2012; **119**: 1572-82. doi: 10.1111/j.1471-0528.2012.03475.x
3. Stensheim H, Moller B, van Dijk T, Fossa SD. Cause-specific survival for women diagnosed with cancer during pregnancy or lactation: a registry-based cohort study. *J Clin Oncol* 2009; **27**: 45-51. doi: 10.1200/JCO.2008.17.4110
4. Smith LH, Danielsen B, Allen ME, Cress R. Cancer associated with obstetric delivery: results of linkage with the California cancer registry. *Am J Obstet Gynecol* 2003; **189**: 1128-35. doi: 10.1067/s0002-9378(03)00537-4
5. Mathews TJ, Hamilton BE. Mean age of mothers is on the rise: United States, 2000-2014. *NCHS Data Brief* 2016; **232**: 1-8. PMID: 26828319
6. Rojas KE, Bilbro N, Manasseh DM, Borgen PI. A review of pregnancy-associated breast cancer: diagnosis, local and systemic treatment, and prognosis. *J Womens Health* 2019; **28**: 778-84. doi: 10.1089/jwh.2018.7264
7. National Comprehensive Cancer Network. Guidelines breast cancer. Version 5.2020. [internet]. Gradishar WJ, Anderson BO, Abraham J, Aft R, Agnese D, Allison KH, et al, editors. [cited 2020 Aug 22]. Available at: [https://www.nccn.org/professionals/physician\\_gls/pdf/breast.pdf](https://www.nccn.org/professionals/physician_gls/pdf/breast.pdf)
8. Peccatori FA, Lambertini M, Scarfone G, Del Pup L, Codacci-Pisanelli G. Biology, staging, and treatment of breast cancer during pregnancy: reassessing the evidences. *Cancer Biol Med* 2018; **15**: 6-13. doi: 10.20892/j.issn.2095-3941.2017.0146

9. Gwyn KM, Theriault RL. Breast cancer during pregnancy. *Curr Treat Options Oncol* 2000; **1**: 239-43. doi: 10.1007/s11864-000-0035-8
10. Genin AS, Lesieur B, Gligorov J, Antoine M, Selleret L, Rouzier R. Pregnancy-associated breast cancers: do they differ from other breast cancers in young women? *Breast* 2012; **21**: 550-5. doi: 10.1016/j.breast.2012.05.002
11. Anders CK, Fan C, Parker JS, Carey LA, Blackwell KL, Klauber-DeMore N, et al. Breast carcinomas arising at a young age: unique biology or a surrogate for aggressive intrinsic subtypes? *J Clin Oncol* 2011; **29**: e18-20. doi: 10.1200/JCO.2010.28.9199
12. Murphy CG, Mallam D, Stein S, Patil S, Howard J, Sklarin N, et al. Current or recent pregnancy is associated with adverse pathologic features but not impaired survival in early breast cancer. *Cancer* 2012; **118**: 3254-9. doi: 10.1002/cncr.26654
13. Claus EB, Schildkraut JM, Thompson WD, Risch NJ. The genetic attributable risk of breast and ovarian cancer. *Cancer* 1996; **77**: 2318-24. doi: 10.1002/(SICI)1097-0142(19960601)77:11<2318::AID-CNCR21>3.0.CO;2-Z
14. Peccatori FA, Azim HA Jr, Orecchia R, Hoekstra HJ, Pavlidis N, Kesic V, et al. Cancer, pregnancy and fertility: ESMO Clinical Practice Guidelines for diagnosis, treatment and follow-up. *Ann Oncol* 2013; **24**(Suppl 6): vi160-70. doi: 10.1093/annonc/mdt199
15. Loibl S, Schmidt A, Gentilini O, Kaufman B, Kuhl C, Denkert C, et al. Breast cancer diagnosed during pregnancy: adapting recent advances in breast cancer care for pregnant patients. *JAMA Oncol* 2015; **1**: 1145-53. doi: 10.1001/jamaoncol.2015.2413
16. National Toxicology Program. NTP monograph: developmental effects and pregnancy outcomes associated with cancer chemotherapy use during pregnancy. *NTP Monogr* 2013; (2): i-214. PMID: 24736875
17. Nettleton J, Long J, Kuban D, Wu R, Shaeffer J, El-Mahdi A. Breast cancer during pregnancy: quantifying the risk of treatment delay. *Obstet Gynecol* 1996; **87**: 414-8. doi: 10.1016/0029-7844(95)00470-x
18. Azim HA Jr, Santoro L, Russell-Edu W, Pentheroudakis G, Pavlidis N, Peccatori FA. Prognosis of pregnancy-associated breast cancer: a meta-analysis of 30 studies. *Cancer Treat Rev* 2012; **38**: 834-42. doi: 10.1016/j.ctrv.2012.06.004
19. Amant F, von Minckwitz G, Han SN, Bontenbal M, Ring AE, Giermek J, et al. Prognosis of women with primary breast cancer diagnosed during pregnancy: results from an international collaborative study. *J Clin Oncol* 2013; **31**: 2532-9. doi: 10.1200/JCO.2012.45.6335
20. U.S. Department of Health and Human Services. Common terminology criteria for adverse events (CTCAE) Version 5.0. [internet]. 2017. [cited 2020 Aug 21]. Available at: [https://ctep.cancer.gov/protocoldevelopment/electronic\\_applications/docs/CTCAE\\_v5\\_Quick\\_Reference\\_5x7.pdf](https://ctep.cancer.gov/protocoldevelopment/electronic_applications/docs/CTCAE_v5_Quick_Reference_5x7.pdf)
21. Martinez MT, Bermejo B, Hernandez C, Gambardella V, Cejalvo JM, Lluch A. Breast cancer in pregnant patients: a review of the literature. *Eur J Obstet Gynecol Reprod Biol* 2018; **230**: 222-7. doi: 10.1016/j.ejogrb.2018.04.029
22. Novotny DB, Maygarden SJ, Shermer RW, Frable WJ. Fine needle aspiration of benign and malignant breast masses associated with pregnancy. *Acta Cytol* 1991; **35**: 676-86. doi: 10.1016/j.ctrv.2012.06.004
23. Woo JC, Yu T, Hurd TC. Breast cancer in pregnancy: a literature review. *Arch Surg* 2003; **138**: 91-8; discussion 9. doi: 10.1001/archsurg.138.1.91
24. Shachar SS, Gallagher K, McGuire K, Zagar TM, Faso A, Muss HB, et al. Multidisciplinary management of breast cancer during pregnancy. *Oncologist* 2017; **22**: 324-34. doi: 10.1634/theoncologist.2016-0208
25. Yang WT, Dryden MJ, Gwyn K, Whitman GJ, Theriault R. Imaging of breast cancer diagnosed and treated with chemotherapy during pregnancy. *Radiology* 2006; **239**: 52-60. doi: 10.1148/radiol.2391050083
26. Committee Opinion No. 723: Guidelines for diagnostic imaging during pregnancy and lactation. *Obstet Gynecol* 2017; **130**: e210-e6. doi: 10.1097/AOG.0000000000002355
27. Nguyen CP, Goodman LH. Fetal risk in diagnostic radiology. *Semin Ultrasound CT MR* 2012; **33**: 4-10. doi: 10.1053/j.sult.2011.09.003
28. Thomsen HS. Contrast media safety-an update. *Eur J Radiol* 2011; **80**: 77-82. doi: 10.1016/j.ejrad.2010.12.104
29. Committee Opinion No. 696: Nonobstetric surgery during pregnancy. *Obstet Gynecol* 2017; **129**: 777-8. doi: 10.1097/AOG.0000000000002014
30. Amant F, Deckers S, Van Calsteren K, Loibl S, Halaska M, Brepoels L, et al. Breast cancer in pregnancy: recommendations of an international consensus meeting. *Eur J Cancer* 2010; **46**: 3158-68. doi: 10.1016/j.ejca.2010.09.010
31. Toesca A, Gentilini O, Peccatori F, Azim HA Jr, Amant F. Locoregional treatment of breast cancer during pregnancy. *Gynecol Surg* 2014; **11**: 279-84. doi: 10.1007/s10397-014-0860-6
32. Gropper AB, Calvillo KZ, Dominici L, Troyan S, Rhei E, Economy KE, et al. Sentinel lymph node biopsy in pregnant women with breast cancer. *Ann Surg Oncol* 2014; **21**: 2506-11
33. Khera SY, Kiluk JV, Hasson DM, Meade TL, Meyers MP, Dupont EL, et al. Pregnancy-associated breast cancer patients can safely undergo lymphatic mapping. *Breast J* 2008; **14**: 250-4. doi: 10.1111/j.1524-4741.2008.00570.x
34. Gentilini O, Cremonesi M, Toesca A, Colombo N, Peccatori F, Sironi R, et al. Sentinel lymph node biopsy in pregnant patients with breast cancer. *Eur J Nucl Med Mol Imaging* 2010; **37**: 78-83. doi: 10.1007/s00259-009-1217-7
35. Fernandez-Delgado J, Lopez-Pedraza MJ, Blasco JA, Andradas-Aragones E, Sanchez-Mendez JJ, Sordo-Miralles G, et al. Satisfaction with and psychological impact of immediate and deferred breast reconstruction. *Ann Oncol* 2008; **19**: 1430-4. doi: 10.1093/annonc/mdn153
36. Mazzola R, Corradini S, Eidemueller M, Figlia V, Fiorentino A, Giaj-Levra N, et al. Modern radiotherapy in cancer treatment during pregnancy. *Crit Rev Oncol Hematol* 2019; **136**: 13-9. doi: 10.1016/j.critrevonc.2019.02.002
37. Raphael J, Trudeau ME, Chan K. Outcome of patients with pregnancy during or after breast cancer: a review of the recent literature. *Curr Oncol* 2015; **22**: S8-18. doi: 10.3747/co.22.2338
38. Beadle BM, Woodward WA, Middleton LP, Tereffe W, Strom EA, Litton JK, et al. The impact of pregnancy on breast cancer outcomes in women. *Cancer* 2009; **115**: 1174-84. doi: 10.1002/cncr.24165
39. Van Calsteren K, Verbesselt R, Ottevanger N, Halaska M, Heyns L, Van Bree R, et al. Pharmacokinetics of chemotherapeutic agents in pregnancy: a preclinical and clinical study. *Acta Obstet Gynecol Scand* 2010; **89**: 1338-45. doi: 10.3109/00016349.2010.512070
40. Cardonick E, Gilmandyar D, Somer RA. Maternal and neonatal outcomes of dose-dense chemotherapy for breast cancer in pregnancy. *Obstet Gynecol* 2012; **120**: 1267-72. doi: 10.1097/AOG.0b013e31826c32d9
41. Hahn KM, Johnson PH, Gordon N, Kuerer H, Middleton L, Ramirez M, et al. Treatment of pregnant breast cancer patients and outcomes of children exposed to chemotherapy in utero. *Cancer* 2006; **107**: 1219-26. doi: 10.1002/cncr.22081
42. Murthy RK, Theriault RL, Barnett CM, Hodge S, Ramirez MM, Milbourne A, et al. Outcomes of children exposed in utero to chemotherapy for breast cancer. *Breast Cancer Res* 2014; **16**: 500. doi: 10.1186/s13058-014-0500-0
43. Gziri MM, Hui W, Amant F, Van Calsteren K, Ottevanger N, Kapusta L, et al. Myocardial function in children after fetal chemotherapy exposure: a tissue Doppler and myocardial deformation imaging study. *Eur J Pediatr* 2013; **172**: 163-70. doi: 10.1007/s00431-012-1849-7
44. Berveiller P, Mir O. Taxanes during pregnancy: probably safe, but still to be optimized. *Oncology* 2012; **83**: 239-40. doi: 10.1159/000341820
45. Zagouri F, Sergentanis TN, Chrysikos D, Dimitrakakis C, Tsigginou A, Zografos CG, et al. Taxanes for breast cancer during pregnancy: a systematic review. *Clin Breast Cancer* 2013; **13**: 16-23. doi: 10.1016/j.clbc.2012.09.014
46. Lambertini M, Peccatori FA, Azim HA Jr. Targeted agents for cancer treatment during pregnancy. *Cancer Treat Rev* 2015; **41**: 301-9. doi: 10.1016/j.ctrv.2015.03.001
47. Isaacs RJ, Hunter W, Clark K. Tamoxifen as systemic treatment of advanced breast cancer during pregnancy – case report and literature review. *Gynecol Oncol* 2001; **80**: 405-8. doi: 10.1006/gyno.2000.6080
48. Cullins SL, Pridjian G, Sutherland CM. Goldenhar's syndrome associated with tamoxifen given to the mother during gestation. *JAMA* 1994; **271**: 1905-6. doi: 10.1001/jama.1994.03510480029018
49. Fejzo MS, MacGibbon KW, Mullin PM. Ondansetron in pregnancy and risk of adverse fetal outcomes in the United States. *Reprod Toxicol* 2016; **62**: 87-91. doi: 10.1016/j.reprotox.2016.04.027
50. Anderka M, Mitchell AA, Louik C, Werler MM, Hernandez-Diaz S, Rasmussen SA. Medications used to treat nausea and vomiting of pregnancy and the risk of selected birth defects. *Birth Defects Res A Clin Mol Teratol* 2012; **94**: 22-30. doi: 10.1002/bdra.22865
51. Xiaoxiao P, Li L, Li M, Qian Z, Chenghao L. [Preliminary study on E-cadherin expression in dexamethasone-induced palatal cleft in mouse]. [Chinese]. *Hua Xi Kou Qiang Yi Xue Za Zhi* 2015; **33**: 581-4. doi: 10.7518/hxkq.2015.06.006

research article

# A protocol for accurate radiochromic film dosimetry using Radiochromic.com

Ignasi Méndez<sup>1</sup>, Juan José Rovira-Escutia<sup>2</sup>, Bozidar Casar<sup>1</sup>

<sup>1</sup> Department for dosimetry and quality of radiological procedures, Institute of Oncology Ljubljana, Ljubljana, Slovenia

<sup>2</sup> Centro Nacional de Dosimetría, INGESA, Valencia, Spain

Radiol Oncol 2021; 55(3): 369-378.

Received 24 June 2021

Accepted 01 July 2021

Correspondence to: Ignasi Méndez, Ph.D., Department for dosimetry and quality of radiological procedures, Institute of Oncology Ljubljana, Zaloška 2, SI-1000 Ljubljana, Slovenia. E-mail: nmendez@onko-i.si

Disclosure: Ignasi Méndez and Juan José Rovira-Escutia are co-founders of Radiochromic.com.

This is an open access article under the CC BY-NC-ND license (<http://creativecommons.org/licenses/by-nc-nd/4.0/>).

**Background.** Radiochromic films have many applications in radiology and radiation therapy. Generally, the dosimetry system for radiochromic film dosimetry is composed of radiochromic films, flatbed scanner, and film analysis software. The purpose of this work is to present the effectiveness of a protocol for accurate radiochromic film dosimetry using Radiochromic.com as software for film analysis.

**Materials and methods.** Procedures for image acquisition, lot calibration, and dose calculation are explained and analyzed. Radiochromic.com enables state-of-the-art models and corrections for radiochromic film dosimetry, such as the Multigaussian model for multichannel film dosimetry, and lateral, inter-scan, and re-calibration corrections of the response.

**Results.** The protocol presented here provides accurate dose results by mitigating the sources of uncertainty that affect radiochromic film dosimetry.

**Conclusions.** Appropriate procedures for film and scanner handling in combination with Radiochromic.com as software for film analysis make easy and accurate radiochromic film dosimetry feasible.

Key words: radiochromic film; dosimetry; protocol, film analysis software

## Introduction

Radiochromic films are extensively employed in radiology and radiation therapy because they have excellent spatial resolution, near water-equivalence,<sup>1,2</sup> and weak energy dependence.<sup>3-8</sup> Furthermore, they can be immersed in water,<sup>9</sup> can be cut, do not need chemical processing, and present low sensitivity to visible light. The active component of radiochromic films are diacetylene monomers which polymerize upon irradiation.<sup>10</sup> Polymerization makes films increasingly dark with the absorbed dose. Changes in the visible absorption spectrum can be measured with a flatbed scanner. Scan pixel values are converted into doses with

software for radiochromic film analysis. Hence, the dosimetry system for radiochromic film dosimetry commonly consists of radiochromic films, flatbed scanner, and film analysis software.

The purpose of this work is to present a protocol for accurate radiochromic film dosimetry using Radiochromic.com (Radiochromic SL, Benifaió, Spain) as software for film analysis.

Radiochromic.com is a software as a service (SaaS) program for radiochromic film dosimetry, radiotherapy QA, and image analysis. It aims to implement state-of-the-art methods and corrections for radiochromic film dosimetry. At the time of writing this work, Radiochromic.com was at version 3.3.

## Materials and methods

### The film-scanner system

#### Radiochromic films

This protocol is designed for the analysis of GafChromic films (Ashland Inc., Bridgewater, NJ, USA). In radiation therapy, GafChromic EBT3 and EBT-XD films are recommended. The difference between EBT3 and EBT-XD films lies in the length of the needles of the active component. EBT-XD needles are shorter, which leads to less darkening for the same absorbed dose and to higher saturation doses. Therefore, EBT-XD films are recommended for higher doses. EBT3 films can be used for applications with doses in the range of 0.01–20 Gy. However, for doses larger than 10 Gy and up to 40 Gy, EBT-XD films are preferred.<sup>10</sup>

EBT3 and EBT-XD films are considered energy independent for MV photon beams. However, they under-respond to photon energies lower than 100 keV<sup>8</sup>, and exhibit LET dependence for protons.<sup>10</sup>

In kV X-rays applications, such as dose measurements in interventional radiology or IORT<sup>11</sup>, XR-RV3 films should be used instead. In the energy range of these applications, films are strongly energy dependent and should be calibrated for each energy in use.<sup>12</sup>

#### Flatbed scanner

Epson Expression 10000-12000XL and Epson Perfection V700-850 flatbed scanner models (Seiko Epson Corporation, Nagano, Japan) are recommended. They have been extensively studied in the literature and possess suitable characteristics for film dosimetry, such as RGB color channels, 16 bit color depth per channel, resolution up to 4800 dpi, reflection and transmission scanning modes, and lamp autocalibration. Epson Expression 10000-12000XL have A3 size, while Epson Perfection V700-850 scanners have A4 size. Epson Expression 10000-12000XL are favored because they are less affected by the lateral artifact.<sup>13-20</sup> Epson scanners can be controlled with the associated Epson Scan software or with alternatives such as VueScan (Hamrick Software, Phoenix, AZ, USA).

Papaconstadopoulos *et al.*<sup>21</sup> found that the slope of the sensitometric curve in reflection scanning was flatter than in transmission mode and considered that the dose range should be reduced accordingly to doses lower than 2 Gy (red channel) and 8 Gy (green channel) in reflection mode. This assumption was called into question by Ramos and

Pérez Azorín<sup>22</sup> who argued that the dose range should not be defined in terms of absolute changes of the signal with the dose but in relative terms by taking into consideration the signal to noise ratio. The protocol presented here is valid for both scanning modes.

#### Sources of uncertainty

Several sources of uncertainty contribute to the total uncertainty of the film-scanner system. Some of them affect radiochromic films, others are exclusive of the scanner, while the rest arise from the interaction between film and scanner.

#### Uncertainties of radiochromic films

Films display variations in the thickness of the active layer<sup>23,24</sup>, causing film heterogeneities and differences between films of the same lot (*i.e.*, intra-lot variations). Also, film darkening continues indefinitely following irradiation, although at an ever slower pace.<sup>25</sup> Humidity and temperature alter film response, yet this influence is reversible as long as the temperature does not reach more than 60°C.<sup>9,10,26,27</sup> Active layer polymerization can be noncatalytic or can also be induced by ultraviolet light.<sup>26</sup> Finally, dust, scratches, and marks modify the response of the system.

#### Uncertainties of the scanner

Despite autocalibrating before each scan, scanners experience inter-scan variations, which cause that repeated scans do not deliver constant responses.<sup>15,18</sup> The signal of the scanner have noise.<sup>14,28,29</sup> The scanner lamp should warm-up before use.<sup>30,31</sup> And other minor sources of uncertainty of the scanner include grid patterns and positional inaccuracies.<sup>15</sup>

#### Uncertainties of the interaction between film and scanner

For a given dose value, the response of the film-scanner system in pixel value decreases with the distance to the center of the scan on the axis parallel to the lamp. Furthermore, this lateral response artifact becomes more important for higher doses.<sup>16,19,32</sup> Radiochromic films polarize light, which means that the response of the system depends on the orientation of the film on the scanner bed.<sup>33</sup> Also, the response depends on film-to-light source distance.<sup>18,34</sup> The effect of the point spread function of the film-scanner system is usually negli-

ble, however, in high contrast regions may become significant.<sup>16</sup> Lastly, even though the addition of microscopic silica particles to the film surface prevents the occurrence of Newton rings<sup>35</sup>, they are still a relevant source of uncertainty for older film models (*i.e.*, EBT2).

### Image acquisition

A protocol for accurate radiochromic film dosimetry must minimize the impact of all those sources of uncertainty. To this end, and regarding image acquisition, our protocol recommends:

1. Keep films in a dry and dark environment.
2. Handle films with care, do not touch them without wearing gloves to prevent marks and scratches.
3. Keep films away from light whenever possible.
4. If films are submerged in water, minimize the time of submersion.
5. Do not bend films when cutting them. Use sharp scissors or, preferably, a guillotine.
6. Films, either entire films or film fragments, shall always keep the same orientation (*i.e.*, portrait or landscape) on the scanner. Label them to keep the orientation with the original sheet and place them consistently on the scanner.
7. Scanning the films prior to and after irradiation delivers more accurate results.<sup>23</sup> However, it compels the use of a frame to place the films at the same position in both occasions and, according to our experience, reduces the uncertainty of film doses in less than 0.5%. Consequently, scanning the films prior to irradiation is optional in this protocol.
8. After irradiation, wait for polymerization to stabilize. For convenience, films are usually scanned 24 h after irradiation. Short waiting times can be employed as well, however, in this case, time windows must be narrower to avoid losing accuracy. For instance, Devic *et al.*<sup>36</sup> found similar errors with waiting-time windows of  $24 \pm 2$  h and  $30 \pm 5$  min. Different waiting-time windows are associated with different sensitometric curves. Even though these differences can be reduced with re-calibration methods<sup>37</sup>, this protocol recommends using the same waiting-time window employed during the calibration to prevent avoidable uncertainties.
9. Warm up the scanner for at least 30 min before use.
10. Before acquisitions, and after pauses, perform several (*e.g.*, five) empty scans to stabilize the scanner lamp.

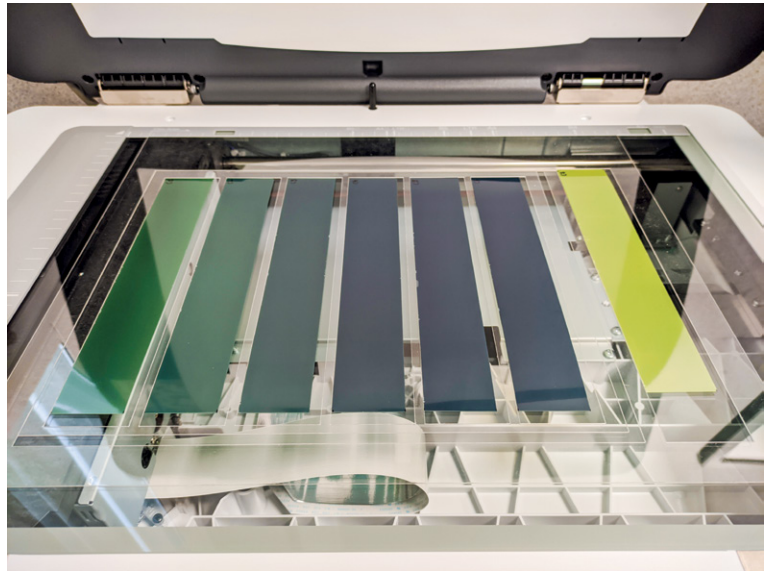


FIGURE 1. Positioning films on the scanner with a frame.

11. Center the film on the scanner. A convenient way to do so is with a frame. To prevent high contrast between frame and film, frames can be built from transparent materials, such as acetate transparencies or PMMA sheets. A set of technical drafts for frames and compression sheets suitable for the scanners recommended in this protocol can be found in the supplementary materials (Figures S1-S8). Figure 1 shows an example on how films can be positioned on the scanner with a frame.
12. Films shall be in perfect contact with the surface of the scanner bed to avoid curling. In transmission mode, place a 2–4 mm thick glass or PMMA sheet on top of the film. The positioning of the compression sheet shall be consistent, therefore, either cover or keep free the autocalibration area for all the scans. In reflection mode, the scanner lid itself compresses the film adequately.
13. Always use the same scanning mode, either reflection or transmission, that was used for the calibration.
14. Maintain a fix scanning area by saving it into the scanning software settings. In this manner, pixel positions on the film match with scanner coordinates, which is imperative when applying lateral corrections or scanning before and after irradiation.
15. Scan with 48 bit RGB mode and all image processing tools turned off.
16. A resolution of 50–75 dpi (0.51–0.35 mm) fits most applications. While for treatments using

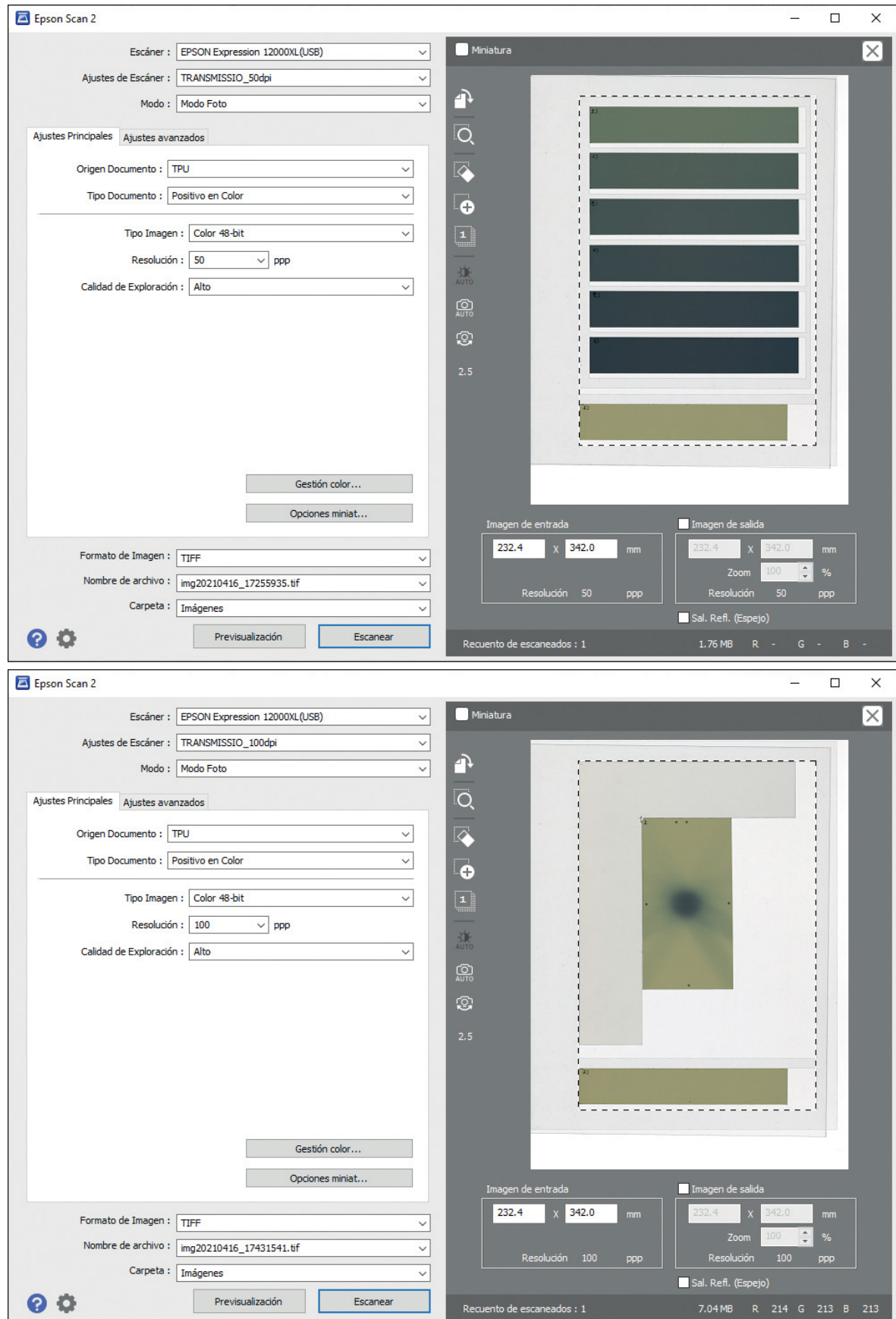


FIGURE 2. Scanner settings for (A) a calibration and (B) a treatment using small fields.

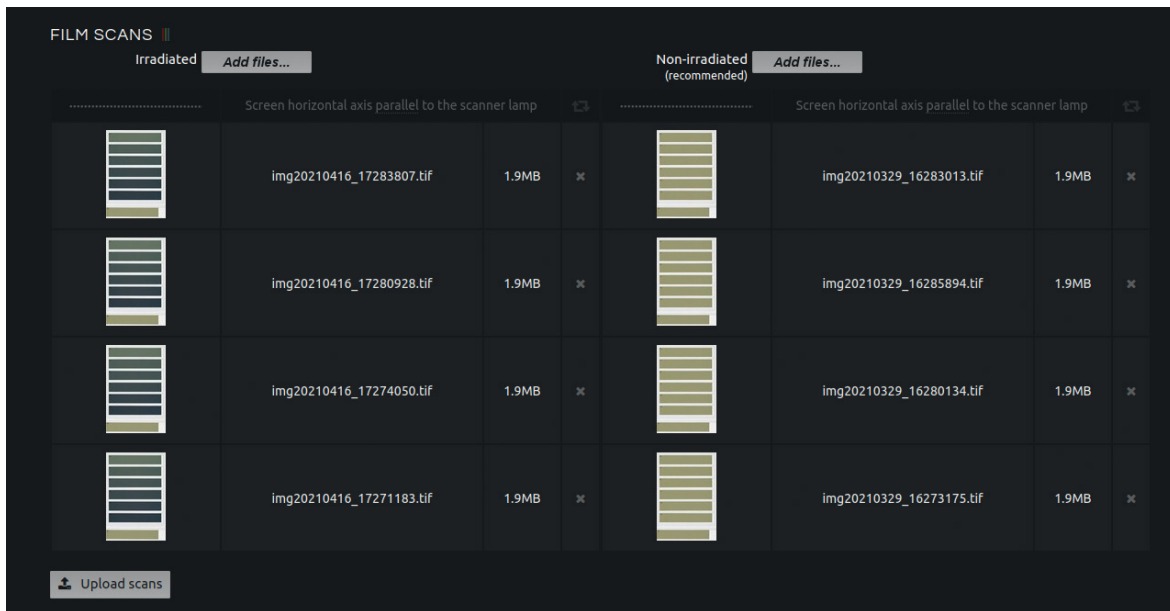


FIGURE 3. Upload films to Radiochromic.com with the correct orientation.

small fields 100–150 dpi (0.25–0.17 mm) may be necessary. In this protocol, higher resolutions are discouraged because they produce larger noise<sup>14,15</sup> and slow down film scanning and analysis. Figure 2 depicts scanner settings for a calibration and a treatment using small fields.

17. Perform four or five repeated scans and discard the first one for each film.
18. Upload the scans to Radiochromic.com selecting the orientation of the scanner lamp on the scans. The orientation should be correct to apply lateral corrections. The software will acquire the average image of the film after irradiation (irradiated film), and optionally before irradiation (non-irradiated film). Figure 3 illustrates how films are uploaded to Radiochromic.com.

## Calibration and lateral correction

### Calibration

A calibration is needed to convert film images into absorbed dose distributions. On Radiochromic.com, film images are converted into doses following the Multigaussian model<sup>23</sup> for multichannel radiochromic film dosimetry. The Multigaussian model considers that the probability density function of the film-scanner system's response given a dose  $D$  follows a multivariate Gaussian distribution, where the response is a vector of pixel values including all color channels and both irradi-

ated and non-irradiated films. Or, in mathematical form,

$$P(\mathbf{z} | D) \sim \mathcal{N}(\boldsymbol{\mu}(D), \boldsymbol{\Sigma}(D)) \quad [1]$$

where  $\mathbf{z}$  is the response vector,  $\boldsymbol{\mu}$  is the expectation vector, and  $\boldsymbol{\Sigma}$  is the covariance matrix.

On Radiochromic.com, a set of known reference doses are associated to regions of interest (ROIs) of a film image during the calibration. The outcome of the software consists of pairing each dose ( $D$ ) with the median pixel values ( $\boldsymbol{\mu}(D)$ ) and covariance matrix ( $\boldsymbol{\Sigma}(D)$ ) of the response on the associated ROI. Radiochromic.com does not fit sensitometric curves, for dose values not included in the calibration,  $\boldsymbol{\mu}(D)$  and  $\boldsymbol{\Sigma}(D)$  are interpolated with natural cubic splines.

### Lateral response correction

Commonly, to correct the lateral artifact, it is necessary to fit the parameters of a function that relates dose and distance to the center of the scan on the axis parallel to the lamp with changes in pixel values. Radiochromic.com integrates the calibration with the fitting of the lateral correction. To do so, the software applies the Lewis and Chan model for the lateral correction:<sup>17,38</sup>

$$v(x) = \alpha_1(x - x_c) + \alpha_2(x - x_c)^2 + \hat{v}(x)(1 + \beta_1(x - x_c) + \beta_2(x - x_c)^2) \quad [2]$$

where  $v$  is the pixel value after correction,  $x$  is the coordinate on the axis parallel to the lamp,  $x_c$  is

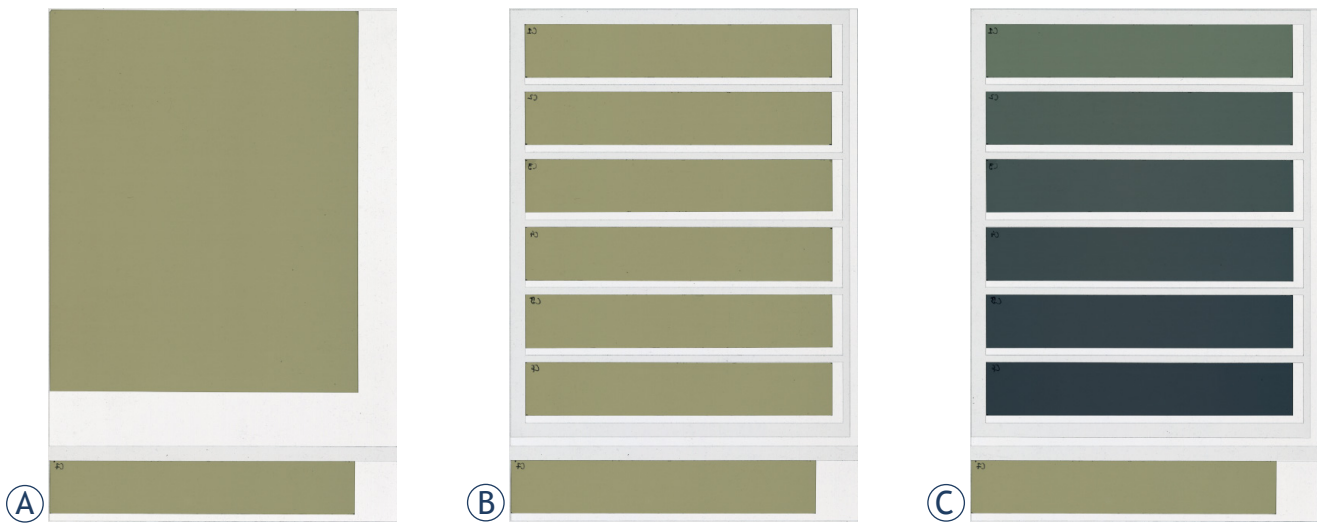


**FIGURE 4.** Scans for a calibration including lateral correction: (A) unexposed image, (B) calibration fragments prior to irradiation, and (C) calibration fragments after irradiation.

the coordinate of the center of the scanner,  $\hat{v}$  is the pixel value before correction, and  $\alpha_1$ ,  $\alpha_2$ ,  $\beta_1$ , and  $\beta_2$  are fitting parameters. As explained by Méndez *et al*<sup>23</sup>, scanning an unexposed film can simplify the process of fitting the parameters. We can rewrite the lateral correction formula as

$$v(x) = v_0 + (\hat{v}(x) - \widehat{v}_0(x))(1 + \beta_1(x - x_c) + \beta_2(x - x_c)^2) \quad [3]$$

where  $v_0$  is the pixel value at zero  $x$  and  $\widehat{v}_0(x)$  is the pixel value before correction as a function of  $x$ , both of them on the unexposed film. Furthermore, if the dose is homogeneous along the axis parallel to the lamp, equation (3) becomes

$$\frac{v - v_0}{\hat{v}(x) - \widehat{v}_0(x)} = 1 + \beta_1(x - x_c) + \beta_2(x - x_c)^2 \quad [4]$$

Radiochromic.com follows equation (4). Thus, in order to calibrate and fit the lateral correction simultaneously, the reference doses should be homogeneous along the axis parallel to the lamp and the image of an unexposed film has to be uploaded to the application too.

### Procedure for the calibration

In this protocol, we expose a calibration procedure for external photon beams, yet, other methods, radiation sources, and applications are possible, provided that they observe four basic principles:

Calibrations are valid for films from the same lot, therefore, each lot of films has to be calibrated at least once. However, since films slowly autopolymerize over time, it is advisable to repeat lot cali-

brations from time to time. Furthermore, since film response depends on humidity and temperature, more accurate film doses can be expected when calibration and film dose measurements are done together.

Uncertainties in the absorbed reference doses will be translated into film dose uncertainties. Hence, it is important to maximize the accuracy of the reference doses. Generally, this can be achieved by irradiating at reference conditions and selecting ROIs with homogeneous doses.

To avoid the lateral response artifact, the ROIs with reference doses should be centered on the scan.

Finally, the reference doses should cover the range of doses of interest to prevent extrapolations.

In accordance with these principles, to calibrate photon beams from a linear accelerator we recommend:

1. If the calibration will include the lateral correction, acquire also the image of an unexposed film.
2. Cut a film into several (*e.g.*, seven) strips with the longer side of the strips parallel to the lamp.
3. Keep one strip unexposed. One-by-one, irradiate the other strips at reference conditions in a water equivalent phantom. Strip doses should go from zero to a dose around 20% larger than the largest dose of interest. If the calibration will include the lateral correction, irradiate the strips with approximately homogeneous doses by using a beam with flattening filter and a 25 cm × 25 cm field.
4. Scan all the calibration strips simultaneously. The irradiated areas of the strips should be centered on the scan. Figure 4 presents scans for a

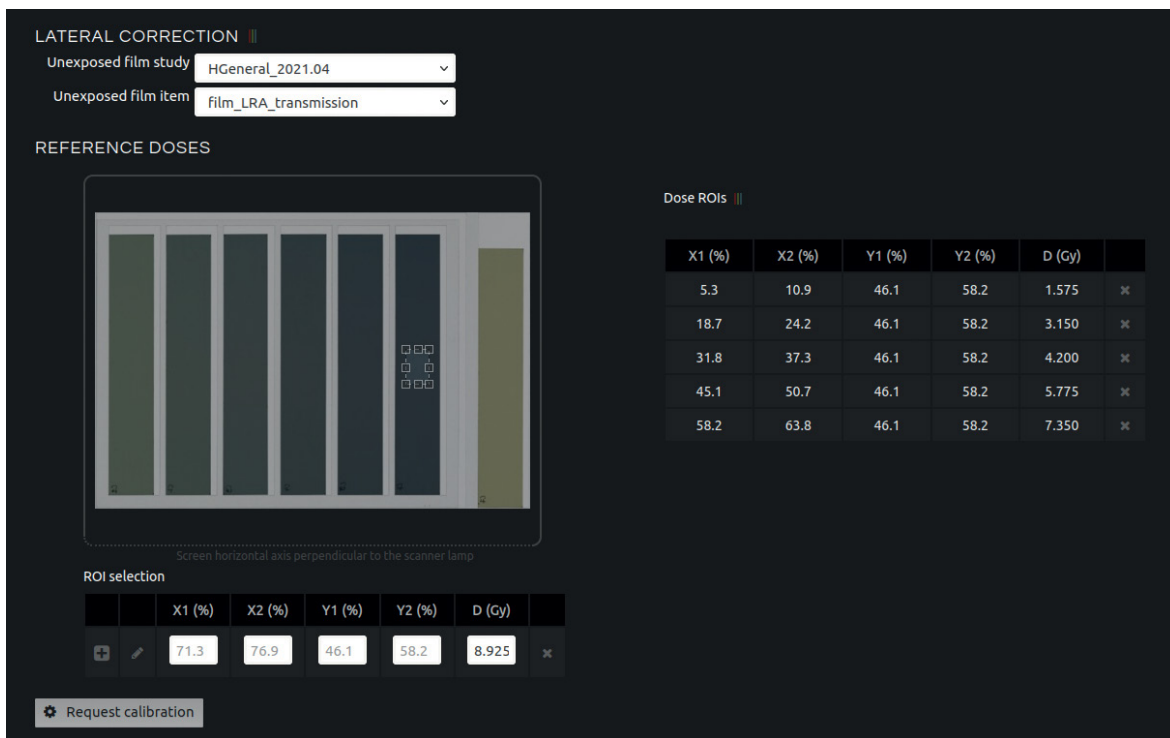


FIGURE 5. Associating reference doses to ROIs for a calibration which includes lateral correction.

calibration including lateral correction. An unexposed image and fragments irradiated with approximately homogeneous doses are necessary, the scan of the calibration fragments prior to irradiation is optional.

- Keep the unexposed strip on the scanner and do not remove it until the next calibration. This will allow easier inter-scan corrections when measuring other films.
- Acquire images into Radiochromic.com verifying that they are correctly oriented. For the calibration, doses should change on the left-right axis of the screen. Correct the orientation if they change on the vertical axis.
- On the Calibration functionality of Radiochromic.com, select the calibration image. Select also the unexposed film image if the calibration will include lateral correction.
- Associate reference doses to ROIs. The ROIs should be centered on the image (and on the scan). To provide enough statistics for the calibration while avoiding the lateral artifact, the length of the ROIs on the axis parallel to the scan should be between 1–4 cm approximately. An example of this process can be found in Figure 5.
- Radiochromic.com provides the mean error of the calibration, which computes the difference between film doses after applying the calibration

to the pixels of the ROIs and reference doses. In our experience, calibrations have mean errors around 1–2.5%. Larger errors may point to flaws in the procedure. Also, they can be expected for low doses, since uncertainties in radiochromic film dosimetry grow fast for doses lower than 1.5 Gy.<sup>39</sup> To reduce uncertainties when measuring low doses with radiochromic films, we recommend to scale the number of MUs. For instance, when measuring MLC transmission with films, we recommend to irradiate with thousands of MUs to achieve film doses around 2 Gy.

### Dose calculation

Once a calibration is made, the procedure to convert film pixel values into doses consists of:

- Scan the film together with the unexposed strip of the calibration. Figure 6 shows an example of film scans before and after irradiation. A piece of transparency sheet was used, in addition to a frame, to position the film consistently on the scanner. However, scanning before irradiation is optional in this protocol.
- Acquire the film image into Radiochromic.com and verify the orientation.
- On the Dosimetry functionality of Radiochromic.com, select the film image and the calibration.

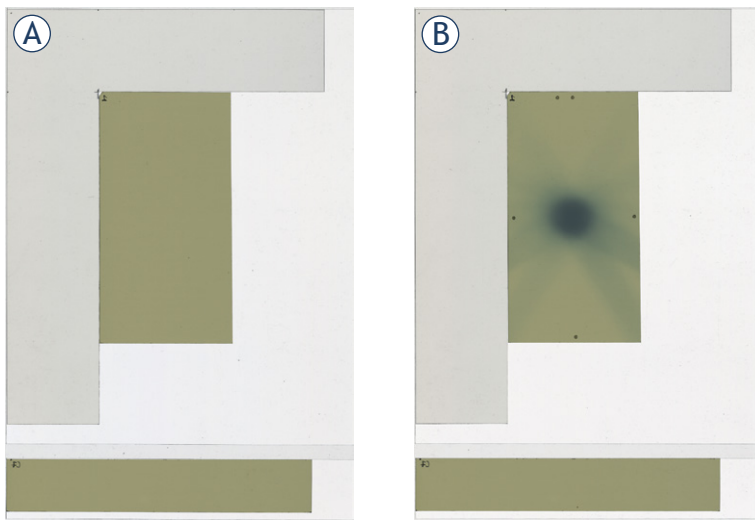


**FIGURE 6.** Scans of a film (A) before and (B) after irradiation. A piece of transparency sheet was used, in addition to a frame, to position the film consistently on the scanner.

As previously mentioned, the software computes film doses with the Multigaussian method. The Multigaussian method is a multichannel method that employs all irradiated color channels or all irradiated and non-irradiated color channels simultaneously to obtain the dose distribution. To include the non-irradiat-

ed channels, both the calibration and the film to measure should be scanned before and after irradiation. Otherwise, only the irradiated channels are evaluated.

4. Keep the default noise reduction, which applies a  $3 \times 3$  square median filter to the dose distribution.
5. Apply the inter-scan correction. To do so, select a ROI on the unexposed strip. The ROI should be centered on the scan to avoid the lateral artifact. For each color channel, the inter-scan correction multiplies each pixel of the image with a factor such that the median pixel value in the ROI coincides with the median pixel value of the unexposed ROI during the calibration. Figure 7 illustrates this process.
6. Re-calibration correction is optional in this protocol. In Radiochromic.com it is composed of inter-scan correction and dose rescaling. To apply dose rescaling, before the irradiation, cut a strip from the film to measure. This strip should be irradiated with a known homogeneous dose and scanned together with the rest of the film and the unexposed strip. Finally, select a ROI of the exposed strip centered on the scan and introduce its dose. Radiochromic.com will rescale film doses in order to match the median dose of the ROI.

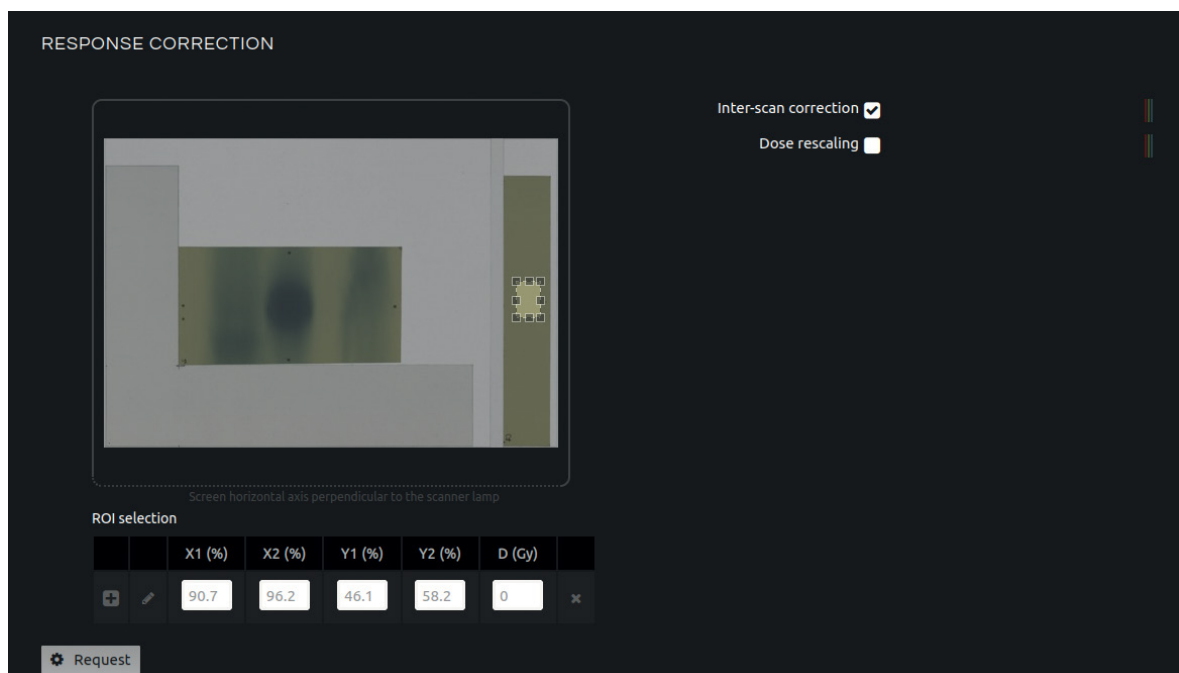


**FIGURE 7.** Applying the inter-scan correction in the film dosimetry functionality of Radiochromic.com.

## Results and discussion

The purpose of this work is to propose an accurate protocol that minimizes the sources of uncertainty that affect radiochromic film dosimetry by implementing appropriate procedures and up-to-date models and corrections. The protocol presented here incorporates the Multigaussian model for multichannel film dosimetry, and lateral, inter-scan, and re-calibration corrections of the response. Procedures for image acquisition, lot calibration, and dose calculation are stated in detail. The accuracy of this protocol has been validated repeatedly in several published studies.<sup>23,40,41</sup>

### Uncertainties of radiochromic films

With respect to the way uncertainties are reduced, variations in the thickness of the active layer are mitigated in this protocol with the Multigaussian model, and to a larger extent if films are scanned before and after irradiation. The evolution of film darkening with post-irradiation time can be managed with a constant waiting-time window post-irradiation. Alternatively, the re-calibration correction can be used, which also mitigates humidity and temperature changes, intra-lot variations, and noncatalytic or ultraviolet-catalyzed polymerization. Dust, scratches, and other marks require a repetition of the measurements. However, repeated measurements with different films also reduce uncertainties due to film heterogeneities, intra-lot variations, and noncatalytic or ultraviolet-catalyzed polymerizations. Therefore, repeating measurements with different films is endorsed when the highest level of accuracy is needed.

### Uncertainties of the scanner

The inter-scan correction mitigates inter-scan variations, which are also reduced by taking repeated scans of the same film. The noise of the scanner signal is reduced by taking repeated scans, by applying a square median filter to the dose distribution, and by the Multigaussian model. By repeating scans, minor positional inaccuracies of the scanner are averaged as well. Multiple measurements with different films reduce scanner noise, inter-scan variations, grid patterns and positional inaccuracies.

### Uncertainties of the interaction between film and scanner

The lateral artifact is mitigated by the lateral correction. The dependency on the orientation of the film on the scanner bed is removed if films always keep the same orientation. And, by scanning in reflection mode or employing a compression sheet if scanning in transmission mode, dependency on film-to-light source distance can be reduced as well.

## Conclusions

This work presents a protocol for accurate radiochromic film dosimetry using Radiochromic.com as software for film analysis. Detailed procedures for image acquisition, lot calibration, and dose calculation are explained and analyzed. State-of-the-art models and corrections for film dosimetry, such as the Multigaussian model, and lateral, inter-scan, and re-calibration corrections of the response, are applied. Proper procedures for film and scanner handling in combination with Radiochromic.com software provide the means for easy and accurate radiochromic film dosimetry.

## References

1. Crijns W, Maes F, van der Heide UA, V den Heuvel F. Calibrating page sized Gafchromic EBT3 films. *Med Phys* 2013; **40**: 012102. doi: 10.1118/1.4771960
2. Niroomand-Rad A, Blackwell CR, Coursey BM, Gall KP, Galvin JM, McLaughlin WL, et al. Radiochromic film dosimetry: Recommendations of AAPM Radiation Therapy Committee Task Group 55. *Med Phys* 1998; **25**: 2093-115. doi: 10.1118/1.598407
3. Rink A, Vitkin IA, Jaffray DA. Energy dependence (75 kVp to 18 MV) of radiochromic films assessed using a real-time optical dosimeter. *Med Phys* 2007; **34**: 458-63. doi: 10.1118/1.2431425
4. Richter C, Pawelke J, Karsch L, Woithe J. Energy dependence of EBT-1 radiochromic film response for photon (10 kVp–15 MVp) and electron beams (6–18 MeV) readout by a flatbed scanner. *Med Phys* 2009; **36**: 5506-14. doi: 10.1118/1.3253902
5. Arjomandy B, Taylor R, Anand A, Sahoo N, Gillin M, Prado K, et al. Energy dependence and dose response of Gafchromic EBT2 film over a wide range of photon, electron, and proton beam energies. *Med Phys* 2010; **37**: 1942-7. doi: 10.1118/1.3253902
6. Lindsay P, Rink A, Ruschin M, Jaffray D. Investigation of energy dependence of EBT and EBT-2 Gafchromic film. *Med Phys* 2010; **37**: 571-6. doi: 10.1118/1.3291622
7. Massillon-JL G, Chiu-Tsao S, Domingo-Munoz I, Chan M. Energy Dependence of the new Gafchromic EBT3 film: dose response curves for 50 kV, 6 and 15 MV x-ray beams. *Int J Radiat Oncol Biol Phys* 2012; **1**: 60-5. doi: 10.4236/ijmpcero.2012.12008
8. Bekerat H, Devic S, DeBlois F, Singh K, Sarfehnia A, Seuntjens J, et al. Improving the energy response of external beam therapy (EBT) GafChromic dosimetry films at low energies ( $\leq 100$  keV). *Med Phys* 2014; **41**: 022101. doi: 10.1118/1.4860157

9. León-Marroquín EY, Lárraga-Gutiérrez JM, Herrera-González JA, Camacho-López MA, Villarreal Barajas JE, García-Garduño OA. Investigation of EBT3 radiochromic film's response to humidity. *J Appl Clin Med Phys* 2018; **19**: 283-90. doi: 10.1002/acm2.12337
10. Niroomand-Rad A, Chiu-Tsao ST, Grams MP, Lewis DF, Soares CG, Van Battum LJ, et al. Report of AAPM Task Group 235 radiochromic film dosimetry: an update to TG-55. *Med Phys* 2020; **47**: 5986-6025. doi: 10.1002/mp.14497
11. Lozares S, Font JA, Gándia A, Campos A, Flamarique S, Ibáñez R, et al. In vivo dosimetry in low-voltage IORT breast treatments with XR-RV3 radiochromic film. *Phys Med* 2021; **81**: 173-81. doi: 10.1016/j.ejmp.2020.12.011
12. McCabe BP, Speidel MA, Pike TL, Van Lysel MS. Calibration of Gafchromic XR-RV3 radiochromic film for skin dose measurement using standardized x-ray spectra and a commercial flatbed scanner. *Med Phys* 2011; **38**: 1919-30. doi: 10.1118/1.3560422
13. Lárraga-Gutiérrez JM, García-Garduño OA, Treviño-Palacios C, Herrera-González JA. Evaluation of a led-based flatbed document scanner for radiochromic film dosimetry in transmission mode. *Phys Med* 2018; **47**: 86-91. doi: 10.1016/j.ejmp.2018.02.010
14. González-López A, Vera-Sánchez JA, Ruiz-Morales C. The incidence of the different sources of noise on the uncertainty in radiochromic film dosimetry using single channel and multichannel methods. *Phys Med Biol* 2017; **62**: N525-36. doi: 10.1088/1361-6560/aa8f74
15. Méndez I, Šljivčić Ž, Hudej R, Jenko A, Casar B. Grid patterns, spatial inter-scan variations and scanning reading repeatability in radiochromic film dosimetry. *Phys Med* 2016; **32**: 1072-81.
16. Battum L van, Huizenga H, Verdaasdonk R, Heukelom S. How flatbed scanners upset accurate film dosimetry. *Phys Med Biol* 2015; **61**: 625-49. doi: 10.1088/0031-9155/61/2/625.
17. Lewis D, Chan MF. Correcting lateral response artifacts from flatbed scanners for radiochromic film dosimetry. *Med Phys* 2015; **42**: 416-29. doi: 10.1118/1.4903758.
18. Lewis D, Devic S. Correcting scan-to-scan response variability for a radiochromic film-based reference dosimetry system. *Med Phys* 2015; **42**: 5692-701. doi: 10.1118/1.4929563
19. Schoenfeld AA, Poppinga D, Harder D, Doerner KJ, Poppe B. The artefacts of radiochromic film dosimetry with flatbed scanners and their causation by light scattering from radiation-induced polymers. *Phys Med Biol* 2014; **59**: 3575-97. doi: 10.1088/0031-9155/59/13/3575
20. Alnawaf H, Yu PK, Butson M. Comparison of Epson scanner quality for radiochromic film evaluation. *J Appl Clin Med Phys* 2012; **13**: 3957. doi: 10.1120/jacmp.v13i5.3957
21. Papaconstadopoulos P, Hegyi G, Seuntjens J, Devic S. A protocol for EBT3 radiochromic film dosimetry using reflection scanning. *Med Phys* 2014; **41**: 122101. doi: 10.1118/1.4901308
22. Ramos L, Perez Azorin JF. Comment on "A protocol for EBT3 radiochromic film dosimetry using reflection dosimetry using scanning" [Med Phys 41(12), 122101 (6pp.) (2014)]. *Med Phys* 2015; **42**: 2096-7. doi: 10.1118/1.4914853
23. Méndez I, Polšak A, Hudej R, Casar B. The multigaussian method: a new approach to mitigating spatial heterogeneities with multichannel radiochromic film dosimetry. *Phys Med Biol* 2018; **63**: 175013.
24. Hartmann B, Martišíková M, Jäkel O. Homogeneity of Gafchromic EBT2 film. *Med Phys* 2010; **37**: 1753-6. doi: 10.1118/1.3368601
25. Andrés C, del Castillo A, Tortosa R, Alonso D, Barquero R. A comprehensive study of the Gafchromic EBT2 radiochromic film. A comparison with EBT. *Med Phys* 2010; **37**: 6271-8. doi: 10.1118/1.3512792
26. Girard F, Bouchard H, Lacroix F. Reference dosimetry using radiochromic film. *J Appl Clin Med Phys* 2012; **13**: 3994. doi: 10.1120/jacmp.v13i6.3994
27. Rink A, Lewis DF, Varma S, Vitkin IA, Jaffray DA. Temperature and hydration effects on absorbance spectra and radiation sensitivity of a radiochromic medium. *Med Phys* 2008; **35**: 4545-55. doi: 10.1118/1.2975483
28. Bouchard H, Lacroix F, Beaudoin G, Carrier J-F, Kawrakow I. On the characterization and uncertainty analysis of radiochromic film dosimetry. *Med Phys* 2009; **36**: 1931-46. doi: 10.1118/1.3121488
29. Van Hoof SJ, Granton PV, Landry G, Podesta M, Verhaegen F. Evaluation of a novel triple-channel radiochromic film analysis procedure using EBT2. *Phys Med Biol* 2012; **57**: 4353-68. doi: 10.1088/0031-9155/57/13/4353
30. Paelinck L, De Neve W, De Wagter C. Precautions and strategies in using a commercial flatbed scanner for radiochromic film dosimetry. *Phys Med Biol* 2007; **52**: 231-42. doi: 10.1088/0031-9155/52/1/015
31. Ferreira B, Lopes M, Capela M. Evaluation of an Epson flatbed scanner to read Gafchromic EBT films for radiation dosimetry. *Phys Med Biol* 2009; **54**: 1073-85. doi: 10.1088/0031-9155/54/4/017
32. Schoenfeld AA, Wieker S, Harder D, Poppe B. The origin of the flatbed scanner artifacts in radiochromic film dosimetry-key experiments and theoretical descriptions. *Phys Med Biol* 2016; **61**: 7704-24. doi: 10.1088/0031-9155/61/21/7704
33. Butson MJ, Cheung T, Yu P. Evaluation of the magnitude of EBT Gafchromic film polarization effects. *Australas Phys Eng Sci Med* 2009; **32**: 21-5. doi: 10.1007/BF03178624
34. Palmer AL, Bradley DA, Nisbet A. Evaluation and mitigation of potential errors in radiochromic film dosimetry due to film curvature at scanning. *J Appl Clin Med Phys* 2015; **16**: 5141. doi: 10.1120/jacmp.v16i2.5141
35. Dreindl R, Georg D, Stock M. Radiochromic film dosimetry: considerations on precision and accuracy for EBT2 and EBT3 type films. *Z Med Phys* 2014; **24**: 153-63. doi: 10.1016/j.zemedi.2013.08.002
36. Devic S, Aldelajjan S, Mohammed H, Tomic N, Liang LH, DeBlois F, et al. Absorption spectra time evolution of EBT-2 model Gafchromic film. *Med Phys* 2010; **37**: 2207-14. doi: 10.1118/1.3378675
37. Ruiz-Morales C, Vera-Sánchez JA, González-López A. On the re-calibration process in radiochromic film dosimetry. *Phys Med* 2017; **42**: 67-75. doi: 10.1016/j.ejmp.2017.08.013
38. Méndez I, Hartman V, Hudej R, Strojnik A, Casar B. Gafchromic EBT2 film dosimetry in reflection mode with a novel plan-based calibration method. *Med Phys* 2013; **40**: 011720. doi: 10.1118/1.4772075
39. Vera-Sánchez JA, Ruiz-Morales C, González-López A. Monte Carlo uncertainty analysis of dose estimates in radiochromic film dosimetry with single-channel and multichannel algorithms. *Phys Med* 2018; **47**: 23-33. doi: 10.1016/j.ejmp.2018.02.006
40. Casar B, Gershkevitch E, Mendez I, Jurković S, Huq MS. A novel method for the determination of field output factors and output correction factors for small static fields for six diodes and a microdiamond detector in megavoltage photon beams. *Med Phys* 2019; **46**: 944-63. doi: 10.1002/mp.13318
41. Casar B, Gershkevitch E, Mendez I, Jurković S, Saiful Huq M. Output correction factors for small static fields in megavoltage photon beams for seven ionization chambers in two orientations – perpendicular and parallel. *Med Phys* 2020; **47**: 242-59. doi: 10.1002/mp.13894

# Primerjava mikrovalovne in radiofrekvenčne ablacije pri zdravljenju raka jeter. Sistematični pregled in metaanaliza

Spiliotis AE, Gäbelein G, Holländer S, Scherber PR, Glanemann M, Patel B

**Izhodišča.** Priporočila izpostavljajo prednosti mikrovalovne pred radiofrekvenčno ablacijo, vendar še vedno ni popolnoma jasna njena superiornost glede učinkovitosti in varnosti. Zato je bil namen raziskave primerjati mikrovalovno in radiofrekvenčno ablacijo pri zdravljenju raka jeter s sistematičnim pregledom literature in metaanalizo pridobljenih podatkov.

**Metode dela.** Metaanalizo smo naredili iz objavljenih raziskavah od leta 2010 naprej po priporočilih PRIZMA. Uporabili smo model naključnih učinkov (*angl. random-effects*) za metaanalizo. Analizirali smo popolno ablacijo, lokalno napredovanje bolezni, oddaljene intrahepatalne ponovitve bolezni ter zaplete po zdravljenju.

**Rezultati.** V analizo smo vključili 4 randomizirane in 11 observacijske raziskave, s skupnim številom 2.169 vključenih bolnikov. Celokupna analiza ni pokazala statistično značilnih razlik med mikrovalovno in radiofrekvenčno ablacijo pri lokalnih napredovanjih bolezni. Analiza podskupine randomiziranih raziskav pri bolnikih z jetrnoceličnim rakom pa je pokazala statistično značilno manj lokalnih napredovanj bolezni po mikrovalovni ablaciji (razmerne obetov [OR] 0,40; 95 % interval zaupanja [CI] 0,18–0,92;  $p = 0,03$ ). Nismo zaznali statistično značilnih razlik med obema ablativnimi tehnikama pri popolnih ablacijah, oddaljenih intrahepatalnih ponovitvah bolezni in pri zapletih, ko smo zdravili tumorje tako manjše kot večje od 3 cm.

**Zaključki.** Uporaba mikrovalovne ablacije je pokazala boljši izhod zdravljenja pri lokalnem napredovanju bolezni v primerjavi z radiofrekvenčno ablacijo pri bolnikih z jetrnoceličnim rakom. Zato bi lahko mikrovalovno ablacijo uporabljali kot metodo izbora pri zdravljenju bolnikov z jetrnoceličnim rakom.

Radiol Oncol 2021; 55(1): 259-267.

doi: 10.2478/raon-2021-0024

# Ocena radiološko neopredeljivih pljučnih nodulov z dinamično pozitronsko emisijsko tomografijo združeno z računalniško tomografsko preiskavo ter perfuzijskimi parametri

Marin A, Murchison JT, Skwarski KM, Tavares AAS, Fletcher A, Wallace WA, Salapura V, van Beek EJR, Mirsadraee S

**Izhodišča.** Razvoj novih slikovnih diagnostičnih tehnologij nam omogoča funkcionalno sledenje radiofarmakov in kontrastnih sredstev v pljučnih nodulih. Namen raziskave je bil oceniti vlogo dinamične  $^{18}\text{F}$ -FDG PET/CT in perfuzijske računalniške tomografije (CT) pri karakterizaciji pljučnih nodulov.

**Bolniki in metode.** V raziskavo smo vključili 20 zaporednih preiskovancev z naključno odkritimi pljučnimi noduli, pri katerih smo opravili preiskavi dinamično  $^{18}\text{F}$ -FDG PET/CT in perfuzijsko CT. V nodulih smo izmerili kopičenje izotopa kot standardno vrednost prevzema ( $\text{SUV}_{\text{max}}$ ); na dinamičnem  $^{18}\text{F}$ -FDG PET/CT smo s Patlakovo metodo določili konstanto fosforilacije ( $K_i$ ); na perfuzijski CT smo s Patlakovim modelom izračunali parameter volumen krvi; z metodo maksimalnega naklona smo določili perfuzijski parameter arterijskega pretoka. Nodule smo razdelili v benigno in maligno skupino na osnovi histološke diagnoze ali 2-letnega sledenja s CT. Parametre smo statistično primerjali med skupinama z neparemtričnim testom Mann-Whitney.

**Rezultati.** Analizirali smo 21 pljučnih nodulov (povprečen premer  $\pm$  standardna deviacija [SD]:  $20,1 \pm 7,5$  mm; 9–29 mm) pri 20 bolnikih (11 moških, 9 žensk, povprečna starost 65,3 leta, starostni razpon 50–76 let). Povprečna  $\text{SUV}_{\text{max}} \pm \text{SD}$  v benigni skupini je bila  $2,2 \pm 1,7$ , v maligni  $7,0 \pm 4,5$ ,  $p = 0,0148$ . Parameter  $K_i$  v benigni skupini je bil  $0,0057 \pm 0,0071 \text{ min}^{-1}$ , v maligni skupini  $0,0230 \pm 0,0155 \text{ min}^{-1}$ ,  $p = 0,0311$ . Povprečen volumen krvi med benignimi noduli je bil  $11,6857 \pm 6,7347 \text{ ml}/100\text{ml}$  ter  $28,3400 \pm 15,9672 \text{ ml}/100\text{ml}$  med malignimi noduli,  $p = 0,0250$ . Povprečen arterijski pretok v maligni skupini je bil  $74,4571 \pm 89,0321 \text{ ml}/100\text{g}/\text{min}$ , v maligni skupini  $89,200 \pm 49,8883 \text{ ml}/100\text{g}/\text{min}$ ,  $p = 0,1613$ .

**Zaključki.** Metabolični parameter  $K_i$  in perfuzijski parameter volumen krvi sta bila značilno višja v malignih pljučnih nodulih. Parameter arterijskega pretoka perfuzijske CT pa ni bil značilno različen.

Radiol Oncol 2021; 55(3): 268-273.  
doi: 10.2478/raon-2021-0018

# Magnetnoresonančna preiskava pri leziji Morel-Lavallee - serija primerov

Šrot Volavc T, Ruprecht M

**Izhodišča.** Namen raziskave je bil narediti pregled značilnosti lezij Morel-Lavallée, ki jih ugotovimo z magnetno resonanco (MR).

**Bolniki in metode.** Retrospektivno smo pregledali dokumentacijo 14 bolnikov s povprečno starostjo 35 let, pri katerih smo z MR diagnosticirali lezijo Morel-Lavallée. Analizirali smo mehanizem poškodbe, čas med poškodbo in preiskavo MR, lokacijo poškodbe, obliko, intenziteto signala na T1 sekvenci in sekvenci protonske gostote z izničenjem signala maščevja, prisotnost (psevdo)kapsule, sept ali vozličev v kolekciji, odtravanje okolnih struktur in nivoje različnih gostot tekočine. Za razvrstitev lezij smo uporabili klasifikacijo Mellado Bencardino.

**Rezultati.** Najbolj pogosta mehanizma poškodbe sta bila zvin ali udarec. Povprečen čas med poškodbo in preiskavo MR je bil 17 dni. Pri 9 bolnikih so bile lezije ob kolenu, pri 5 bolnikih pa ob kolku. Pri 12 bolnikih so bile kolekcije vretenaste oblike, pri dveh pa ovalne. Pri 9 bolnikih so bile hipointenzivne na sekvenci T1 in hiperintenzivne na sekvenci protonske gostote z izničenjem signala maščevja. 4 kolekcije so imele srednjo intenziteto signala na T1 in visoko na sekvenci protonske gostote z izničenjem signala maščevja. Ena je imela srednjo intenziteto signala na obeh sekvencah. (Psevdo)kapsulo smo našli v 3 ter septa in vozliče v 4 primerih. Znakov odtravanja ali nivojev različnih gostot tekočine v kolekcijah nismo našli. Po klasifikaciji Mellado Bencardino smo 9 primerov uvrstili v tip 1 (serom), enega v tip 2 (subakutni hematoma) in 4 v tip 3 (organizirajoč kronični hematoma).

**Zaključki.** Značilnost lezije Morel-Lavallée je vretenasta kolekcija med globokim podkožnim maščevjem ter mišično fascijo po strižni poškodbi. Z MR lahko lezije razdelimo v šest tipov, od katerih so najpogostejši serom, subakutni hematoma in kronični organizirajoči hematoma.

Radiol Oncol 2021; 55(3): 274-283.

doi: 10.2478/raon-2021-0032

## So z radioterapijo povzročeni kavernomi pomembna klinična najdba? Rezultati dolgotrajnega spremljanja preživelih z rakom v otroštvu z magnetnoresonančnim slikanjem možganov

Becker L, Gebauer J, Kuchler J, Staackmann C, Schacht H, Lauten M, Jensen-Kondering U, Schramm P, Langer T, Neumann A

**Izhodišča.** Z radioterapijo povzročeni kavernomi, ki nastanejo po obsevanju glave, imajo neznano tveganje za krvavitev. Tveganje za krvavitev iz kavernomov, ki jih ni povzročilo obsevanje sicer lahko predvidimo z razvrščanjem magnetnoresonančnih (MR) posnetkov po Zabramskem. Namen pričujoče raziskave je bil, da bi z dolgotrajnim sledenjem bolnikov, ki so preživeli rak v otroštvu, z MR slikanjem ocenili tveganje za krvavitev iz takšnih kavernomov.

**Bolniki in metode.** Retrospektivno smo analizirali podatke dolgotrajnega sledenja 36 preživelih bolnikov z rakom v otroštvu. Imeli so izhodiščno diagnozo akutno levkemijo ( $n = 18$ ) ali možganski tumor ( $n = 18$ ) in smo jih zdravili z obsevanjem glave. V obdobju dolgotrajnega sledenja smo z radioterapijo povzročene kavernome, ki smo jih ugotovili na MR posnetkih (1,5 ali 3 Tesla), razvrstili s klasifikacijo po Zabramskem. Bolnike smo uvrstili v skupino z visokim (Zabramski tip I, II ali V) ali nizkim (tip III ali IV) tveganjem za krvavitev.

**Rezultati.** Pri 18 bolnikih (50 %) smo našli z radioterapijo povzročeni kavernom, ki je bil pomembno povezan z izhodiščno tumorsko entiteto ( $p = 0,023$ ) in kumulativno dozo sevanja na možgane ( $p = 0,016$ ). Pri vseh 9 preživelih, ki so imeli v mladosti meduloblastom, se je razvil kavernom. Samo pri 3/36 (8 %) preživelih z rakom v otroštvu (1 bolnik z akutno limfoblastno levkemijo [Zabramski tip II] in 2 bolnika z meduloblastomom [tip I in tip II]) smo kavernom razvrstili v skupino z visokim tveganjem za krvavitev; ostale z radioterapijo povzročene kavernome smo opredelili ko Zabramski tipa IV z nizkim tveganjem za krvavitev. Pri nobenem izmed preživelih z rakom v otroštvu in z radioterapijo povzročenim kavernomom ni prišlo do simptomatske krvavitve.

**Zaključki.** Z radioterapijo povzročenim kavernomom je pogost kasen učinek pri preživelih bolnikih, ki so zboleli za raka v otroštvu in smo jih zdravili z obsevanjem glave. Pojavi se pri polovici teh bolnikov. Vendar pa je bilo samo nekaj z radioterapijo povzročenim kavernomom (pri 8 % preživelih z rakom v otroštvu) razvrščenih v skupino z visokim tveganjem za krvavitev. Pri nobenem izmed naših bolnikov, ki so preživeli raka v otroštvu in imeli z radioterapijo povzročeni kavernom se ni pojavila simptomatska krvavitev. Sklepamo lahko, da je z radioterapijo povzročeni kavernom na MR posnetkih možganov najdba z nizkim tveganjem in praviloma benignim potekom.

Radiol Oncol 2021; 55(3): 284-291.  
doi: 10.2478/raon-2021-0015

# Sialendoskopsko in CT navigacijsko usmerjanje pri kirurškem zdravljenju sialolitiazze

Aničin A, Urbančič J

**Izhodišča.** Kombinirani sialendoskopsko asistirani pristop je dodobra uveljavljen v kirurgiji sialolitiazze. V primeru proksimalno ležečih kamnov je transkutani sialendoskopsko asistirani pristop z ohranitvijo obušesne in odstranitvev podčeljustne žleze prvi namen zdravljenja. Nedavno smo za izboljšanje rezultatov teh zahtevnih operacij dodali tudi kirurško računalniškotomografsko (CT) navigacijo.

**Bolniki in metode.** V raziskavo smo vključili vse bolnike, ki so bili napoteni na sialendoskopijo ali sialendoskopsko asistirano operacijo v terciarno ustanovo med januarjem 2012 in oktobrom 2020. Od novembra 2019 smo v primerih domnevno slabega endoskopskega prikaza kamna dodali tudi CT navigacijo. Ocenjevali smo parametre bolezni, diagnostične postopke, sialendoskopske najdbe in izide z ali brez uporabe optične kirurške navigacije.

**Rezultati.** Pri 372 bolnikih smo opravili 178 uspešnih odstranitvev slinskih kamnov, med katerimi je bilo 118 kombiniranih sialendoskopsko asistiranih pristopov, vključno s 16 transkutanimi operacijami proksimalnih kamnov, 10 submandibularnimi in 6 parotidnimi. Kirurško navigacijo smo uporabili pri šestih bolnikih, štirikrat pri podčeljustni in dvakrat pri obušesni sialolitiazzi. V vseh primerih so bili to neotipljivi kamni, med sialendoskopijo nevidni ali delno vidni. Uspeli smo ohraniti pet od šestih žlez slinavk.

**Zaključki.** Dodatek CT navigacije k sialendoskopsko asistiranim posegom za odstranitev neotipljivih, sialendoskopsko slabo vidnih in zagozdenih kamnov predstavlja pomembno prednost pri obvladovanju sialolitijaze. Z doslednim izvajanjem sialendoskopije in z njo povezanih ohranitvenih postopkov smo znatno zmanjšali potrebo po sialadenektomiji pri bolnikih z obstruktivno boleznijo žlez slinavk.

Radiol Oncol 2021; 55(3): 292-304.  
doi: 10.2478/raon-2021-0033

## Morfološke značilnosti cirkulirajočih tumorskih celic raka dojke po fizikalnem in biološkem načinu izolacije

Jesenko T, Modic Ž, Grašič Kuhar C, Čemažar M, Matkovič U, Miceska S, Varl J, Kuhar A, Kloboves-Prevodnik V

**Izhodišča.** Cirkulirajoče tumorske celice (CTC) so postale pomemben napovedni dejavnik pri raku dojke. Vzpostavili so različne metode za njihovo izolacijo, ki temeljijo na njihovih fizikalnih ali bioloških lastnostih. Za njihovo vizualizacijo po izolaciji večinoma uporabljajo imunofluorescenčna barvanja, s katerimi pa ne moremo dobiti podatkov o celični morfologiji.

**Materiali in metode.** Izvedli smo raziskavo, v kateri smo primerjali, kako dva različna načina izolacije CTC vplivata na morfologijo celic. Morfologijo smo analizirali z metodami, ki jih uporabljamo v rutinski citopatološki diagnostiki. Neposredno smo primerjali morfologijo celic po fizikalni (Parsortix®) in biološki (MACS®) metodi izolacije CTC.

**Rezultati.** V predkliničnem delu raziskave smo ugotovili, da obe metodi ohranita viabilnost in antigen-ske lastnosti celične linije raka dojke MCF7. Opazili smo nekaj znakov degeneracije – nabrekanje celic, brste citoplazme, nitaste izrastke ter citoplazemske vakuole. V kohorti bolnic z metastatskim rakom dojke se je izkazalo, da so morfološke lastnosti odvisne od metode izolacije. Po fizikalnem načinu izolacije smo določili CTC z ohranjenimi morfološki lastnostmi. Po biološkem načinu izolacije je bila večina CTC tako morfološko degeneriranih, da je bilo njihovo identiteto težko potrditi na podlagi morfološke ocene.

**Zaključki.** Glede na rezultate lahko zaključimo, da je fizikalni način izolacije primerna metoda za detekcijo CTC z ohranjeno morfologijo in je zato primerna za uporabo v rutinskem citopatološkem laboratoriju.

Radiol Oncol 2021; 55(3): 305-316.  
doi: 10.2478/raon-2021-0020

## Simvastatin učinkovito ubija radiorezistentne celice raka dojke

Aschenbrenner B, Negro G, Savic D, Sorokin M, Buzdin A, Ganswindt U, Čemažar M, Serša G, Skvortsov S, Skvortsova I

**Izhodišča.** Statini so nizko molekularni inhibitorji 3-hidroksi-3-metilglutaril-koencima A reduktaze, ki jih uporabljamo za zniževanje ravni holesterola in lipidnih neravnotežij. Novejše raziskave nakazujejo pozitivne učinke statinov pri zdravljenju raka dojke s podaljšanjem časa do ponovitve bolezni. Mehanizmi delovanja pa ostajajo neraziskani.

**Materiali in metode.** V raziskavi na starševskih in radiorezistentnih celicah raka dojke smo uporabili simvastatin, ki je eden od najbolj pogosto predpisanih statinov. Na treh različnih celičnih linijah raka dojke in njihovih rezistentnih podlinijah smo raziskali njegov potencialen radiosenzibilizirajoči učinek ter vpliv na preživetje in migracijo celic.

**Rezultati.** V primerjavi s starševskimi celičnimi linijami je bilo v radiorezistentnih celičnih linijah MDA-MB-231-RR, T47D-RR in Au565-RR povečano izražanje MHGCR, ki je bilo povezano z aktivacijo epitelno-mezenhimalnega prehoda. Ubijanje radiorezistentnih rakavih celic je bilo povezano z aktivacijo različnih signalnih poti, ki so vpletene v apoptozo in avtofagijo. V prisotnosti simvastatina je bila zmanjšana migracija celic, ter izražanje vimentina, povečano pa je bilo izražanje E-kadherina.

**Zaključki.** Rezultati raziskave nakazujejo, da lahko simvastatin učinkovito odstranjuje radiorezistentne celice raka dojke in zmanjšuje njihov mezenhimalni fenotip.

Radiol Oncol 2021; 55(3): 317-322.  
doi: 10.2478/raon-2021-0025

# Petletno spremljanje in klinični izid pri evtirotičnih bolnikih z nodusi v ščitnici

Bajuk Studen K, Gaberšček S, Pirnat E, Zaletel K

**Izhodišča.** Nodusi v ščitnici so zelo pogosti. Določanje optimalnih intervalov spremljanja nesumljivih nodusov v ščitnici še vedno predstavlja izziv. V raziskavi smo obravnavali kohorto bolnikov, ki smo jim diagnosticirali nodus v ščitnici ter ga ocenili kot nesumljivega in zdravljenje ni bilo indicirano. Bolnike smo pet let po diagnozi povabili na pregled, da bi ponovno ultrazvočno ocenili velikost nodusa in da bi ugotovili, ali potrebujejo klinično obravnavo.

**Bolniki in metode.** Retrospektivno smo zbrali osnovne podatke o bolnikih in ultrazvočnih značilnostih nodusov. Ob ponovnem obisku smo opravili ultrazvok ščitnice.

**Rezultati.** V raziskavo smo vključili 118 bolnikov (107 žensk / 11 moških, starih  $56,8 \pm 13,4$  let), ki so imeli izhodiščno 203 noduse v ščitnici s povprečnim največjim premerom nodusa  $10,5 \pm 7,4$  mm. Po 5 letih se je 58 (28,6 %) od 203 nodusov pomembno povečalo, 27 (13,3 %) pomembno zmanjšalo, 104 (51,2 %) pa je ostalo nespremenjenih. Štirinajst (6,9 %) nodusov je izginilo, odkritih je bilo 26 novih s povprečnim največjim premerom  $7,7 \pm 5,0$  mm. Ob preverjanju kliničnega poteka bolezni nismo odkrili nobenega primera raka ščitnice. Zdravljenja ni potrebovalo 107 (90,7%) bolnikov. Štirje (4,2%) bolniki so bili napoteni na tiroidektomijo zaradi rasti nodusov. Dva bolnika (1,7 %) sta potrebovala zdravljenje hipertiroze. Štirje bolniki (3,4 %) raziskave niso zaključili.

**Zaključki.** Z raziskavo smo preverili naravni potek bolezni pri bolnikih z nesumljivimi nodusi v ščitnici. Ugotovili smo, da je 71,4 % nodusov ostalo glede na velikost nespremenjenih, se je zmanjšalo ali so celo izginili. Večina bolnikov je ostalo klinično stabilnih in pet let po diagnozi ni potrebovalo zdravljenja.

Radiol Oncol 2021; 55(3): 323-332.

doi: 10.2478/raon-2021-0012

## Vloga režnjev v rekonstrukciji tkivnih vrzeli po resekciji lokoregionalno napredovalega raka lateralne lobanjske baze. Izkušnje terciarnega otorinolaringološkega centra

Vozel D, Pukl P, Grošelj A, Aničin A, Strojman P, Battelino S

**Izhodišča.** Namen raziskave je bil prikazati pomen obsežne resekcije in rekonstrukcije z režnji pri zdravljenju lokoregionalno napredovalega raka lateralne lobanjske baze.

**Bolniki in metode.** Naredili smo retrospektivno analizo bolnikov z rakom lateralne lobanjske baze, ki smo jih zdravili z namenom ozdravitve v terciarnem otorinolaringološkem centru med leti 2011 in 2019.

**Rezultati.** Opravili smo analizo 12 bolnikov z lokoregionalno napredovalim rakom lateralne lobanjske baze. Lateralno resekcijo temporalne kosti smo izvedli pri devetih (75 %) bolnikih, delno parotidektomijo pri šestih (50 %), totalno parotidektomijo pri enem (8,3 %), ipsilateralno selektivno disekcijo vratu pri osmih (66,7 %) in ipsilateralno modificirano radikalno disekcijo vratu pri enem bolniku (8,3 %). Tkivno vrzel smo rekonstruirali s prostim sprednje-stranskim stegenskim režnjem, prostim radialnim podlahtnim režnjem ali z vezanim mišično-kožnim režnjem mišice *pectoralis major* pri dveh bolnikih (17 %) za vsak reženj. Povprečno celokupno preživetje je bilo 3,1 leta (standardna deviacija [SD] = 2,5), preživetje brez bolezni pa 100 %. Ob prekinitvi zbiranja podatkov je bilo živih 83 % analiziranih bolnikov in 100 % bolnikov, pri katerih smo opravili rekonstrukcijo z režnjem.

**Zaključki.** Ugoden lokalni nadzor raka lateralne lobanjske baze lahko dosežemo z obsežno lokoregionalno resekcijo, ki ji sledi rekonstrukcija tkivne vrzeli s prostim ali vezanim režnjem. Smiselno je razmisliti o univerzalnem registru tovrstnega raka v centrih, ki zdravijo to bolezen, da bi olajšali analizo in multicentrične raziskave.

Radiol Oncol 2021; 55(3): 333-340.  
doi: 10.2478/raon-2021-0023

# Sodobno stanje v intraoperativni radioterapiji dojk z elektroni po intraoperativni uvedbi ultrazvoka

Vidali C, Severgnini M, Bellio G, Giudici F, Milan V, Pellin Z, Savatovic S, Scomersi S, Fastner G, Ciabattoni A, Bortul M

**Izhodišča.** Intraoperativno radioterapijo dojk z elektroni lahko uporabimo v klinični praksi tako za elektivno (delno) obsevanje dojk pri bolnicah z nizkim tveganjem za ponovitev bolezni, kot tudi za predvideno dodatno dozo. Pri tem namestimo zaščitni disk med preostalo dojko in prsno fascijo, da za zaščitimo tkivo pod tarčnim volumnom. Cilj pričujoče raziskave je bil oceniti vlogo intraoperativnega ultrazvoka pri izboljšanju kakovosti intraoperativne radioterapije dojk z elektroni.

**Bolniki in metode.** Intraoperativno radioterapijo dojk smo v Trstu uvedli leta 2012, tehniko pa izboljšali leta 2014 z intraoperativnim ultrazvokom. Za merjenje debeline obsevalne tarče smo uporabili iglo in intraoperativni ultrazvok. S slednjim smo tudi preverjali pravilni položaj zaščitnega diska. Primarni cilj raziskave je bila ocena učinkovitosti intraoperativnega ultrazvoka pri zmanjševanju tveganja za premik diska povezanega z intraoperativno radioterapijo, sekundarni cilj pa je bila analiza akutne in pozne toksičnosti. Primerjali smo dve skupini bolnic, ki smo jih zdravili z intraoperativno radioterapijo dojk z elektroni kot dodatkom doze, ob uporabi intraoperativnega ultrazvoka in igle (skupina 1) ali samo iglo (skupina 2). Akutno in pozno toksičnost smo ocenili s potrjenimi sistemi točkovanja.

**Rezultati.** Med junijem 2012 in oktobrom 2019 je bilo 109 primernih bolnic, ki smo jih vključili v raziskavo (kar ustreza 110 primerom, ena bolnica je bila namreč zdravljena z dvostransko konzervativno operacijo in dvostransko intraoperativno radioterapijo dojk z elektroni). 38 bolnic smo razvrstili v skupino 1 in 72 v skupino 2. Ciljna debelina, izmerjena z ultrazvočno sondo in z iglo, je bila podobna (povprečna razlika 0,1 mm;  $p = 0,38$ ). Odstotek bolnic, pri katerih je bil zaščitni disk popolnoma poravnana, se je po uvedbi intraoperativnega ultrazvoka povečal iz 23 % na več kot 70 %. Poleg tega so imele bolnice, kjer smo uporabili intraoperativni ultrazvok, manj akutne toksičnosti zaradi radioterapije (36,8 % vs. 48,6 %;  $p = 0,33$ ), razlika pa ni bila statistično pomembna. Pozna toksičnost je bila podobna ne glede na uporabo intraoperativnega ultrazvoka: 39,5 % vs. 37,5 % ( $p = 0,99$ ).

**Zaključki.** Pri intraoperativni radioterapiji dojk z elektroni je intraoperativni ultrazvok omogočil natančnejše merjenje ciljne globine in hkrati zmanjšal premik med kolimatorjem in zaščitnim diskom. Z ultrazvočno vodenim posegom smo zmanjšali akutno toksičnosti, čeprav ne statistično značilno.

# Predoperativna serumska koncentracija tumorskega označevalca CA-125 kot napovedni dejavnik obsega citoredukcije pri bolnicah z epiteljskim rakom jajčnikov

Merlo S, Drmota E, Bešić N, Kovačević N

**Izhodišča.** Rak jajčnikov je sedmi najpogostejši rak pri ženskah in osmi najpogostejši vzrok smrti zaradi raka. Zaradi pomanjkanja učinkovitih diagnostičnih postopkov in nespecifičnih simptomov ga v 75 % primerov odkrijemo v napredovali fazi. Vrednost tumorskega označevalca CA-125 je povišana pri več kot 85 % žensk z napredovalim epiteljskim rakom jajčnikov. Standardno zdravljenje je primarna citoreduktivna operacija z dopolnilno kemoterapijo, novejši pristop pa je predoperativna kemoterapija, ki ji nato sledi intervalna citoreduktivna operacija. Več raziskav je želelo odgovoriti, ali predoperativna koncentracija serumskega CA-125 lahko vpliva na izbiro in izid zdravljenja. Namen pričujoče raziskave je bil analizirati izkušnje posamičnega celostnega onkološkega centra glede preoperativne uporabnosti določanja serumskega nivoja tumorskega označevalca CA-125.

**Bolnice in metode.** Na Onkološkem Inštitutu Ljubljana smo izvedli retrospektivno raziskavo pri 253 bolnicah, ki smo jih zdravili zaradi raka jajčnikov, FIGO stadij IIIc in IV. Bolnice smo razdelili v dve skupini glede na osnovni način zdravljenja. V prvo skupino, ki smo jo zdravili s predoperativno kemoterapijo, smo vključili 215 bolnic, v drugo skupino, ki smo jo zdravili s primarno citoreduktivno operacijo pa 38 bolnic. Razlike med značilnostmi bolnic smo primerjali s hi-kvadrat testom in ANOVO. S pomočjo Kaplan-Meierjeve metode smo izračunali preživetje brez ponovitve bolezni in celokupno preživetje.

**Rezultati.** Mediana vrednost tumorskega označevalca CA-125 je bila višja v prvi skupini, ki smo jo zdravili s predoperativno kemoterapijo v primerjavi drugo skupino s primarno citoreduktivno operacijo (972 IU/ml vs. 499 IU/ml). Preživetje brez ponovitve bolezni pa je bilo v prvi skupini nižje kot v drugi (8 mesecev [95 % IZ: 6,4–9,5] vs. 18 mesecev [95 % IZ: 12,5–23,4]). Prav tako je bilo celokupno preživetje v prvi skupini, ki smo jo zdravili s predoperativno kemoterapijo, nižje kot v drugi, ki smo jo zdravili s primarno citoreduktivno operacijo (25 mesecev [95 % IZ: 20,6–29,5]) vs. 46 mesecev [95 % IZ: 32,9–62,1]).

**Zaključki.** Predoperativna vrednost tumorskega označevalca CA-125 do 500 IU/ml je obetajoč napovedni dejavnik, s katerim bi lahko predvideli vsaj optimalno primarno citoredukcijo.

Radiol Oncol 2021; 55(3): 347-353.  
doi: 10.2478/raon-2021-0027

# Napovedni vpliv z vnetjem povezanih označevalcev pri bolnikih z jetrnimi metastazami uvealnega melanoma, ki smo jih zdravili s transarterijsko jetrno kemoperfuzijo

Ludwig JM, Haubold J, Bauer S, Richly H, Siveke JT, Wimmer J, Umutlu L, Schaarschmidt BM, Theysohn JM

**Izhodišča.** Namen raziskave je bil oceniti, kakšen napovedni pomen imajo z vnetjem povezani označevalci pri bolnikih z neoperabilnimi jetrnimi metastazami uvealnega melanoma, ki smo jih zdravili s transarterijsko jetrno kemoperfuzijo.

**Bolniki in metode.** Retrospektivno smo ocenili 54 bolnikov (44 % moških, mediana starost: 61 let). Bolnike smo zdravili z melfalanom (92 %) ali fotemustinom (8 %), enkratno ali z več ponovitvami (mediana 3 zdravljenja; razpon: 1–11). Upoštevali smo naslednje z vnetjem povezane označevalce: razmerje (nevtrofilci/nl)/(limfociti/nl) (NLR), sistemski imunskovnetni indeks (trombociti/nl×nevtrofilci/nl)/(limfociti/nl) (SII) in razmerje (trombociti/nl)/(limfociti/nl) (PLR). Mejo z namenom dihotomizacije smo postavila na mediano (z vnetjem povezani označevalci, teža bolezn) ali pa na zgornjo raven normalnih vrednosti. Analizo Kaplan-Meier smo naredili za mediano vrednost celokupnega preživetja v mesecih in Coxov proporcionalni model tveganj za uni- in multivariatno razmerje ogroženosti (HR) z 95 % intervalom zaupanja (IZ).

**Rezultati.** Mediano skupno preživetje bolnikov, k smo jih vključili v raziskavo, je bilo 7,7 (6,3–10,9) meseca. V univariatni analizi je bilo celokupno preživetje daljše za bolnike z nizkim C reaktivnim proteinom (CRP; 13,5 proti 5,2;  $p = 0,0005$ ), nizkim SII (10,8 proti 5,6;  $p = 0,0005$ ), nizkim NLR (11,1 proti 6,3;  $p = 0,0045$ ), nizko aspartat aminotransferazo AST (11,5 proti 5,6;  $p = 0,015$ ), alanin aminotransferazo (ALT; 11,5 proti 5,6;  $p = 0,01$ ) in tumorskim bremenom 50 % (8,2 proti 4,8;  $p = 0,007$ ). Multivariatna analiza je potrdila nizek CRP (HR: 0,29, 0,11–0,7;  $p = 0,005$ ), nizek SII (HR: 0,19, 0,11–0,7;  $p = 0,008$ ) in nizek ALT (HR: 0,13, 0,02–0,63;  $p = 0,011$ ) kot neodvisne napovedne dejavnike podaljšane celokupnega preživetja. Bolniki z zvišanimi pomembnimi dejavniki v multivariatni analizi  $\leq 1, 2, 3$  so imeli mediano preživetja 14,9, 7,7 in 3,9 meseca,  $p = 0,0001$ .

**Zaključki.** Z vnetjem povezani označevalci (CRP, SII) in AST določeni pred zdravljenjem so bili neodvisni napovedni dejavniki preživetja pri bolnikih z uvealnimi melanomskimi metastazami v jetrih, zdravljenimi s transarterijsko jetrno kemoperfuzijo. Kombinacija označevalcev bi lahko pomagala prepoznati bolnike, ki bi lahko imeli koristi od zdravljenja.

Radiol Oncol 2021; 55(3): 354-361.

doi: 10.2478/raon-2021-0019

## Neželeni učinki zdravljenja z imunoterapijo pri slovenskih bolnikih z metastatskim melanomom kažejo sorazmerje z boljšimi rezultati zdravljenja

Mesti T, Čeplak Mencin V, Boshkoska BM, Ocvirk J

**Izhodišča.** Imunoterapija z zaviralci CTLA-4 in zaviralci PD1 kontrolnih točk je prinesla preboj v zdravljenju in napovedi poteka bolezni pri bolnikih z metastatskim melanomom. Preživetje teh bolnikov se je od pričakovanega časa preživetja, krajšega od 12 mesecev, povečalo na vsaj štirideset mesecev. Vendar ima imunoterapija s protitelesi proti CTLA-4 ali z zaviralci PD1 samimi ali v kombinaciji široko paleto pomembnih imunskih posledic. Cilj raziskave je bil oceniti korelacijo imunsko pogojenih neželenih dogodkov z izidi zdravljenja. Izide zdravljenja smo opredelili kot pomembne razlike v skupni stopnji odziva in preživetju bolnikov brez napredovanja bolezni.

**Bolniki in metode.** Naredili smo retrospektivno analizo bolnikov z metastatskim melanomom, ki smo jih zdravili z imunoterapijo leta 2020 na Onkološkem inštitutu v Ljubljani. V raziskavo smo vključili samo bolnike z radiološko oceno odziva na imunoterapijo. Bolnike smo razdelili v dve kohorti: kohorto bolnikov z imunsko povezanimi neželenimi dogodki (skupina irAE) in kohorto bolnikov brez imunsko povezanih neželenih dogodkov (skupina NirAE). Za raziskovanje razlik v preživetju brez napredovanja bolezni med kohorto irAE in kohorto NirAE smo uporabili analizo preživetja, Coxov model sorazmerij tveganj s kovariantami časa do napredovanja in neželenih dogodkov. Uporabili smo tudi H-test Kruskal-Wallis.

**Rezultati.** Med 120 bolniki, zdravljenimi z imunoterapijo, smo odziv na zdravljenje radiološko ocenili pri 99 bolnikih: pri 38 bolnikih v kohorti irAE in pri 61 bolnikih v kohorti NirAE. Skupni stopni odziva za kohorto irAE in NirAE sta bila 57 % in 37 %. Preživetje brez napredovanja bolezni je bil bistveno boljše za kohorto irAE (301,6 dni) kot za kohorto NirAE (247,29 dni). Rezultati regresijske analize preživetja so pokazali znatno povečanje verjetnosti preživetja, 80 % za kohorto irAE in manj kot 60 % za kohorto NirAE.

**Zaključki.** Bolniki z metastatskim melanomom, zdravljeni z imunoterapijo, pri katerih so se razvili imunsko povezani neželeni dogodki, so pokazali boljše rezultate zdravljenja z boljšo skupno stopnjo odziva in daljšim časom do napredovanja bolezni kot bolniki, ki niso razvili imunsko povezanih neželenih dogodkov. Prav tako se je pomembno povečala verjetnosti preživetja.

Radiol Oncol 2021; 55(4): 362-368.  
doi: 10.2478/raon-2021-0022

## Nosečniški rak dojke. Retrospektivna kohortna raziskava

Matos E, Ovčariček T

**Izhodišča.** Nosečniški rak dojke je redka bolezen. Je posebna oblika raka dojke, za katerega je značilen agresiven fenotip. Osrednji namen raziskave je bil oceniti, kako mednarodne smernice za obravnavo teh bolnic uresničujemo pri vsakodnevnem kliničnem delu.

**Bolnice in metode.** V retrospektivni raziskavi predstavljava skupino nosečih bolnic z rakom dojke, ki smo jih zdravili v terciarni ustanovi med leti 2007 in 2019 in povzemava ključna priporočila za njihovo obravnavo. Podatke sva pridobili iz elektronske podatkovne baze Onkološkega inštituta Ljubljana. Zajeli sva podatke o značilnosti bolnicah, njihovih tumorjev ter podatki o izhodu bolezni matere in stanju otroka.

**Rezultati.** Vključitvenim zahtevam je ustrezalo 14 bolnic. Tumorji so bili večinoma visoke stopnje malignosti, trojno negativni ali HER2 pozitivni, pri dveh bolnicah je bila bolezen že ob postavitvi diagnoze razsejana. Za vsako bolnico smo načrt zdravljenja izdelali v okviru multidisciplinarnega tima. Vse, razen dveh bolnic, so rodile ob načrtovanem terminu in brez pomembnih zapletov. Osem bolnic je bilo zdravljenih s sistemsko kemoterapijo, vse so dobile antracikline, ena tudi taksane. Odstopanje od mednarodnih priporočil smo našli samo pri eni bolnici, kjer je bilo uporabljeno modrilo za ugotavljanje varovalne bezgavke.

**Zaključki.** Obravnavo raka dojke v nosečnosti predstavlja velik strokovni in etični izziv. Načrt zdravljenja mora biti za vsako posamezno bolnico narejen v okviru multidisciplinarnega tima. Nosečniški rak dojke zdravimo podobno kot pri ostalih bolnicah z rakom dojke in tako da hkrati upoštevamo nosečnost.

Radiol Oncol 2021; 55(3): 369-378.  
doi: 10.2478/raon-2021-0034

## Protokol za natančno radiokromsko dozimetrijo z uporabo programske opreme Radiochromic.com

Méndez I, Rovira-Escutia JJ, Casar B

**Izhodišča.** Radiokromski filmi imajo širok spekter uporabe v radiologiji in radioterapiji. Dozimetrični sistem za radiokromsko filmsko dozimetrijo sestoji iz radiokromskih filmov, ploščatega optičnega bralnika in programske opreme za analizo filmov. Namen tega dela je predstavitev učinkovitost protokola za natančno radiokromsko filmsko dozimetrijo z uporabo programske opreme za analiziranje filmov Radiochromic.com.

**Metode.** Predstavili in pojasnili smo postopke za pridobivanje in analizo slik, kalibracijo filmov in izračun absorbirane doze. Programska oprema Radiochromic.com omogoča uporabo najsodobnejših modelov za izračun in popravke pri radiokromski filmski dozimetriji: multigausssov model za večkanalno filmsko dozimetrijo, module za popravke odzivov v stranski smeri in med posameznimi skeni ter modul za ponovitevno umeritev odziva filmov.

**Rezultati.** Predstavljen protokol zagotavlja natančno določitev absorbirane doze s sočasno omejitvijo merilnih negotovosti, ki vplivajo na kakovost rezultatov pri radiokromski filmski dozimetriji.

**Zaključki.** Opisani postopki za uporabo filmov in ploščatega optičnega bralnika zagotavljajo enostavno in natančno izvajanje radiokromske filmske dozimetrije ob uporabi programske opreme Radiochromic.com.